ROLE OF FOOD MATERIAL PROPERTIES ON THE MECHANISMS OF SOLID FOOD DISINTEGRATION DURING GASTRIC DIGESTION

A thesis presented in partial fulfilment of the requirements for the degree of

Doctor of Philosophy

in

Food Technology

at Massey University, Palmerston North,
New Zealand.

GEESHANI MADUWANTHI SOMARATNE

2020

To my beloved Amma & Thaththa for raising me to believe that all good things are possible…….

Abstract

The stomach is, after the mouth; the major organ for the breakdown of foods by a complex interaction of biochemical and mechanical mechanisms driven by the diffusion of gastric juice and the peristaltic activity of the stomach. The degree of fragmentation of solid food in the stomach and consequent release of nutrients is largely dependent on the food material properties. Despite extensive research directed at the gastric digestion, the establishment of the proper relationship between the initial material properties of foods and their subsequent breakdown during gastric digestion is still far from being fully understood.

To bridge the aforementioned knowledge gap, the aim of this thesis was to characterise the relationship between material properties of solid foods (composition and structure) and their disintegration behaviour in the stomach. Sweet potato (steamed and fried) and egg white gels (pH 5 and pH 9 EWGs) were used as starch and protein based-product models, respectively, to develop experimental models to characterise not only the diffusion of gastric juice into the food matrix, but also the mechanisms underlying the biochemical and mechanical degradation of the food matrix during *in vitro* gastric digestion.

Overall results revealed that the porous network created during frying facilitated a faster gastric acid penetration into the sweet potato food matrix than occurred in the less porous steamed sweet potato. Consequently, the fried sweet potato matrix underwent a faster collapsing and quicker softening time during *in vitro* gastric digestion than the more compact and denser structure of steamed sweet potato. This led to the faster disintegration and subsequent release of β-carotene in the human gastric simulator from the fried sweet potato matrix. A similar effect was demonstrated with the EWG, where the loose protein network of pH 5 EWG exhibited a significantly higher rate of pepsin diffusion, softening, nutrient release and mechanical breakdown compared to the more tightened gel microstructure found in the pH 9 EWG. In conclusion, gastric disintegration and nutrient release within the solid food structures is mainly controlled by the initial food microstructure and composition. Such knowledge will help to identify key factors for the designing of health-promoting food formulations.

Acknowledgments

Undertaking this PhD has been a rewarding and truly life-changing experience for me. It would not have been possible for me to complete my doctoral dissertation without the remarkable support that I have received from many amazing people. Therefore, I would like to take the opportunity to express my sincere gratitude to all of them.

I would like to begin by thanking my big supervisory panel! It was a privilege to work with the six best and most renowned food scientists in the World. Although working with six supervisors was the biggest challenge of my PhD journey, they were also my biggest strength. I could not have asked for a better supervisory panel; you have all been incredible role models in my academic life!

At the outset, I wish to express my sincere appreciation to my chief supervisor, Dr. Jaspreet Singh, for his guidance and all the worthwhile discussions, especially during the initial and final stages of my PhD. I greatly appreciate the freedom you have given me to find my own research path. My sincere gratitude is reserved for Associate Professor Aiqian Ye, my Massey co-supervisor, for his invaluable suggestions, encouragement, insightful comments and hard questions! Our discussions always clarified my questions, and it has been a great opportunity to learn from your food hydrocolloids and digestion related research expertise.

I would like to express my sincere thanks to Dr. Maria J. Ferrura, external co-supervisor, for accepting me as a PhD student in first place and helping me to start my doctoral research in New Zealand (Massey University). Unexpectedly, within the first day of my candidature, you announced your plan for joining Fonterra Research and Development Centre in Palmerston North, New Zealand. As a result, you transferred your role of main supervisor to Dr. Jaspreet Singh and you continued to support me in various ways as my external co-supervisor. It was you who gave me the initial idea of this research project and, subsequently, you also helped me to develop the design of this project. You have always been reachable throughout the project despite your tight schedule. Many thanks for initiating the wonderful collaboration with the French research team, which provided me with the opportunity to complete part of my PhD research in France, a truly pleasurable experience for me.

I could not have imagined that I would have the great opportunity to work with Distinguished Professor R. Paul Singh. I am greatly indebted to you Sir, for your invaluable time, co-operation, and generosity which made this PhD possible. Your important suggestions and advice are simply priceless! As a person with an amicable and

positive disposition, I was blessed to have an advisor like you. You are the best role model in my academic life!

I am extremely grateful to my overseas co-supervisors, Professor Francoise Nau and Dr. Didier Dupont for their invaluable guidance, encouragement and academic stimulus. Both of you provided valuable feedback on the development of all manuscripts and other publications and you were always easily accessible to discuss research related questions and ideas. My sincere gratitude also goes to both of you for offering me the internship opportunity in your research group and guiding me on the exciting project in UMR1253, INRA, Agrocampus Ouest, Rennes, France.

A special note of thanks should again be given to Professor Francoise Nau for her warm welcome and hospitality during my first few days in Rennes, France and continuous help and support during my internship period. I consider it a great opportunity to share your office for the five months. Even though I could not improve my French, I learnt many good things from you. You provided me a perfect role model not only as a great leader in your academic field, but also as a great researcher!

Chapters 6 and 7 would not have come to a successful completion, without the help I received from Associate Professor Juliane Fluory. Despite your busy schedules, you taught me to use the confocal microscope from the basic principles to complex diffusion related applications. Moreover, you were kind enough to undertake the editing of my publications and I acknowledge the meticulous work you have done. Working with you was very productive and pleasurable. You are the best mentor within my PhD journey!

I would like to express my sincere gratitude to Distinguished Professor Harjinder Singh (Director, Riddet Institute) and Professor Marlena Kruger (Associate Dean Higher Degree Research) for great support and guidance to ensure common agreement about my PhD research direction among the supervisory panel. I also want to take a moment to express a profound appreciation to my confirmation committee members, particularly Professor Matt Golding (Examiner of the confirmation report) and Professor Julian Heyes (Post-Graduate Coordinator) for investing their time and providing interesting and valuable feedback to modify my PhD research proposal at the beginning.

I would like to express my deepest appreciation to the Riddet Institute, a premier national centre for fundamental and strategic scientific research in food, not only for providing the funding which allowed me to undertake this doctoral research, but also for giving me the opportunity to attend conferences, workshops and invaluable internship opportunities. Particularly, I gratefully acknowledge the funding received towards my doctoral study from the Riddet Institute CoRE research programme. I am also grateful

for the funding received through the Riddet Institute Overseas Placement Award to undertake part of my PhD study in France.

The administrative staff of the Riddet Institute, Ms. Ansley Te Hiwi, Ms. Terri Palmer, Ms. Hannah Hutchinson and Dr. Sarah Golding have been very kind and patient and always willing to lend their administrative services whenever I approached them, and I acknowledge and appreciate them for all their great efforts. Likewise, Mr. John Henley-King (CoRE Business Manager), the late Ms. Fliss Stibbards (Senior Finance Administrator), Ms. Meg Wedlock and Ms. Angela Gemmell (Finance Administrators) of the Riddet Institute have been kind enough to extend their help regarding the financial matters at various phases of my research and I do hereby acknowledge all of them! Moreover, I would like to express my special appreciation to Mr. Matt Levin (Computer Consultant) for all his invaluable Information Technology and Systems support throughout my doctoral research study. Matt was kind enough to create my lightbox which was the key component of the experimental set-up in Chapters 5 and 8. I really acknowledge the meticulous work he has done. Dr. Catriona Hay kindly agreed to do the proofreading and I would like to express my deepest gratefulness for her diligent editing of my PhD thesis.

I am extremely grateful to Ms. Janiene Gilliland, Ms. Maggie Zou, Mr. Chris Hall, Mr. Warwick Johnson, Mr. Steve Glasgow, Ms. Michelle Tamehana, Ms. Chanapha Sawatdeenaruenat (Nok) and Mr. Jack Cui for providing the laboratory inductions, training in the use of laboratory instruments and equipment, ordering of chemicals and all the scientific advice. I would like to express my special appreciation to the Manawatū Microscopy Imaging Centre (MMIC) for helping me to observe the evolution of microstructure changes in my product models as a result of digestion. In particular, I would like to thank, Ms. Niki Minards (confocal microscopy and scanning electron microscopy) and Ms. Jordan Taylor (light microscopy and transmission electron microscopy) for their enormous contributions.

My thanks also go out to the support I received from the collaborative work I undertook with AgResearch, Palmerston North. I would like to sincerely thank Dr. Marlon Reis for his exceptional assistance and guidance to apply Hyperspectral imaging on tracing the gastric juice diffusion process for the first time. Ms. Cheerie Wang, your countless contributions to the Hyperspectral experiment was deeply appreciated. I am also extremely grateful to my friends, Ms. Chathurika Samarakoon and Mr. Hasitha Priyashantha, who gave me the first idea of using Hyperspectral imaging in my PhD. Chapters 3 and 6 would not have been published without all your great contributions!

I would like to acknowledge, and express my appreciation for, the countless support received through the collaborative work undertaken with the UMR1253, INRA,

Agrocampus Ouest, Rennes, France. In particular, Dr. Amélie Deglaire, Professor Catherine Guerin, Dr. Thomas Croguennec, Dr. Marie-Françoise Cochet, Dr. Romain Jeantet and Dr. Valérie Lechevalier for their warm welcome in Agrocampus Ouest, Rennes and their willingness to help in any situation. I am also very grateful to the administrative staff; especially Ms. Laurence Fauvel, Ms. Anne Giboulot, Ms. Nathalie Hommet, Ms. Monique Bouriel and Mr. Dominica Volland for their administrative assistance throughout my internship period. Additionally, I would like to acknowledge Ms. Claire Prioul for providing me the laboratory induction, Mr. Jean-Jacques Dubois for analysing the protein content of egg white samples and Dr. Jordane Ossemond for helping me to use the confocal microscope.

All former and current researchers of the Riddet Institute have played an important role in my journey as a PhD fellow and I would like to thank a few of them personally. Dr. Cintia Dias, Dr. Teresa Wegrzyn, Dr. Carlos Montoya, Dr. Natascha Strobinger, Dr. Parbhu Balan, Dr. Parthasarathi Subramanian, Dr. Prateek Sharma, Dr. Arup Nag and Dr. Devastotra Poddar, many thanks for your generous sharing of personal and scholarly experiences and suggestions at various stages of my PhD journey.

I would like to thank all my current and former friends from the Riddet Institute and Massey Institute of Food Science and Technology, Isuri Jayawardana (My elder sister from another mom!), Sewuese Okubanjo (My PhD problem solver!), Jane Lin (My fairy friend!), Muhammad Syahmeer How (My loving younger brother!), Marion Hubert (My French teacher!), Gurpreet Singh, Nina Yang, Nicole Yu-Fang Chen, Anika Hoogeveen, Feng Ming Chian, Chih-Chieh Chuang, Thomas Do, Hoang Du Le, Xiaoye He (Rachael), Akashdeep Singh, Siqi Li, Nan Luo, Alice Mao, Jing Feng, Marina Marinea, Natasha Nayak, Sarah Priour, Yonatan Souid, Edward de Haas, Philipp Schulze, Nikhila Mary Vijay (Niki), Debashree Roy, Akila Srinivasagam, Xin Wang, Jessie Zhu, Maheeka Weerawarna and late Harjot Khaira (I really miss you Harjot, May you attain supreme bliss of Nibbana!) with whom I have shared moments of happiness but also various difficulties as a PhD fellow during the last three years. It was a pleasure to sit with you in the same office and to share the laboratory spaces. Thanks for all your fascinating corridor chats, simulating coffee and lunch breaks, surprise parties, PhD student gatherings and for all the fun we have had in the last three years.

An unforgettable time during my PhD was my visit to France for five months. The warm welcome and fabulous support of my friends, particularly Elham, Ashkan (Dr. A. Madadlou), Sanda, Carlos and Manon from the UMR1253, INRA, Agrocampus Ouest, Rennes, France. I would also like to thank Paul Capela for being the best lab mate ever and for us surviving together in France!

Words cannot express how grateful I am to my New Zealand Aunt (Ms. Anoma Kariyawasam), Uncle (Mr. Sena Kariyawasam), their eldest daughter (Ms. Sadamali Kariyawasam) and the youngest daughter (Ms. Thushari Kariyawasam) for all of the sacrifices that they have made on my behalf during my PhD journey. You all treated me as a family member! The success of my PhD story was entirely due to the support received from the Kariyawasam family!

I am indebted to all my relations in New Zealand who opened their homes to me during my PhD journey. In particularly, I am very grateful to my beautiful cousin sister (Ms. Kumari Gamlath) and her family for helping me immensely in numerous ways during various stages of my PhD. And of course, a big thank you to my loving cousin brother (Mr. Snajaya Rajakaruna) and sister (Ms. Thanuja Herath) for helping me enormously and especially for offering me delicious foods from time to time.

My life in France was made more enjoyable due to the presence of my mom's cousin sister and I would like to extend my deepest gratitude to my Aunt (Ms. Nali Rupasinghe), my Uncle (Mr. Parakrama Rupasinghe) and their loving sons, Vithum and Jewin for their great care and hospitality. Thank you all for making my stay in Paris such an unforgettable experience!

I would like to thank Dr. Ishani Soysa, Dr. Nihal Jayamaha, Dr. Thiagarajah Ramilan, Professor Ravi Ravindran, and Dr. Rana Ravindran for their invaluable guidance, personal and scholarly support and constant encouragement throughout my research work. This thesis would not have come to a successful completion, without the help I received from Dr. Nirosha Priyadarshani. Thank you so much my loving sister, Nirosha, for your unconditional and tremendous support to clarify all my questions related to the data analysis using Matlab.

New Zealand, and in particular Palmerston North, was not only a place where I did my doctoral research but also felt like heaven similar to my sweet home in Sri Lanka, due to the love and caring support received from the brothers and sisters from another mother. Among them, I would like to particularly express my sincere gratitude to Ms. Umani Walallawita, Mr. Harshana Jayarathna, Mr. Asela Rupasgnhe, Mr. Sanjaya Fernando, Ms. Pushpa Gunawardhane, Ms. Ayanthi Matharage, Mr. Buddhi Somaweera, Ms. Pavithra Ariyarathne, Mr. Shanka Samarasinghe, Mr. Muditha Peiris, Ms. Nissansaala Pallawala, Mr. Sagara Kumara, Dr. Nirosha De Silva, Ms. Vishna Weerarathne, Ms. Tharanga Wedikula and Mr. Chanjief Chandrakumar for all your fabulous supports at various stages of my PhD journey. Some special words of gratitude go to my loving friend, Ms. Nipuna Perera who has always been a major source of support when things would get a bit discouraging. Not only as a good friend, but also you acted as an elder sister from time to time during my PhD journey.

I would also like to acknowledge all my lecturers from the University of Peradeniya, Sri Lanka who were the first to inspire me to start a PhD, helped me to make the right decision and have supported me ever since. Additionally, I am indebted to all my teachers and schools (Hillwood College and Mahamaya College, Kandy) for providing me a platform to broaden my knowledge and inculcating soft skills, time management skills and creativity in me!

I am extremely grateful to all my good old Sri Lankan friends, SPINTAG group (especially Ms. Akemi Wijayabahau) and BFST-09 group (especially Ms. Ayesha Satharasinghe, Ms. Chathurika Abeyratne, Mr. Reshan Jayawardhana, Mr. Dimuthu Gunasekara and Mr. Prasad Wijekoon). Thanks, folks, for always being there for me!

I would like to say a heartfelt thank you to my own loving elder brother, (Mr. Buddhika Somaratne), sister-in-law, (Mrs. Sachithra Karunarathne) and my darling niece, (Thiseja Somaratne) not only for their all the support and encouragement but also taking care of our parents, when I was studying abroad. My deepest thanks also go to all my relations who all helped me in numerous ways during various stages of my PhD.

Finally, my wholehearted gratitude goes to my beloved Amma (Mom) and Thaththa (Dad). They have been living every single minute for my brother and me. Without them, I would not have had the courage to embark on this PhD journey in the first place. Thank you for teaching me that all good things are always possible! You are always right! Yes, I did it and thus I dedicate my PhD dissertation to you!

Geeshani Somaratne
April 2020

Table of Contents

Abstract I
Acknowledgments II
Table of Contents VIII
List of Tables XIII
List of Figures XVII
List of Abbreviations XXII
List of Publications XXIII

Chapter One 1
1.Introduction and Thesis Outline 1
1.1 Research Background and Rationale of the Thesis 1
1.2 Overall Goal and Research Questions of the Thesis 3
1.3 Research Approach 4

Chapter Two 8
2. Food Material Properties as Determining Factors in Nutrient Release during Human Gastric Digestion: Literature Review* 8
2.1 Abstract 8
2.2 Introduction 9
2.3 Functional Anatomy of the Human Stomach and Gastric Secretion 12
2.4 Experimental Approaches to Evaluate Gastric Digestion 14
2.5 Role of Food Material Properties on the Gastric Digestion Process 17
2.5.1 The Chemical Nature of Food Matrix Determines the Biochemical Disintegration 17
2.5.2 Food Structure Regulates the Food Transit in the Gastrointestinal Tract 18
2.5.3 Food Structure Determines Mass Transfer Process during Gastric Juice Diffusion 19
2.5.4 Food Microstructure is one of the Determining Factors for Gastric Enzyme Diffusion and Activity 22
2.5.5 Physical Disintegration of Foods as a Result of Complex and Combined Mechanisms 26
2.6 Nutrient Release during Gastric Digestion 29
2.6.1 Mechanisms of Nutrient Release 29
2.6.2 Modelling Nutrient Release Kinetics 31
2.7 Conclusions and Perspectives 34

Chapter Three 36
3. Characterisation of Steamed and Fried Sweet Potatoes Microstructure and its Relationship with Acid and Moisture Diffusivity during Static In Vitro Gastric Digestion* 36
3.1 Abstract 36
3.2 Introduction 37
3.3 Materials and Methods 39
3.3.1 Materials 39
3.3.2 Sweet Potato Sample Preparation 39

3.3.3 Observation of Initial Microstructure....40
3.3.4 Formulation of Simulated Digestive Fluids....40
3.3.5 Static *In Vitro* Digestion....40
3.3.6 Hyperspectral Image Acquisition....43
3.3.7 Moisture Content Determination....43
3.3.8 Total Acid Content Determination....43
3.3.9 Hyperspectral Images Pre-Processing....44
3.3.10 Model Development to Predict Moisture and Acid Distribution....44
3.3.11 Visualisation and Prediction of the Spatiotemporal Distribution of Acid and Moisture....45
3.3.12 Acid and Moisture Diffusion Modelling....46
3.3.13 Statistical Analysis....47
3.4 Results and Discussion....47
3.4.1 Choice of Experimental Parameters....47
3.4.2 Microstructure of the Raw Sweet Potatoes is Influenced by the Cooking Treatment....47
3.4.3 Moisture and Acid Content of the Cooked Sweet Potatoes is Influenced by the Cooking Treatment....49
3.4.4 Moisture Content Prediction....49
3.4.5 Acid Content Prediction....52
3.4.6 Spatiotemporal Distribution of Moisture in Sweet Potatoes Structures During Gastric Digestion....54
3.4.7 Spatiotemporal Distribution of Acid in Sweet Potatoes Structures During Gastric Digestion....57
3.4.8 Impact of Sweet Potatoes Structures on Diffusion Kinetics of Water During Gastric Digestion....57
3.4.9 Impact of Sweet Potatoes Structures on Diffusion Kinetics of Acid During Gastric Digestion....58
3.4.10 Performance comparison of the Fick's second law and the power-law diffusion models....63
3.5 Conclusions....64

Chapter Four....65
4. Characterisation of Microstructural Changes and Nutrient Release in Steamed and Fried Sweet Potatoes during Static *In Vitro* Gastric Digestion*....65
4.1 Abstract....65
4.2 Introduction....66
4.3 Materials and Methods....67
4.3.1 Materials....67
4.3.2 Sweet Potato Sample Preparation and Cooking....67
4.3.3 Static *In Vitro* Digestion....68
4.3.4 Scanning Electron Microscopy....69
4.3.5 Light Microscopy and Transmission Electron Microscopy....69
4.3.6 Analysis of β-carotene Release During Gastric Digestion....70
4.3.7 Modelling the Kinetics of β-carotene Release over Digestion Time....71
4.3.8 Statistical Analysis....72
4.4 Results and Discussion....73

4.4.1 Surface Microstructure of the Cooked Sweet Potatoes is Influenced by the In Vitro Gastric Digestion 73
4.4.2 Cellular Structure of the Cooked Sweet Potatoes is Influenced by the In Vitro Gastric Digestion..... 73
4.4.3 ß-carotene Release from Sweet Potato Food Matrix due to Gastric Digestion ..82
4.5 Conclusions 85

Chapter Five 86
5. Role of Gastric Juice Diffusion on Softening and Mechanical Disintegration of Steamed and Fried Sweet Potatoes during *In Vitro* Gastric Digestion* 86
5.1 Abstract 86
5.2 Introduction 87
5.3 Materials and Methods 89
5.3.1 Materials 89
5.3.2 Sweet Potato Sample Preparation and Cooking 89
5.3.3 Static *In Vitro* Digestion 89
5.3.4 Hardness Determination using Texture Profile Analysis 89
5.3.5 Weibull Model Parameters and Softening Half-Time Determination..... 90
5.3.6 Mechanical Disintegration of Cooked Sweet Potatoes using a Human Gastric Simulator 90
5.3.7 Determination of Particle Size Distribution using Image Analysis 91
5.3.8 Modelling of Particle Breakdown during Gastric Digestion 92
5.3.9 Modelling the ß-carotene Release Kinetics 93
5.3.10 Statistical Analysis 93
5.4 Results and Discussion 94
5.4.1 Choice of Experimental Parameters 94
5.4.2 Softening Kinetics of Sweet Potatoes during Gastric Phase is Influenced by the Initial Cooked Sweet Potatoes Characteristics 94
5.4.3 Mechanisms of Particle Breakdown Depend on the Initial Structure of Steamed and Fried Sweet Potatoes 97
5.4.4 Role of Biochemical and Mechanical Effects on the Breakdown Process of Steamed and Fried Sweet Potatoes 101
5.4.5 Role of Biochemical and Mechanical Effects on the ß-Carotene Release from Steamed and Fried Sweet Potatoes 105
5.5 Conclusions 108

Chapter Six 109
6. Characterisation of Egg White Gels Microstructure and its Relationship with Pepsin, Acid and Moisture Diffusivity During Static In Vitro Gastric Digestion* ...109
6.1 Abstract 109
6.2 Introduction 110
6.3 Materials and Methods 112
6.3.1 Materials 112
6.3.2 Preparation of Egg White Solution 112
6.3.3 Egg White Gel Preparation for Microstructure Study 113
6.3.4 Egg White Gel Preparation for the Fluorescence Recovery After Photobleaching Analysis 113
6.3.5 Egg White Gel Preparation for the Hyperspectral Imaging 113

6.3.6 Pepsin Labeling....113
6.3.7 Confocal Imaging....114
6.3.8 Image Analysis....114
6.3.9 Fluorescence Recovery After Photobleaching Analysis....116
6.3.10 Fluorescence Recovery After Photobleaching Data Analysis....116
6.3.11 Determination of Acid and Moisture Diffusivity using Hyperspectral Imaging....118
6.3.12 Statistical Analysis....118
6.4 Results and Discussion....119
6.4.1 Observation of Native Egg White Gels Microstructure....119
6.4.2 Microstructural Parameters of Native Egg White Gels....119
6.4.3 Effective Diffusion Coefficients of FITC-pepsin and FITC–dextran in Egg White Gels....122
6.4.4 Reduced Diffusion Coefficients of FITC-pepsin and FITC–dextran in Egg White Gels....124
6.4.5 Moisture and Acid Content of Egg White Gels....126
6.4.6 Moisture Content Prediction....126
6.4.7 Acid Content Prediction....129
6.4.8 Spatiotemporal Distribution of Moisture in Egg White Gel Structures during Gastric Digestion....130
6.4.9 Spatiotemporal Distribution of Acid in Egg White Gel Structures during Gastric Digestion....131
6.4.10 Impact of Egg White Gel Structures on Diffusion Kinetics of Water during Gastric Digestion....131
6.4.11 Impact of Egg White Gel Structures on Diffusion Kinetics of Acid during Gastric Digestion....137
6.5 Conclusions....140

Chapter Seven....141
7. Characterisation of Microstructural Disintegration and Nutrient Release in pH 5 and pH 9 Egg White Gels during Static *In Vitro* Gastric Digestion*....141
7.1 Abstract....141
7.2 Introduction....142
7.3 Materials and Methods....143
7.3.1 Materials....143
7.3.2 Preparation of Heat-induced Egg White Gels....144
7.3.3 Spectral Properties of TRITC-dextran in EWGs at Different pH....144
7.3.4 Time-lapse Confocal Microscopic Observations during *In Vitro* Gastric Digestion....145
7.3.5 Quantification of Protein Particle Area Fraction....147
7.3.6 Modeling the Kinetics of TRITC-Dextran Release over Digestion Time....147
7.3.7 Statistical Analysis....148
7.4 Results and Discussion....149
7.4.1 Egg White Gel Microstructure Impacts the Disintegration by Pepsin.....149
7.4.2 pH Cannot Be Avoided as A Key Parameter for Egg White Gel Disintegration by Pepsin....150
7.4.3 In These Experimental Conditions, Egg White Gel Disintegration by Pepsin was Mainly Driven by a Surface Erosion Phenomenon....155

7.4.4 TRITC-dextran (4.4 kDa) can be Considered as a Peptide Release Marker in Egg White Gel Matrices during Gastric Digestion 155
7.4.5 Egg White Gel Characteristics Determine the Extent of TRITC-Dextran Release by Pepsin Action 156
7.5 Conclusions 160

Chapter Eight 161
8. Role of gastric Juice Diffusion on Softening and Mechanical Disintegration of pH 5 and pH 9 Egg White Gels During *In Vitro* Gastric Digestion* 161
8.1 Abstract 161
8.2 Introduction 162
8.3 Materials and Methods 163
8.3.1 Materials 163
8.3.2 Preparation of Egg White Gels 164
8.3.3 Static *In Vitro* Digestion 164
8.3.4 Hardness Determination using Texture Profile Analysis 164
8.3.5 Weibull Model Parameters and Softening Half-Time Determination. 164
8.3.6 Mechanical Disintegration of Egg White Gels Using a Human Gastric Simulator 164
8.3.7 Determination of Particle Size Distribution using Image Analysis 164
8.3.8 Modelling of Particle Breakdown during Gastric Digestion 165
8.3.9 Statistical Analysis 165
8.4 Results and Discussion 165
8.4.1 Softening Kinetics of Egg White Gels during Gastric Phase is Influenced by the Initial Egg White Gel Characteristics 165
8.4.2 Mechanisms of Particle Breakdown Depend on the Initial Structure of the Egg White Gels 168
8.4.3 Role of Biochemical and Mechanical Effects on the Breakdown Process of pH 5 and pH 9 Egg White Gels 173
8.5 Conclusions 176

Chapter Nine 177
9. Overall Discussion, Conclusions and Future Recommendations 177
9.1 Overall Discussion and Conclusions 177
9.2 Future Recommendations 185
References 189
Appendix 1 206
Appendix 2 213
Appendix 3 216
Appendix 4 217
DRC 16 Forms 218
Copyright Permissions 224

List of Tables

Table 2.1: Summary of *in vitro* static and dynamic gastric digestion models 15

Table 2.2: D_{eff} of water in different solid food matrices 20

Table 2.3: D_{eff} of acid in different solid food matrices 21

Table 2.4: Summary of mathematical models for drug/nutrient release kinetics 33

Table 3.1: Preparation of SSF at pH 7 41

Table 3.2: Preparation of SGF at pH 3 41

Table 3.3: Moisture Contents (% wet basis) and acid contents (mg HCl/g of sample) of sweet potatoes during 240 min of *in vitro* gastric digestion 50

Table 3.4: Performance of the PLS regression model for moisture content, for HSI quantification on SSP and FSP 51

Table 3.5: Performance of the PLS regression model for acid content, for HSI quantification on SSP and FSP 52

Table 3.6: The rate of moisture diffusion (k), diffusion exponent (n), diffusion mechanism and effective diffusivity (D_{eff} ± SD of n=3) for water in SSP and FSP.. .. 61

Table 3.7: The rate of acid diffusion (k), diffusion exponent (n), diffusion mechanism and effective diffusivity (D_{eff} ± SD of n=3) for acid in SSP and FSP..... 62

Table 4.1: Fitting parameters for the ß-carotene release data fitted with the weibull model and the power-law model 84

Table 5.1: Changes in the hardness (N) of the steamed and fried sweet potatoes during *in vitro* gastric digestion 96

Table 5.2: Parameter values of weibull function (Eq. 5.1) fitted to the softening curves of the steamed and fried sweet potatoes during *in vitro* gastric digestion.. 97

Table 5.3: Mixed weibull distribution parameters. Values are given as averages (n = 3) with SD 103

Table 5.4: Parameter values of weibull function (Eq. 5.4 and Eq. 5.5) fitted to the ß-carotene (%) release profiles of the steamed and fried sweet potatoes 104

Table 6.1: Quantitative parameters characterising the microstructure of pH 5 and pH 9 EWGs obtained from image analysis on binary confocal micrographs 120

Table 6.2: D_{eff} values relating to the mobility of FITC-pepsin and FITC-dextran in water and EWGs. 124

Table 6.3: Reduced diffusion coefficient (Dr) values relating to the mobility of FITC-pepsin and FITC-dextran. 125

Table 6.4: Net charge of the pepsin and major egg white proteins at pH 5 and pH 9. The given net charge values and the estimated pI of the proteins were calculated by using the online Protein Calculator v3.4 (http://protcalc.sourceforge.net/). 125

Table 6.5: Moisture Contents (% wet basis) and acid contents (mg HCl/g of sample) of EWGs during 240 min of in vitro gastric digestion 127

Table 6.6: Performance of the PLS regression model for moisture content, for HSI quantification on pH 5 and pH 9 EWGs 129

Table 6.7: Performance of the PLS regression model for acid content, for HSI quantification on pH 5 and pH 9 EWGs 129

Table 6.8: The rate of moisture diffusion (k), diffusion exponent (n), diffusion mechanism and effective diffusivity (Deff ± SD of n=3) for water in pH 5 and pH 9 EWGs. 136

Table 6.9: The rate of acid diffusion (k), diffusion exponent (n), diffusion mechanism and effective diffusivity (D_{eff} ± SD of n=3) for acid in pH 5 and pH 9 EWGs..... .139

Table 7.1: Fitting parameters for the TRITC-dextran release data fitted with the weibull model and the power-law model 158

Table 8.1: Changes in the hardness (N) of the pH 5 and pH 9 EWGs during *in vitro* gastric digestion 166

Table 8.2: Parameter values of weibull function (Eq. 5.1) fitted to the softening curves of the pH 5 and pH 9 EWGs during *in vitro* gastric digestion 167

Table 8.3: Mixed weibull distribution parameters. Values are given as averages (n = 3) with SD..... 175

List of Figures

Figure 1.1: Overview of the experimental approach 7

Figure 2.1: The physicochemical processes of food disintegration showing how the food bolus simultaneously undergoes breakdown and nutrient release inside the stomach 10

Figure 2.2: Main factors influencing nutrient release kinetics during gastric digestion 11

Figure 2.3: Structural arrangement of the human stomach 14

Figure 2.4: Comparison of the diffusion coefficients (D_{eff}) of pepsin in semi-solid gels with the D_{eff} of pepsin in liquid. Note that all the diffusion experiments were performed at 20 °C. 24

Figure 3.1: Schematic diagram of the gastric acid and moisture diffusion and HSI experimental procedure of SSP as an example 42

Figure 3.2: CLSM images of (a) raw, (b) steamed and (c) fried sweet potatoes. SEM images of (d) raw, (e) steamed and (f) fried sweet potatoes. “IS” denotes the intercellular spaces, “SG” denotes strach granules, “GS” denotes cells filled with gelatinised starch, “white arrow” denotes β-carotene crystals and “oil” represent the canola oil accumulation in intercellular spaces. Blue colour of CLSM images represents cell walls, magenta (Figure 3.2 (c)) colour represents the oil, green colour of CLSM images reprents other intercellualr content including starch granules and red-orange thin strands represent auto-fluorescence carotenoids crystals. The obtained Figure 3.2 (a) and (b) were a combination of images from three channels, namely a differential interference contrast (DIC) microscopy image, an image from the green and blue fluorescence and Figure 3.2 (c) was a combination of four channels including a differential interference contrast (DIC) microscopy image, an image from the red, green and blue fluorescence. 48

Figure 3.3: Predicted versus measured values of moisture in (a) SSP and (b) FSP for the best PLS models (calibration data set), expressing the moisture content as wet basis. The solid line shows the calibration line of the PLS regression model. Performance of the PLS regression model for moisture indicated as the determination coefficients (R^2) 51

Figure 3.4: Predicted versus measured values of acid in (a) SSP and (b) FSP for the best PLS models (calibration data set), expressing the acid content as mg HCl/g of sample. The solid line shows the calibration line of the PLS regression model. Performance of the PLS regression model for acid indicated as determination coefficients (R^2). 53

Figure 3.5: Spatiotemporal moisture content distribution maps of (a) SSP and (b) FSP generated by using the optimal PLS models. (Note that the colour scale of an individual sweet potatoes structure represents a different range of moisture (%) content) 55

Figure 3.6: Spatiotemporal acid content distribution maps of (a) SSP and (b) FSP generated by using the optimal PLS models. (Note that the colour scale of an individual sweet potatoes structure represents a different range of acid (mg HCl/g of sample) content) 56

Figure 3.7: Plots of moisture concentration ratio as a function of digestion time (s) for the (a) SSP and (b) FSP. Circles represent average experimental values (n = 3) and error bars represent the SD of the mean. The prediction of the model of the Fick's second law (Eq. 3.1) and the power-law model (Eq. 3.2) are represented by solid and dashed lines, respectively. 59

Figure 3.8: Plots of acid concentration ratio as a function of digestion time (s) for the (a) SSP and (b) FSP. Circles represent average experimental values (n = 3) and error bars represent the SD of the mean. The prediction of the model of the Fick's second law (Eq. 3.1) and the power-law model (Eq. 3.2) are represented by solid and dashed lines, respectively. 60

Figure 4.1: Schematic representation of sample preparation for SEM 69

Figure 4.2: Schematic representation of sample preparation for LM and TEM 70

Figure 4.3: Surface microstructure changes of SSP during simulated *in vitro* gastric digestion. (a) Before digestion (0 min), Samples taken after (b) 10min, (c) 20 min, (d) 40 min, (e) 60 min, (f) 120 min, (g) 180 min and (h) 240 min of gastric digestion. As artefacts produced by freeze-drying are present, these micrographs do not necessarily represent the structure prior to freeze-drying. 75

Figure 4.4: Surface microstructure changes of FSP during simulated *in vitro* gatsric digestion. (a) Before digesion (0 min), Samples taken after (b) 10min, (c) 20 min, (d) 40 min, (e) 60 min, (f) 120 min, (g) 180 min and (h) 240 min of gatrsic digetsion. As artefacts produced by freeze-drying are present, these micrographs do not necessarily represent the structure prior to freeze-drying. 76

Figure 4.5: Centre location of microstructure changes of SSP during simulated *in vitro* gastric digestion. (a) Before digestion (0 min), Samples taken after (b) 10min, (c) 20 min, (d) 40 min, (e) 60 min, (f) 120 min, (g) 180 min and (h) 240 min of gastric digestion. 77

Figure 4.6: Surface location of microstructure changes of SSP during simulated *in vitro* gastric digestion. (a) Before digestion (0 min), Samples taken after (b) 10min, (c) 20 min, (d) 40 min, (e) 60 min, (f) 120 min, (g) 180 min and (h) 240 min of gastric digestion. 78

Figure 4.7: Centre location of microstructure changes of FSP during simulated *in vitro* gastric digestion. (a) Before digestion (0 min), Samples taken after (b) 10min, (c) 20 min, (d) 40 min, (e) 60 min, (f) 120 min, (g) 180 min and (h) 240 min of gastric digestion. 79

Figure 4.8: Surface location of microstructure changes of FSP during simulated *in vitro* gastric digestion. (a) Before digestion (0 min), Samples taken after (b) 10min, (c) 20 min, (d) 40 min, (e) 60 min, (f) 120 min, (g) 180 min and (h) 240 min of gastric digestion. 80

Figure 4.9: TEM images obtained after 4 hours of static *in vitro* gastric digestion; (a-d) SSP and (e-h) FSP. 81

Figure 4.10: ß-carotene (%) release profiles of the SSP and FSP matrix during simulated gastric digestion. Values are given as averages (n = 3) ± SD of the mean. The prediction of the weibull model (Eq. 4.2) are represented by solid lines. The different

letters within each bar correspond to significance level ($p<0.05$) as determined using multiple comparison of means (Tukey test). 84

Figure 5.1: Characterisation of broken particles into fine debris, fragments and undamaged product based on their relative size to the original one before comminution, according to Drechsler and Ferrua (2016)..... 92

Figure 5.2: Softening curves of the steamed and fried sweet potatoes matrix during *in vitro* gastric digestion based on the hardness (N) measurements. Values are given as averages (n = 3) with error bars as SD (some are too small to be visible). The solid line represents the predicted values from the average weibull model parameters from the three digestion trials (shown in Table 5.1) for 240 min total digestion time. SSP: Steamed sweet potatoes. FSP: Fried sweet potatoes 96

Figure 5.3: Examples illustrating the characterisation of broken SSP particles surface area (0-240 min digestion time) to determine the underlying mechanisms of SSP breakdown during the gastric phase..... 99

Figure 5.4: Examples illustrating the characterisation of broken FSP particles surface area (0-240 min digestion time) to determine the underlying mechanisms of FSP breakdown during the gastric phase..... 100

Figure 5.5: Graphical illustration of the influence of gastric juice soaking time on the cumulative size distribution of particle surface areas of (a) SSP and (b) FSP. Values are given as averages (n=3) with error bars as SD 104

Figure 5.6: Temporal evolution of weight parameter (α) of the mixed weibull function (proportion of small particles within breakdown sweet potatoes samples). Values are given as averages (n = 3) with error bars as SD. The different letters within each bar correspond to significance level ($p<0.05$) as determined using multiple comparison of means (Tukey test). SSP: Steamed sweet potatoes and FSP: Fried sweet potatoes. . 105

Figure 5.7: Graphical illustration of the influence of gastric juice soaking time on the ß-carotene (%) release profiles of the steamed and fried sweet potato matrix. Values are given as averages (n = 3) with error bars as SD. The prediction of the model of the weibull function (Eq. 5.4) are represented by solid lines. 107

Figure 6.1: Schematic representation of the confocal micrographs segmentation procedure 115

Figure 6.2: pH 5 EWG (a) and pH 9 EWG (b) micrographs obtained from the confocal imaging. 120

Figure 6.3: Distribution of particle aggregate sizes (μm) in confocal micrographs of (a) pH 5 EWG and (b) pH 9 EWG. Distribution of inter-particle aggregate distances in confocal micrographs of (c) pH 5 EWG and (b) pH 9 EWG. The average curve (red solid line) of each graph was obtained from 30 individual curves (grey solid lines). 121

Figure 6.4: Representative FRAP profiles and images before bleaching and after 0 and 2.73 s (30th post-bleaching image) for diffusion of (a) FITC-pepsin in water, (b) FITC-dextran in water, (c) FITC-pepsin in pH 5 EWG, (d) FITC-dextran in pH 5 EWG, (e) FITC-pepsin in pH 9 EWG and (f) FITC-dextran in pH 9 EWG. Data points (black colour) denote the normalized experimental data and solid lines (red colour) denote the data curve fit. 123

Figure 6.5: Predicted versus measured values of moisture in (a) pH 5 EWG and (b) pH 9 EWG for the best PLS models (calibration data set), expressing the moisture content as wet basis. The solid line shows the calibration line of the PLS regression model. Performance of the PLS regression model for moisture indicated as the determination coefficients (R^2)..... 128

Figure 6.6: Predicted versus measured values of acid in (a) pH 5 EWG and (b) pH 9 EWG for the best PLS models (calibration data set), expressing the acid content as mg HCl/g of sample. The solid line shows the calibration line of the PLS regression model. Performance of the PLS regression model for acid indicated as determination coefficients (R^2)..... 130

Figure 6.7: Spatiotemporal moisture content distribution maps of (a) pH 5 EWG and (b) pH 9 EWG generated by using the optimal PLS models. 132

Figure 6.8: Spatiotemporal acid content distribution maps of (a) pH 5 EWG and (b) pH 9 EWG generated by using the optimal PLS models. (Note that the colour scale of an individual EWG structure represents a different range of acid (mg HCl/g of sample) content)..... 133

Figure 6.9: Plots of moisture concentration ratio as a function of digestion time (s) for the (a) pH 5 EWG and (b) pH 9 EWG. Circles represent average experimental values (n = 3) and error bars represent the SD of the mean. The prediction of the model of the Fick's second law (Eq. 3.1) and the power-law model (Eq. 3.2) are represented by solid and dashed lines, respectively. 135

Figure 6.10: Plots of acid concentration ratio as a function of digestion time (s) for the (a) pH 5 EWG and (b) pH 9 EWG. Circles represent average experimental values (n = 3) and error bars represent the SD of the mean. The prediction of the model of the Fick's second law (Eq. 3.1) and the power-law model (Eq. 3.2) are represented by solid and dashed lines, respectively. 138

Figure 7.1: Diagram of the IBIDI gel system experimental device for monitoring the *in situ* disintegration of the model EWGs..... 146

Figure 7.2: Typical time-lapse fluorescence imaging of changes of (a) pH 5 EWG and (b) pH 9 EWG microstructure with no SGF or pepsin (control experiment). No change of microstructure and no photo bleaching of the fluorescent dye was occurring with time due to confocal imaging in both (a) pH 5 EWG and (b) pH 9 EWG 151

Figure 7.3: Typical time-lapse fluorescence imaging of changes of (a) pH 5 EWG and (b) pH 9 EWG microstructure during diffusion of SGF at pH 2 (Control experiment). No change of network microstructure and fluorescence intensity was observed in both (a) pH 5 EWG and (b) pH 9 EWG microstructure during diffusion of SGF. 152

Figure 7.4: (a) Typical time-lapse fluorescence imaging of changes of pH 5 EWG microstructure during diffusion of SGF at pH 2 containing 8,000 U/mL of pepsin. (b) Visualisation of changes of corresponding area fraction of pH 5 EWG microstructure during gastric digestion through a heat-map diagram (red = no particle on the confocal image) 153

Figure 7.5: (a) Typical time-lapse fluorescence imaging of changes of pH 9 EWG microstructure during diffusion of SGF at pH 2 containing 8,000 U/mL of pepsin. (b) Visualisation of changes of corresponding area fraction of pH 9 EWG microstructure

during gastric digestion through a heat-map diagram (red = no particle on the confocal image) 154

Figure 7.6: TRITC-dextran emission spectra of (a) pH 9 EWG, and (b) pH 5 EWG at different pH conditions..... 156

Figure 7.7: Percentage of TRITC-dextran release from pH 9 EWG (squares) and pH 5 EWG (circles) over time using either SGF-pepsin solution (filled symbols) or SGF solution without pepsin (open symbols). Values represent averages (n = 3 replicates) with error bars representing the SD. Dashed lines show the model representations of the weibull function applied to the entire TRITC-dextran release profiles..... 157

Figure 8.1: Softening curves of the pH 5 and pH 9 EWGs during *in vitro* gastric digestion based on the hardness (N) measurements. Values are means (n = 3) with error bars as SD. The solid lines represent the predicted values from the average weibull model parameters shown in Table 8.2. 166

Figure 8.2: Examples illustrating the characterisation of broken pH 5 EWG particles surface area (0-240 min digestion time) to determine the underlying mechanisms of pH 5 EWG breakdown during the gastric phase..... 171

Figure 8.3: Examples illustrating the characterisation of broken pH 9 EWG particles surface area (0-240 min digestion time) to determine the underlying mechanisms of pH 9 EWG breakdown during the gastric phase..... 172

Figure 8.4: Cumulative particle surface area distributions for (a) pH 5 and (b) pH 9 EWGs after 10 min HGS, depending on the time of prior gastric juice soaking. Values are given as averages (n = 3) with error bars as SD..... 174

Figure 8.5: Temporal evolution of weight parameter (α) of the mixed weibull function (proportion of small particles within samples) for pH 5 and pH 9 EWG submitted to 10 min HGS after 0 to 240 min prior gastric digestion. Values are given as averages (n = 3) with error bars as SD. Different letters indicate significant difference ($p<0.05$) as determined using multiple comparison of means (Tukey test)..... 176

Figure 9.1: Schematic overview of unravelling the physicochemical process of gastric digestion..... 177

Figure 9.2: Summary of role of starch-based model food structures on the mechanisms of solid food disintegration during *in vitro* gastric digestion..... 183

Figure 9.3: Summary of role of protein-based model food structures on the mechanisms of solid food disintegration during *in vitro* gastric digestion..... 184

List of Abbreviations

ANOVA	Analysis of Variance
AOAC	Association of Official Agricultural Chemists
CLSM	Confocal Laser Scanning Microscopy
D_{eff}	Effective Diffusivity
Dr	Reduced Diffusion Coefficient
EWG	Egg White Gel
FCS	Fluorescence Correlation Spectroscopy
FITC	Fluorescein Isothiocyanate
FRAP	Fluorescence Recovery After Photobleaching
FSP	Fried Sweet Potatoes
HGS	Human Gastric Simulator
HSI	Hyperspectral Imaging
LM	Light Microscopy
LVs	Latent Variables
MRI	Magnetic Resonance Imaging
PLS	Partial Least Squares
R^2	Coefficient of Determination
RMSE	Root Mean Square Error
RMSEC	Root Mean Square Error of Calibration
RMSEP	Root Mean Square Error of Prediction
ROI	Region of Interest
RQ	Research Questions
SD	Standard Deviation
SEM	Scanning Electron Microscopy
SGF	Simulated Gastric Fluid
SSE	Sums of Square Error
SSF	Simulated Salivary Fluid
SSP	Steamed Sweet Potatoes
TEM	Transmission Electron Microscopy
TRITC	Tetramethyl Rhodamine Isothiocyanate

List of Publications

Peer-reviewed paper

Somaratne, G., Ferrua, M. J., Ye, A., Nau, F., Floury, J., Dupont, D. and Singh, J. (2020). Food material properties as determining factors in nutrient release during human gastric digestion: A Review. *Critical Reviews in Food Science and Nutrition,* Accepted.

Somaratne, G., Reis, M. M., Ferrua, M. J., Ye, A., Nau, F., Floury, J., Dupont, D., Singh, R. P. and Singh, J. (2019). Mapping the spatiotemporal distribution of acid and moisture in food structures during gastric juice diffusion using Hyperspectral Imaging. *Journal of Agricultural and Food Chemistry*, 67(33), 9399-9410.

Somaratne, G., Nau, F., Ferrua, M. J., Singh, J., Ye, A., Dupont, D., Singh, R. P. and Floury, J. (2019). Characterisation of egg white gel microstructure and its relationship with pepsin diffusivity. *Food Hydrocolloids*, Accepted. Volume 98, January 2020, 105258.

Somaratne, G., Nau, F., Ferrua, M. J., Singh, J., Ye, A., Dupont, D., Singh, R. P. and Floury, J. (2019). *In situ* disintegration of egg white gels by pepsin and kinetics of nutrient release followed by time-lapse confocal microscopy. *Food Hydrocolloids*, Accepted. Volume 98, January 2020, 105258.

Somaratne, G., Ferrua, M. J., Ye, A., Nau, F., Dupont, D., Singh, R. P. and Singh, J. (2020). Egg white gel structures determines gastric juice diffusion with consequences on softening and mechanical disintegration during *in vitro* gastric digestion. *Food Research International,* Submitted.

Somaratne, G., Ferrua, M. J., Ye, A., Nau, Dupont, D., Singh, R. P. and Singh, J. (2020). Role of biochemical and mechanical disintegration on β-carotene release from steamed and fried sweet potatoes during *in vitro* gastric digestion. *Food Research International*, Submitted.

Conference abstracts and presentations

Somaratne, G. M., Singh, J., Ferrua, M. J., Ye, A., Dupont, D., Nau, F. and Singh, R. P. Role of gastric juice diffusion into steamed and fried orange-fleshed sweet potatoes on the macro- and micro-structural changes and nutrient release during static *in vitro* gastric digestion. NZIFST Annual Conference 2017 – Nelson, New Zealand. 4-6 July 2017 (oral presentation).

Somaratne, G. M., Singh, J., Ferrua, M. J., Ye, A., Dupont, D., Nau, F. and Singh, R. P. Diffusion of gastric juice and release of nutrients in fried and steamed orange-fleshed sweet potatoes during *in vitro* gastric digestion. 7th International Symposium on "Delivery of Functionality in Complex Food Systems", Auckland, New Zealand. 5-8 November 2017 (poster presentation).

Somaratne, G. M., Reis, M. M., Ferrua, M. J., Ye, A., Dupont, D., Nau, F., Floury, Singh, R. P. and Singh, J. Feasibility of using hyperspectral imaging to predict gastric juice diffusion into solid food structures during gastric digestion. 19th IUFoST World Food Congress Food Science & Technology, Mumbai, India. 23-27 October 2018 (poster presentation).

Somaratne, G., Nau, F., Ferrua, M. J., Singh, J., Ye, A., Dupont, D., Singh, R. P. and Floury, J. Mapping the spatiotemporal disintegration and release of nutrient from egg white gel microstructure during *in vitro* gastric digestion. 8th International Symposium on "Delivery of Functionality in Complex Food Systems", Porto, Portugal. 7-10 July 2019 (poster presentation).

Somaratne, G., Nau, F., Ferrua, M. J., Singh, J., Ye, A., Dupont, D., Singh, R. P. and Floury, J. Role of native egg white protein gel microstructure on the diffusion of gastric pepsin. 8th International Symposium on "Delivery of Functionality in Complex Food Systems", Porto, Portugal. 7-10 July 2019 (poster presentation).

Somaratne, G., Ferrua, M. J., Ye, A., Nau, F., Dupont, D., Singh, R. P. and Singh, J. Role of food initial microstructure on the softening kinetics of solid foods during simulated gastric digestion. 5th International Conference on "Food Structures, Digestion & Health", Rotorua, New Zealand. 30th September to 3rd October 2019 (poster presentation).

Somaratne, G., Ferrua, M. J., Ye, A., Nau, F., Dupont, D., Singh, R. P. and Singh, J. Role of gastric juice diffusion on disintegration kinetics of solid foods during *in vitro* gastric digestion. 5th International Conference on "Food Structures, Digestion & Health", Rotorua, New Zealand. 30th September to 3rd October 2019 (poster presentation).

Chapter One

1. Introduction and Thesis Outline

This chapter provides an overview of the background, rationale, research goals and approach of the thesis.

1.1 Research Background and Rationale of the Thesis

After the oral cavity, human stomach is the second major organ where masticated food structures are broken down for further digestion and final absorption in the small intestine (Bornhorst & Singh, 2014; Bornhorst & Singh, 2012; McClements *et al.,* 2008). During gastric digestion, a complex interaction of biochemical and mechanical processes disintegrates food structures into a product called chyme (Kong & Singh, 2010; Singh, Ye, & Ferrua, 2015). Biochemical processes are driven by the diffusion of acid and enzymes (i.e. gastric pepsin and lipase) into food matrix (Mennah-Govela & Bornhorst, 2016a, b; Minekus *et al.,* 2014) while, the mechanical processes are driven by peristalsis contractions of the stomach wall (Kong & Singh, 2008a; Singh *et al.,* 2015). Gastric wall contraction further fractionates the ingested solid particles into little pieces which in terms facilitates the biochemical degradation, by increase the surface area exposed to the gastric environment. Similarly, the biochemical degradation of the food products facilitates its mechanical breakdown (Bornhorst, Kostlan, & Singh, 2013; Kong & Singh, 2010).

Our understanding of the gastric digestion has evolved significantly over the past few decades, with several *in vitro*, *in vivo* and *in silico* gastric digestion models being developed to better understand the phenomena involved (Bornhorst & Singh, 2014; Ferrua & Singh, 2010; Ferrua, Kong, & Singh, 2011; Kong & Singh, 2010; Minekus *et al.,* 2014). However, studying the complex multistage process of human gastric digestion is technically difficult and costly (Bornhorst & Singh, 2014; Kong & Singh, 2008a). Thus, little is still known of the relationship that exists between the initial structure and composition of foods and their disintegration behaviour (Bornhorst & Singh, 2014; Singh *et al.,* 2015). There are even uncertainties about some of the specific mechanisms such as gastric juice diffusion process, nutrient release and particle size reduction process involved during gastric digestion (Drechsler & Ferrua, 2016; Kong & Singh, 2010; Mennah-Govela & Bornhorst, 2016a, b).

The biochemical digestion of foods in the stomach are driven by two simultaneous and counter-current mass transfer mechanisms (Kong & Singh, 2011). On one hand, it involves the diffusion of acid and enzyme from the gastric medium into the

food material, and on the other hand it involves the release of nutrients from the interior of the food structure to the gastric medium (Kong & Singh, 2009a, b; Singh *et al.,* 2015). The rate of which these mass transfer phenomena occur is governed by the dynamic interaction between concentration gradients and material properties of the foods (Singh *et al.,* 2015). Based on optical image analysis techniques using coloured dyes (i.e Methylene blue), it has been shown that the heterogeneity of food structures influence the spatial distribution of gastric fluid within the food matrix (Mennah-Govela, Bornhorst, & Singh, 2015; Kong & Singh, 2011; Van Wey *et al.,* 2014; Widjaja, 2010). However, the major drawback of optical imaging using coloured dyes is the ability to truly represent the diffusion rate of gastric juice due to differences in the size of Methylene blue (molar mass: 319.85 g/mol) and gastric juice constituents (mainly moisture molar mass: 18.06 g/mol and acid molar mass: 36.46 g/mol) (Widjaja, 2010). Alternatively, Kong *et al.* (2013), investigated the spatial and temporal distribution of water in gastric juice and swelling of peanuts during gastric digestion using Magnetic Resonance Imaging (MRI) technique. MRI has a significant advantage because MRI does not require the use of added dyes or labelling methods for visualisation of different chemical components in the gastric fluid (Kong *et al.,* 2013).

Furthermore, some studies have focused on identifying the diffusion coefficients of gastric acid and moisture into different food matrix, including carrots (Kong & Singh, 2011), cooked sweet potatoes (Mennah-Govela & Bornhorst, 2016a, b) and rice (Mennah-Govela *et al.,* 2015). But, due to the lack of sufficiently sensitive measurement techniques, little is known about the relationship that exist between the diffusion rate of gastric juice and the initial structure of the food and the microstructural changes during the biochemical process (Mennah-Govela & Bornhorst, 2016b; Singh *et al.,* 2015). Disruption of natural food microstructure due to biochemical degradation may influence the release, transformation and subsequent absorption of nutrients in the digestive tract (Grassby *et al.,* 2014; Mennah-Govela *et al.,* 2015). Development of a more fundamental understanding of the mechanisms coupling the rate of gastric juice diffusion with the microstructural degradation of foods and subsequent release of nutrients is essential for the design of novel food structures with enhancing functional and nutritional benefits.

Similarly, understanding the solid food breakdown mechanisms is crucial in developing a quantitative understanding of the kinetics of nutrient release during gastric digestion process (Grassby *et al.,* 2014; Kong & Singh, 2008a) and its relationship to the initial composition and structure of the foods. Mathematical models and mechanisms have been proposed to characterise the *in vitro* and *in vivo* breakdown of solid food during gastric digestion (Ferrua & Singh, 2010; Ferrua *et al.,* 2011; Guo *et al.,* 2015; Kong & Singh, 2009b, 2010). Food scientists have shown that, the particle size distribution in

a solid food during gastric digestion can be successfully fitted well to a Weibull distribution and/or a mixed Weibull distribution (Bornhorst *et al.,* 2013; Bornhorst *et al.,* 2014; Drechsler & Ferrua, 2016; Ferrua & Singh, 2010; Guo *et al.,* 2015). However, little is still known on the underlying mechanical mechanism governing the breakdown behaviour of different food structures within the stomach.

Fragmentation and erosion are expected to be the main factor during the breakdown of solid foods during gastric processing (Kong & Singh, 2008b, Kong & Singh, 2009b). The level of fragmentation and/or erosion experienced by foods during digestion can be quantified by changes in the particle size distribution during the process (Bornhorst *et al.,* 2013; Guo *et al.,* 2015). Drechsler and Ferrua, (2016) proposed a possible methodology to determine the relative contribution of erosive and fracture mechanisms to the breakdown behaviour of the solid food. Up to date, little is known of the role of gastric juice absorption and biochemical degradation on the physical breakdown mechanism of solid foods. Furthermore, the establishment of valid correlations between the *in vivo* and *in vitro* behaviour of foods disintegration during digestion remain to be achieved.

All the above, emphasize the necessity for a better characterisation of the mechanisms of solid food disintegration during gastric digestion. To bridge this knowledge gap, by taking an alternative approach to current *in vitro* static and dynamic gastric models, this Doctoral research study uncoupled the role of biochemical and mechanical mechanisms occurring during gastric digestion and thereby expected to develop a more complete picture of the physicochemical process driving the disintegration of solid foods during gastric digestion.

1.2 Overall Goal and Research Questions of the Thesis

Overall Goal: To better understand the mechanisms and the relative role of biochemical and mechanical process, occurring during gastric digestion, on the disintegration behaviour of solid foods of different compositions and structures.

Research Questions (RQs)

RQ 1: How do food composition and structure influence the diffusion of gastric juice in terms of acid, moisture and pepsin diffusion within the food structure, the mechanism of biochemical degradation (acid and enzymatic) and nutrient release?

RQ 2: How do the biochemical degradation (acid and enzymatic) and material properties of foods during digestion influence the rate of softening, subsequent breakdown mechanics, and nutrient release as a result of the mechanical stresses occurring in the stomach?

RQ 3: How do food composition and structure influence the relative role of biochemical and mechanical processes on the disintegration of solid foods during gastric digestion?

1.3 Research Approach

To answer these RQs, this study uncouples the biochemical and mechanical phenomena during gastric digestion, by combining the use of the static *in vitro* digestion and a dynamic human gastric simulator (HGS) to simulate key processes occur during the gastric phase.

Figure 1.1 outlines the brief summary of the experimental design of the thesis. In this study, two different 'natural' solid foods, sweet potatoes and egg white gels (EWGs) were selected as product models for starch and protein rich food, respectively. Each product was processed/cooked in two different ways to achieve different structures. The starch and protein-based model foods cover many of the common compositions and structures of natural and processed solid food and they are expected to cover a wide range of breakdown pathways encountered during gastric digestion. This study excluded liquid foods because they do not need significant physical breakdown during gastric digestion. It can be defined solid foods as it has a definite shape and structure that do not naturally conform to the shape of the container where it is placed. In this study, EWGs was considered as solid foods, despite being a liquid entrapped inside a three-dimensional colloidal polymer network. Details of the selected product models and their preparation as a model food for digestion simulation are as follows.

Product model (1): Orange-fleshed sweet potatoes (*Ipomoea batatas* [L.] Lam) was used to develop the starch-based product model. Sweet potatoes are an extremely important starchy dietary staple of the tropical and subtropical areas in many parts of the world (Van Jaarsveld *et al.,* 2006). It is consumed in a variety of ways including boiled, fried, steamed, and microwave steamed (Tumuhimbise, Namutebi, & Muyonga, 2009; Van Jaarsveld *et al.,* 2006). Thus, steaming and frying cooking methods were selected in this study as thermal treatments that may be used by a typical consumer. The orange-fleshed sweet potato could be considered as an excellent source of β-carotene (Tumuhimbise *et al.,* 2009; Van Jaarsveld *et al.,* 2006). Thus, β-carotene was used as a target nutrient to study its

release during gastric digestion. Throughout this thesis, steamed sweet potatoes and fried sweet potatoes refer to SSP and FSP, respectively.

Product model (2): EWGs were used in this study as a model protein-based food. It is highly used in the food industry as food gels mainly due to their functional and nutritional properties (Nyemb *et al.,* 2016a, b). In the present study, EWGs with two different microstructures but equal protein concentration (10%) were produced by varying the pH conditions (pH 5 and pH 9). Throughout this thesis, the EWGs of pH 5 and pH 9 refers to pH 5 EWG and pH 9 EWG, respectively. Tetramethylrhodamine isothiocyanate (TRITC)-dextran (4.4 kDa) was incorporated into the EWGs as a model fluorescent molecule of peptide-like size, to trace its release due to the pepsin action.

The research questions were completed through six different research chapters. Chapter 3 described how SSP and FSP microstructures impact the diffusion of acid and water during static *in vitro* gastric digestion. Apart from that, this chapter also focused on the feasibility of hyperspectral imaging (HSI), in the range 550–1700 nm, for predicting total acid and moisture distributions in food matrices during *in vitro* gastric juice diffusion process. The main strength of this technique is that it is a label-free technique, which allows studying the diffusion of gastric fluid in different food structures during *in vitro* gastric digestion without using any indicator dye to represent the gastric fluid. Chapter 4 described how SSP and FSP food structures impact the microstructural disintegration by gastric fluid diffusion and subsequent kinetics of β-carotene release during the simulated static gastric environment. Chapter 5 was designed to investigate the role of gastric juice diffusion on the rate of softening and mechanical disintegration of SSP and FSP.

Chapter 6 described how different pH 5 and pH 9 EWG microstructures impact the diffusion of pepsin, acid and water during static *in vitro* gastric digestion. The microstructures of the protein gels were observed using a relatively new high-resolution confocal microscopic technique, followed by image analysis. The effective diffusivity (D_{eff}) of fluorescein isothiocyanate (FITC) labelled-pepsin was measured in the EWGs, using the fluorescence recovery after photobleaching (FRAP) technique. In parallel to chapter 3, chapter 6 also investigated the spatial and temporal distribution of gastric acid and water in pH 5 and pH 9 EWGs using the HSI techniques. Impacts of EWG microstructure on the spatiotemporal disintegration by gastric juice diffusion and kinetics of nutrient release (i.e. TRITC-dextran release) during simulated static gastric environment were investigated in Chapter 7 using a novel time-lapse confocal

microscopy-based methodology. Chapter 8 was designed to investigate the role of gastric juice diffusion on the rate of softening and mechanical disintegration of pH 5 and pH 9 EWG structures.

The final chapter of the thesis mainly discusses the key levers driving the dynamic of gastric digestion, identify existing challenges and recommended future considerations. It discusses the role of initial food material properties on the diffusion of gastric juice (pepsin, acid and moisture) and the subsequent biochemical and mechanical disintegration of foods and the subsequent release of nutrient during simulated digestion. Apart from that, the final chapter of the thesis also identified the existing challenges of uncoupling the physicochemical process of *in vitro* gastric digestion and recommended future perspectives regarding the gastric digestion of solid foods.

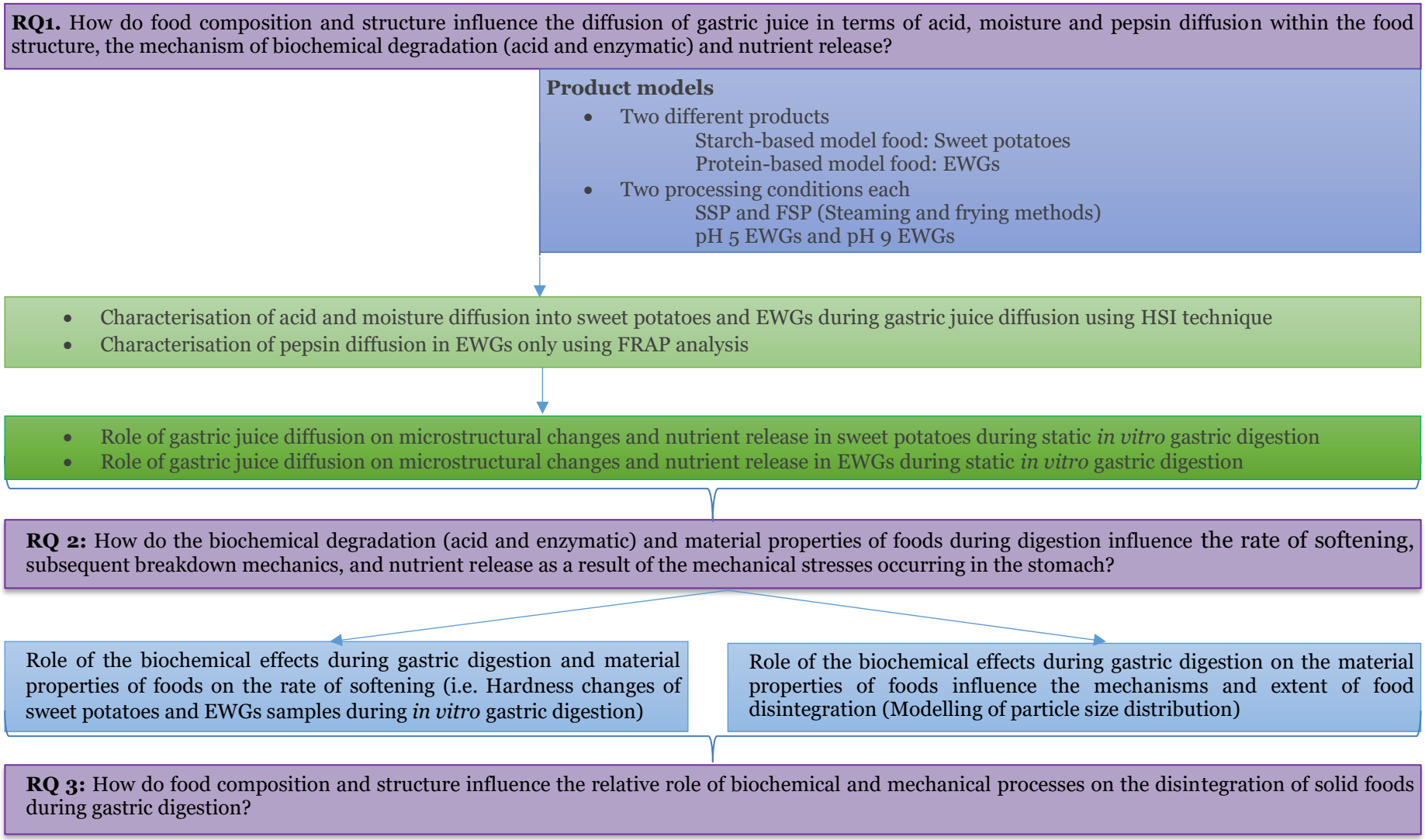

Figure 1.1: Overview of the experimental approach

Chapter Two

2. Food Material Properties as Determining Factors in Nutrient Release during Human Gastric Digestion: Literature Review*

2.1 Abstract

The fundamental mechanisms of nutrient release from solid foods during gastric digestion consist of multiple elementary processes. These include the diffusion of gastric juice into the food matrix and its simultaneous enzymatic degradation and mechanical breakdown by the peristaltic activity of the stomach. Understanding the relative role of these key processes, in association with the composition and structure of foods, is of paramount importance for the design and manufacture of novel foods possessing specific target behaviour within the body. This literature review section covers the past and current literature with respect to the in-stomach processes leading to the biochemical and physical disintegration of solid foods and the release of nutrients. This literature review section outlines recent progress in experimental and modelling methods used for studying food disintegration mechanisms and concludes with a discussion on potential future research directions in this field. Information from pharmaceutical science-based modeling approaches describing nutrient release kinetics as a result of food disintegration in the gastric environment is also reviewed. Future research aimed at understanding the disintegration of foods in the stomach may lead to the development of novel foods that are nutritious, healthy, and satisfy consumer demand.

*Chapter two has published as a peer-reviews paper: Somaratne, G., Ferrua, M. J., Ye, A., Nau, F., Floury, J., Dupont, D. and Singh, J. (2020). Food material properties as determining factors in nutrient release during human gastric digestion: A Review. *Critical Reviews in Food Science and Nutrition*. Accepted.

2.2 Introduction

The digestion of food is a complex phenomenon essential for sustaining the health and well-being of humans, in which nutrients are extracted from the ingested food matrix through enzymatic, chemical and mechanical transformations (Kong and Singh 2008a; Singh *et al.,* 2015). The digestive system consists of the long hollow muscular gastrointestinal tube starting from the oral cavity and ending at the anus (Bornhorst & Singh, 2014). The mode of nutrient release during digestion is greatly influenced by initial food material properties and how they change when exposed to the physicochemical environment of the digestive tract (Floury *et al.,* 2018; Mishra, Hardacre, & Monro, 2012; Nyemb *et al.* 2016a, b).

The mouth and stomach are mainly responsible for food disintegration, while the final stages of digestion and nutrient absorption occur in the small intestine (Bornhorst & Singh, 2014). Initial physicochemical transformation of food matrices begins in the oral cavity during mastication (Gray-Stuart, 2016). During this process, ingested solid and semi-solid foods are broken down into small particles (De-Wijk, Janssen, & Prinz, 2011). During mastication, the biochemical disintegration of foods is initiated as a result of the action of salivary enzymes. Saliva plays a key role in the formation of a bolus that is easily swallowed and transferred from the mouth to the stomach via the oesophagus (Foegeding *et al.,* 2011).

The stomach is the second major compartment where food particles are disintegrated (Kong & Singh, 2008a, b). Therefore, the stomach plays a crucial role in nutrient release mechanisms and the process of chyme formation for subsequent nutrient absorption in the small intestine (Hyslop, 1980; Kong & Singh, 2008b). From an engineering point of view, the gastric digestion process can be considered as a series of unit operations including mixing, grinding, diffusing, sieving and pumping (Bornhorst *et al.,* 2016; Urbain *et al.,* 1989). If the steps of food gastric digestion are considered in isolation as a set of unit operations, then a simple diagram can be drawn as shown in Figure 2.1. When the food bolus enters the stomach, gastric juice is secreted, resulting in acid and enzymatic hydrolysis of the food. Then the gastric juice diffusion, combined with the hydrodynamic physical breakdown of food particles, govern the nutrient release from food matrices (Kong & Singh 2009a, b; Van Wey *et al.,* 2014). Gastric juice is responsible for heat and mass transport between the food matrix and the surrounding gastric environment. The mass transport phenomenon depends mainly on the composition of the gastric juice content, and on the structure and composition of the food system (Mennah-Govela & Bornhorst, 2016a, b).

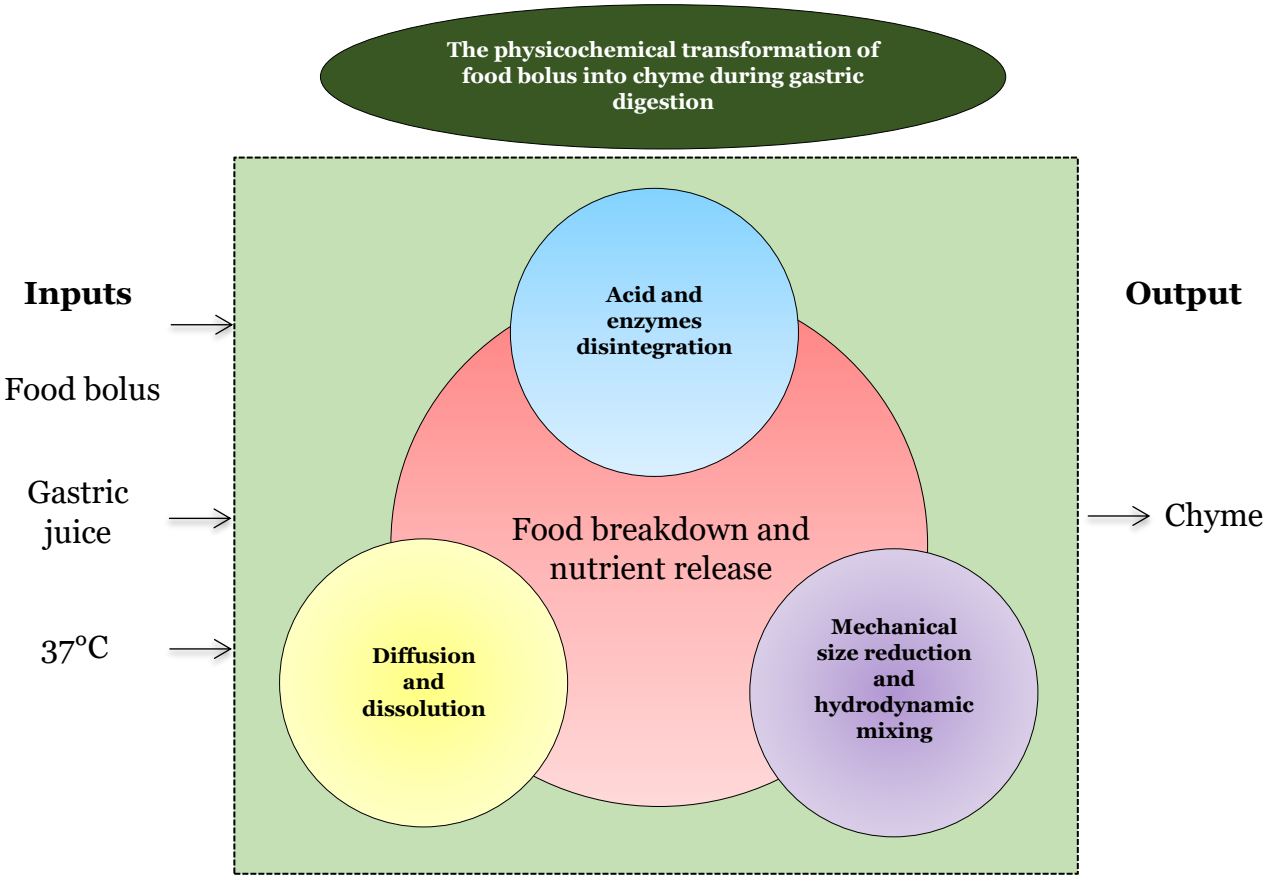

Figure 2.1: The physicochemical processes of food disintegration showing how the food bolus simultaneously undergoes breakdown and nutrient release inside the stomach

Understanding the mechanisms and identifying the key parameters that govern nutrient release from food within the stomach are one of the major steps toward accurately predicting the nutrient bioavailability profile. Thus, the solid food disintegration during gastric digestion has been extensively investigated in the past few decades by researchers and industry in multiple fields such as medicine, food science, nutrition, pharmacology and microbiology (Bornhorst & Singh, 2014). To address this issue, several *in vitro* and *in vivo* digestion models were developed to mimic the physicochemical modifications that occur during gastric digestion (Guerra *et al.,* 2012). However, information about solid food disintegration behaviour during gastric digestion remains unclear because studying this complex multistage process is technically difficult and costly. There are even uncertainties about some of the specific mechanisms involved during gastric digestion, such as gastric juice diffusion, nutrient release and particle size reduction process (Drechsler & Ferrua, 2016; Guerra *et al.,* 2012).

The aim of this chapter is to gather the most recent scientific information about the disintegration of solid foods during gastric digestion, in order to identify any gaps/limitations in current knowledge. In particular, how the gastric juice and mechanical contraction forces contribute to the gastric food disintegration process is reviewed. Solid food disintegration is described as a series of sub processes from the diffusion of gastric juice into the food matrix, biochemical degradation and physical breakdown of the food matrix, to the final nutrient release. These different processes are affected by multiple complex factors such as the structural and compositional characteristics of the food matrix, the physicochemical properties of the nutrients, gastric environment, and the possible interactions between these factors (Flores & Kong, 2017; Singh *et al.,* 2015). These main factors are summarised in Figure 2.2 and extensively discussed below. This review will focus only on solid and semi-solid foods, not on liquid foods because they do not need significant physical breakdown during gastric digestion.

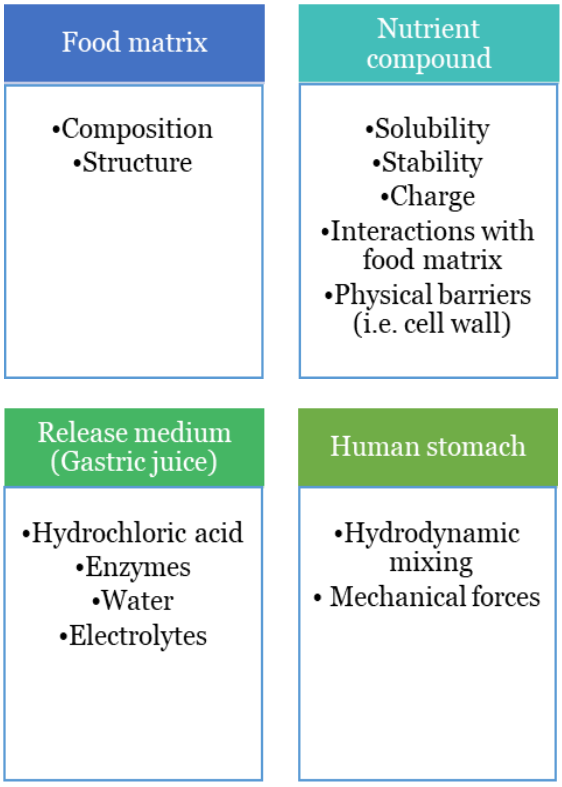

Figure 2.2: Main factors influencing nutrient release kinetics during gastric digestion

2.3 Functional Anatomy of the Human Stomach and Gastric Secretion

The human stomach is located on the left side of the upper abdomen cavity and positioned between the end of the oesophagus and the beginning of the small intestine (Deshpande *et al.*, 1996). As shown in Figure 2.3, it is a "J" shaped expanded muscular bag-like structure with three major compartments including the fundus, the body, and the pylorus (Ferrua & Singh, 2010). The dome-shaped area of the upper curvature of the stomach is known as the fundus (Hellstrom, Gryback, & Jacobsson, 2006; Schulze, 2006). The body is the largest portion of the three sections of the stomach (Deshpande *et al.*, 1996; Hellstrom *et al.,* 2006; Schulze, 2006). The pylorus is the lower section of the stomach that is subdivided into two parts, known as the antrum and the pyloric canal (Bornhorst & Singh, 2012; Schulze, 2006). The antrum, which is shaped like a tapered tube, is where the food is exposed to physiological shear stresses and grinding forces (Deshpande *et al.*, 1996; Kong & Singh, 2010). The pyloric canal is located at the end of the stomach and connects to the duodenum, acting as a sieve and pump (Bornhorst *et al.,* 2016; Bornhorst & Singh, 2012; Deshpande *et al.,* 1996). It facilitates emptying of the gastric digesta into the small intestine for further digestion and nutrient absorption (Bornhorst *et al.,* 2016; Kelly, 1980).

The stomach can again subdivide into 2 regions known as the proximal and the distal regions (Bornhorst & Singh, 2012; Kelly, 1980). The proximal region represents the fundus and about one-third of the stomach body. This region mainly regulates the gastric emptying of liquids and stores partially digested food materials received from the oesophagus (Urbain *et al.,* 1989). The remaining two-thirds of the stomach body, the antrum and the pylorus, represent the distal region (Bornhorst & Singh, 2012; Kelly, 1980). This region can be considered as a mixer, grinder, sieve and pump which serves to reduce solid particle size so that they can pass through the pyloric sphincter into the small intestine (Kelly, 1980; Schulze, 2006; Urbain *et al.,* 1989).

The stomach has two sphincters and two curvatures (greater and lesser curvatures) (Bornhorst & Singh, 2012; Schulze, 2006). The lower oesophageal sphincter, which is located at the junction of the oesophagus and stomach, releases the bolus into the stomach and prevents gastro-oesophageal reflux (Castell *et al.,* 2004). The pyloric sphincter, which is located at the junction of the stomach and the duodenum, controls the release of gastric chyme at a controlled rate from the stomach into the duodenum for the absorption process (Deshpande *et al.*, 1996).

The human gastric wall is lined with mucosa, sub-mucosa, muscularis propria and serosa (Montgomery, Mulberg, & Grand, 1999; Tortora & Derrickson, 2008; Treuting, Dintzis, & Montine, 2017). The interior surface of the gastric wall is rough, with

thick and longitudinally oriented folds to increase the surface area (Tortora & Derrickson, 2008; Treuting *et al.,* 2017). Specialized epithelial cells secrete the different compounds that make up the gastric juice. The gastric juice is the main physiological secretion of the human stomach and plays an important role in the overall digestion process (Bornhorst & Singh, 2012). Hydrochloric acid and intrinsic factor are secreted by the parietal cells, which are mainly found in the fundus of the stomach (Allen & Flemström, 2005; Bornhorst & Singh, 2012; Hunt *et al.,* 2015). Intrinsic factor plays a dominant role in the absorption of vitamin B12 in the gastrointestinal tract (Pavelka & Roth, 2010). Chief cells and neck cells are typically found in the distal region of the stomach. Chief cells are mainly responsible for the synthesis of pepsinogen, the proenzyme for pepsin, and gastric lipase, whereas neck cells secrete the mucus (Hunt *et al.,* 2015; Montgomery *et al.,* 1999). Mucus acts as a physical barrier to protect the stomach cell wall from gastric acid (Allen & Garner, 1980). Gastric juice also contains various electrolytes such as sodium, potassium, calcium, magnesium, bicarbonate and phosphate (Flores & Kong, 2017; Singh *et al.,* 2015). Bicarbonate is synthesized by specialized cells in the lining of the stomach in order to neutralize HCl, thereby protecting the cell lining of the stomach (Allen & Flemström, 2005; Allen & Garner, 1980). Low concentrations of bile acids and phospholipids are also found in gastric juice (Minekus *et al.,* 2014). The characteristic temperature of gastric juice is 37°C, which is the optimum temperature for the optimum function of gastric enzymes (Minekus *et al.,* 2014).

Gastric juice is an acidic secretion ranging between pH 2 to pH 3 (Lu *et al.,* 2010). The average intra-gastric fasting or resting pH in the stomach of healthy humans is around pH 2, which is controlled by hydrochloric acid. When the food bolus is ingested into the stomach, the intragastric pH can increase due to the buffering effect of the ingested food and then returns to baseline due to secretion of gastric acid from the gastric wall (Bornhorst & Singh, 2014; Malagelada, Go, & Summerskill, 1979).

In normal healthy individuals, the stomach can secrete 2 to 3 litres of gastric juice daily (Kong & Singh, 2008a). However, the production of gastric juice, and its composition depends on many factors and shows high inter- and intra-individual variation (Bornhorst, 2017). The fasting or ingesting conditions, and the consistency of the ingested food decide the total volume of gastric secretion (Marciani *et al.,* 2001). For example, a larger amount of gastric juice is secreted for a solid meal compared to a liquid meal (Moore *et al.,* 1984).

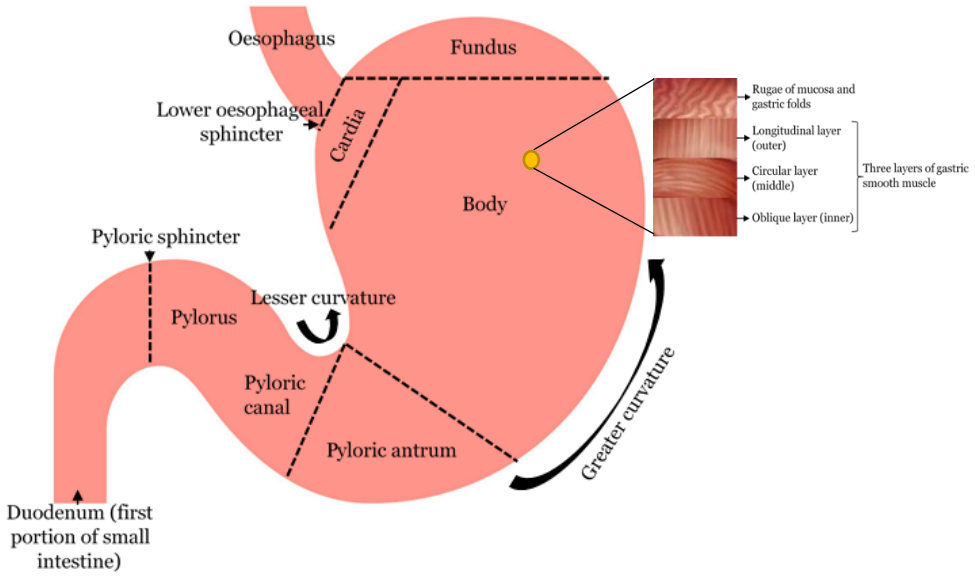

Figure 2.3: Structural arrangement of the human stomach

2.4 Experimental Approaches to Evaluate Gastric Digestion

In vivo animal trials or, better yet, human clinical trials are considered the "gold standard" for addressing digestion-related research studies (Yao, Gibson, & Shepherd, 2013). Although these *in vivo* studies provide the most accurate representation of the complexity of the digestion process, they are associated with several practical and logistical constraints including; high cost, ethical issues and length of time (Ulleberg *et al.,* 2011). As a result, *in vitro* laboratory-scale digestion models are increasingly used as an alternative to *in vivo* digestion methods. These models are relatively quick, less labour intensive, lower cost and do not have ethical constraints compared to *in vivo* studies (Bornhorst & Singh, 2014).

Available *in vitro* gastric digestion systems can be further sub-divided into two categories, static models and dynamic models, and these have been applied in many foods, nutrition and health studies (Kong & Singh, 2010; Minekus *et al.,* 2014). Previous reviews by Bornhorst and Singh (2014) and Kong and Singh (2008a), extensively describe the important aspects of static and dynamic gastric digestion models. Recently, two reviews underlined the correlations observed between *in vivo* and *in vitro* data obtained with static (Bohn *et al.*, 2018) and dynamic (Dupont *et al.*, 2018) digestion models and emphasized what could be predicted by these models. Thus, a brief overview of *in vitro* static and dynamic gastric digestion models and their advantages, as well as limitations are summarised in Table 2.1.

Table 2.1: Summary of *in vitro* static and dynamic gastric digestion models

	Static *in vitro* gastric digestion models	Dynamic *in vitro* gastric digestion models
Brief description	• Most simple and common *in vitro* gastric digestion model which can be performed in a simple water bath or a bioreactor • Foods are mixed with a simulated digestion fluid and incubated at 37◦C with or without agitation	• Prototypes of simulated dynamic gastric digestion models were introduced by several previous studies that can simulate pH kinetics, continued inflow of digestive enzymes, chyme mixing and gastric emptying
Examples	• Single static bioreactors (Guerra *et al.,* 2012) • Water bath incubation models (Mennah-Govela & Bornhorst, 2016a, b) • INFOGEST standardised digestion method (Minekus *et al.,* 2014)	• The TNO Gastro-Intestinal Model (TIM) of the TNO Nutrition and Food Research Centre - (Minekus, 2015) • Human gastric simulator (HGS) - (Kong & Singh, 2010) • Gastric Digestion Simulator - (Kozu *et al.,* 2014) • Dynamic gastric model of the Institute of Food Research (IFR) - (Thuenemann *et al.,* 2015) • Special gastric simulation models developed using texture analyser - (Chen *et al.,* 2011) • Computer-aided model to simulate the motility pattern of the stomach and to characterise the fluid–mechanical forces (Ferrua *et al.,* 2011; Ferrua & Singh, 2010; Kozu *et al.,* 2010)

Advantages	• Suitable for large pre-screening approaches, • Simulate the biochemical breakdown, • Allows identification and quantification of the nutrient release and • Less tedious and less costly (Bornhorst & Singh, 2014; Guerra *et al.,* 2012)	• Simulate the change of physicochemical and enzymatic conditions along the gastric digestion, as well as the mechanical processes and • Important to identify the influence of dynamic stomach environment on nutrient bio-accessibility (Bornhorst & Singh, 2014; Guerra *et al.,* 2012)
Limitations	• Not representing the mechanical forces (peristaltic movements) and gastric emptying and • Difficult to simulate pH changes and secretion of gastric juice mechanisms (Bornhorst & Singh, 2014; Guerra *et al.,* 2012)	• More complex and expensive compared to static *in vitro* methods and • Impossible to simulate hormonal and nervous control (Bornhorst & Singh, 2014; Kong & Singh, 2010)

Although these *in vitro* systems may be suitable for a wide range of foods, none of these systems can completely represent complex human gastric digestion which involves the actions of different accessory organs, hormones and mechanical processes (Kong & Singh, 2010). Thus, future research and technological innovations are still required to further improve *in vitro* models to incorporate more precisely the gastric emptying process, hormone and nervous control and complexity of peristaltic contractions, as well as to simulate the gastric environment of specific populations such as the infants or the elderly. In addition, these models also require systematic validation with *in vivo* data prior to widespread use.

2.5 Role of Food Material Properties on the Gastric Digestion Process

2.5.1 The Chemical Nature of Food Matrix Determines the Biochemical Disintegration

The biochemical breakdown of foods occurs due to hydrochloric acid and enzymes found in the gastric juice (Bornhorst & Singh, 2012; Kong & Singh, 2011). During the biochemical process of digestion, the stomach mainly acts as a small-scale bioreactor filled with gastric juice (Bornhorst *et al.,* 2016). Due to the complex nature of these biochemical reactions, the overall mechanism of acid and enzymatic degradation of the food is not fully understood (Floury *et al.,* 2018).

The main proteolytic enzyme found in gastric juice is pepsin, which breaks down proteins into peptides in the acidic environment of the stomach (Minekus *et al.,* 2014; Singh *et al.,* 2015). Pepsin activity (approximately 2000 U/mL) is high in the gastric compartment and the pepsin secretion increases with digestion time from 0.26 (30 min of gastric digestion) to 0.58 mg/mL (180 min of gastric digestion) (Minekus *et al.,* 2014). The hydrochloric acid found in the gastric juice plays a key role by activating the proenzyme, pepsinogen, into its active form, pepsin, and unravelling ingested proteins so that gastric enzymes can easily attack their protein substrates (Singh *et al.,* 2015). Pepsin digests dietary protein into peptides in the stomach after which, the chyme (partially digested food) enters the small intestine for further digestion by pancreatic protease enzymes (Kong & Singh, 2008a). One more enzyme found in gastric juice is gastric lipase, which breaks down lipids (Capuano, 2017). However, the activity of gastric lipase is remarkably low in the human stomach (10–120 U/mL), consequently very little ingested lipid is hydrolyzed by gastric lipase by the time the food leaves the stomach (Sams *et al.,* 2016; Singh & Gallier, 2014). The digestion of lipids in chyme is mainly carried out by pancreatic lipase (Bornhorst & Singh, 2012; Minekus *et al.,* 2014). The

hydrochloric acid referred to above also aids gastric digestion by creating the optimal pH for pepsin (pH 1-2) and gastric lipase (pH 4-5.4) (Minekus *et al.,* 2014; Sams *et al.,* 2016).

As described earlier, gastric acid assists in denaturation of digested food and degradation of the food structures (Kong & Singh, 2009b; Mennah-Govela & Bornhorst, 2016b). Moreover, gastric acid plays a significant role in the breakdown of the cell wall structure of plant-based foods to a varying extent (Bornhorst, Ferrua, & Singh, 2015). Previous studies have provided evidence that, diffusion of gastric acid may be capable of disintegrating the pectin in the cell walls, thus reducing their cohesiveness and increasing the intercellular spaces of the cell wall matrix of plant-based food, mainly within the surface of the food matrix (Kong & Singh, 2009a; Mennah-Govela & Bornhorst, 2016a; Widjaja, 2010). However, the mechanism for pectin solubilisation of the plant cell walls during digestion is not clear (Diaz, Anthon, & Barrett, 2007). Acid hydrolysis of glycosidic linkages within pectin strands in the gastric environment may also contribute to cell-cell separation (Garna *et al.,* 2006; Kong & Singh, 2009a; Mennah-Govela & Bornhorst, 2016a, b). The displacement of Ca^{2+} cross-links by H^{+} or solubilisation of calcium ions in the middle lamella in the gastric medium also destabilize pectin (Garna *et al.,* 2006; Krall & McFeeters, 1998).

It is believed that gastric juice does not contribute significantly to the digestion of starch-based foods, because the activity of salivary amylase is inhibited by the low pH of the gastric acid (Bornhorst, Singh, & Heldman, 2011; Bornhorst & Singh, 2012; Pedersen *et al.,* 2002). However, enzymatic digestion of starch may take place in the stomach before hydrochloric acid diffuses inside the food matrix to inactivate the salivary α-amylase (Bornhorst & Singh, 2012; Capuano, 2017; Fried, Abramson, & Meyer, 1987).

2.5.2 Food Structure Regulates the Food Transit in the Gastrointestinal Tract

In order to show that food structure affects the transit of food in the different compartments of the gastrointestinal tract, six dairy matrices of identical composition but different structures were given to six multi-cannulated and catheterized mini pigs. The 6 matrices did not contain fat and were raw milk, heat treated milk (10 min at 90°C), an acid gel obtained by coagulating the heat-treated milk with glucono-delta lactone, a stirred acid gel made of heated milk and 2 rennet gels designed with raw or heat-treated milk (Barbé *et al.,* 2013). Gastric emptying half-time was shown to be dramatically impacted by the food structure even if all the six samples were perfectly isoenergetic (Le Feunteun *et al.,* 2014). Determination of the kinetics of milk protein digestion and amino acid absorption after the ingestion in either liquid or gel form (acid and rennet gels) showed that the gelation of milk slowed down the outflow of the meal from the stomach,

slowed down the subsequent absorption of amino acids, and subsequently decreased their bioavailability in peripheral blood (Barbé *et al.,* 2014). The nature of the matrix seemed to affect the release of the gastrointestinal hormones involved in appetite regulation, with the gel matrices appearing to be potentially more satiating. It was also shown that two gels with the same composition and similar rheological and structural properties but differ in their mode of coagulation (acidification/renneting), exhibited different behaviors during digestion. Indeed, ingestion of the rennet gel resulted in lower levels of both proteins in the duodenum and lower levels of amino acids in the plasma, compared with ingestion of the acid gel. This was due to the formation of a coagulum with high stiffness after ingestion of the rennet gel, under the simultaneous action of the stomach acidity and the rennet, leading to very long retention of the rennet matrix in the stomach (Barbé *et al.,* 2014). The plasma cholecystokinin and ghrelin concentrations suggested a potentially more satiating effect of the rennet gel compared to the acid gel.

2.5.3 Food Structure Determines Mass Transfer Process during Gastric Juice Diffusion

Gastric juice diffusion into the food matrix is responsible for mass transport between the food matrix and the gastric juice. This mass transfer phenomenon depends mainly on the composition of the gastric juice and the structure and composition of the food matrix (Kong & Singh, 2011; Kong *et al.,* 2011, 2013). As described earlier, gastric juice is mainly comprised of water, acid, electrolytes and enzymes (Flores & Kong, 2017). This section reviews the influence of food material properties on the electrolytes, acid and water migration into the solid food matrix during gastric digestion.

The diffusion of gastric juice occurs mainly as water and acid diffusion into the food matrix due to water and acid concentration gradients, respectively (Mennah-Govela & Bornhorst, 2016b). In addition to that, there is a net movement of electrolyte ions such as Cl^-, HCO_3^- and Na^+ etc. from the gastric juice into the food matrix if their concentration is higher in the gastric juice than in the food (Singh *et al.,* 2015). Electrolytes in the gastric juice mainly contribute to buffering action during gastric digestion (Minekus *et al.,* 2014). During diffusion, gastric juice penetrates from the external surface and gradually transfers towards the centre of the food bolus resulting in hydration of the food matrix and biochemical digestion, which degrades the structural integrity of the food micro- and macro-structure, thus improving the disintegration rate (Kong & Singh, 2009a, 2009b; Mennah-Govela & Bornhorst, 2016a). In addition, based on the initial temperature of ingested food, heat transfer occurs until food and gastric juice temperature has reached thermal equilibrium of 37 °C, which is the optimum temperature for pepsin activity (Kong & Singh, 2009b).

As shown in Table 2.2 and 2.3, many previous attempts to model gastric juice diffusion into different food matrices have shown that, as theoretical support, Fick's second law of diffusion can be applied successfully (Mennah-Govela & Bornhorst, 2016b; Mennah-Govela *et al.,* 2015; Widjaja, 2010). In contrast, Van Wey *et al.* (2014), applied a nonlinear regression model to examine the D_{eff} of gastric juice using raw carrots and Edam cheese as product models. These studies mainly used conventional and gravimetric methods (mass uptake and acid determination using potentiometric titrations) to determine the gastric juice diffusion process (Mennah-Govela & Bornhorst, 2016a, b; Mennah-Govela *et al.,* 2015). Unfortunately, these techniques can generate very little information about temporal changes of gastric juice distribution within the food matrix.

Table 2.2: D_{eff} of water in different solid food matrices

Food structure	D_{eff} (10^{-10} m^2/s)	Reference
Raw frankfurters	26.6	(Ozvural & Bornhorst, 2018)
Frankfurters boiled for 3 min	15.1	
Frankfurters boiled for 6 min	25.6	
Frankfurters boiled for 9 min	15.8	
Frankfurters boiled for 12 min	5.52	
Frankfurters boiled for 15 min	18.8	
Frankfurters fried for 3 min	13.8	
Frankfurters fried for 6 min	16.4	
Frankfurters fried for 9 min	8.26	
Boiled sweet potatoes	10.0	(Mennah-Govela & Bornhorst, 2016b)
Steamed sweet potatoes	21.0	
Microwave steamed sweet potatoes	1.0	
Fried sweet potatoes	2.0	
Mild boiled sweet potatoes	3.52	(Mennah-Govela & Bornhorst, 2016a)
Severely boiled sweet potatoes	3.81	
Mild steamed sweet potatoes	7.85	
Severely steamed sweet potatoes	5.94	

Note: D_{eff}: Effective Diffusivity. All of the studies used similar static *in vitro* gastric digestion methodology at pH 1.8. Water diffusion was measured by the Association of Official Agricultural Chemists (AOAC) oven drying method. Fick's second law was used to estimate the D_{eff} of water within almost all the product models.

Table 2.3: D_{eff} of acid in different solid food matrices

Food structure	D_{eff} (10^{-10} m^2/s)	Reference
White medium grain rice	95.0	(Mennah-Govela *et al.,* 2015)
White long grain rice	187.0	
Brown medium grain rice	373.0	
Brown long grain rice	240.0	
Boiled potatoes	10.3	(Widjaja, 2010)
Boiled sweet potatoes	0.09	(Mennah-Govela & Bornhorst, 2016b)
Steamed sweet potatoes	0.13	
Microwave steamed sweet potatoes	0.09	
Fried sweet potatoes	0.16	
Mild boiled sweet potatoes	5.9	(Mennah-Govela & Bornhorst, 2016a)
Severely boiled sweet potatoes	11.4	
Mild steamed sweet	0.03	
Severely steamed sweet potatoes	2.92	

Note: D_{eff}: Effective Diffusivity. All of the studies used similar static *in vitro* gastric digestion methodology at pH 1.8. Acid diffusion was measured via potentiometric titration, except boiled potatoes for which Widjaja, (2010) used methylene blue dye indicator. Fick's second law was used to estimate the D_{eff} of acid within almost all the product models.

Due to the heterogeneous nature of the food matrix, it is important to explore the spatiotemporal distribution of gastric juice within different solid foods to gain better insight about gastric digestion. Direct and indirect imaging techniques have been identified as promising methods for studying the diffusion of gastric fluids into food structure (Kong *et al.,* 2011, 2013; Van Wey *et al.,* 2014). Indirect imaging methods were developed using methylene blue-like dyes to represent the gastric juice diffusion (Van Wey *et al.,* 2014; Widjaja 2010), but its applicability to truly represent the gastric acid concentration is still questionable. More sophisticated methods using MRI, attenuated total reflection-Fourier transform infrared (ATR-FTIR) imaging, or HSI enables the study of the direct spatiotemporal diffusion of gastric fluids into food microstructure without using any indicator dyes (Pu & Sun, 2015; Punčochová *et al.,* 2015; Richardson *et al.,* 2005; Zhu *et al.,* 2016).

Net solid transfer from the food into gastric juice is governed predominantly by the internal resistance within the food matrix rather than external resistance (Widjaja, 2010). Thus, the rate of gastric juice diffusion is largely determined by the physical

properties of foods such as food composition, textural and microstructural properties and eventual physical barriers (i.e. such as cell wall and rice bran layer etc.) (Bornhorst *et al.,* 2011; Mennah-Govela & Bornhorst, 2016b; Parada & Aguilera, 2007).

As shown in Table 2.2 and 2.3, the D_{eff} of water and acid differ in solid foods with different structures. Previous literature supported that different food processing methods such as heating, roasting, grinding and/or fermentation may affect the diffusion of acid and water within the food matrix during gastric digestion (Kong *et al.,* 2013; Kong & Singh, 2009a). As examples, boiling and frying processes influence the structural properties of beef frankfurters and may lead to the lower estimated D_{eff} of water into the boiled and fried samples compared to that of the raw frankfurter (Ozvural & Bornhorst, 2018). Interestingly, Mennah-Govela and Bornhorst (2016a, b), reported that acid diffusivity during *in vitro* digestion differs from water diffusivity and highlights that both diffusion parameters should be estimated separately. These studies also revealed that the cooking method affected the rate of gastric acid and water diffusion into sweet potato during simulated gastric digestion. Kong *et al.* (2013), demonstrated faster diffusion of water in gastric juice into fried peanuts, followed by roasted, boiled, and raw peanuts using MRI; these apparent differences were attributed to the difference in structural properties of the different peanut products. For instance, during the roasting and frying process, intercellular and intracellular porous channels are created inside the food matrix, which is vital for the penetration of gastric juice that may assist effective gastric digestion (Kong & Singh, 2009a). Moreover, Kong *et al.* (2011), further revealed that the bran layer on brown rice inhibited the absorption of water and acid during gastric digestion using MRI. Similarly, Mennah-Govela *et al.* (2015), reported that acid diffusion into rice boluses is influenced by rice type, variety, and the presence of α-amylase. Using time-lapse synchrotron deep-UV microscopy methodology, Floury *et al.* (2018), reported that, compared to acid dairy gels, rennet gels form compact protein aggregates due to acid diffusion from the simulated gastric juice and consequently, the kinetics of proteolysis were much slower for the rennet gel as a result of reduced pepsin accessibility to its substrate.

2.5.4 Food Microstructure is One of the Determining Factors for Gastric Enzyme Diffusion and Activity

Underpinning knowledge of the diffusion of gastric juice into solid food matrices has mainly focused on acid and water diffusion (Mennah-Govela & Bornhorst, 2016a; Van Wey *et al.,* 2014), while there are limited research findings available for gastric enzyme diffusion. However, studying enzyme diffusion is important because it informs about how the gastric enzymes, including pepsin and lipase, interact with the food

components and contribute to the delivery of nutrients (Nyemb *et al.,* 2016a; Singh *et al,* 2015). The most promising approaches for quantitative analysis of the gastric enzymes' mobility are Fluorescence Recovery After Photo-bleaching (FRAP) and Fluorescence Correlation Spectroscopy (FCS) (Luo *et al.,* 2017; Thévenot *et al.,* 2017).

Thévenot *et al.* (2017), successfully investigated the diffusion coefficient of pepsin in the native microstructure of dairy gel models using the FRAP method. In this study, pepsin was tagged with FITC before incorporation into the rennet gels. The FRAP method consists of a bleaching phase of FITC-pepsin obtained by exposing the region of interest (ROI) to a high-intensity laser ray under confocal laser scanning microscopy (CLSM) guidance, followed by a recovery phase monitored with a low-intensity laser ray. The recovery of fluorescence results from the diffusion of unbleached FITC-pepsin molecules toward the ROI and bleached molecules out of the ROI. The increment in mean FITC-pepsin fluorescence intensity after photobleaching was then monitored over time. By assuming that the recovery of the fluorescence profile occurs by diffusion that is consistent with Fick's second law, the D_{eff} of FITC-pepsin can be determined (Thévenot *et al.,* 2017). Luo *et al.* (2017), used FCS to determine the diffusivity of pepsin in whey protein gel matrices and its effect on digestion. FCS involves the quantification of the fluctuation of fluorescently labelled pepsin (i.e. Alexa Fluor® 633- Pepsin) followed by autocorrelation analysis to determine the D_{eff} of the pepsin fluorophore (Luo *et al.,* 2017).

The major drawback associated with both FRAP and FCS techniques is the labeling reaction inactivates the pepsin because it takes place at a denaturing pH for the protein (Thévenot *et al.,* 2017; Luo *et al.,* 2017). Moreover, these analyses were carried out at neutral pH, where pepsin has no activity. Thus, it was difficult, in both studies, to get information about how pepsin diffusion was affected by the structural breakdown of the food matrix due to biochemical disintegration, which occurs *in vivo*.

However, as shown in Figure 2.4, it is interesting to note that these techniques were able to demonstrate that the diffusion of pepsin differs in semi-solid foods with different structures. Luo *et al.* (2017) and Thévenot *et al.* (2017), found that the steric hindrance in the food structure resulted in slower rate of pepsin diffusion compared with pepsin diffusion in water (Tyn & Gusek, 1990). Thévenot *et al.* (2017), further highlighted that the increase of casein concentration of rennet gels from 32.5 to 130 g/kg resulted in the simultaneous decrease of pore sizes and increase of tortuosity, which reduced the diffusion of FITC-pepsin by a factor 2.4. Moreover, Luo *et al.* (2017), reported that the network of the 20 wt% whey protein gel had a smaller pore size than the 15 wt% whey protein gel network, in agreement with the lower diffusion rates of Alexa Fluor® 633-Pepsin in the 20 wt% whey protein gel. Thus, as shown in both studies, protein gels with

higher protein fraction have greater hindrance on the pepsin mobility (Luo *et al.,* 2017; Thévenot *et al.,* 2017).

It is important to note that the food structure and/or composition might not be the only explanation for the different rates of pepsin diffusion. Other factors, such as the enzyme's affinity towards the food protein network, may also impact diffusion (Marimuthu & Schätzlein, 2013). For example, pepsin has been reported to form a temporary complex with some food proteins due to electrostatic interactions, which might reduce the overall pepsin diffusivity within the food matrices (Nyemb *et al.,* 2016a). Moreover, the apparent size of pepsin has been reported to vary depending on the pH, its size increasing at pH higher than 6.5 (Campos & Sancho, 2003). This pH-dependant change in size of pepsin may have an influence on its further diffusion properties inside the food matrix depending on its initial pH, as reported in Nyemb *et al.* (2016a).

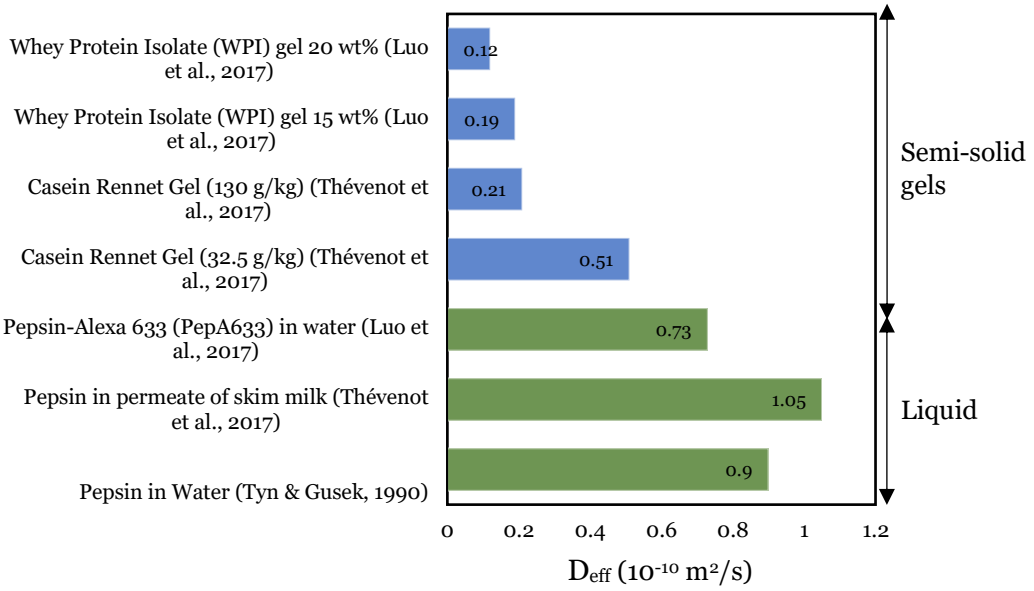

Figure 2.4: Comparison of the diffusion coefficients (D_{eff}) of pepsin in semi-solid gels with the D_{eff} of pepsin in liquid. Note that all the diffusion experiments were performed at 20 °C

To explore qualitatively the diffusion of pepsin and hydrolysis kinetics of protein gels during simulated gastric digestion, Floury *et al.* (2018), recently developed an *in situ* methodology based on the real time-lapse synchrotron deep-UV microscopy technique. Furthermore, Luo *et al.* (2017), employed scanning electron microscopy (SEM) to observe the effect of pepsin diffusion on the microstructure of whey protein isolate gels. Both studies highlighted that, within their experimental conditions (static *in vitro* model of gastric digestion), pepsin had limited penetration depth into the dairy gel matrices

and, as a result, gastric digestion was largely limited to the surface erosion (Floury *et al.,* 2018; Luo *et al.,* 2017).

Moreover, several *in vitro* studies have allowed us to obtain a deeper insight of how the food microstructure, mainly protein hydrogels, hinders the proteolysis process during the gastric digestion. As examples, Nyemb *et al.* (2016a, b), have shown that the digestibility of EWGs and the profiles of peptides released, were modulated by the microstructure: larger pores of the granular-spongy (pH 5) and intermediate (pH 7) EWGs enhanced pepsin activity compared to the smooth-rigid (pH 9) and fracturable (pH 2) EWGs. Tomczynska-Mleko (2015), and Tomczyńska-Mleko *et al.* (2016), revealed that aerated egg protein gels with a higher concentration of ions disintegrated faster than the low ion concentrated gels in their artificial human stomach environment. They reported that an increase in ion (i.e. calcium or magnesium) concentration resulted in a rougher surface and less smooth microstructure in aerated egg protein gels, which enabled fast proteolysis during the gastric phase. In the study of Opazo-Navarrete *et al.* (2018), soy protein isolate gel was hydrolyzed very slowly compared to pea protein isolate gel, which also correlates well with the high porosity of the pea protein isolate gel.

The food macro- or microstructure might not be the only factor influencing the different proteolysis kinetics of food matrices during *in vitro* digestion. Pepsin activity is strongly affected by pH (Campos & Sancho, 2003) and thus, the pH buffering capacity of food protein must be taken into account when describing the gastric digestibility of foods (Dekkers *et al.,* 2016; Sicard *et al.,* 2018). For example, Nau *et al.* (2019), confirmed *in vivo* that the higher intra-gastric pH appeared to be determined by the higher initial pH of the EWGs. The reported optimum pH for pepsin activity is pH 2.0 and falls to less than 50% of its maximum activity when the pH exceeds pH 3.0 (Kondjoyan, Daudin, & Santé-Lhoutellier, 2015). If pH value exceeds pH 8.0, pepsin can be denatured, which can result in irreversible inactivation (Kozlov *et al.,* 1979; Sicard *et al.,* 2018; Koufman & Johnston, 2012). Thus, overall pepsin activity and subsequent proteolysis kinetics in the food matrix depends on the intragastric pH which is determined by the ratio of gastric juice to food quantity and the buffering capacity of the ingested food.

Studies on the effect of food composition and structure on the pepsin diffusivity and protein digestibility of complex food proteins, including plant and meat proteins, are still limited (Opazo-Navarrete *et al.,* 2018). Thus, further research is necessary to adapt the promising methods (i.e. FRAP or FSC) to the determination of pepsin diffusion behaviour of a wide variety of solid food matrix in general, from protein-based food to more complex food structures. Moreover, further research still needs to focus on: (i) the development of techniques to determine the impact of gastric pH profiles on the proteolytic digestion and (ii) the determination of the actual pepsin diffusion that is

involved in enzymatic reactions during food protein digestion. In addition to that, research regarding the gastric lipase diffusivity and its activity within lipid-based solid foods are still largely unknown, which merits future investigations.

2.5.5 Physical Disintegration of Foods as a Result of Complex and Combined Mechanisms

The homogeneous mixing of the food around the stomach and the mechanical disintegration of food is controlled by involuntarily contraction and relaxation of smooth muscle in the gastric wall, which is known as gastric peristalsis or antral contraction waves (Kelly, 1980; Schulze, 2006). From an engineering point of view, this dynamic process is more or less similar to what occurs in a mixing tank (Bornhorst *et al.,* 2016). The motility pattern of the human stomach is mainly regulated by both neural and hormonal actions (Guerra *et al.,* 2012).

When food bolus is ingested, the state of the stomach changes from resting to a fed state, at which point antral contraction waves begin and move from the fundus to the pylorus until the chyme is emptied from the stomach (Kong & Singh, 2008a). During this fed stage, approximately 2-3 peristaltic contractions occur concurrently per minute (Bornhorst & Singh, 2012). The average mechanical contraction forces of the human stomach vary from 1.50 N under fasting state to 1.89 N under fed conditions (Kamba *et al.,* 2000). In addition to the peristaltic contractions, movement of ingested food from the top to the bottom of the stomach is also governed by the tonic contractions (Pal, Brasseur, & Abrahamsson, 2007). Two different flow types generate as a result of these mechanical contractions. They are flow vortices (eddies) and retropulsive jet. The pattern of flow vortices (eddies) is responsible for the homogenous mixing of gastric juice throughout the stomach, whereas the retropulsive jet movement is responsible for continuous mixing and emulsifying of the gastric juice and ingested food (Schulze, 2006). The magnitude of the stomach forces and other antral contraction wave parameters (frequency and speed) are influenced by biological factors including age, body mass index, hormonal factor, gender, blood glucose level and diseased states. Thus, the pattern of solid food disintegration within the human stomach for the same food may vary depending on an individual person (Kamba *et al.,* 2000; Kelly, 1980).

Gastric mixing caused by gastric peristalsis induces gastric fluid shear forces, dissolution and melting of food, food breakdown, pH distribution, and gastric emptying (Kelly, 1980; Bornhorst, 2017). All these processes are dependent on the rate of gastric juice addition, heat flow and surface area change as food matrix is physically broken down (Kong & Singh, 2009b). However, previous studies reported that the solid and nutrient release of almonds (Kong & Singh, 2009a) and bolus disintegration of different

types of bread (Bornhorst *et al.,* 2011) was not significantly affected by the hydrodynamic conditions (mixing and shearing effect) of surrounding gastric fluid.

Apart from biochemical disintegration, food is broken up to 1-2 mm size by the action of the physical forces of the stomach (Chen *et al.,* 2011). The proposed mechanisms of the disintegration of solid foods in the gastric environment are fragmentation and/or erosion (Guo *et al.,* 2015; Drechsler & Ferrua, 2016). Fragmentation can be defined as the breakdown of large food particles into several smaller daughter pieces, whereas surface erosion can be defined as the wearing away of the small food particles from the food surface (Drechsler & Ferrua, 2016). Fragmentation and surface erosion mechanisms increase the overall surface area, which provides additional contact area for gastric juice to absorb enhances the surface area for enzymatic attack and tenderizes the food matrix, leading to increased nutrient release within the stomach (Kong & Singh, 2009b). The repeated hydrodynamic mixing of and mechanical forces on gastric contents, together with the biochemical degradation, assist the progressive digestion of solid foods and finally, the formation of a semi-solid mixture called chyme (Bornhorst & Singh, 2012). The gastric chyme is then delivered into the small intestine for further digestion and absorption (Kong & Singh, 2008a).

The degree of disruption to the food structure by fragmentation and/or erosion can be quantified by assessing the particle size distribution (Bornhorst *et al.,* 2013; Guo *et al.,* 2015). Drechsler and Ferrua (2016), proposed a possible methodology to determine the contribution of erosive and fracture mechanisms to the breakdown behaviour of solid food. Previous studies have demonstrated that, in addition to these two breakdown processes, gastric temperature, acidity, and enzyme of gastric juice show a synergistic effect on solid food breakdown mechanisms (Kong & Singh, 2009b). Therefore, it is also important to identify the role that gastric juice absorption and biochemical degradation have on the physical breakdown mechanism of solid foods (Drechsler & Ferrua, 2016). Furthermore, the establishment of valid correlations between the *in vivo* and *in vitro* behaviour of food disintegration during digestion merits in future investigations.

It is well established that food material properties play an important role in the breakdown processes of food during gastric digestion (Bornhorst, Ferrua, & Singh, 2015). The physical properties of food such as particle size, density, texture, and microstructure are significant in determining how easily it can be disintegrated in the stomach (Kong & Singh, 2009b). Food particles with large size and density require extra time for size reduction in the stomach, resulting in lengthy gastric emptying times. As an example, the gastric emptying half-time is 70±10 min for the 0.25 mm chicken liver particles compared to 117±19 min for the 10 mm liver particles (Weiner *et al.,* 1981). In addition,

an *in vitro* study revealed that 3% of the carotenoid was released from raw carrot pieces, while 21% were released from the homogenized pulped carrots (Hedren, Diaz, & Svanberg, 2002).

Furthermore, soft food particles disintegrated at a considerably faster rate and released more nutrients than harder ones. For instance, Guo *et al.* (2015), studied how mechanical forces of the human stomach altered the whey protein emulsion gel microstructure and reported that, in the presence of pepsin, the soft whey protein emulsion gel emptied faster from the HGS compared to the hard gel, due to the increased rate of disintegration. *In vivo* studies carried out by Marciani *et al.* (2001), also showed that soft agar gels had a faster gastric emptying rate than rigid hard gels. Moreover, Kozu *et al.* (2014), highlighted that Kinugoshi-Tofu particles in the largest fraction disintegrated more easily and quickly inside the gastric digestion simulator model than Momen-Tofu particles and these results could be due to the higher breaking stress and Young's modulus of Kinugoshi-Tofu. Kong and Singh (2008b), developed a model stomach system to investigate the kinetics of food disintegration during digestion and demonstrated that the disintegration kinetics of raw carrots, cooked carrots and ham were largely decided by the initial hardness of the foods.

In addition to the aforementioned physical properties, physical barriers present in the food matrix, and interactions of chemical components within the food structure, significantly influence the food disintegration during gastric digestion. For instance, using *in vivo* and *in vitro* studies, Bornhorst *et al.,* (2013), Kong *et al.* (2011) and Wu *et al.* (2017), highlighted that the bran layer on brown rice significantly delayed rice disintegration and slowed down gastric emptying, as it inhibited the absorption of gastric juice, leading to decreased texture degradation. In contrast to brown rice, white rice reported a higher rate of disintegration and gastric emptying (Kong *et al.,* 2011). Several *in vivo* and *in vitro* studies reported that the physical disintegration of plant-based foods is limited by the cell wall in the plant-food matrix, which may act as a physical 'barrier' towards the gastric juice and to the subsequent release of nutrients into the aqueous phase of the gastric digesta (Bordoloi, Singh, & Kaur, 2012a, b; Grundy *et al.,* 2015; Tydeman *et al.,* 2010). Moreover, complex interactions that occur during cooking and/or digestion within the macronutrients of different types of solid foods may also affect the food disintegration kinetics within the stomach (Bornhorst & Singh, 2012). As an example, protein–starch interactions in bread dough significantly reduced the rate of disintegration and subsequent blood glucose response (Jenkins *et al.,* 1987; Parada & Santos, 2016).

Different mathematical models and mechanisms have been proposed to characterise the *in vitro* and *in vivo* breakdown of solid food during gastric digestion

(Drechsler & Ferrua, 2016; Ferrua & Singh, 2010; Guo *et al.,* 2015; Kong & Singh, 2009b; Kong & Singh, 2010). Food scientists have shown that the particle size distribution in a solid food during gastric digestion can be successfully fitted to a Weibull distribution and/or a mixed Weibull distribution (Bornhorst *et al.,* 2013; Bornhorst & Singh, 2014; Drechsler & Ferrua, 2016; Guo *et al.,* 2015). These models successfully simulate the particle size distribution in the food bolus for a limited range of foods including whey protein emulsion gels (Guo *et al.,* 2015), almonds (Bornhorst *et al.,* 2014), potatoes (Drechsler & Ferrua, 2016) and rice (Bornhorst *et al.,* 2013). However, it is important to evaluate how these models perform for a wider range of foods that have different compositions and structures.

2.6 Nutrient Release during Gastric Digestion

2.6.1 Mechanisms of Nutrient Release

During gastric digestion, the mechanisms of acid and enzymatic hydrolysis, gastric juice diffusion and physical breakdown govern the rate and mode of nutrient release from food matrices (Kong & Singh, 2009a, 2009b). This concept of nutrient release for absorption during gastric digestion is known as the nutrient bio-accessibility, which is a major limiting step of nutrient bioavailability for intestinal absorption (Mennah-Govela & Bornhorst, 2016a, b).

Release of nutrients and bioactive compounds from the food matrix due to disintegration mechanisms inside the stomach involve single or multiple stages: (a) diffusion through food matrix, (b) food matrix relaxation due to swelling and/or (c) food matrix erosion/degradation (Flores & Kong, 2017; Kong *et al.,* 2011; *Peng et al.,* 2010).

(a) Diffusion through food matrix

Diffusion of solutes/nutrients through the hydrated food matrix due to the concentration gradient is one of the major mechanisms that may individually or simultaneously affect the release of nutrients during gastric digestion process (Kong & Singh, 2011; Peng *et al.,* 2010). It is known that there are two mechanisms of nutrient diffusion phenomena; in the first one, the nutrient moves from the food matrix interior towards the surface; and in the second one, the nutrient is transferred from the food surface to the gastric fluid (Kong & Singh, 2009b). When the nutrient concentration of the food matrix becomes equal to the nutrient concentration of the aqueous gastric medium, no further diffusion takes place and the nutrient concentration at this stage is called the equilibrium nutrient concentration (Kong *et al.,* 2011; Mennah-Govela &

Bornhorst, 2016b). Although there are works related to nutrient transfer in solid foods, mainly covering diffusion aspects, there is still a necessity of additional studies in order to achieve a more complete knowledge.

(b) Food matrix relaxation due to swelling

The swelling of the food matrix is the result of a series of processes that start with gastric juice penetration, which induces a conformation change due to hydration and unravelling of the solid food matrix (Kong & Singh, 2011; Mennah-Govela & Bornhorst, 2016b). In the area of pharmaceutical studies, the rate of polymer hydration and swelling is an important aspect in controlling the rate of drug release from polymeric matrices (Siepmann & Peppas, 2012). In view of this, a more complete knowledge of the food matrix swelling behaviour due to the diffusion of gastric juice is useful because it might affect the nutrient release during digestion. However, currently there is limited information available in the literature on the swelling kinetics of foods during gastric digestion and its relationship with nutrient release.

Studies of plant-based foods including almonds (Bornhorst *et al.,* 2014; Kong & Singh, 2009a), and rice (Kong *et al.,* 2011) showed that food particles increased in weight due to gastric juice penetration and also demonstrated an increase in volume during the initial stages of gastric digestion. These studies further reported that significant water absorption and swelling of the ingested food in the stomach phase may help to control obesity-related diseases due to the rapid generation of satiety feeling due to a larger increase in food matrix volume (Kong & Singh, 2009a). Furthermore, Kong *et al.* (2013), studied the absorption of water and the swelling of peanuts during gastric digestion using MRI and reported that fried peanuts swelled the most, followed by the boiled peanuts. They further revealed that solid release was greater in fried peanut food matrix followed by boiled peanuts during the gastric digestion process.

Tydeman *et al.* (2010), reported that the cell-wall swelling of plant-based food matrix is significant, primarily in the simulated gastric environment. This swelling behaviour is also accompanied by an increase in pore size within the cell wall, which can have direct effects on the mobility of cell wall-degrading enzymes and acid during gastric digestion (Grassby *et al.,* 2014). Another study also reported that swelling of semi-solid food matrices might contribute to enzyme diffusion and nutrient release during digestion (Guo, Bellissimo, & Rousseau, 2017). Since the semi-solid food matrix was composed of both polymer and nutrient molecules, the swelling effect caused a uniform volume expansion, causing the opening of pores throughout the matrix structure. For effective diffusion of nutrient molecules to occur, the pore size of the swollen matrix must greatly

exceed the size of the hydrophilic or hydrophobic bioactive compound entrapped within the food matrix (Siepmann *et al.,* 1999; Singh *et al.,* 2015).

(c) Food matrix erosion/degradation

The effects of the food matrix degradation due to gastric digestion are measured as the erosion of the food material over digestion time (Kong & Singh, 2011). The erosion can occur through acid and enzyme hydrolysis as well as mechanical disintegration (Grassi & Grassi, 2005; Kong & Singh, 2009b). Erosion of the food matrix can be segregated into two distinct categories: bulk erosion and surface erosion (Grassi & Grassi, 2005; Von-Burkersroda, Schedl, & Göpferich, 2002). In the case of bulk erosion, the food matrix degrades uniformly throughout the bulk of the material and the volume of the food remains constant while the mass of the food material reduces (Von-Burkersroda *et al.,* 2002). In the case of surface erosion, the food matrix degrades from the outer surface of the food matrix which is in direct contact with the surrounding gastric environment. Thus, the volume of the material decreases with digestion time (Von-Burkersroda *et al.,* 2002). As an example, for surface erosion, Kong and Singh (2009a), observed that surface cell arrangement was disrupted during *in vitro* gastric digestion and the intracellular contents, such as lipid and protein, of damaged cells were released.

2.6.2 Modelling Nutrient Release Kinetics

Mathematical modelling of nutrient release kinetics during gastric digestion provides the basis for the study of nutrient release from the food matrix over a period of gastric digestion, which helps to assess the biological outcome of released nutrient (Flores & Kong, 2017). There have been a few research studies that have described nutrient release kinetics as a result of *in vitro* digestion by combining experimental concentration-time profiles and corresponding theoretical or empirical models (Grassby *et al.,* 2014; Kong & Singh, 2011).

The food breakdown process, and subsequent nutrient release inside the human stomach might be described in a similar manner to drug dissolution and absorption (Bornhorst *et al.,* 2015). The pharmaceutical industry has extensively investigated the various kinetics models in order to predict drug performance (i.e. the extent and mechanism of release of active compound) after ingestion (Costa & Lobo, 2001; Grassi & Grassi, 2005; Jeong *et al.,* 2007). Some of these models have been successfully applied to nutrient release kinetics in food-related applications (Kong & Singh, 2011; Tomczynska-Mleko, 2015; Tomczyńska-Mleko *et al.,* 2016). Thus, this section focuses on

information from pharmaceutical studies to determine the kinetic models of nutrient release during the gastric digestion and thereby to understand the main mechanisms involved in the release process.

Four commonly used equations for modelling release kinetics in pharmacological studies are summarised in Table 2.4. They include Higuchi, Korsmeyer-Peppas, Peppas-Sahlin and Weibull equations. Higuchi model is the first mathematical model that describes drug release from a matrix system (Higuchi, 1963). It describes the release of the bioactive compound as a diffusion process based on Fick's law, square root time-dependent (Higuchi, 1963). However, Higuchi's model does not provide additional insights into a release mechanism (Flores & Kong, 2017).

To understand the dissolution mechanisms of the bioactive compound from the drug-incorporated matrix, a simple relationship that described drug release based on the power-law equation was proposed by Korsmeyer and Peppas (Ritger & Peppas, 1987; Flores & Kong, 2017). Using the diffusion exponent value (n), this model can predict the mechanism of drug release. For a thin film, values of $n=0.5$ indicate that drug release is governed by diffusion-controlled processes (Fickian diffusion), as in the Higuchi model. If the diffusion exponent is in the range of $0.5<n<1$, it indicates that drug release is governed by both diffusion-controlled and erosion-controlled (anomalous diffusion) processes. Finally, when $n>1$, it indicates that drug release is governed by erosion-controlled processes only (case III transport) (Flores & Kong, 2017; Ritger & Peppas, 1987). The appropriate n values for other geometries are given in Table 2.4.

Tomczynska-Mleko (2015), and Tomczynska-Mleko *et al.* (2016), studied the release of calcium and magnesium ions from aerated EWGs in an artificial stomach environment. They successfully applied the Korsmeyer and Peppas model and concluded that the nutrient release from the selected egg gel matrix occurred by Fickian diffusion. Later, the Peppas and Sahlin model was developed to account for the approximate contributions of the effects of Fickian diffusional and erosion-controlled (case II transport) mechanisms (Peppas & Sahlin, 1989). Although this model is successfully used to describe the drug release kinetics (Grassi & Grassi, 2005), it has not been used in food-related applications.

Table 2.4: Summary of mathematical models for drug/nutrient release kinetics

Model (References)	Equation	Mechanisms of release			
Higuchi (Higuchi, 1963)	$\frac{M_t}{M_0} = k_H\, t^{0.5}$	Diffusion-controlled (Fickian diffusion)			
Ritger-Peppas (Ritger & Peppas 1987; Yin *et al.* 2013; Flores & Kong 2017)	$\frac{M_t}{M_0} = k_P\, t^n$	Diffusional exponent (n)			
		Thin film	Cylinder	Sphere	Mechanism
		n≤0.5	n≤0.45	n≤0.43	Diffusion-controlled (Fickian diffusion)
		0.5≤n< 1	0.45≤n< 0.89	0.43 ≤n<0.85	Diffusion- and erosion-controlled (Anomalous diffusion)
		n>1	n>0.89	n>0.85	Erosion-controlled
Peppas-Sahlin (Peppas & Sahlin 1989)	$\frac{M_t}{M_0} = k_d\, t^n + k_r\, t^{2n}$	$k_d\, t^n$ for diffusion-controlled $k_r\, t^{2n}$ for erosion-controlled			
Weibull (Kong *et al.*, 2011)	$\frac{M_t}{M_0} = e^{-(kt)\beta}$ $t_{1/2} = \frac{1}{k}(\ln(2))^{1/\beta}$	β > 1; sigmoidal curve β = 1; exponential curve β < 1; parabolic curve			

- M_t is the amount of drug/nutrient (mg) release at digestion time t, M_o is the amount of drug/nutrient (mg) at digestion time = 0
- In Higuchi model k_H is the Higuchi release rate constant ($min^{-0.5}$)
- In Korsmeyer-Peppas model k_p is the Korsmeyer-Peppas release rate constant (min^{-n}) and n is the diffusional exponent (dimensionless).
- In Peppas-Sahlin model k_d is the diffusion release rate constant (min^{-n}), k_r is the relaxation release rate constant (min^{-2n}) and n is the diffusional exponent (dimensionless).
- In Weibull model k is the scale parameter (min^{-1}), which may indicate the rate of drug/nutrient release and β is the distribution shape factor (dimensionless). $t_{1/2}$ is the time (min) necessary for the initial drug/nutrient concentration to be reduced by 50%

The Weibull model has been extensively used in pharmacological research to model the dissolution profile of active drug compounds in a polymer matrix (Bornhorst *et al.,* 2015; Costa & Lobo, 2001; Jeong *et al.,* 2007). Similarly, the Weibull equation was applied to describe the solid release kinetics of carrots during *in vitro* simulated gastric digestion (Kong & Singh, 2011). In the Weibull model, parameter 'k' denotes a scale parameter that describes the rate of active compound release from the matrices, while 'β' describes the shape of the release curve progression (Bornhorst *et al.,* 2015). For $\beta = 1$, the shape of the curve corresponds exactly to the shape of an exponential profile, if $\beta > 1$, the shape of the curve gets sigmoidal, whereas the shape of the curve is parabolic if $\beta < 1$ (Flores & Kong, 2017). Using these Weibull parameters, a release half time can be calculated as the time necessary for the initial concentration of the active compound to be reduced by 50% (Kong & Singh, 2011). Since the release half time incorporates both the k and β parameters from the Weibull model, it defines the complete characteristics of the curve more accurately than either of the Weibull parameters on their own (Bornhorst *et al.,* 2015).

2.7 Conclusions and Perspectives

This review aimed to develop a more complete picture of the physicochemical breakdown process driving the disintegration of solid foods during gastric digestion. The disintegration process of foods within the human stomach is extremely complex, involving many different physical, physicochemical, and biochemical mechanisms. These fundamental mechanism(s) governing nutrient release is highly dependent on the food's material properties; particularly its composition and structure, which can change as digestion proceeds. Moreover, food structure regulates food transit in the gastric phase. But our understanding of how various foods with different compositions and structures are affected by these processes remains incomplete.

Water, acid and enzymes in the gastric fluid are the main stimuli for the release of nutrients from the food matrix due to the diffusion of gastric juice. The food material properties have a marked effect on the acid and enzymatic degradation of the food matrix. Currently, a limited number of experimental methodologies allow us to monitor the diffusion of gastric components under normal gastric conditions. Thus, techniques, including sophisticated imaging techniques (i.e. MRI, HSI, CLSM etc), need to be developed further to quantify the spatial and temporal movement of the water, acid, and enzymes during gastric digestion of solid foods. This will allow us to gain a better understanding of the gastric process and mechanisms involved in the

nutrient release of solid foods which could be applied for the development of foods with enhanced functionality.

In the last few years, there has been an increase in research on understanding the physicochemical breakdown of different solid food structures inside the human stomach. This has led to the development of various human gastric simulator models, as well as mathematical approaches to model erosion, fragmentation, and changes in food particle size distribution during gastric digestion. But there is still much work to be done in this field in order to accurately model the actual process of food mechanical disintegration in the stomach.

In addition, different mechanisms of nutrient release during gastric digestion have been reviewed here. However, the understanding of how various foods with different compositions, physical properties, and structures impact the nutrient release during gastric digestion remains incomplete. Another less studied aspect is the modelling of nutrient release kinetics during solid food disintegration in the stomach, in connection with the different mechanisms that can occur. Various theoretical, semi-empirical, and empirical models have been successfully applied to model the release kinetics of encapsulated biomaterials from drug polymers. These models of pharmaceutical studies can be utilized to systematically study the mode and rate of the nutrient release from food matrices during the gastric digestion process. Moreover, to better elucidate nutrient release mechanisms during gastric digestion, it is crucial to building up the connection between *in vitro* and *in vivo* nutrient release kinetics through proper correlation analysis.

Finally, to fully exploit the relationship between food material properties, solid food disintegration mechanisms inside the stomach, and its health outcomes, an integrated approach involving researchers from different disciplines (nutrition, pharmaceutical, and biomedical sciences, food science, materials science, etc.) will be required. Understanding the effects of food material properties on the mechanisms of solid food disintegration and nutrient bio-accessibility during gastric digestion is crucial for developing a new generation of foods with improved health and wellness, as well as to validate health claims for functional foods.

Chapter Three

3.Characterisation of Steamed and Fried Sweet Potatoes Microstructure and its Relationship with Acid and Moisture Diffusivity during Static *In Vitro* Gastric Digestion*

3.1 Abstract

The diffusion of gastric juice is one of the key parameters driving solid food disintegration within the stomach. This chapter aimed to investigate the feasibility of using hyperspectral imaging (HSI) to characterise the diffusion of acid and water within steamed sweet potatoes (SSP) and fried sweet potatoes (FSP) during *in vitro* gastric digestion. SSP and FSP samples were exposed to *in vitro* gastric digestion before scanning by HSI. Afterward, the moisture or acid present in the digested sample was analysed for calibration purposes. Calibration models were subsequently built using partial least squares (PLS). The PLS models indicated that the full-wavelength spectral range (550–1700 nm) had a good ability to predict the spatial distribution of acid (R_{cal}^2>0.90) and moisture (R_{cal}^2>0.90). The spatiotemporal distributions of moisture and acid were mapped across the digested sweet potatoes matrix, and they were shown to depend on the initial microstructure of sweet potatoes. Effective diffusivity (D_{eff}) of acid and moisture was described mathematically using Fick's second law. Results indicate that open-porous matrix and interconnected pores of the fried samples (D_{eff} = 3.2±0.2x10^{-9} m^2/s) facilitate the faster rate of gastric acid diffusion than the compactly dense structure of steamed samples (D_{eff} = 1.6±0.4x10^{-9} m^2/s). The current findings further indicate that the D_{eff} of acid does not follow the same trend as the D_{eff} of moisture during simulated gastric digestion of cooked sweet potatoes. Thus, acid and moisture diffusion into the solid foods during gastric digestion should be estimated, separately.

*Chapter three published as a peer-reviewed paper: Somaratne, G., Reis, M. M., Ferrua, M. J., Ye, A., Nau, F., Floury, J., Dupont, D., Singh, R. P. and Singh, J. (2019). Mapping the spatiotemporal distribution of acid and moisture in food structures during gastric juice diffusion using Hyperspectral Imaging. *Journal of Agricultural and Food Chemistry*, 67(33), 9399-9410.

3.2 Introduction

Gastric secretion from the stomach is an important biological fluid in the entire digestive system (Bornhorst & Singh, 2014). It is an acidic and diluted aqueous solution containing electrolytes and digestive enzymes such as pepsin and lipase (Mennah-Govela & Bornhorst, 2016a, b; Minekus *et al.,* 2014). The average pH of gastric acid secreted from the stomach wall of healthy humans is around pH 2, which is controlled by hydrochloric acid (Lu *et al.,* 2010). During digestion, gastric moisture and acid contribute to hydration and acid hydrolysis of food, respectively, and thereby alter the external attributes (i.e. softening of the food matrix) and the internal attributes (i.e. chemical composition, pH) of the food structure (Kong *et al.,* 2013; Mennah-Govela *et al.,* 2015). Thus, the diffusion of gastric juice within food matrices in the gastric environment is one of the fundamental parameters that contribute to overall food disintegration and nutrient release during gastric digestion (Mennah-Govela & Bornhorst, 2016b). Nevertheless, the mechanism by which the diffusion of moisture and acid of the gastric juice affect the disintegration of food is still far from being fully understood (Mennah-Govela & Bornhorst, 2016a, b).

Classical characterisations of moisture and acid penetration in food systems during gastric juice diffusion have employed integral gravimetric techniques. As examples, previous studies have focused on identifying the gastric acid and/or moisture diffusion coefficient of different food matrices including rice (Mennah-Govela *et al.,* 2015), cooked sweet potatoes (Mennah-Govela & Bornhorst, 2016a, b) and frankfurters (Ozvural & Bornhorst, 2018) using an oven drying method and potentiometric titration, respectively. In these studies, the transport of gastric components into food matrix during gastric digestion was typically characterised by moisture or acid gain into the food product from the surrounding experimental gastric environment using the Fick's second law of diffusion (Mennah-Govela & Bornhorst, 2016a, b; Mennah-Govela *et al.,* 2015; Ozvural & Bornhorst, 2018). While the calculated diffusivity value describes on overall gastric juice gain over digestion time, it does not represent any spatial information in regard to the diffusion process. Furthermore, gastric juice diffusion as a function of time is often insufficient to allow the investigation of the underlying mechanism of moisture or acid penetration during gastric digestion, particularly in heterogeneous food systems (Van Wey *et al.,* 2014; Widjaja, 2010).

Thus, to gain insight into spatiotemporal gastric juice migration, the diffusion of gastric juice into different food products such as white potatoes (Widjaja, 2010), carrots and cheese (Van Wey *et al.,* 2014) has been characterised based on an optical image analysis technique. In these studies, the intensity of methylene blue colour is used to

detect the spatial and temporal changes in gastric fluid distribution allowing it to be indirectly modelled by the Fick's second law (Widjaja, 2010). However, the use of methylene blue and similar coloured dyes as reliable indicators of the gastric juice have remained unanswered. Alternatively, Kong *et al.* (2013), studied the spatial and temporal distribution of gastric juice and swelling of peanuts during gastric digestion using the MRI technique. MRI has significant advantages compared to the optical imaging method for the characterisation of gastric juice diffusion process because it relies on the characteristic absorption and emission of energy from corresponding protons in the digested sample (Grover *et al.,* 2015). Therefore, MRI does not require the use of added dyes or labelling methods for visualisation of different chemical components in the gastric fluid (Kong *et al.,* 2013).

Similar to MRI, HSI is a labelling free analytical approach used in food science-related research, which is becoming increasingly important in revealing the spatiotemporal distribution of chemical composition within foods. HSI obtains the electromagnetic spectrum for each pixel in the tested image and this information then create a three-dimensional data set, which can be analysed to characterise the physical and chemical topographies of the product being scanned (ElMasry *et al.,* 2012). HSI is used to predict the spatial distribution of sucrose, caffeine, and trigonelline in single green coffee beans (Caporaso *et al.,* 2018), moisture in red meat (Kamruzzaman, Makino, & Oshita, 2016a, b) and moisture in dehydrated prawns (Wu *et al.,* 2012). Moreover, the distribution of acid and moisture in a vinegar culture during solid-state fermentation was successfully distinguished with this technique by noting the spectral differences between each component (Zhu *et al.,* 2016). The success of these studies stimulate us to apply a similar technique of HSI to obtain quantitative information about the spatiotemporal distribution of gastric fluid components in a food matrix. To our knowledge, no study has been reported on using HSI technique to evaluate the gastric juice diffusion phenomenon during gastric digestion.

The main aim of this chapter was to explore the feasibility of HSI, in the range 550–1700 nm, for predicting total acid and moisture distributions in steamed and fried sweet potatoes matrices during *in vitro* gastric juice diffusion process using partial least squares (PLS) regression models. Consequently, these models can be used to visualise the distribution of acid and moisture within the digestive SSP and FSP matrix at a single-pixel level. Moreover, SSP and FSP were selected as starch-based product models to identify the effect of the microstructural characteristics of solid foods on the diffusion of gastric acid and moisture into the food matrix in the gastric environment.

3.3 Materials and Methods

3.3.1 Materials

Orange-fleshed sweet potatoes and canola oil were purchased from a local supermarket in Palmerston North, New Zealand. The sweet potatoes were stored at room temperature (25 °C) and used within no more than two days. To reduce the influence of possible variations among the initial samples, the same batch of sweet potatoes was used for the entire analysis. Pepsin (from porcine gastric mucosa, ≥ 250 U/mg solid), gastric lipase analogue (from *Aspergillus niger*≥120,000 U/mg solid) and α-amylase (from *Aspergillus oryzae*, ≥30 U/mg) were purchased from Sigma–Aldrich, USA. All other chemicals were of analytical grade. Milli-Q water (Millipore Corp., Bedford, MA, USA) was used for all experiments.

3.3.2 Sweet Potato Sample Preparation

Orange-fleshed sweet potatoes were peeled with a hand-peeler. Then, cylindrical sweet potatoes with a dimension of 30 mm length and 20 mm diameter were cut from sweet potato core using a cutting bore.

SSP were prepared according to the method described by Drechsler and Ferrua (2016). Prior to steaming, water was placed at the bottom of the steam cooker and heated up to boiling over 15 min. The temperature of the generated steam reached up to 100±3 ◦C. Then, ten cylindrical samples of sweet potatoes were steamed over 1500 mL of boiling water using a steamer pot (25 cm diameter) with a 1.5 mm stainless steel sieve mesh for 10 min and then removed.

The frying method adopted in this study is a method that is typically used in the production of deep-fried potato chips (Farinu & Baik, 2007). Initially, the canola oil was filled in a Breville Deep Fryer and pre-heated to 180±2 °C before frying. Then, 10 cylindrical samples of sweet potatoes were placed in a wire mesh basket, which was immersed in the oil for 5 min, after the set temperature was reached. A thermocouple was kept inside the frying container during cooking to measure the temperature profile over time to ensure similar cooking conditions for each batch. After frying, the batch of the samples was taken out of the oil and allowed to drain for 3 min before blotting off the surface oil using an absorbent paper. The details of the development of starch-based product models (SSP and FSP) and their initial parameters such as weight of the sample, microstructure, diameter and length were given in Appendix 1.

3.3.3 Observation of Initial Microstructure

Scanning electron microscopy (SEM): SEM was done to determine the changes of the surface microstructure of sweet potatoes after cooking. Raw and cooked sweet potato samples were snap-freeze using liquid N_2 and freeze-dried. The freeze-dried samples were mounted on the stub and sputter-coated with gold in a sputter coater (SCD 050, Balzers, Liechtenstein). Then the sample was viewed using a scanning electron microscope (FEI Quanta 200 FEI Electron Optics, Eindhoven, The Netherlands) at an accelerating voltage of 20kV at different magnifications and representative images were selected.

Confocal laser scanning microscopy (CLSM): The microstructure of raw and cooked samples was observed by a CLSM (Leica, Germany) with 40× oil immersion lens. Calcofluor white (2%) was used to detect the cell wall. Acridine orange (1%) was used to stain starch granules. Differential interference contrast mode was used to detect the β-carotene. Nile red (1%) was used to stain for oil in FSP. The samples were excited using an argon laser at 405 nm for Calcofluor white, at 488 nm for Nile red, at 500 nm for Acridine orange, and at 488 nm for auto-fluorescence of carotenoids.

3.3.4 Formulation of Simulated Digestive Fluids

The solutions of simulated digestion fluids (SSF: simulated salivary fluid and SGF: simulated gastric fluid) were prepared as shown in Table 3.1 and 3.2, respectively. The volumes were calculated for a final volume of 500 mL for each simulated fluid. The stock solutions were prepared and stored at −20 °C with a small headspace. They were warmed at 37 °C before the digestion procedure.

3.3.5 Static *In Vitro* Digestion

Before the *in vitro* gastric digestion study, plastic caps were fixed to the top and bottom of the prepared sweet potatoes cylinders using an acid-resistant silicon adhesive (Silcoset 158, Acc Silicones, UK) to achieve the gastric juice diffusion only in the radial direction (Figure 3.1 (a)).

Cylindrical sweet potatoes samples were digested according to the harmonized INFOGEST protocol (Minekus *et al.,* 2014). The sample was first submitted to a 2 min oral phase by mixing the cylindrical food sample with SSF electrolyte stock solution. After addition of SSF, salivary α-amylase was added to achieve 75 U/mL in the final mixture, followed by CaCl2 to achieve 0.75 mM in the final mixture and the required amount of water to dilute the stock solution of SSF. The sample was kept at a 37 °C shaking water bath (BS-11, Lab Companion) at 50 rpm.

Table 3.1: Preparation of SSF at pH 7

SSF at pH 7			
Constituent	Stock conc. (g/L)	Stock conc. (mol/L)	Vol. of stock (mL)
KCl	37.3	0.5	15.1
KH_2PO_4	68	0.5	3.7
$NaHCO_3$	84	1	13.6
$MgCl_2(H_2O)_6$	30.5	0.15	0.15
$(NH_4)_2CO_3$	48	0.5	0.06
For pH adjustment			
HCl	-	6	0.09
$CaCl_2(H_2O)_2$ and α-amylase are not added to the simulated digestion fluids			
$CaCl_2(H_2O)_2$	44.1	0.3	25 µL per 5 mL SSF
α-amylase	1500 U/mL	-	0.5 mL per 5 mL SSF

Source: Minekus *et al.,* (2014). SSF: Simulated Salivary Fluid

Table 3.2: Preparation of SGF at pH 3

SGF at pH 3			
Constituent	Stock conc. (g/L)	Stock conc. (mol/L)	Vol. of stock (mL)
KCl	37.3	0.5	6.9
KH_2PO_4	68	0.5	0.9
$NaHCO_3$	84	1	12.5
NaCl	117	2	11.8
$MgCl_2(H_2O)_6$	30.5	0.15	0.4
$(NH_4)_2CO_3$	48	0.5	0.5
For pH adjustment			
HCl	-	6	1.3
$CaCl_2(H_2O)_2$ and α-amylase are not added to the simulated digestion fluids			
$CaCl_2(H_2O)_2$	44.1	0.3	0.2 mL per 10 mL SGF
Porcine pepsin	25 000 U/mL	-	1.6 mL per 10 mL SGF
Gastric Lipase	2400 U/ml	-	1 mL per 10 mL SGF

Source: Minekus *et al.,* (2014). SGF: Simulated Gastric Fluid

Subsequently, the sample was mixed with SGF and the pH value of the samples was immediately adjusted at a value of 3.0. Porcine pepsin and lipase were added to achieve 2000 U/mL and 120 U/mL in the final digestion mixture, respectively. Then CaCl2 was added to achieve 0.075 mM in the final digestion mixture. Finally, the required amount of water was added to the mixture to dilute the stock solution of SGF. A mass ratio of 1:10 between the cylindrical sweet potatoes sample and gastric fluid was used. As shown in Figure 3.1 (b), the sample was then placed inside the shaking water bath (37 °C, 50 rpm).

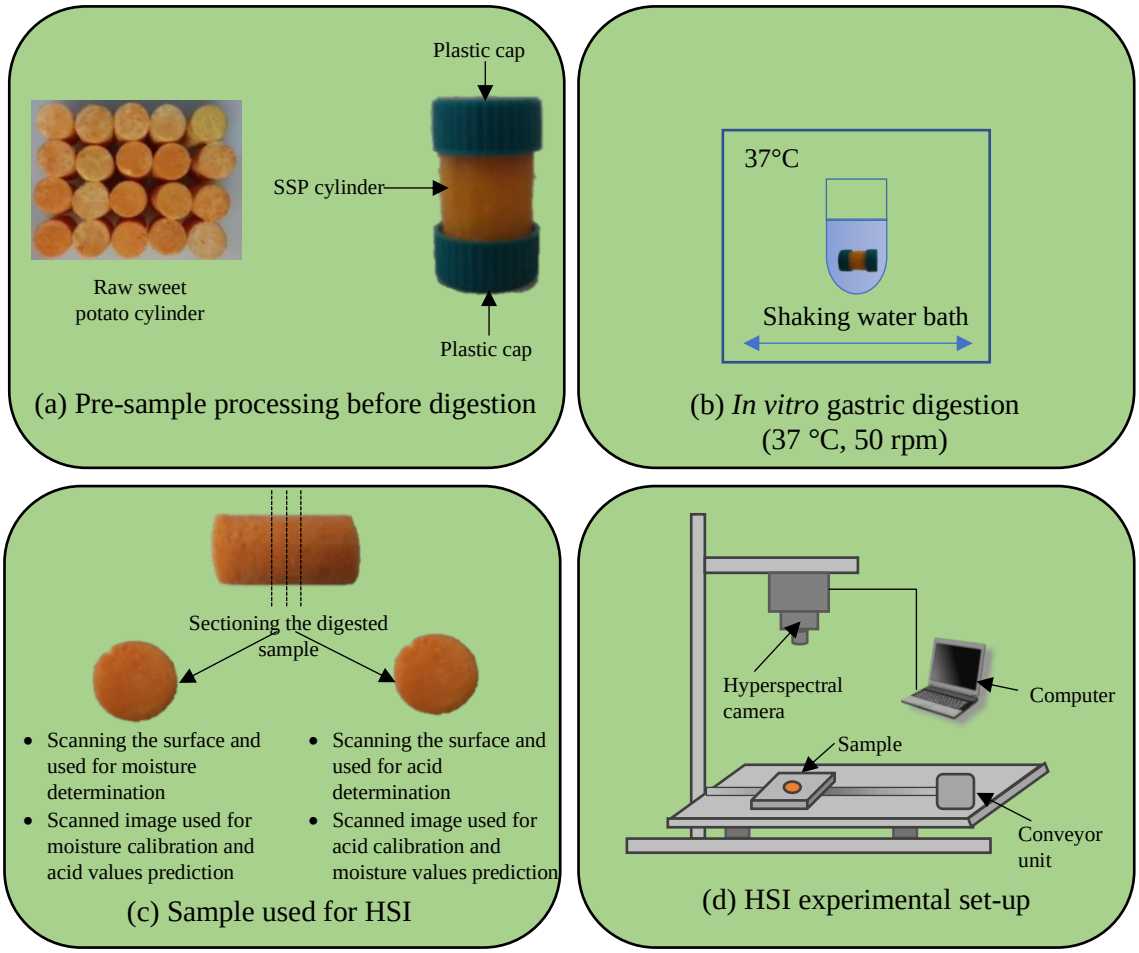

Figure 3.1: Schematic diagram of the gastric acid and moisture diffusion and HSI experimental procedure of SSP as an example

Separate samples were prepared for each digestion time of 0, 10, 20, 40, 60, 120, 180 and 240 min, respectively. Simulated digestions were performed in triplicate for each food system and digestion time point. After being digested, cylindrical samples were removed from the digestive fluid and two slices (5±0.5 mm of thickness) were obtained from the central parts of each digested sweet potatoes matrix using a surgical scalpel

blade. As illustrated in Figure 3.1 (c), two slices from food cylinders of one digestion time were used, one for calibration of moisture or acid and the other for prediction. Two different slices belonging to the same cut surface of the digested food cylinder at each digestion time were scanned with a HSI system described below. After scanning, one set of slices was used to determine the moisture whereas the other set of slices was used to determine the acid content using the laboratory method described below.

3.3.6 Hyperspectral Image Acquisition

A schematic diagram of the hyperspectral scanning experimental set-up is shown in Figure 3.1 (d). The HSI system used in this study includes a computer-controlled movable stage, with data acquisition and control software of Hyperspec III. A VIS-InGaAs hyperspectral camera which acquires 235 bands in the spectral range from 548 nm to 1701 nm, and a Headwall spectrograph (Model 1003B-10151, Headwall Photonics, Fitchburg, MA, USA) attached to the hyperspectral camera. An optical fiber illumination liner (12" Light line, A08905, Schott Lighting, and Imaging) was used to illuminate the sample. A 35 mm lens with an f/stop of 1.65 was placed in front of the hyperspectral camera, exposure time of 34 ms, with a frame period of 40 ms and translation speed of 6 mm/s, resulting in a square pixel size of 0.14 mm x 0.14 mm. The digested slice of the sweet potatoes was placed in the sample holder and transported to a conveyor unit. When the sample moved within the field of view at a constant speed of 2.08 mm/s, the images and spectra were acquired by the hyperspectral camera and sent to the computer for storage and post-processing. The obtained raw images were calibrated automatically by the system using a white and a dark reference image. The white image was obtained by scanning a uniform white Spectralon tile and the dark reference was obtained with the light off the covering of the lens.

3.3.7 Moisture Content Determination

After image acquisition, reference moisture contents of the one sweet potato slice (5±0.5 mm of thickness) at different digestion stages were determined by the thermo-gravimetric method. The sample was dried in a convective hot-air oven at 105 °C to constant weight for 16 hours. Samples before and after oven drying were weighed. The moisture content was calculated on a wet basis (AOAC method, 2005).

3.3.8 Total Acid Content Determination

After image acquisition, reference total acid content (in terms of mg of HCl/g sample) of another digested sweet potato slice (5±0.5 mm of thickness) at different

digestion stages was determined by potentiometric titration (Mennah-Govela & Bornhorst, 2016a, b). First, each slice of the sample was weighed and mixed with 20 mL of deionized water. The mixture was homogenized at 4,600 rpm for 5 min. The initial pH of the homogenized sample was measured using a portable pH meter. Potentiometric titrations were performed to measure sample acidity, by adding sodium hydroxide (0.01 N NaOH) until the sample reached a pH of 8.2±0.05.

3.3.9 Hyperspectral Images Pre-Processing

The acquired hyperspectral images were saved in a raw format as a three-dimensional (3-D) hypercube consisting of two spatial dimensions (x = 180 pixels and y = 320 pixels) and one spectral dimension (λ = 235 bands) from which both the physical and the chemical properties of the samples could be obtained. The initial stage in the hyperspectral image process was in reducing the dataset by removal of background data and retaining key qualitative data (food slice or ROI) using a principal component analysis. The resulting image spectra were processed to reduce scattering effects, using standard normal variate, the Savitzky-Golay smoothing process, and multiplicative scatter correction (Caporaso *et al.,* 2018; Zhu *et al.,* 2016). For each slice of sweet potato image, the mean spectrum was extracted by averaging the spectra of each pixel in the ROI. The mean spectral data for each sample were used in the next stage of the analysis. The Prediktera Evince software 2.7.2 (Prediktera AB, Umeå, Sweden) was used for images pre-processing and mean spectrum extraction.

3.3.10 Model Development to Predict Moisture and Acid Distribution

Among the 48 scanned samples from each sweet potato food system (two food slices from one replicate x 8 digestion times x 3 replicates), samples were divided into two sample sets such as calibration set and prediction set. A calibration sample set consisted of 24 samples (first food slice from one replicate x 8 digestion times x 3 replicates). The mean spectra obtained were linked to the reference moisture or acid contents of digested sweet potato slice using a PLS regression analysis to develop a calibration model. Thus, the calibration sample set was used for developing the PLS regression model. A full cross-validation (leave-one-out) method was applied to the calibration set to determine the optimal number of latent variables (LVs). Then, this calibration model was applied to the prediction sample set which consists of 24 samples (corresponding second sweet potato slice from one replicate x 8 digestion times x 3 replicates). The prediction set used for model validation and verification of the prediction performance of the calibration models. The development of the calibration and prediction models were performed using the Prediktera Evince software 2.7.2

(Prediktera AB, Umeå, Sweden). Performance of the calibration and prediction models were evaluated using several statistical parameters, including coefficient of determination (R^2) between measured and predicted value, root mean square error (RMSE) of calibration (RMSEC), RMSE of prediction (RMSEP) and the number of LVs. A good model should have a high R^2 and a low RMSE. In addition to that, a good model also should have a lower number of LVs than the number of samples (Caporaso *et al.,* 2018; Kamruzzaman *et al.,* 2016a, b).

3.3.11 Visualisation and Prediction of the Spatiotemporal Distribution of Acid and Moisture

With the help of the developed PLS models, the total acid and moisture of each pixel in the hyperspectral image were predicted and their spatial distributions were shown with linear color scales. For predicting moisture and acid content in all pixels of the sample, the developed PLS model for each steamed and fried food system was transferred to each pixel of the image. After multiplying the model's regression coefficient by the spectrum of each pixel in the image, a prediction chemical image was built and exhibited the spatial distribution of total acid and moisture of the sample. The resulting chemical images are generally referred to as the "distribution map" (Kamruzzaman *et al.,* 2016a) which was generated using the Prediktera Evince software 2.7.2 (Prediktera AB, Umeå, Sweden).

During the visualisation process, each pixel in the digested food matrix image was assigned to a specific colour from the HSV (hue, saturation, lightness) color space, based on predicted moisture or acid content for that pixel, which facilitates the elucidation of moisture or acid diffusion process. Note that each product model has a different range of moisture or acid distribution during gastric digestion. Instead of using the same color scale for each product model, color scale with different range of moisture or acid content of an individual steamed and fried structure was used to represent hyperspectral images. This helped to clearly identify the spatiotemporal distribution patterns of gastric acid or moisture within the SSP and FSP structure during gastric digestion.

Finally, the predicted spatiotemporal distribution of acid and moisture values of the digested samples were generated. The average acid and moisture content of each sample (average of acid and moisture content of pixel in the ROI) were determined as a function of digestion times using the Evince 2.7.0 hyperspectral image analysis software package (Prediktera AB, Umeå, Sweden).

3.3.12 Acid and Moisture Diffusion Modelling

To study the kinetics and mechanism of acid and moisture diffusion from the selected product models, two different kinetic models were considered to fit the experimental data. The experimental data fitting was carried out using *nlinfit*, a nonlinear regression function in Matlab (R2016a, USA).

Fick's second law

Considering that the model food behaves like an infinite cylinder, a theoretical model (Eq. 3.1) based on Fick's second law was applied, considering the following assumptions: (i) negligible external resistance to mass transfer; (ii) isotropic and homogenous material; (iii) negligible material shrinkage (Crank, 1979). The experimental concentration ratio results were applied to fit the following analytical solution of Fick's second law for obtaining the value of the D_{eff}.

$$Concentration\ ratio\ (CR) = \frac{C_e - C_{(t)}}{C_e - C_0} = \frac{4}{\pi^2} \sum_{n=1}^{\infty} \frac{\pi^2}{R^2 \delta n^2} \exp(-D_{eff}\ t\ {\delta_n}^2) \qquad \text{(Eq. 3.1)}$$

Where CR is the acid or water concentration ratio, $C_{(t)}$ is the concentration of acid or water (mg HCl/g of sample or g H2O/g of sample), C_o is the initial concentration (mg HCl/g of sample or g H2O/g of sample), C_e is the equilibrium concentration (mg HCl/g of sample or g H2O/g of sample), R is the radius of the sample before digestion (m), t is the digestion time (s), D_{eff} is the effective diffusion coefficient (radial direction, m^2/s) and δn are the Bessel function roots (n=100). To prove negligible material shrinkage, the diameter changes after gastric digestion for each food structures were measured, and data are given in Appendix 4.

The power-law model (Ritger-Peppas model)

The mechanism and kinetics of moisture and acid diffusion during gastric digestion were deduced from the fitting of the experimental acid or moisture concentration ratio to the Ritger-Peppas model (Ritger & Peppas, 1987). It is based on the power-law and widely used to describe water diffusion profiles into high-amylose starch tablets (Ghosal *et al.,* 2012; Russo *et al.,* 2007; Thérien-Aubin *et al.,* 2005).

$$CR = \frac{C_e - C_{(t)}}{C_e - C_0} = 1 - kt^n \qquad \text{(Eq. 3.2)}$$

Where t is the digestion time, k is a parameter related to the velocity of the diffusion, and n is the diffusional exponent, which indicates the diffusion mechanism. For cylinders, when n<0.45, the diffusion mechanism can be hypothesized as purely Fickian diffusion. When 0.45<n<0.89, the transport mechanisms are hypothesized to be both Fickian

diffusion and erosion controlled. When the value of n is greater than 0.89, a pure erosion-controlled mechanism is generally observed (Ritger & Peppas, 1987; Russo *et al.,* 2007).

3.3.13 Statistical Analysis

An analysis of variance (ANOVA) was conducted using a 2-factor factorial design to determine differences in acid and moisture uptake during simulated gastric digestion. The factors were food types (SSP, FSP), and digestion time (0–240 min). A Tukey multiple comparison test was implemented to investigate the differences among means when the main effects were significant. The Student's t-test was used to assess differences in Fick's second law and the power-law model parameters. Minitab 17 software was used for statistical analysis.

3.4 Results and Discussion

3.4.1 Choice of Experimental Parameters

Even though the size of sweet potatoes cylinders selected for the diffusion study is larger than the actual size range (0.1 to 5 mm) (Jalabert-Malbos *et al.,* 2007) of particulates what would normally enter the stomach after mastication, it was chosen for easy sample preparation to achieve one-dimensional diffusion process. In addition to that, a larger size sample was required to achieve the objective of the study because the food samples should not completely break down during the 4 hours of gastric digestion period in order to improve the visualisation of the gastric acid and moisture distribution. The maximum digestion time of 240 min was selected to cover residence time for gastric exposure as most solid foods are emptied within 3-4 hours (Gardner *et al.,* 2002). In this study, a mass ratio of 1:10 between the cylindrical sweet potatoes sample and gastric fluid was used, in order to avoid considerably changes in gastric juice volume and pH during the experiments (Kong & Singh, 2011).

3.4.2 Microstructure of the Raw Sweet Potatoes is Influenced by the Cooking Treatment

Representative CLSM and SEM images of raw and cooked sweet potato samples are shown in Figure 3.2. The storage parenchyma of the raw sweet potatoes was found to be composed of polyhedral cells (Figure 3.2 (a) and (d)). Figure 3.2 (a) showed that β-carotene-containing membrane-bound semi-crystalline structures encapsulated in intact cells which is responsible for the orange colour of sweet potato flesh (Tumuhimbise *et al.,* 2009).

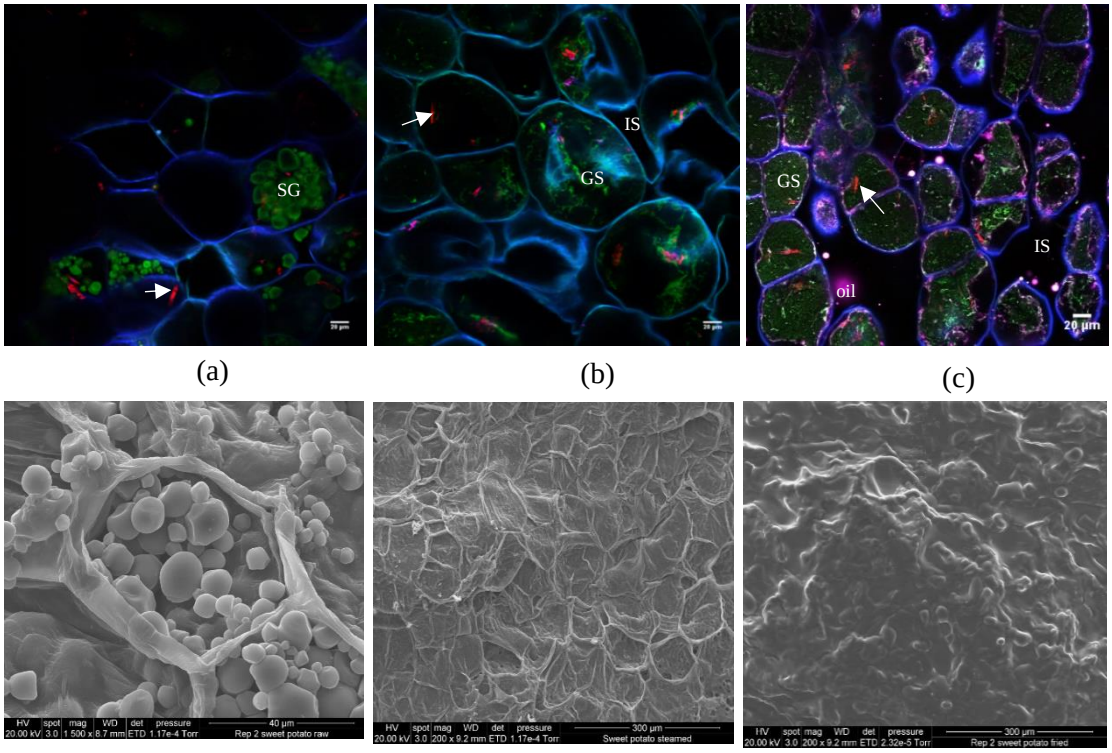

Figure 3.2: CLSM images of (a) raw, (b) steamed and (c) fried sweet potatoes. SEM images of (d) raw, (e) steamed and (f) fried sweet potatoes. "IS" denotes the intercellular spaces, "SG" denotes starch granules, "GS" denotes cells filled with gelatinised starch, "white arrow" denotes β-carotene crystals and "oil" represent the canola oil accumulation in intercellular spaces. The blue colour of CLSM images represent cell walls, magenta (Figure 3.2 (c)) colour represents the oil, green colour of CLSM images reprents other intercellular content including starch granules and red-orange thin strands represent auto-fluorescence carotenoids crystals. The obtained Figure 3.2 (a) and (b) were a combination of images from three channels, namely a differential interference contrast (DIC) microscopy image, an image from the green and blue fluorescence and Figure 3.2 (c) was a combination of four channels including a differential interference contrast (DIC) microscopy image, an image from the red, green and blue fluorescence.

Both SEM and CLSM images further revealed apparent differences in the microstructure of sweet potatoes parenchyma after steaming and frying. The most common structural changes observed with the steaming and frying comprise the starch gelatinisation (absence of starch granules) and cell-cell separation due to degradation of cell wall components including middle lamella (Bordoloi *et al.,* 2012a; Tumuhimbise, *et al.,* 2009). Furthermore, as observed in Figure 3.2 (c), the fried samples showed that the

cells are more separated. As a result, the volume of the intercellular space increased and oil was accumulated in intercellular spaces. In contrast, the steamed samples (Figure 3.2 (b)) had a homogeneous compact structure and showed reasonable preservation of the cell wall outline of the parenchyma tissue. Moreover, the surface microstructural changes of the sweet potato samples due to the cooking effect can be clearly visible using SEM as shown in Figure 3.2 (e) and (f). SSP surface demonstrated smooth cell surfaces and intact cells (Figure 3.2 (e)). In contrast, FSP surface demonstrated wrinkled cell surfaces that represent the crust of the fried matrix (Figure 3.2 (f)).

3.4.3 Moisture and Acid Content of the Cooked Sweet Potatoes is Influenced by the Cooking Treatment

Moisture and acid content were significantly influenced by cooking method, and the digestion time ($p<0.05$, Table 3.3). FSP had a significantly lowest initial moisture compared to the SSP (71.0 % compared to < 83.8 %). FSP exhibited comparatively high acid content than steamed once (0.86 mg HCl/g of the sample compared to < 1.1 mg HCl/g of the sample). Both steamed and fried sweet potatoes had significant increases in moisture and acid content during the 240 min gastric digestion period ($p<0.05$).

3.4.4 Moisture Content Prediction

Table 3.4 shows the main statistics used to evaluate the performance of the developed calibration and prediction models for predicting the moisture content of the examined SSP and FSP samples. Calibration models generated using hyperspectral data with R^2 values of greater than 0.70 can be considered as good enough for prediction purposes (Caporaso *et al.,* 2018; Williams & Sobering, 1996). Thus, it was observed that the PLS calibration models based on full spectra had a very good ($R_{cal}^2>0.70$) (Caporaso *et al.,* 2018; Williams & Sobering, 1996) moisture prediction accuracy for both steamed and fried food matrices, with $R_{cal}^2>0.90$ and RMSEC<0.48 (Table 3.4). The predicted versus measured plots for the best PLS calibration models for moisture content are shown in Figure 3.3. The application of HSI has been reported previously for moisture determination in biological products (i.e. mango, banana and strawberry), demonstrating a similar prediction performance of $R^2\geq0.90$ of PLS regression calibration built on the wavelengths of 400 nm and 1000 nm (ElMasry *et al.,* 2007; Pu & Sun, 2015; Rajkumar *et al.,* 2012).

Table 3.3: Moisture contents (% wet basis) and acid contents (mg HCl/g of sample) of sweet potatoes during 240 min of *in vitro* gastric digestion.

Moisture content (% wet basis)	Digestion time (min)							
	0	10	20	40	60	120	180	240
SSP	83.75 ± 1.44^{Ac}	83.87 ± 0.41^{Ac}	84.90 ± 0.41^{Ab}	85.82 ± 0.21^{Ab}	86.12 ± 0.31^{Ab}	86.67 ± 0.68^{Bb}	87.28 ± 0.61^{Ba}	88.09 ± 0.26^{Ba}
FSP	71.00 ± 5.28^{Bd}	70.46 ± 4.41^{Bd}	75.97 ± 0.60^{Bd}	84.39 ± 1.55^{Abc}	84.85 ± 4.37^{Ab}	89.49 ± 2.00^{Aab}	90.91 ± 7.38^{Aab}	94.34 ± 1.65^{Aa}
Acid contents (mg HCl/g of sample)								
SSP	0.86 ± 0.07^{Be}	0.86 ± 0.04^{Be}	0.88 ± 0.19^{Bed}	1.11 ± 0.06^{Bd}	1.26 ± 0.07^{Bb}	1.20 ± 0.05^{Bcb}	1.34 ± 0.03^{Bb}	1.47 ± 0.06^{Ba}
FSP	1.04 ± 0.23^{Af}	1.25 ± 0.29^{Ae}	1.45 ± 0.27^{Ade}	1.63 ± 0.26^{Ac}	1.77 ± 0.18^{Abc}	1.91 ± 0.26^{Aab}	1.86 ± 0.36^{Aab}	2.25 ± 0.22^{Aa}

A-C Means within each column followed by different superscript letters are significantly different ($p<0.05$).

a-f Means within each line followed by different superscript letters are significantly different ($p<0.05$).

SSP: Steamed sweet potatoes, FSP: Fried sweet potatoes

Values represent averages (n = 3) ± standard deviation (SD).

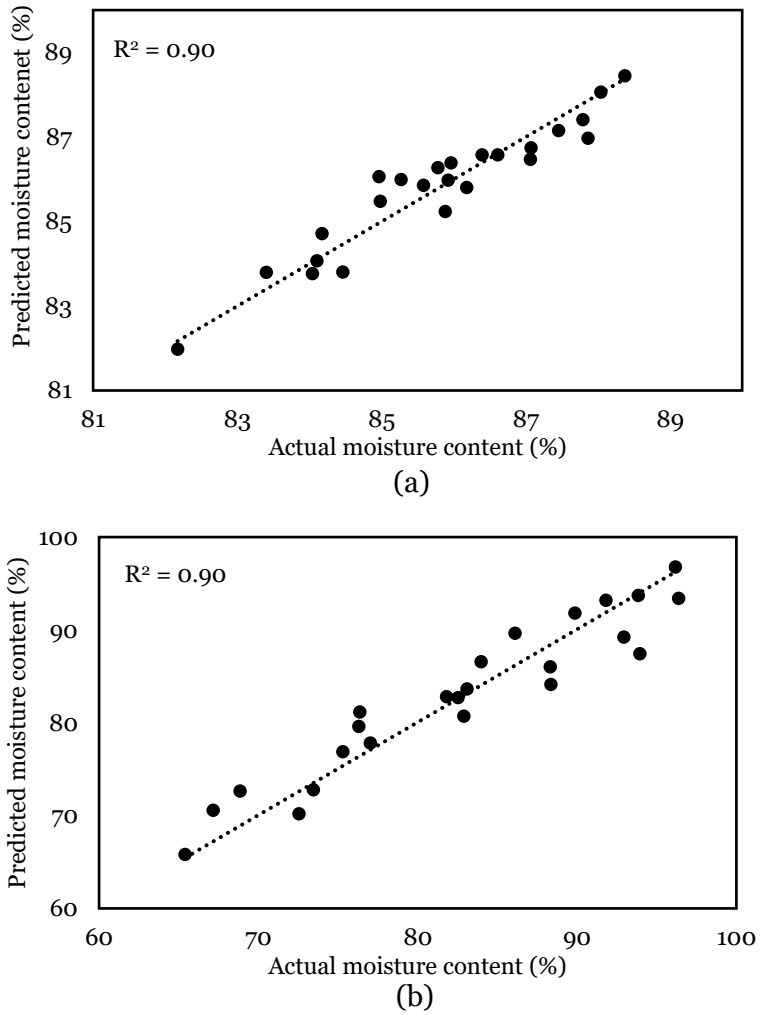

Figure 3.3: Predicted versus measured values of moisture in (a) SSP and (b) FSP for the best PLS models (calibration data set), expressing the moisture content as wet basis. The solid line shows the calibration line of the PLS regression model. Performance of the PLS regression model for moisture indicated as the determination coefficients (R^2).

Table 3.4: Performance of the PLS regression model for moisture content, for HSI quantification on SSP and FSP

		Calibration		Prediction	
	LVs	R_{cal}^2	RMSEC	R_{pred}^2	RMSEP
SSP	4	0.90	0.48	0.87	0.71
FSP	3	0.90	0.27	0.83	0.42

LVs: latent variables. Sample size (n): 24. Spectral range: 550–1700 nm. R_{cal}^2 = coefficient of determination of calibration, R_{pred}^2 = coefficient of determination of prediction, RMSEC = root mean square error of calibration. RMSEP = root mean square error of prediction. SSP: Steamed sweet potatoes, FSP: Fried sweet potatoes.

In this study, all PLS models appeared to be acceptable since not more than four factors (LVs) were used in the development of calibration models (Table 3.4). When the calibrated model was used to predict the samples, the prediction results were also desirable, with a R_{pred}^2>0.83 between the measured and the predicted values for both food types and the RMSEP<0.71 for steamed and fried sweet potatoes (Table 3.4).

3.4.5 Acid Content Prediction

The main statistics used to evaluate the performance of the developed calibration and prediction models for predicting acid content of the examined steamed and fried sweet potatoes samples are given in Table 3.5. The predicted versus measured plots for the best PLS regression models for acid content are shown in Figure 3.4. The performance of the PLS model was good (R_{cal}^2>0.7) (Caporaso *et al.,* 2018; Williams & Sobering, 1996) for acid prediction in SSP (R_{cal}^2 = 0.90) and FSP (R_{cal}^2 = 0.90). It was also demonstrated that all calibrated models had good performance with the low RMSEC<0.15. The R^2 (0.90) of the PLS calibration models obtained in this study was comparable to those reported previously by the application of HSI on vinegar culture to investigate their acid content, with R^2 of the PLS model equal to 0.86 (Zhu *et al.,* 2016). The PLS regression model appeared to be robust since less than four factors (LVs) were used in the calibration model development in SSP and FSP product models (Table 3.5). When the acid calibrated model was applied to the prediction set, the results were applicable with R_{pred}^2>0.80 between the measured and the predicted values and the RMSEP<0.22 for steamed and fried sweet potatoes (Table 3.5).

Table 3.5: Performance of the PLS regression model for acid content, for HSI quantification on SSP and FSP

		Calibration		Prediction	
	LVs	R_{cal}^2	RMSEC	R_{pred}^2	RMSEP
SSP	4	0.90	0.06	0.91	0.07
FSP	4	0.90	0.15	0.80	0.22

LVs: latent variables. Sample size (n): 24. Spectral range: 550–1700 nm. R_{cal}^2 = coefficient of determination of calibration, R_{pred}^2 = coefficient of determination of prediction, RMSEC = root mean square error of calibration. RMSEP = root mean square error of prediction. SSP: Steamed sweet potatoes, FSP: Fried sweet potatoes.

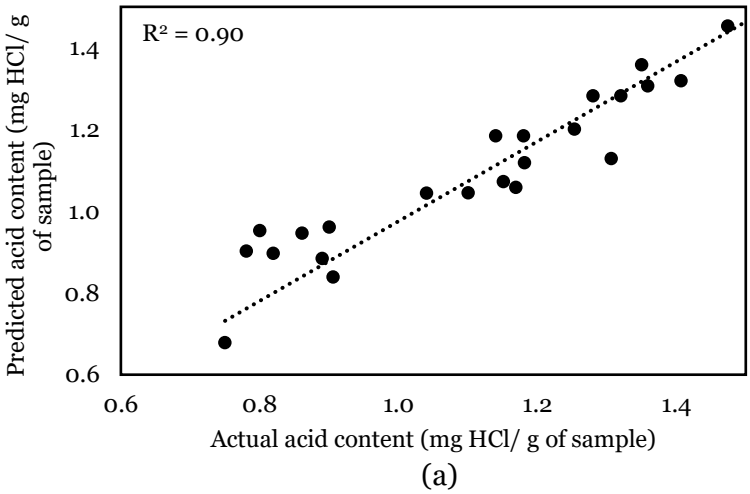

(a)

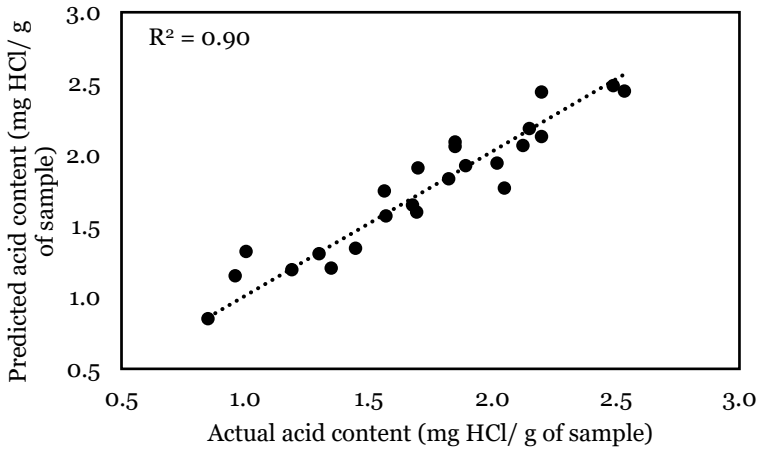

(b)

Figure 3.4: Predicted versus measured values of acid in (a) SSP and (b) FSP for the best PLS models (calibration data set), expressing the acid content as mg HCl/g of sample. The solid line shows the calibration line of the PLS regression model. Performance of the PLS regression model for acid indicated as determination coefficients (R^2).

3.4.6 Spatiotemporal Distribution of Moisture in Sweet Potatoes Structures During Gastric Digestion

The developed PLS regression models for the prediction of moisture in steamed and fried sweet potatoes matrixes were applied to HSI hypercubes to visualise the spatial moisture distribution of digested samples with different digestion times. Figure 3.5 shows the final visualised image of the moisture distribution of selected product models at eight different gastric digestion times. Although there was variation in the distribution in moisture content across the steamed and fried food matrices, there was a general trend of increase in overall moisture content represented by the shift from blue to red (Figure 3.5). This is an indication of sweet potatoes food matrices absorbing moisture during their gastric digestion.

More specifically, the majority of pixels within the SSP before gastric digestion indicated a high and quite homogeneous moisture content (83%) (Figure 3.5 (a)). When the digestion progress, the gastric juice diffusion resulted in an isotropic change of the moisture distribution as evidenced by the shift towards the higher end of the scale (i.e. to red). After 240 min digestion, almost all the pixels were at this end of the scale, corresponding to an average moisture content of 83.3% to 88.2%.

As shown in Figure 3.5 (b), in comparison to steaming, frying created two different regions within the food matrix before digestion: an outer layer corresponding to the crust that could be easily recorded visually, and an interior part or core, in agreement with previous findings (Alam & Takhar, 2016; Sumnu & Sahin, 2008). The crust region showed a uniform moisture distribution, with relatively low moisture content (<50%). In contrast, the inner core was much wetter with a moisture content higher than 80%. During the digestion process, it is noteworthy that the distinction between these two parts (crust and core) persisted for a long time: both regions were still easily distinguished after 120 min of digestion. The diffusion process of gastric juice which can be interpreted as transport in a gradient of concentration, quickly resulted in a very high moisture content (around 90% as soon as 40 min digestion) in the inner core, whereas the crust remained dryer (around 75% after 120 min digestion); even more, moisture content as low as 50% were still locally observed after 180 min digestion. This indicates that the crust might permeable and allow diffusion into the core of the sample. Moreover, compared to the moisture content of FSP (71.0±5.3%), as the SSP (83.8±1.4%) have a higher content of moisture at the start, the moisture concentration gradient between gastric medium and the steamed sweet potato is lower and there is less intense gradient and therefore lower transport of moisture into the product.

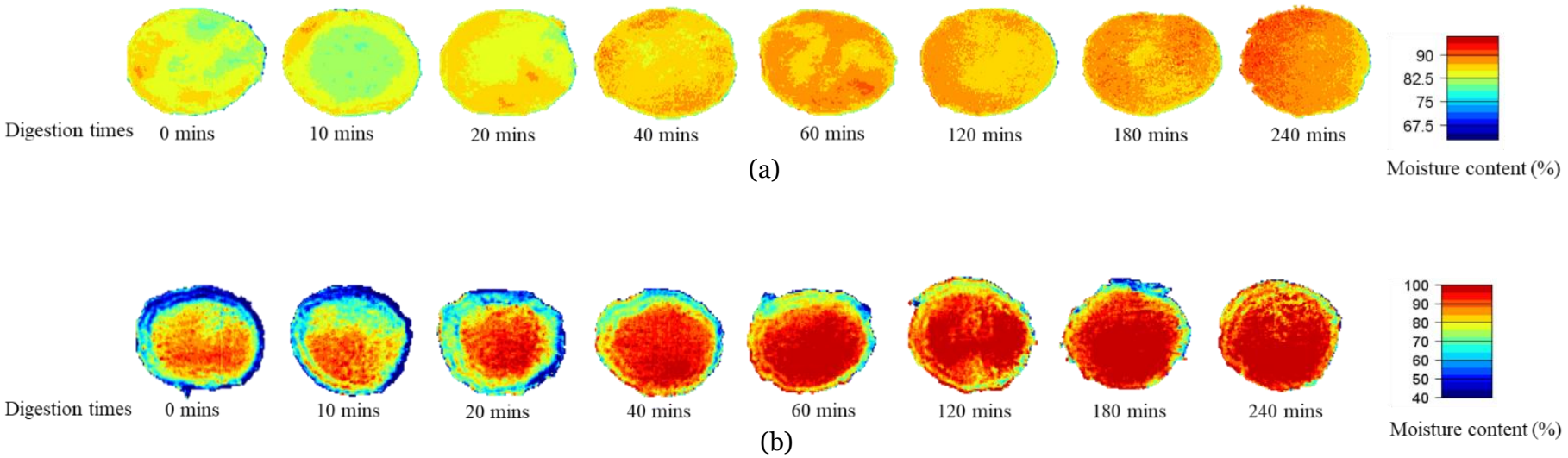

Figure 3.5: Spatiotemporal moisture content distribution maps of (a) SSP and (b) FSP generated by using the optimal PLS models. (Note that the colour scale of an individual sweet potatoes structure represents a different range of moisture (%) content)

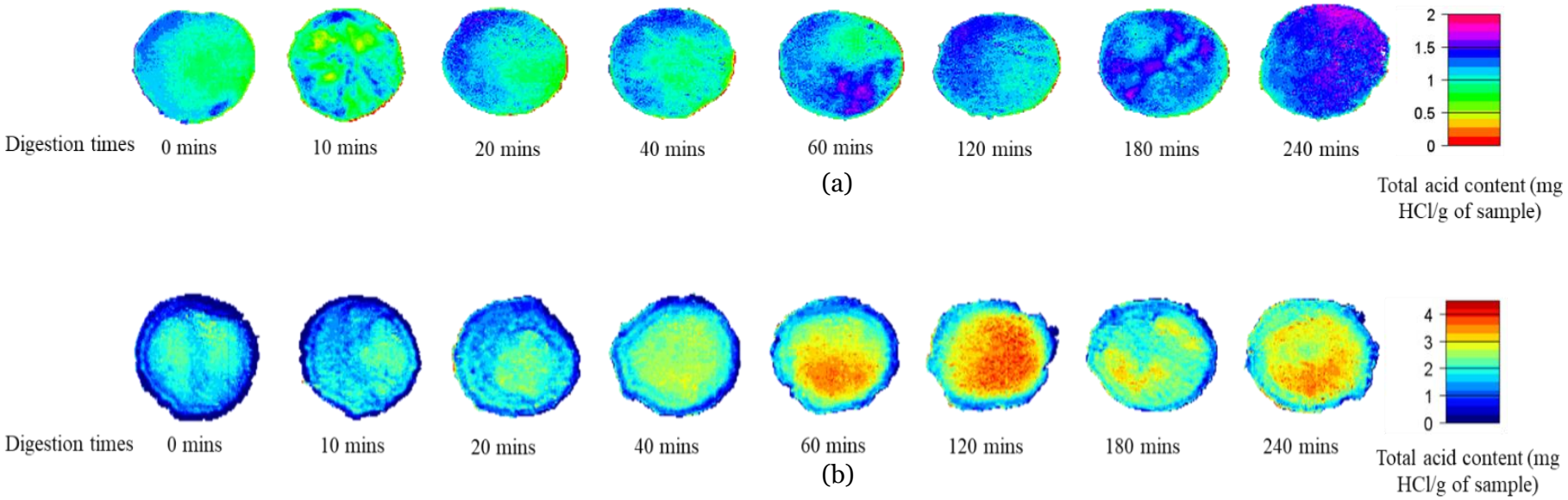

Figure 3.6: Spatiotemporal acid content distribution maps of (a) SSP and (b) FSP generated by using the optimal PLS models. (Note that the colour scale of an individual sweet potatoes structure represents a different range of acid (mg HCl/g of sample) content)

3.4.7 Spatiotemporal Distribution of Acid in Sweet Potatoes Structures During Gastric Digestion

The spatiotemporal distribution of acid in sweet potatoes structures during gastric digestion is displayed in Figure 3.6. A non-uniform acid distribution was observed in non-digested SSP (Figure 3.6 (a)). When immersed in the gastric fluid, gastric acid advanced rapidly and anisotropically to the centre of the sample, as shown by the blue area of the images. This may be due to the inherent variations including irregular pore path distribution within the cooked sweet potato matrix (Mennah-Govela & Bornhorst, 2016b). An uneven acid distribution was observed in non-digested FSP, with lower acid content in the crust region and higher acid content in the middle of the sample (Figure 3.6 (b)). Similar to SSP, upon immersion, a rapid gain of acid was observed in FSP. Moreover, it can be clearly observed that for SSP and FSP, the pattern of water (Figure 3.5 (a) and (b)) and acid (Figure 3.6 (a) and (b)) distribution during gastric digestion were not similar.

3.4.8 Impact of Sweet Potatoes Structures on Diffusion Kinetics of Water During Gastric Digestion

Figure 3.7 illustrates the concentration ratio of moisture uptake into the steamed and fried sweet potatoes structures as a function of digestion time. The *in vitro* moisture gain concentration profiles of different sweet potatoes structures could be expressed by the Fick's second law, as the diffusion model provided a moderate fit for both seamed and fried matrix of the data sets (R^2>0.91). The D_{eff} of gastric moisture was estimated for each sweet potato structure and is shown in Table 3.6.

The sweet potatoes structure significantly affected the diffusion kinetics of moisture during gastric digestion ($p<0.05$). There is a trend that may show a significantly higher effective water diffusivity in SSP (D_{eff} = 2.2±0.8 x10^{-9} m^2/s) than FSP (D_{eff} = 1.9±0.5 x10^{-9} m^2/s). Mennah-Govela and Bornhorst (2016b), reported similar trends of diffusion of water in steamed and fried sweet potatoes during gastric juice diffusion.

To confirm the diffusion mechanism, the data were fitted with the power-law model (Ritger & Peppas, 1987). The model parameters and goodness of fit (R^2>0.94) are shown in Table 3.6. The water diffusion exponent (n) was found to be higher than 0.45 and lower than 0.89 for the steamed and fried sweet potatoes, which implies that the transfer of water did not follow a pure Fickian diffusion behaviour, but rather coupled diffusion and erosion mechanisms in both matrices. Hence, the diffusion of water due to the concentration gradient coupled with the erosion of food structure due to acid hydrolysis of cellular structure (Mennah-Govela & Bornhorst, 2016a, b; Van Wey *et al.,*

2014) might be the predominant mechanisms for the water diffusion in the steamed and fried sweet potatoes during *in vitro* gastric juice diffusion. Thus, the plant cell wall of SSP and FSP can be degraded by the acid contained in the gastric fluid (Mennah-Govela & Bornhorst, 2016a) which facilitates the diffusion of water in gastric fluid.

However, Figure 3.5 (a) and 3.5 (b) illustrate that the hydrolysis of the sweet potato food matrix is not predominant because no significant reduction in the steamed or fried food matrix's shape was observed, even after 4 hours of gastric digestion. In addition to that, the diameter changes of steamed and fried sweet potatoes with digestion time is negligible (Table 1, Appendix 4). This observation is supported by the previous study (Mennah-Govela & Bornhorst, 2016b). These authors reported that although cooked sweet potatoes cubes remained visually intact after 4 hours of digestion, microstructural erosion of the sweet potato matrix (i.e. cell wall separation and cell wall breakdown) after 4 hours of digestion were observed in the center of the cube.

3.4.9 Impact of Sweet Potatoes Structures on Diffusion Kinetics of Acid During Gastric Digestion

The acid concentration ratio data as a function of the digestion time (t) were fitted into the Fick's second law and the power-law models as listed in Eq. 3.1 and Eq. 3.2, respectively (Figure 3.8). The results of the model parameters and the R^2 are listed and compared in Table 3.7. The acid diffusion based on the Fick's second law model provided a good fit for the FSP data set ($R^2>0.97$), apart from SSP ($R^2=0.85$). The sweet potato structures significantly affected the diffusion kinetics of acid during gastric digestion ($p<0.05$). There is a trend of significant ($p<0.05$) faster acid D_{eff} in FSP (D_{eff} = $3.2\pm0.2x10^{-9}$ m^2/s) and slower diffusivity in SSP (D_{eff} = $1.6\pm0.4x10^{-9}$ m^2/s). Microstructure analysis results (Figure 3.2) indicate that open-porous matrix and interconnected pores of the fried samples might facilitate the faster rate of hydrochloric acid diffusion than the compactly dense structure of steamed samples. These results are in agreement with Mennah-Govela and Bornhorst (2016b).

Moreover, it can be observed that for steamed and fried sweet potatoes, the trend of water and acid diffusivity were not equivalent. For example, in FSP the diffusivity of acid (D_{eff} = $3.2\pm0.2x10^{-9}$ m^2/s) was higher than in SSP (D_{eff} = $1.6\pm0.4x10^{-9}$ m^2/s). In contrast, in SSP the diffusivity of water (D_{eff} = 2.2 ± 0.8 $x10^{-9}$ m^2/s) was higher than in FSP (D_{eff} = 1.9 ± 0.5 $x10^{-9}$ m^2/s) during gastric digestion. Similarly, the spatiotemporal distribution patterns of water (Figure 3.5 (a) and (b)) and acid (Figure 3.6 (a) and (b)) were also not equivalent within steamed and fried sweet potatoes. These results are confirmed by the previous study of Mennah-Govela and Bornhorst (2016b). These authors reported that there was not a consistent trend of water and acid diffusivity across

sweet potatoes with different structures, and thus they should be estimated separately. However, the reason for different trends of moisture and acid diffusivity across steamed and fried sweet potatoes are not clear which is merits future investigation.

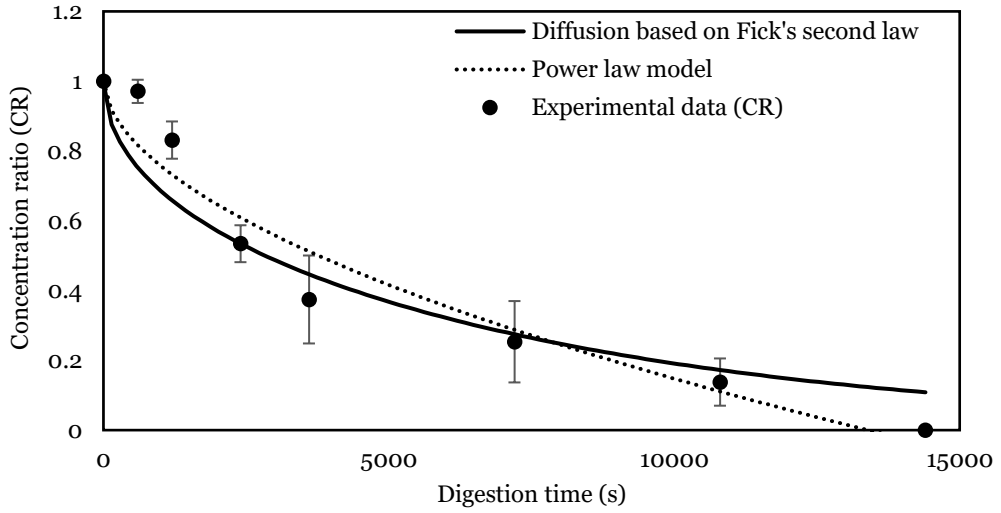

(a)

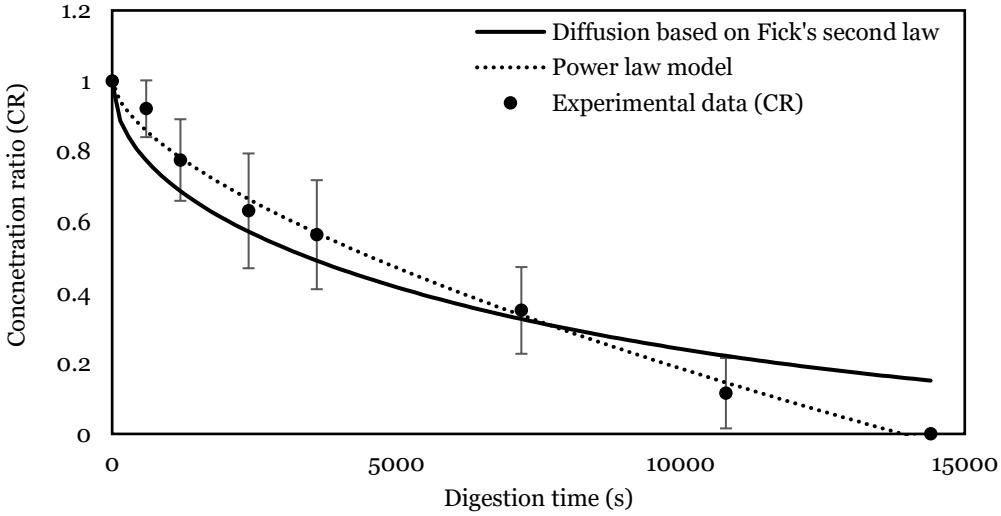

(b)

Figure 3.7: Plots of moisture concentration ratio as a function of digestion time (s) for the (a) SSP and (b) FSP. Circles represent average experimental values (n = 3) and error bars represent the SD of the mean. The prediction of the model of the Fick's second law (Eq. 3.1) and the power-law model (Eq. 3.2) are represented by solid and dashed lines, respectively.

The power-law model had an acceptable R^2 (>0.98) for all the product models. The predicted diffusion behaviour of acid in SSP is both Fickian diffusion and erosion

controlled, whereas the Fickian diffusion should be responsible for the observed acid diffusion behaviour in FSP.

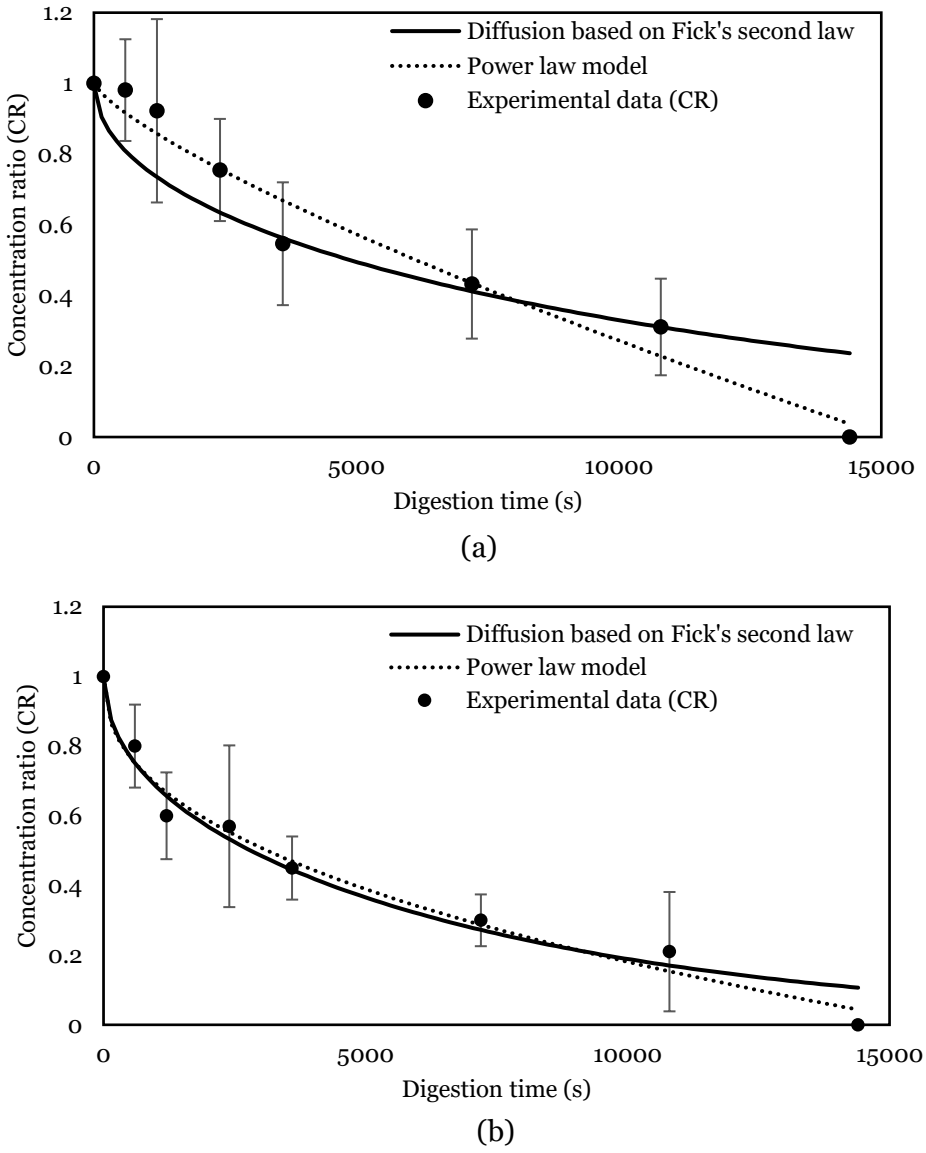

Figure 3.8: Plots of acid concentration ratio as a function of digestion time (s) for the (a) SSP and (b) FSP. Circles represent average experimental values (n = 3) and error bars represent the SD of the mean. The prediction of the model of the Fick's second law (Eq. 3.1) and the power-law model (Eq. 3.2) are represented by solid and dashed lines, respectively.

Table 3.6: The rate of moisture diffusion (k), diffusion exponent (n), diffusion mechanism and effective diffusion coefficients (D_{eff} ± SD of n=3) for water in SSP and FSP.

	Power-law model					Fick's second law model		
	R^2	SSE	k	n	Diffusion mechanism	R^2	SSE	D_{eff} (m^2/s) ± SD
SSP	0.94	0.03	0.006 ± 0.003^{a}	0.56 ± 0.06^{a}	Erosion controlled + Fickian diffusion	0.91	0.08	$2.2\pm0.8x10^{-9a}$
FSP	0.99	0.01	0.003 ± 0.001^{b}	0.62 ± 0.06^{a}	Erosion controlled + Fickian diffusion	0.92	0.06	$1.9\pm0.5x10^{-9b}$

R^2: Coefficient of determination, SSE: Error sum of squares, SSP: Steamed sweet potatoes, FSP: Fried sweet potatoes

a-b Means within each column followed by different superscript letters are significantly different ($p<0.05$).

Table 3.7: The rate of acid diffusion (k), diffusion exponent (n), diffusion mechanism and effective diffusion coefficients (D_{eff} ± SD of n=3) for acid in SSP and FSP.

	Power-law model					Fick's second law model		
	R^2	SSE	k	n	Diffusion mechanism	R^2	SSE	D_{eff} (m^2/s) ± SD
SSP	0.97	0.03	0.0006 ± 0.0003^{b}	0.76 ± 0.044^{a}	Erosion controlled + Fickian diffusion	0.85	0.11	$1.6\pm0.4x10^{-9\,b}$
FSP	0.98	0.01	0.016 ± 0.0120^{a}	0.44 ± 0.05^{b}	Fickian diffusion	0.97	0.02	$3.2\pm0.2x10^{-9\,a}$

R^2: Coefficient of determination, SSE: Error sum of squares, SSP: Steamed sweet potatoes, FSP: Fried sweet potatoes

a-b Means within each column followed by different superscript letters are significantly different ($p<0.05$).

3.4.10 Performance Comparison of the Fick's Second Law and the Power-law Diffusion Models

In this study, the Fick's second law was used to predict the acid and moisture diffusivity within the steamed and fried sweet potatoes whereas the power-law model was used to identify the mechanism of diffusion during gastric digestion. In the power-law model, three types of diffusion mechanisms are proposed; Pure Fick's diffusion, both erosion-controlled and Fick's diffusion and purely erosion-controlled mechanism (Russo *et al.,* 2007; Thérien-Aubin *et al.,* 2005). However, in order to apply for the Fick's second law, the diffusion of moisture or acid should govern by the pure Fickian diffusion with the assumption of negligible shrinkage of the food matrix during digestion (Crank, 1979).

However, the microstructural changes due to the diffusion of gastric acid and moisture is an important aspect of manipulating the rate of gastric acid and moisture diffusivity from different food matrices (Mennah-Govela & Bornhorst, 2016b; Van Wey *et al.,* 2014; Widjaja, 2010). These microstructural changes could modify the acid and enzyme diffusion path during the digestion process and, as a consequence, change the value of the acid and moisture effective diffusion coefficient obtain using the Fick's law models. This fact is supported by the results of this study. Results indicate that both erosion-controlled and Fickian diffusion govern the diffusion of moisture within SSP and FSP and the diffusion of acid within SSP structure during gastric digestion.

Interestingly, if the diffusion mechanism is governed by the erosion-controlled and Fickian diffusion, then the data set was fitted with the Fick's law model with low R^2. For examples, the Fick's law model provided a moderate fit for the diffusion of moisture into SSP and FSP (R^2>0.91) compared to the power-law model (R^2>0.98) because diffusion of moisture into SSP and FSP regulated by both erosion-controlled and Fickian diffusion mechanism. In addition to that, the Fick's law model provided a good fit for the diffusion of acid into FSP (R^2=0.97), with the exception of SSP (R^2=0.85), because diffusion of acid into SSP regulated by the both erosion-controlled and Fickian diffusion mechanism. Therefore, future works should take into account microstructural degradation when modelling the gastric juice diffusion process. In addition to that, elucidation on the specific microstructural changes and subsequent nutrient release that controls the diffusion of gastric juice into differing sweet potatoes matrices is an area that merits future investigation.

3.5 Conclusions

This study is the first reported application of HSI for the prediction of the spatiotemporal distribution of gastric juice within solid food matrixes during *in vitro* gastric juice diffusion process. In this study, the quantitative relationships between hyperspectral data and the reference acid and moisture of digested sweet potatoes samples were successfully developed based on PLS regression with the good prediction performance. These PLS models were applied pixel-wise to the hyperspectral images of the digested samples to produce chemical images for visualising moisture and acid distribution with different digestion times. From the gastric juice mapping results, the overall D_{eff} of hydrochloric acid into FSP (D_{eff} = $3.2x10^{-09}$ m^2/s) is greater than SSP (D_{eff} = $1.6x10^{-09}$ m^2/s). Cooking treatment (steaming and frying) influenced the microstructure of the cooked sweet potatoes. Frying not only dehydrates the samples but also caused a disruption of cell arrangement and the creation of a porous network. These factors can directly contribute to the higher overall diffusivity of hydrochloric acid within the fried samples. In contrast, compact dense microstructure of steamed sweet potatoes leads to a slower overall diffusivity of hydrochloric acid. Moreover, there was not a consistent trend of water and acid diffusivity across sweet potatoes with steamed and fried structures, and thus they must be assessed separately. Overall, the results of this chapter offer convincing evidence that HSI provides more qualitative and quantitative information on the nature of the moisture and acid penetration into solid food structures during the gastric juice diffusion process. However, to better elucidate the gastric fluid diffusion observed in the gastric environment, the proposed HSI can be improved in the future to investigate the pH changes and associated macro- and microstructural changes in digested sweet potatoes matrix while diffusion of gastric fluid.

Chapter Four

4. Characterisation of Microstructural Changes and Nutrient Release in Steamed and Fried Sweet Potatoes during Static *In Vitro* Gastric Digestion*

4.1 Abstract

β-carotene from sweet potatoes have been shown to play an important role in the prevention of vitamin A deficiency, but little is known about their bioaccessibility in the stomach. The aim of this chapter was to characterise the microstructural changes and β-carotene release in steamed sweet potatoes (SSP) and fried sweet potatoes (FSP) due to the diffusion of gastric juice into the food structures during static *in vitro* gastric digestion. Steamed and fried sweet potatoes cubes (5 cm^3) underwent static *in vitro* digestion by incubation in simulated oral and gastric fluids at different time intervals for up to 240 min. Although the gross structure of SSP and FSP cubes was found to be relatively unaffected by *in vitro* gastric digestion, based on the findings of light microscopy and scanning electron microscopy, at the cellular level, some cell-wall separation and loss of intercellular content were observed. Transmission electron microscopy provided a closer look on the changes in cell walls after gastric digestion and loss of the middle lamella and destruction of cell walls were evident in both SSP and FSP. Cellular breakdown of cooked sweet potatoes microstructure associated with the diffusion of gastric acid helping to significantly increase the release of ß-carotene from steamed and fried sweet potatoes with the gastric digestion time. However, cooking treatment (steaming and frying) may not influence the release of ß-carotene from sweet potatoes during static *in vitro* gastric digestion. In both steamed and fried sweet potatoes, cellular degradation was mainly observed at the food surface compared to the interior matrix. Thus, surface erosion of cellular structure is possibly the underlying mechanism of ß-carotene release during static *in vitro* gastric digestion.

*Part of chapter four submitted as a peer-reviewed paper: Somaratne, G., Ferrua, M. J., Ye, A., Nau, Dupont, D., Singh, R. P. and Singh, J. (2020). Role of biochemical and mechanical disintegration on β-carotene release from steamed and fried sweet potatoes during *in vitro* gastric digestion. *Food Research International*, Submitted.

4.2 Introduction

β-carotene is the predominant natural pigments principally responsible for the characteristic deep-orange colour of sweet potatoes (Bengtsson *et al.,* 2010; Tumuhimbise *et al.,* 2009). It has attracted considerable attention as epidemiological evidence continues to suggest that it may provide protection against cancers and other degenerative diseases (Low, D'Arcy, & Gidley, 2015). This could be due to its biological and physicochemical properties, especially related to its effects as a natural antioxidant and its provitamin A activity (Low *et al.,* 2015; Schweiggert *et al.,* 2014).

Orange-fleshed sweet potatoes and related products are one of the major sources of β-carotene compounds in the human diet and they can be an efficient way to deal with Vitamin A Deficiency (Islam *et al.,* 2016). β-carotene is physically encapsulated within the parenchyma cells of sweet potato tubers (Mennah-Govela & Bornhorst, 2016a, b). Thus, bioaccessibility of carotenoids requires the breaking down of cell walls and preceding release from the food matrix during food processing and/or digestion for subsequent absorption of the small intestine (Mennah-Govela & Bornhorst, 2016b; Tumuhimbise *et al.,* 2009).

Mastication is often the first step of food disintegration, where the process of breaking down solid foods into smaller particle sizes and forming a food bolus (Chen, 2009, 2015). Then food bolus is transported through the esophagus to the stomach. The stomach is the major compartment where the size of food particulates is reduced after oral mastication (Kong & Singh, 2008a). During gastric digestion, mechanical and biochemical breakdown of food bolus occur due to both stomach contractions and gastric secretions, respectively (Bornhorst & Singh, 2014). The diffusion of gastric juice into the food matrix is one of the key parameters that leads to biochemical degradation and subsequent nutrient release from plant-based food structures during the gastric phase (Mennah-Govela & Bornhorst, 2016a, b). However, there is still a limited understanding of the contribution of hydrochloric acid to the structural breakdown of food and the consequent mechanism of nutrient release during gastric digestion. Kong and Singh (2009a), reported the microstructural breakdown of almond tissue due to the diffusion of hydrochloric acid and acid hydrolysis during the simulated *in-vitro* gastric environment. Moreover, the same research group described the solid release kinetics of carrots in a simulated gastric environment, as an indicator of nutrient release due to the diffusion of gastric fluid (Kong & Singh, 2011).

Previous studies provide evidence that the cooking methods of sweet potatoes such as boiling, steaming, frying, and microwave steaming would induce structural changes in sweet potatoes (Mennah-Govela & Bornhorst, 2016a, b). These structural

modifications play a predominant role in physicochemical changes such as food matrix softening, matrix swelling, cell-cell separations, cell wall breakdown and solid release as a result of *in vitro* gastric digestion (Mennah-Govela & Bornhorst, 2016a, b). During simulated or real gastric digestion, the physical barriers such as cell wall to the release of β-carotene from sweet potatoes cells may be ruptured (Bengtsson *et al.,* 2010). However, gastric juice penetration effects on β-carotene release from sweet potatoes have not been reported. Moreover, the changes in microstructural properties such as cell wall degradation, cell-cell separation and pore size distribution of sweet potatoes due to the diffusion of the gastric juice has received less attention. These microstructural properties are very important in modelling nutrient release kinetics during gastric digestion process (Mennah-Govela & Bornhorst, 2016b). To bridge the aforementioned knowledge gap, the objective of this chapter 4 was to characterise the microstructural degradation and subsequent release of β-carotene in steamed and fried sweet potatoes during static *in vitro* gastric digestion.

4.3 Materials and Methods

4.3.1 Materials

Orange-fleshed sweet potatoes and canola oil were purchased from a local supermarket in Palmerston North, New Zealand. To reduce the influence of possible variations among the initial samples, the same batch of sweet potatoes was used for the entire analysis. Pepsin (from porcine gastric mucosa, ≥ 250 U/mg solid), gastric lipase (from *Aspergillus niger*≥120,000 U/mg solid) and α-amylase (from *Aspergillus oryzae*, ≥30 U/mg) were purchased from Sigma–Aldrich, USA. Standard of β-carotene Type I (95% purity, UV) was obtained from Sigma Aldrich. All other chemicals were of analytical grade. The simulated salivary fluid (SSF) and simulated gastric fluid (SGF) were prepared using the electrolyte stock solutions according to the harmonized protocol within the INFOGEST Network (Minekus *et al.,* 2014) described in section 3.3.4.

4.3.2 Sweet Potato Sample Preparation and Cooking

Orange-fleshed sweet potatoes were peeled with a hand-peeler and cut into strips using a DiTo-Sama® vegetable slicer and dicer machine, followed by cutting the strips into cubes (approximately 5 mm^3) using a sharp knife. Any strips containing curve surfaces were discarded and cubes were only selected from the interior of the sweet potato tuber. The size of the orange-fleshed sweet potatoes cubes was selected to be 5 mm in length, width and thickness, which is more or less similar to the upper limit of the

actual size range of raw vegetable particulates after oral mastication (Hoebler, 2000; Jalabert-Malbos *et al.,* 2007).

SSP were prepared according to the method described by Drechsler and Ferrua (2016). Prior to steaming, water was placed at the bottom of the steam cooker and heated up to boiling over 15 min. The temperature of the generated steam reached up to 100±3 ◦C. Then, 50 g of sweet potato cubes were steamed over 1500 mL of boiling water using a steamer pot (25 cm diameter) with a 1.5 mm stainless steel sieve mesh for 5 min and then removed.

The frying method adopted in this study is a method that is typically used in the production of deep-fried potato chips (Farinu & Baik, 2007). Initially, the canola oil was filled in a Breville Deep Fryer and pre-heated to 180±2 °C before frying. Then, 50 g of sweet potato cubes were placed in a wire mesh basket, which was immersed in the oil for 1.5 min, after the set temperature was reached. A thermocouple was kept inside the frying container during cooking to measure the temperature profile over time to ensure similar cooking conditions for each batch. After frying, the batch of samples was taken out of the oil and allowed to drain for 3 min before blotting off the surface oil using an absorbent paper.

Preliminary studies were conducted by changing different steaming and frying time in order to get the similar initial composition and microstructure of steamed and fried sweet potato cylinders (described in the section 3.3.2), respectively (Details are given in Appendix 1 and 2).

4.3.3 Static *In Vitro* Digestion

SSP and FSP samples were digested according to the harmonized INFOGEST protocol (Minekus *et al.,* 2014) as described in section 3.3.5. Briefly, either steamed or fried orange-fleshed sweet potatoes cubes (5 g) sample was mixed with 4 mL of pre-heated (37 °C) SSF electrolyte stock solution. Then 0.5 mL salivary α-amylase solution of 1500 U/mL, 25 µL of 0.3 M $CaCl_2$ $(H_2O)_2$ and 975 µL of water were added and thoroughly mixed. The sample was incubated for 2 minutes at 37°C at 50 rpm in a shaking water bath (BS-11, Lab Companion).

After the oral phase, the sample was mixed with 7.5 mL of previously warmed (37 °C) SGF electrolyte stock solution and 5 µL of 0.3 M $CaCl_2$ $(H_2O)_2$. The pH was adjusted to 3.0 with 1 M HCl. Then, 1.6 mL porcine pepsin stock solution (2000 U/mL in the final mixture) and 1.0 mL lipase (120 U/mL in the final mixture) was added and the volume was adjusted to 20 mL with water. The sample was incubated at 37 °C at 50 rpm in a shaking water bath (BS-11, Lab Companion).

The individual sample was used for each replicate of each digestion time. Thus, 24 samples from one cooking treatment (either steamed or fried) were prepared according to the above procedure and placed into the shaking water bath at 37 °C at 50 rpm and incubated at different time intervals up to 4 hours (0 min – control sample, 10 min, 20 min, 40 min, 60 min, 120 min, 180 min, and 240 min). The order in which the samples were digested *in vitro* was randomised. After static *in vitro* digestion samples were immediately analysed for their β-carotene release and microstructural changes (as described below).

4.3.4 Scanning Electron Microscopy

SEM was done to determine the changes of the surface microstructure of SSP and FSP after gastric digestion. Immediately after each digestion time, sweet potato samples were snap-freeze using liquid N_2 and freeze-dried. The freeze-dried samples were mounted on the stub and sputter-coated with gold in a sputter coater (SCD 050, Balzers, Liechtenstein). As shown in Figure 4.1, the digested surface of the cube was viewed using a scanning electron microscope (FEI Quanta 200 FEI Electron Optics, Eindhoven, The Netherlands) at an accelerating voltage of 20kV at different magnifications and representative images were selected.

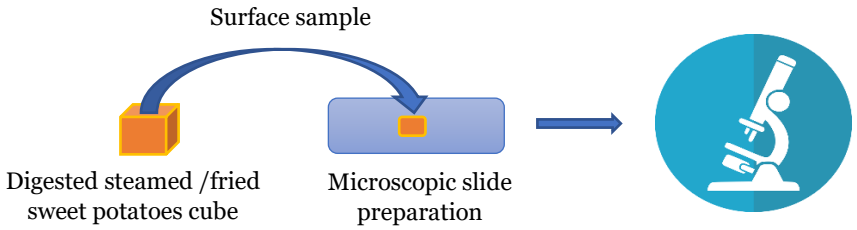

Figure 4.1: Schematic representation of sample preparation for SEM

4.3.5 Light Microscopy and Transmission Electron Microscopy

The cross-sections of both steamed and fried sweet potato cubes before and after simulated digestion were determined using LM and TEM (Figure 4.2).

Samples were pre-fixed in Modified Karnovsky's Fixative (3% Gluteraldehyde (v/v) 2% Formaldehyde (w/v) in 0.1M Phosphate Buffer (pH 7.2)) for at least 2 hours. The sample was then washed thrice, 10 min each, with 0.1 M phosphate buffer (pH 7.2) and secondarily fixed in 1% Osmium Tetroxide in 0.1 M phosphate buffer for one hour. Then, samples were rinsed again three times with 0.1 M Phosphate Buffer (pH 7.2) and dehydrated through a graded acetone series (25%, 50%, 75%, 95%, 100%) for 10-15 min

each, and three changes of 95% acetone for 10 min each, followed by two changes of 100% acetone for one hour each. The samples were then put into 50:50 resin:acetone and placed on the stirrer overnight. This was replaced by fresh 100% resin (Procure 812, ProSciTech Australia) for 8 hours on the stirrer. This step was repeated twice more (overnight in 100% resin, 8 hours in 100% resin). Samples were then embedded in moulds with fresh resin and cured in a 60°C oven for 48 hours. For the light microscopy, sample sections were cut at 1 micron using a glass knife on the ultramicrotome (Leica EM UC7, Germany) and heat fixed onto glass slides. These were stained with 0.05% Toluidine Blue for approximately 12 seconds and viewed under the light microscope (Zeiss Axiophot Microscope with Differential Interference Contrast Optics and Colour CCD camera, Germany).

For the sample preparation of TEM, the block was trimmed down to the selected area and cut using a Diamond Knife (Diatome, Switzerland) at 100 nm. These were stretched with chloroform vapour and mounted on a grid using a Quick Coat G pen (Daido Sangyo, Japan). Grids were stained in Saturated Uranyl Acetate in 50% Ethanol for 4 min, washed with 50% ethanol and MilliQ water and then stained in Lead Citrate (Venable and Coggeshall, 1965) for a further four minutes. This was followed by a wash in MilliQ water. Samples were viewed using a transmission electron microscopy (FEI Tecnai G2 Spirit BioTWIN, Czech Republic).

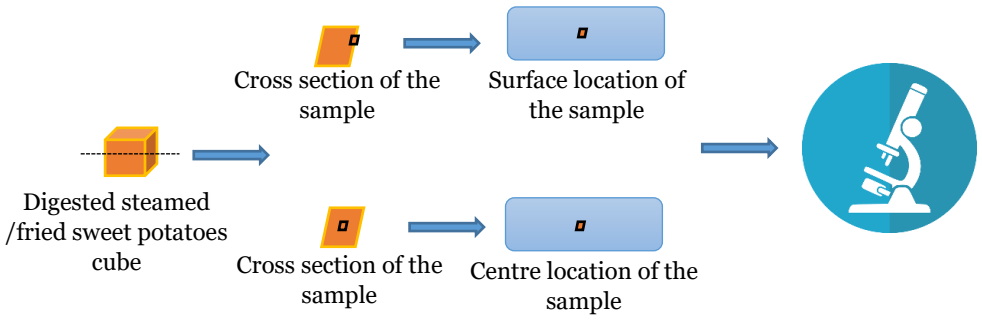

Figure 4.2: Schematic representation of sample preparation for LM and TEM

4.3.6 Analysis of β-carotene Release during Gastric Digestion

Fried and steamed sweet potato samples were subjected to simulated digestion (oral and gastric phase) as described by section 4.3.3. Immediately after each digestion time, sweet potato samples were snap-freeze using liquid N_2 and stored at −80 °C. Then the dry matter content of digested samples was obtained by freeze-drying and powdered using a coffee grinder and passed through a 0.2 mm mesh. All samples were stored in dark conditions for analyses. The sample preparation procedure was also made in dim light.

Standard preparation: The standard β-carotene stock solution at 1 mg/mL concentration was prepared by dissolving standard in acetone. The working standard solutions of 16, 8, 4, 2, 1 and 0.50 mg/mL were prepared. All solutions were protected against the light with aluminium foil.

Extraction of β-carotene after digestion and analysis: Remaining β-carotene was extracted from digested sweet potato samples as described by Biswas, Sahoo, and Chatli (2011). For β-carotene extraction, 0.5 g of freeze-dried each digested sweet potato sample was accurately weighed in a glass test tube. Then, 5 mL of acetone was added to it, and the tube was held for 15 min with occasional shaking, vortex at high speed for 10 min, and finally centrifuged at 1370 g for 10 min. The supernatant was collected into a separate test tube, and the remaining ß-carotene compound was re-extracted (until it gives a colourless residue) with 5 mL of acetone followed by centrifugation once again as above. Both of the supernatants were pooled together and then passed through the Whatman filter paper No. 42 into 25 mL volumetric flask. The carotenoid extract was then made up to 25 mL using acetone. The absorbance of the extract was determined at 449 nm wavelength in a UV-Vis spectrophotometer. A cuvette containing acetone was used as a blank to calibrate the spectrophotometer to the zero points. β-carotene release (%) was calculated as follows.

$$\beta\text{-carotene release (\%)} = ((\beta_o - \beta_t)/\beta_o) \times 100 \qquad \text{(Eq. 4.1)}$$

Where β_o is initial β-carotene (Total β-carotene μg/g dry matter) and β_t (Total β-carotene μg/g dry matter) is the remaining β-carotene content after digestion time t.

4.3.7 Modelling the Kinetics of β-carotene Release over Digestion Time

The experimental β-carotene release data were fitted with the Weibull distribution function and the power-law mathematical models using Matlab (R2016a, Mathworks, Natick, MA, USA), as described below. Coefficient of determination (R^2) and the error sum of squares (SSE) were used to determine the quality of the goodness of fit.

The Weibull model: The Weibull distribution function, widely used to describe drug dissolution and nutrient release kinetics during *in vitro* analysis (Carbinatto *et al.,* 2014; Kong & Singh, 2011), was used to model the β-carotene release during static *in vitro* gastric digestion.

$$\beta\text{-carotene release (\%)} = 1 - e^{-kt(\beta)} \qquad \text{(Eq. 4.2)}$$

Where k defines the time scale of the process (min^{-1}) associated with the rate constant of β-carotene release and β is a shape parameter that characterises the shape of the release

curves (Kong & Singh, 2011). The half-time ($t_{1/2}$), the time to reach 50% loss of total β-carotene, was calculated as the following equation.

$$t_{(\frac{1}{2})} = \left(\frac{-\ln 0.5}{k}\right)^{\frac{1}{\beta}} \qquad \text{(Eq. 4.3)}$$

The power-law (Krosmeyer-Peppas) model: In order to gain some insight into the β-carotene release rate and mechanism from the steamed and fried sweet potatoes during static *in vitro* gastric digestion, a very simple and semi-empirical equation to describe drug release from polymeric systems, the power-law model (Krosmeyer-Peppas model), was applied (Carbinatto *et al.,* 2014; Sankalia, Sankalia, & Mashru, 2008; Sriamornsak, Thirawong, & Korkerd, 2007).

$$\text{β-carotene release (\%)} = kt^n \quad \text{(Eq. 4.4)}$$

In this equation, k is the rate constant and n is the release exponent, indicative of the mechanism of the β-carotene release. When the exponent n assumes a value of $n<0.5$, the β-carotene release mechanism can be hypothesized as purely Fickian diffusion. When $0.5<n<1.0$, the β-carotene release mechanisms are hypothesized to be both Fickian diffusion and erosion controlled. When the value of n is greater than 1.0, a pure erosion-controlled mechanism is generally governed the β-carotene release mechanism (Sriamornsak *et al.,* 2007).

4.3.8 Statistical Analysis

An ANOVA was conducted using a 2-factor factorial design to determine differences in β-carotene release during static *in vitro* gastric digestion. The factors were cooking treatment (SSP and FSP), and digestion time (0-240 min). The Tukey test was used to analyse the differences between means and statistical significance was assessed at a level of $p<0.05$. The student t-test was used to assess differences in the β-carotene release model parameters. Minitab 17 software was used for statistical analysis.

4.4 Results and Discussion

4.4.1 Surface Microstructure of the Cooked Sweet Potatoes is Influenced by the *In Vitro* Gastric Digestion

The surface microstructural changes of the sweet potato samples due to the gastric digestion effect can be clearly visible using scanning electron micrographs as shown in Figures 4.3 and 4.4. Non-digested steamed sweet potato (Figure 4.3(a)) surface demonstrates smooth cell surfaces and the starch granules were gelatinised with water absorption and were expanded (the starch granules swollen and fused together). During frying, the temperature gradient between the sweet potato and the oil caused water loss and oil uptake in the cubes and eventually led to a compact, wrinkled and oil-immersed surfaces (Figure 4.4(a)). Other researchers have reported similar morphologies in cooked potatoes (Bordoloi *et al.,* 2012a; Pedreschi *et al.,* 2008). The microstructure changes of potatoes with steaming and frying cooking methods during simulated *in vitro* digestion were shown in Figures 4.3 and 4.4, the surface structures of cooked sweet potatoes after digestion were significantly changed in all types of cooking methods. However, the possibility of some artifacts produced due to freeze-drying cannot be ruled out. When the digestion progress, the surface microstructure of digested sweet potatoes (both fried and steamed) showed many opened and ruptured cells, as well as many cells, lost their cellular contents as a result of gastric digestion. There were apparent differences (mainly surface microstructural degradation) in between the surface microstructure of steamed and fried sweet potatoes after the similar gastric digestion time (i.e. Figure 4.3 (b,c,d,e,f,g and h) verses Figure 4.4 (b,c,d,e,f,g and h)).

4.4.2 Cellular Structure of the Cooked Sweet Potatoes is Influenced by the *In Vitro* Gastric Digestion

LM was used to observe the microstructural changes of the cross-sections of steamed and fried sweet potato cubes after simulated gastric digestion. Figures 4.5, 4.6 and 4.7, 4.8 show the centre and surface of SSP and FSP samples, respectively. SSP parenchyma cells (Figure 4.5 (a) and 4.6 (a)) were observed to be completely filled with gelatinised starch matrix after steaming, which is in agreement with the results reported by previous studies (Bordoloi *et al.,* 2012a). The images in fried samples (Figure 4.7 (a) and 4.8 (a)) show that the cells are more separated and cell arrangement was extensively disrupted. As a result, the volume of the intercellular space increased and oil was accumulated in intercellular spaces after frying compared to the SSP. Thus, the microstructure of sweet potatoes is significantly influenced by the method of

cooking/processing. Changes in the mechanical properties and integrity of cell walls of potato and sweet potato tubers during cooking are mainly attributed to the changes affecting cell wall and middle lamella components (Bordoloi *et al.,* 2012; Tian *et al.,* 2016). The middle lamella is mainly composed of pectin (structural heteropolysaccharide) that has been reported to degrade during thermal processing (Bordoloi *et al.,* 2012a, b). Although the cooked sweet potato cubes remained visually intact and not completely break down after 4 hours of static *in vitro* gastric digestion, LM images demonstrate that the microstructure of sweet potatoes is significantly influenced by simulated gastric digestion. All these digested steamed and fried sweet potato samples show that before digestion, the cells are complete and without breakage, however after diffusion of gastric juice, cell wall breakage can be observed in the centre (Figures 4.5 and 4.7) and surface location (Figures 4.6 and 4.8) of both of SSP (Figures 4.5 and 4.6) and FSP (Figures 4.6 and 4.8). More broken cells and the empty cells can be observed in the surface area of both steamed and fried sweet potatoes compared to the centre, which is the first site that contact with gastric juice (Figures 4.6 and 4.8). These figures also demonstrate that intracellular solid contents including β-carotene within the first few surface cellular layers were lost during digestion. However, the possibility of some artefacts produced due to the sweet potato sample preparation for the microscopy analysis. FSP show very limited cell wall degradation in the centre of digested cubes after simulated gastric digestion (Figure 4.7) compared with SSP (Figure 4.5). However, gaps between cells and more intercellular and intracellular spaces can be observed after digestion in FSP, which may be due to the looser structure of fried potatoes than steamed ones.

Transmission electron micrographs provide a closer look at the changes in SSP and FSP microstructure after simulated gastric digestion. Loss of the middle lamella (pectin) and cell separation were observed, and the cell wall degradation and breakage were clearly seen in both steamed and fried sweet potato cylinders after *in vitro* static gastric digestion (Figure 4.9). The degradation of the cell wall may be related to the acidic environment of the gastric juice and the hydrochloric acid was capable of hydrolyse the pectin in the cell wall (Kong & Singh, 2011). According to Kong and Singh (2009a, 2011), the cell wall degradation may be the most important mechanism for the release and digestion of intracellular content by creating the pathways through which the enzyme and acid can access to the intracellular lipid and proteins contents by breaking the cell walls. However, it is important to note that the majority of the cells located in the centre of the sweet potato cubes stayed intact after 4 hours of static *in vitro* gastric digestion. This showed that gastric acid had no major effect on the complete breakdown of steamed/fried sweet potato cell walls even after 4 hours of gastric digestion.

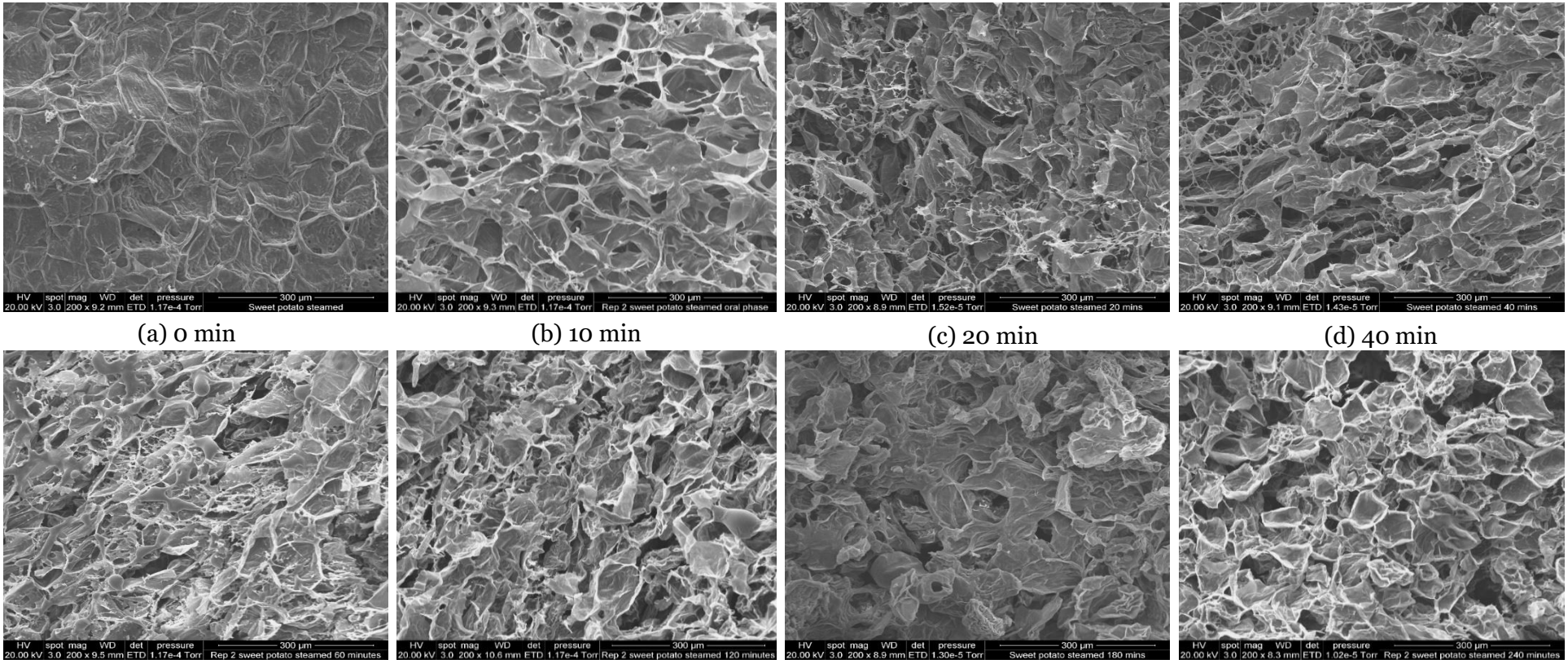

(a) 0 min (b) 10 min (c) 20 min (d) 40 min

(e) 60 min (f) 120 min (g) 180 min (h) 240 min

Figure 4.3: Surface microstructure changes of SSP during simulated *in vitro* gastric digestion. (a) Before digestion (0 min), Samples were taken after (b) 10min, (c) 20 min, (d) 40 min, (e) 60 min, (f) 120 min, (g) 180 min and (h) 240 min of gastric digestion. As artefacts produced by freeze-drying are present, these micrographs do not necessarily represent the structure prior to freeze-drying.

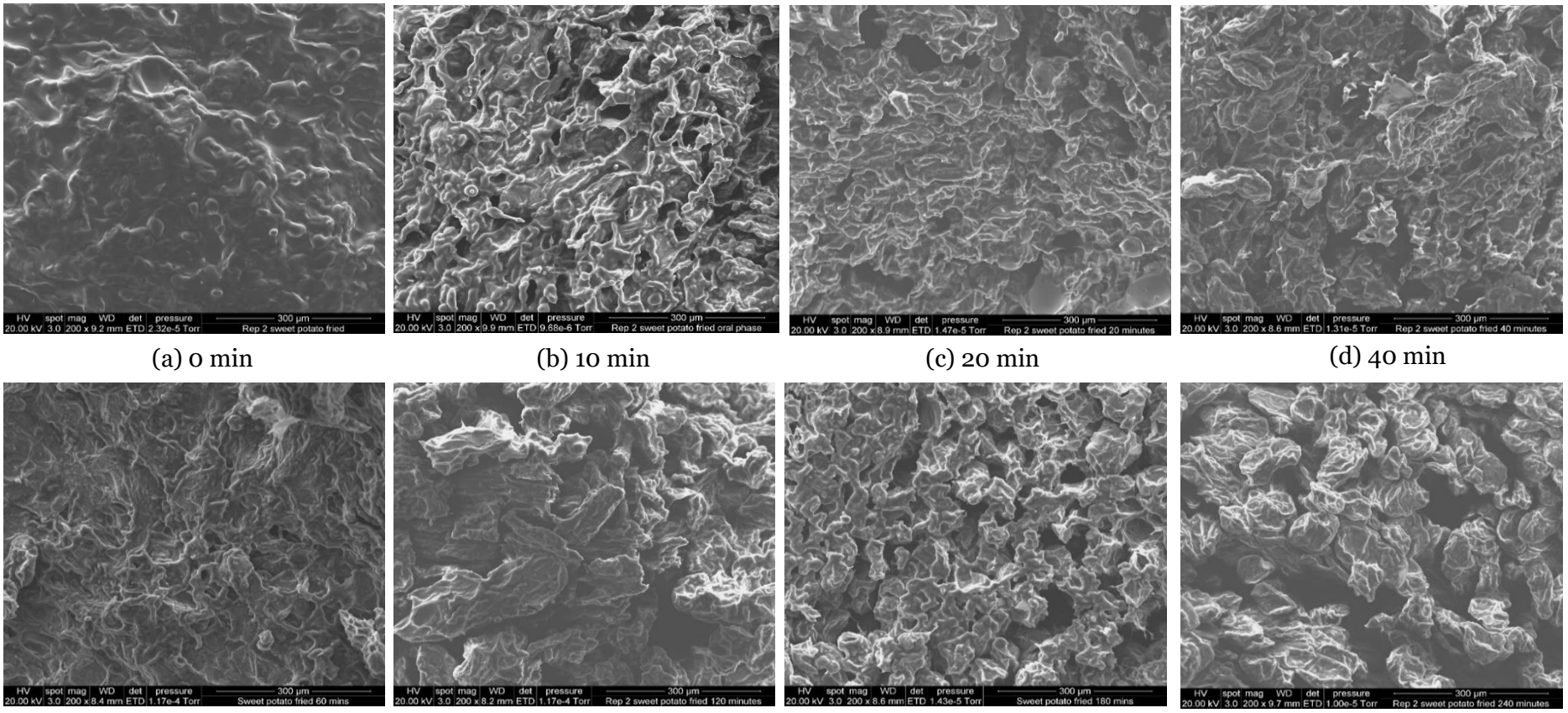

(a) 0 min (b) 10 min (c) 20 min (d) 40 min

(e) 60 min (f) 120 min (g) 180 min (h) 240 min

Figure 4.4: Surface microstructure changes of FSP during simulated *in vitro* gastric digestion. (a) Before digestion (0 min), Samples were taken after (b) 10min, (c) 20 min, (d) 40 min, (e) 60 min, (f) 120 min, (g) 180 min and (h) 240 min of gastric digestion. As artefacts produced by freeze-drying are present, these micrographs do not necessarily represent the structure prior to freeze-drying.

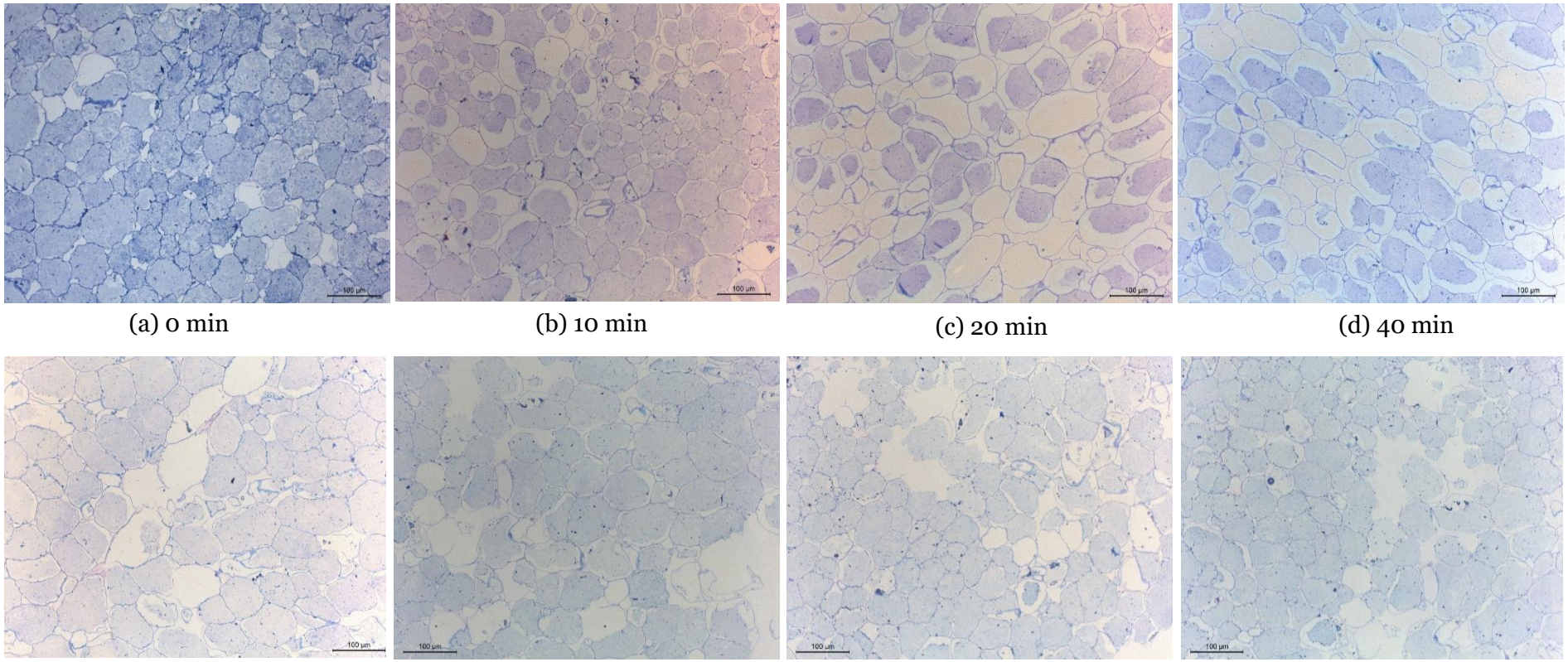

(a) 0 min (b) 10 min (c) 20 min (d) 40 min

(e) 60 min (f) 120 min (g) 180 min (h) 240 min

Figure 4.5: Centre location of microstructure changes of SSP during simulated *in vitro* gastric digestion. (a) Before digestion (0 min), Samples were taken after (b) 10min, (c) 20 min, (d) 40 min, (e) 60 min, (f) 120 min, (g) 180 min and (h) 240 min of gastric digestion.

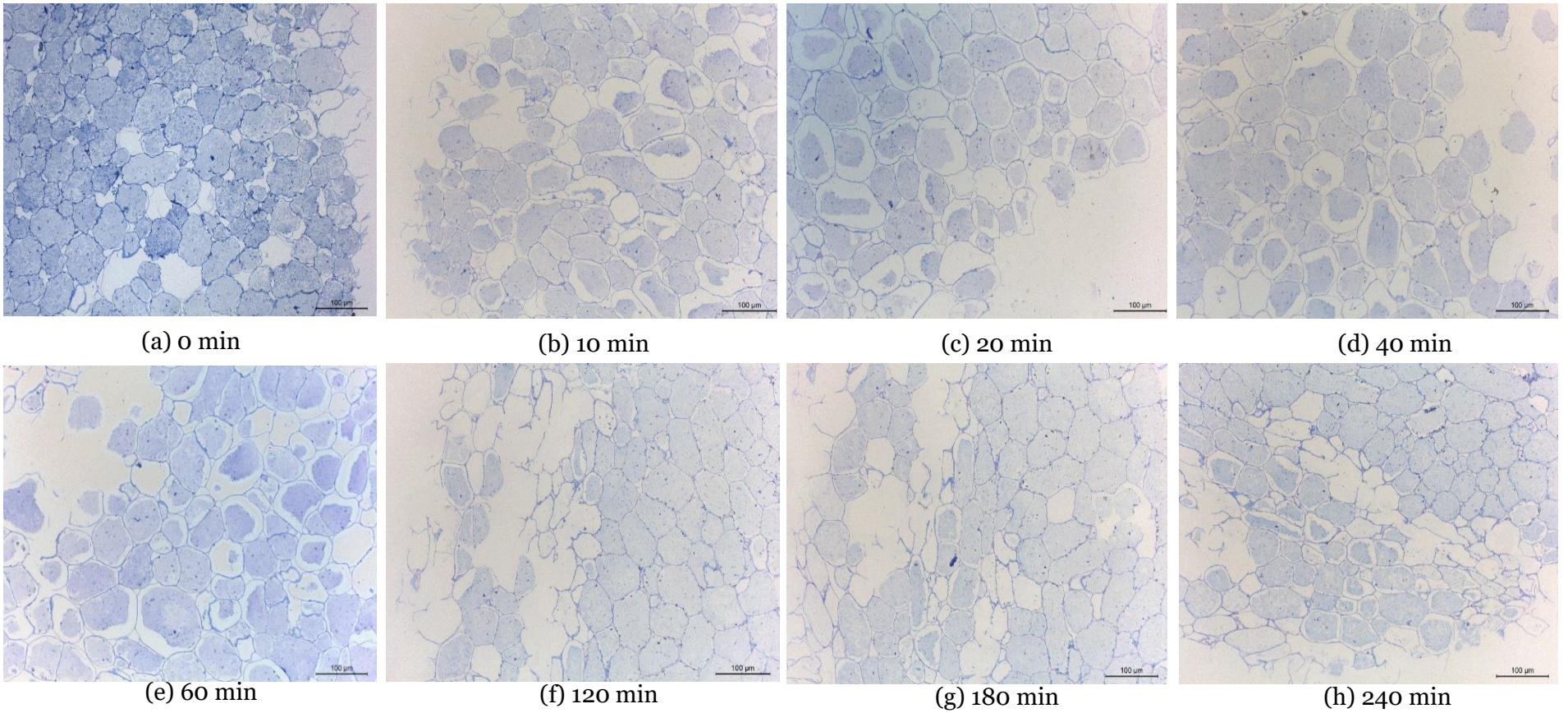

Figure 4.6: Surface location of microstructure changes of SSP during simulated *in vitro* gastric digestion. (a) Before digestion (0 min), Samples were taken after (b) 10min, (c) 20 min, (d) 40 min, (e) 60 min, (f) 120 min, (g) 180 min and (h) 240 min of gastric digestion.

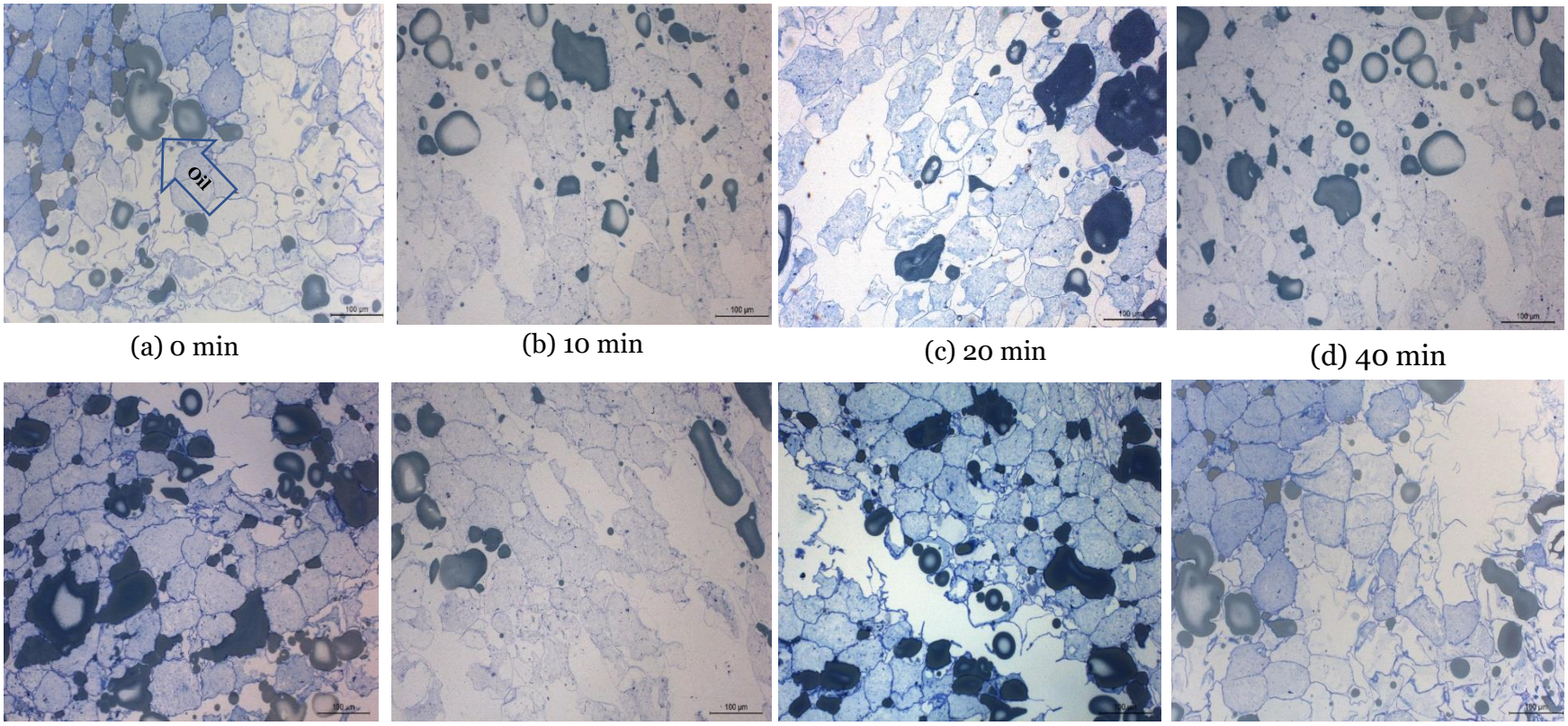

(a) 0 min (b) 10 min (c) 20 min (d) 40 min

(e) 60 min (f) 120 min (g) 180 min (h) 240 min

Figure 4.7: Centre location of microstructure changes of FSP during simulated *in vitro* gastric digestion. (a) Before digestion (0 min), Samples were taken after (b) 10min, (c) 20 min, (d) 40 min, (e) 60 min, (f) 120 min, (g) 180 min and (h) 240 min of gastric digestion.

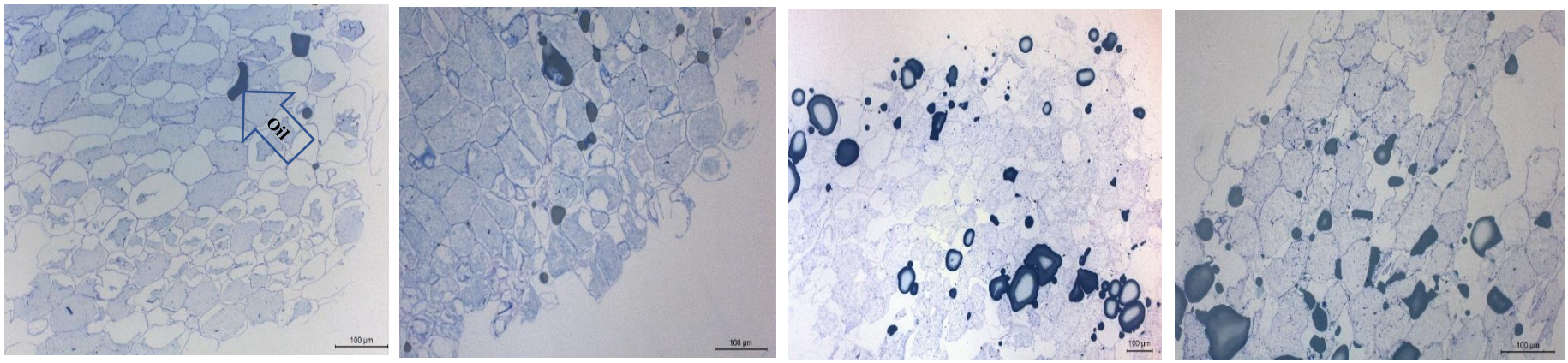

(a) 0 min (b) 10 min (c) 20 min (d) 40 min

(e) 60 min (f) 120 min (g) 180 min (h) 240 min

Figure 4.8: Surface location of microstructure changes of FSP during simulated *in vitro* gastric digestion. (a) Before digestion (0 min), Samples were taken after (b) 10min, (c) 20 min, (d) 40 min, (e) 60 min, (f) 120 min, (g) 180 min and (h) 240 min of gastric digestion.

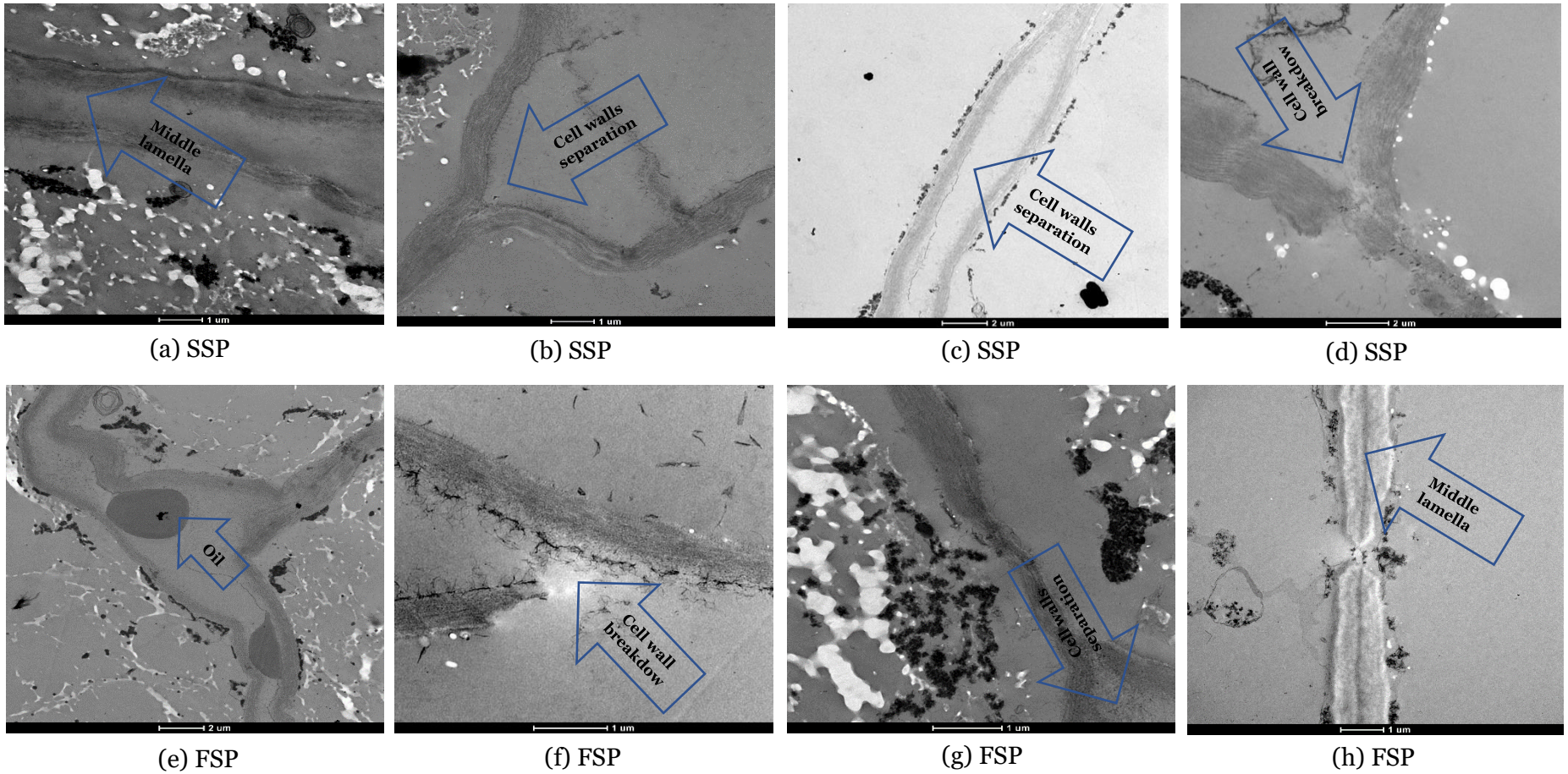

Figure 4.9: TEM images obtained after 4 hours of static *in vitro* gastric digestion; (a-d) SSP and (e-h) FSP

4.4.3 ß-carotene Release from Sweet Potato Food Matrix due to Gastric Digestion

The initial ß-carotene content differed with cooking method from 381.13±19.39 µg/g dry matter in SSP to 334.84±15.03 µg/g dry matter in FSP. In frying samples, frying temperature (180 °C) may reduce ß-carotene content because ß-carotene degrades when exposed to long preparation times and high temperatures (Howard *et al.,* 1999). Studies show that sweet potatoes processing methods prior to consumption may significantly reduce the amount of remaining β-carotene that is available for release and absorption in the human gastro-intestinal tract but increases its bio-accessibility (Tumuhimbise *et al.,* 2009). Several studies have shown that in plant-food matrix, carotenoids occur as membrane-bound semi-crystalline structures within the cells and heat treatments could increase the bioavailability of carotenoids by disrupting or softening plant cells and carotenoids-protein complexes (Lemmens *et al.,* 2010).

Figure 4.10 shows the β-carotene release profiles of the steamed and fried sweet potatoes during simulated gastric digestion. As expected, digestion time significantly ($p<0.05$) influenced the total amount of β-carotene released, but β-carotene release was not statistically ($p>0.05$) influenced by the cooking method and the interaction between the digestion time × cooking method. Both steamed and fried sweet potatoes had a slightly similar total β-carotene loss percentage at the end of 4 hours of gastric digestion (17.56±3.3% and 18.29±0.7%, respectively).

Based on the coefficient values ($R^2>0.97$), the Weibull function fitted well to the β-carotene release data for both steamed and fried sweet potatoes (Table 4.1). The reported release rate constants of the Weibull function (k) and the half-time $t_{1/2}$ (the time to reach 50% loss of total β-carotene) demonstrated that, both steamed and fried sweet potatoes showed a nearly similar rate of β-carotene release during static *in vitro* gastric digestion. The β parameter was used as a structure factor to determine the pattern of β-carotene release during digestion. Both steamed and fried sweet potatoes showed the value of $\beta < 1$, which is suggested that β-carotene release proceeded in two phases: 1) a higher initial rate of β-carotene release followed by; 2) an exponential decrease in the loss of β-carotene with digestion time.

Based on the coefficient values ($R^2=0.99$), the power-law model fitted well to the β-carotene release data for both steamed and fried sweet potatoes (Table 4.1). The reported release rate constants of the power-law model (k) demonstrated that, both steamed and fried sweet potatoes showed a nearly similar rate of β-carotene release ($k=0.19\ min^{-1}$).

However, according to the findings of chapter 3 revealed that the gaps between cells and more intercellular and intracellular spaces can be observed after frying of FSP and as a result, gastric juice penetrates into this food matrix faster than SSP. Yet, the difference in the initial microstructure of the cooked sweet potatoes, the different rate of hydrochloric acid diffusion and the different effect on the microstructure during digestion did not affect the release of β-carotene. These results point toward that in the absence of mechanical forces of the human stomach, β-carotene release from sweet potato food matrix during gastric digestion may be largely independent of the different structure between steamed and fried samples.

For the power-law model, the value of release exponent (n) is correlated with the mechanism that drives the nutrient release process during gastric digestion (Carbinatto *et al.,* 2014). The release exponent (n) values of steamed and fried samples presented as n = 0.75 (Table 4.1) indicate that the release occurred according to an anomalous mechanism (non-Fickian transport). This suggested that more than one mechanism may be involved to release ß-carotene from the sweet potatoes during diffusion of simulated gastric fluid. Thus, the combination of passive diffusion of gastric juice and erosion of cooked sweet potatoes matrix due to acid hydrolysis could be the possible mechanisms that responsible for the ß-carotene release. As shown in microstructure analysis results, the majority of the cells located in the centre of the sweet potato cylinders stayed intact after 4 hours of gastric acid diffusion study. Thus, acid hydrolysis of the cellular structure had only a greater effect on the breakdown of cell walls in the surface of the structure, which is the first site that contact with gastric juice and subsequently release ß-carotene from both steamed and fried sweet potatoes. Nevertheless, the cell wall in the centre of the sweet potato matrix may act as a physical 'barrier' towards the interactions of gastric acid and to the release of ß-carotene into the gastric digesta. The microscopic observations also suggests that in the fried samples, although the gastric acid is rapidly diffuse into the food matrix (as described in Chapter 3), gastric juice is not going inside the cells due to the fact that accumulated canola oil around the cell walls may inhibit the degradation of cell walls by gastric acid. This finding is supported by the previous study (Mennah-Govela & Bornhorst, 2016b). This observation is in agreement with both steamed and fried samples having the similar rate of ß-carotene release during static *in vitro* gastric digestion.

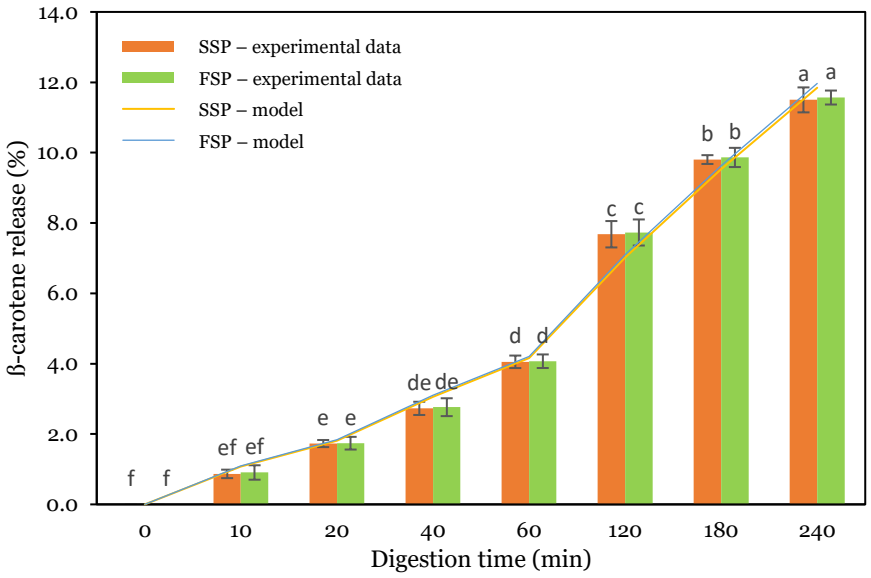

Figure 4.10: ß-carotene (%) release profiles of the SSP and FSP matrix during simulated gastric digestion. Values are given as averages (n=3) ± SD of the mean. The prediction of the model of the Weibull model (Eq. 4.2) are represented by solid lines. The different letters within each bar correspond to the significance level ($p<0.05$) as determined using multiple comparisons of means (Tukey test).

Table 4.1: Fitting parameters for the ß-carotene release data fitted with the Weibull model and the power-law model

Cooking method	Weibull model fitting parameters				
	k (min^{-1})	β	R^2	SSE	$t_{1/2}$ (hours)
SSP	$4.9\times10^{-4}\pm0.00^a$	0.98 ± 0.01^a	0.97	0.00	24 ± 1^a
FSP	$5.1\times10^{-4}\pm0.00^a$	0.99 ± 0.00^a	0.98	0.00	23 ± 1^a
	Power-law model fitting parameters				
	k	n	R^2	SSE	Release mechanism
SSP	0.19 ± 0.02^a	0.75 ± 0.02^a	0.99	0.92	Anomalous transport
FSP	0.19 ± 0.01^a	0.75 ± 0.01^a	0.99	1.00	Anomalous transport

R^2 is the goodness of fit; SSE is error sum of squares; k is the rate of ß-carotene release (min^{-1}); ß is the distribution shape factor (dimensionless); $t_{1/2}$ is the ß-carotene release half time (hours); k is the rate constant and n is the release exponent for the power-law model, SSP: Steamed sweet potatoes and FSP: Fried sweet potatoes

Means within each column followed by different superscript letters are significantly different ($p<0.05$)

4.5 Conclusions

SSP and FSP microstructure was expected to play an important role in the food matrix disintegration as well as the release of ß-carotene. Cooking treatment (steaming and frying) may influence the microstructure of the cooked sweet potatoes. Frying not only dehydrates the samples but also caused a disruption of cell arrangement and the creation of a porous network. As expected, the digestion time mainly influenced the disintegration of cellular sweet potatoes matrix and subsequent release of ß-carotene from steamed and fried sweet potatoes. However, cooking treatment (steaming and frying) may not influence the release of ß-carotene from sweet potatoes during static *in vitro* gastric digestion. In the absence of mechanical forces generated by the stomach, biochemical digestion had not a greater effect on the complete breakdown of cell walls within the sweet potato food matrix and the release of ß-carotene in both steamed and fried sweet potatoes. Cell wall in the plant-food matrix may act as a physical 'barrier' towards the interactions of gastric juice and to the release of nutrients into the aqueous phase of the gastric digesta. Moreover, in both steamed and fried sweet potatoes, cellular degradation was mainly observed at the food surface compared to the interior matrix. Thus, surface erosion of cellular structure is possibly the underlying mechanism of ß-carotene release by hydrochloric acid in these experimental conditions.

Chapter Five

5. Role of Gastric Juice Diffusion on Softening and Mechanical Disintegration of Steamed and Fried Sweet Potatoes during *In Vitro* Gastric Digestion*

5.1 Abstract

The knowledge of the influence of gastric juice diffusion into food structures on the rate of softening and mechanical disintegration of the food matrix during gastric digestion is crucial in formulating food that delivers desirable nutrient bioavailability. The aim of this work was to investigate the role that gastric juice diffusion plays in the softening and disintegration kinetics of steamed sweet potatoes (SSP) and fried sweet potatoes (FSP) during *in vitro* gastric digestion. SSP and FSP samples (5 cm^3 cubes) were subject to *in vitro* digestion by incubation in simulated gastric fluid at different time intervals for up to 240 min. The hardness of the digested sweet potato cubes was measured using a Texture Analyser and softening kinetics were fitted to the Weibull model. Results revealed that FSP (initial hardness: 4.83±0.36 N) had the shortest softening half-time (218±32 min), indicating the quickest rate of softening, whereas SSP (initial hardness: 4.61±0.24 N) had the longest softening half-time (381±97 min), indicating the slowest rate of softening during *in vitro* gastric digestion. The digested samples were then immediately exposed to mechanical forces generated by the human gastric simulator (HGS) for 10 min to investigate the influence that gastric juice diffusion has on the breakdown behaviour and β-carotene release from the steamed and fried sweet potatoes. When described in terms of the particle surface area, results suggested that breakdown of sweet potato within the HGS followed a bimodal distribution. The breakdown behaviour of the disintegrated samples was characterised by fitting the cumulative distributions of particle surface areas to a mixed Weibull function (R^2>0.99). The weight of fine particles (α) showed that regardless of gastric juice diffusion, the FSP (α = 0.15±0.00) disintegrated into more fine particles than SSP (α = 0.11±0.02). The diffusion of gastric juice not only enhanced abrasion of the matrix of sweet potatoes into fine particles (<1 mm^2) but also increased the β-carotene release during 240 min of gastric digestion. In particular, FSP exhibited significant ($p<0.05$) breakdown and subsequent β-carotene release over time than steamed once. In conclusion, the overall sweet potatoes disintegration and subsequent ß-carotene as a result of gastric juice diffusion was greatly influenced by the characteristics of SSP and FSP.

*Part of chapter five submitted as a peer-reviewed paper: Somaratne, G., Ferrua, M. J., Ye, A., Nau, Dupont, D., Singh, R. P. and Singh, J. (2020). Role of biochemical and mechanical disintegration on β-carotene release from steamed and fried sweet potatoes during *in vitro* gastric digestion. *Food Research International*, Submitted.

5.2 Introduction

The second major physicochemical transformation of food matrices occurs in the stomach after oral digestion (Kong & Singh, 2008a; Singh *et al.,* 2015). In recent years, the relationship between food material properties, mainly composition and structure and food disintegration behaviour inside the stomach has been the focal point of much food scientific investigation (Bornhorst *et al.,* 2015; Bornhorst & Singh, 2014; Singh *et al.,* 2015). Various approaches, including *in vivo*, *in silico* and *in vitro* techniques have been employed for such investigations (Bornhorst & Singh, 2014; Ferrua & Singh, 2010; Ferrua *et al.,* 2011). For examples, Guo *et al.* (2015), studied the influences of whey protein emulsion gels structuring in gastric disintegration using the dynamic human gastric simulator (HGS). They concluded that the differences in the breakdown of soft and hard gels in the HGS were mainly due to the emulsion gel structures, which may result in different sets of peptides in the digestion (Guo *et al.,* 2015). Similarly, Kozu *et al.* (2014), reported that the size distribution of two types of Tofu, Kinugoshi, and Momen particles after the dynamic gastric digestion simulator experiments were affected by the structural differences of tofu samples. Nau *et al.* (2019), and Nyemb *et al.* (2016a, b), also conducted a series of *in vitro* and *in vivo* studies and demonstrated that egg white protein gel structure impacts on peptide kinetics profile during gastric digestion. Moreover, several *in vitro* and *in vivo* studies reported that the physicochemical structure including cell wall barrier of the plant food tissues are critical factors that influence the food breakdown in the stomach, thus influencing the bioaccessibility of entrapped nutrients (Bornhorst *et al.,* 2014; Kong & Singh, 2009a; Lemmens *et al.,* 2010; Tydeman *et al.,* 2010).

Gastric processing combines several physicochemical processes (diffusion of gastric fluid, heat transfer, fragmentation, dissolution, enzymatic reactions, etc.) that lead to the formation of a chyme ready to be entered into the small intestine (Kong & Singh, 2008a; Kong & Singh, 2009b). Diffusion of gastric fluid along with acid hydrolysis and enzymatic action help to soften food texture, thus improving the disintegration rate (Drechsler & Bornhorst, 2018; Kong & Singh, 2009b). Previous studies have attempted to classify solid foods according to the softening kinetics of foods during gastric digestion with the use of texture analysis methods (Bornhorst *et al.,* 2015; Drechsler & Bornhorst, 2018). This classification system is known as food breakdown classification system which can classify foods based on their material properties and behaviour during *in vitro* gastric digestion (Bornhorst *et al.,* 2015). It is essential to apply this classification methodology in a wide variety of food matrices in order to help predict food behaviour *in vivo*. In addition, the mechanism by which the gastric juice diffusion affects physical

disintegration of food is not fully understood. Only one study, from Drechsler and Ferrua, (2016), has attempted to understand the physicochemical processes occurring during gastric digestion. However, this study highlighted that the proposed methodology does not actually reflect the dynamic environment that food experiences *in vivo* and therefore, this needs to be considered in future studies (Drechsler & Ferrua, 2016).

In addition to the gastric juice, the mechanical action and hydrodynamic mixing generated by the antral wave contractions of the stomach muscles also play a critical role in gastric digestion (Ferrua & Singh, 2010; Kong & Singh, 2008a). Fragmentation and/or erosion are the governing mode(s) of the disintegration of solid foods in the simulated gastric environment (Kong & Singh, 2009b; Lentle & Janssen, 2011). These modes depend not only on the internal cohesive force of the food matrix but also on the physical forces acting on the food (Kong & Singh, 2009b). The decrease in the degree of food structure by fragmentation and/or erosion can be quantified by the particle size distribution. Moreover, Drechsler and Ferrua (2016), developed a novel methodology to determine the contribution of erosion and fracture mechanisms to the breakdown behaviour of solid food. Even though work still needs to be done in modelling particle size distribution during gastric digestion, there is ample evidence that the particle size distribution in solid foods (i.e. whey protein emulsion gels, almonds, potatoes, and rice) during gastric digestion can be successfully fitted well to Rosin-Rammler distribution function and/or a mixed Weibull distribution (Bornhorst *et al.,* 2013*,* 2014; Drechsler & Ferrua, 2016; Guo *et al.*, 2015; Kong *et al.,* 2011).

Using steamed and fried sweet potatoes as product models, the aim of this chapter is to investigate the influence of gastric juice on the softening kinetics and the breakdown mechanics of SSP and FSP during *in vitro* gastric digestion. To achieve this aim, the HGS was employed to provide a suitable *in vivo* mechanical destructive force on food samples (Guo *et al.,* 2015). This work contributes to a better understanding of underpinning knowledge of the food disintegration in the human stomach which will help in the development of the specific functional foods that help in the prevention of degenerative diseases.

5.3 Materials and Methods

5.3.1 Materials

All the materials used in this study is similar as described in the previous 4.3.1 materials section.

5.3.2 Sweet Potato Sample Preparation and Cooking

Sweet potato sample preparation as well as steaming and frying cooking procedures used in this study is similar as described in the previous 4.3.2 sweet potato sample preparation and cooking section.

5.3.3 Static *In Vitro* Digestion

Static *in vitro* digestion procedure used in this study is similar as described in the previous 4.3.3 static *in vitro* digestion section. Briefly, each steamed/fried sweet potatoes sample (100g) was first submitted to a 2 min *in vitro* oral phase by mixing the steamed/fried sweet potatoes sample with simulated saliva containing 75 U/mL amylase (1 mL SSF/g food sample) using a 37 °C shaking water bath (BS-11, Lab Companion) at 50 rpm. Next, the sample was mixed with SGF and the pH was adjusted to 3.0 with 1 M HCl. Then the sample was mixed with pepsin (2000 U/mL) and lipase (120 U/mL) and the sample was then placed inside the shaking water bath (37 °C, 50 rpm).

The individual sample was used for each replicate of each digestion time. Thus, 24 samples from SSP and FSP were prepared according to the above procedure and placed into the shaking water bath at 37 °C at 50 rpm and incubated at different time intervals up to 4 hours (0 min – control sample, 10 min, 20 min, 40 min, 60 min, 120 min, 180 min and 240 min). The order in which the samples were digested *in vitro* was randomised. Immediately after each digestion time, steamed/fried sweet potatoes samples were neutralized using 0.5 M NaHCO3. Then steamed and fried sweet potatoes cubes were separated from the gastric juice using a sieve and then following textural, mechanical breakdown and β-carotene release measurements of steamed and fried sweet potato cubes were measured, immediately.

5.3.4 Hardness Determination using Texture Profile Analysis

The texture profile analysis of digested steamed and fried sweet potatoes cube was performed using a Texture Analyser TA-XTPlus (Texture Technologies, Stable Microsystems, Surrey, UK). One sweet potato cube was placed on the base plate of the TA-XTPlus with a cylindrical flat-end aluminium probe (35 mm in diameter) using a 50

kg load cell. The crosshead speed was 0.5 mm/s, with a rest period of 5 s between cycles and the deformation was 50% of the original length. The maximum force (N) recorded during the compression measurement (peak force of the first compression cycle in N) is referred to as the hardness of the sample. Three separate replicates were performed for each cooking treatment (SSP and FSP) and digestion time point, and eight determinations were performed per replicate for each gastric digestion time.

5.3.5 Weibull Model Parameters and Softening Half-Time Determination

The hardness change kinetics were fit to the Weibull model, according to Bornhorst *et al.* (2015), using the following equation:

$$\frac{\mathrm{Ht}}{\mathrm{Ho}} = e^{-kt(\beta)} \quad \text{(Eq. 5.1)}$$

where H_t is the hardness (N) at time t; H_o is the initial hardness (N); k is the scale parameter, which may indicate the rate of change in hardness (min^{-1}); t is the digestion time (min); and β is the distribution shape factor (dimensionless). The goodness of fit between the experimental and predicted values was determined using the error sum of squares (SSE) and the coefficient of determination (R^2).

The softening half-time ($t_{1/2}$) was calculated as the time required for the initial hardness to be reduced by 50% using the following equation:

$$t_{(\frac{1}{2})} = \left(\frac{-\ln 0.5}{k}\right)^{\frac{1}{\beta}} \quad \text{(Eq. 5.2)}$$

where k is the scale parameter and β is the distribution shape factor of the Weibull model.

5.3.6 Mechanical Disintegration of Cooked Sweet Potatoes using a Human Gastric Simulator (HGS)

The influence of gastric juice diffusion into the steamed and fried sweet potatoes cubes on their breakdown behaviour was analysed by exposing the soaked samples to a dynamic HGS for 10 min. The HGS provides a realistic and predictive simulation of mechanical and grinding forces within the human stomach (Ferrua & Singh, 2015; Kong & Singh, 2010). The latex stomach chamber was lined with a thin polyester mesh bag (pore size of the mesh bag is approximately 1 mm), which permits only particle size of less than 1 mm to pass as a gastric digesta. A plastic tube was connected to the bottom of the stomach chamber in order to remove the gastric digesta (particles of size < 1 mm) from the system during the digestion process. The peristaltic contractions on 4 sides of the latex stomach chamber were generated by six pairs of equally spaced rollers attached with the four conveyor belts. The mechanical contraction frequency was 3 times/min,

mimicking the actual stomach peristalsis. The temperature inside the human gastric chamber was maintained at 37 °C.

The method of operating the HGS was adapted from the procedures described by Guo *et al.,* (2015). Steamed and fried sweet potatoes samples (100 g) were subjected to simulated static *in vitro* digestion (oral and gastric phase) as described in section 5.3.3. Then, the digested sample with neutralized gastric juice was loaded into the stomach chamber. For control sample (0 min digestion), steamed and fried sweet potatoes samples (100 g) were directly loaded into the HGS, and instead of neutralized gastric juice, an equal amount of water was added into the stomach chamber. The samples were exposed to the mechanical forces applied by the HGS for 10 min and then, gastric digesta were removed from the bottom of the stomach, manually.

The particle size distributions of the combined digesta (i.e. the cumulative emptied digesta and the digesta retained in the simulated latex stomach chamber) were measured by an image analysis method as described below.

5.3.7 Determination of Particle Size Distribution using Image Analysis

The breakdown mechanics of the steamed and fried sweet potatoes were assessed on combined digesta, which included the cumulative emptied digesta and the digesta retained in the simulated latex stomach chamber. It was characterised based on image analysis of their particle size distributions according to the method described by Drechsler and Ferrua (2016). Three representative aliquots of the sub-samples (5 mL) were randomly taken for each combined digesta and dispersed in 20–30 mL of water in a rectangular petri dish (12.2 cm×8.0 cm). In order to prevent the particles coming into contact with each other during imaging, the number of petri dishes required was increased from 3 to 10, as soaking time progressed. Particles were dyed with an iodine solution (Lugol's 1%) to increase their contrast against the background. Each petri dish was manually shaken to ensure good dispersion and placed on an LED lightbox and the image was captured using a digital camera (Nikon 1 V1, AF-S DX Micro NIKKOR 40 mm f/2.8G macrolens). The number and surface area of all the particles present in each individual petri dish was then analysed using a custom-built code program in Matlab 2013a (MathWorks, Natick, Mass., USA) software and the results were expressed as a cumulative percentage of the surface area of the particles. To facilitate the comparison among different treatments, the size distribution of the particles was analysed over one hundred size classes ranging from 10^{-4} mm^2 to 100 mm^2.

As illustrated in Figure 5.1, Drechsler and Ferrua (2016), developed a framework to characterise the damage mechanisms undergone by the potato samples during the simulated gastric phase. In particular, based on the size distribution of compressed

particles compared to their initial size (A0~25 mm²), it is possible to quantify the amount of product associated with undamaged particles (A0>15 mm²), fragments (1.75 mm2<A0<15 mm²), chips (1 mm2<A0<1.75 mm²) and fine debris (A0<1 mm²) during the gastric digestion process (Drechsler & Ferrua, 2016). Based on this classification framework, we have evaluated the contribution of surface erosion and particle fragmentation on the breakdown of sweet potato particles due to the exposure of gastric juice and the mechanical forces generated by the HGS.

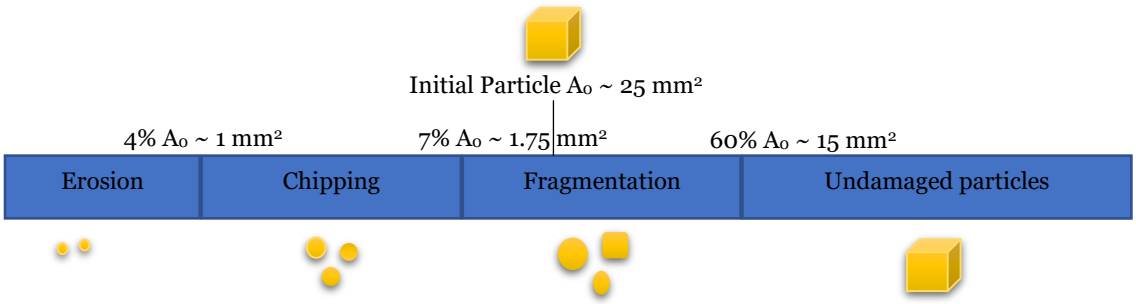

Figure 5.1: Characterisation of broken particles into fine debris, fragments and undamaged product based on their relative size to the original one before comminution, according to Drechsler and Ferrua (2016).

5.3.8 Modelling of Particle Breakdown during Gastric Digestion

The earlier study by Drechsler and Ferrua (2016), reported that the mixed Weibull distribution function can successfully be used to describe the extent and the mechanism of particle breakdown of potatoes during *in vitro* gastric digestion. This research highlighted that the double-form of breakage distribution function (i.e. mixed Weibull distribution function) may be more appropriate to describe the particle surface area distribution of a comminuted food than the single-form breakage distribution function such as a Rosin Rammler distribution function.

Thus, the cumulative percentage of particle surface area ($F_{(x)}$) for each sample and digestion time was fit to a mixed Weibull distribution function as follows. A mixture of Weibull distribution, involving two shape parameters (k), two scale parameters (λ), and one weight parameter (α).

$$F_{(x)} = \alpha\left(1 - e^{-\left(\frac{x}{\lambda 1}\right)^{k1}}\right) + (1-\alpha)\left(1 - e^{-\left(\frac{x}{\lambda 2}\right)^{k2}}\right) \quad \text{(Eq. 5.3)}$$

where $F_{(x)}$ is the cumulative particle size distribution of the sample (0 to 1); x ($x = A/A_0$) is the particle surface area (A mm²) in relationship to its initial value (A_0 mm²); α is a mixing weight parameter that represents the proportion of the first mode (left Weibull

distribution); λ1 and λ2 are the scale parameters established by left (first mode) and right (second mode) Weibull distribution, respectively; and k1 and k2 are the shape parameters established by left (first mode) and right (second mode) Weibull distribution, respectively. The model parameters were determined using nonlinear regression techniques in Matlab (MathWorks, Natick, Mass., USA). The more details of the method for estimating parameters of mixed Weibull distribution and the used custom-built code program in Matlab has been outlined by Drechsler and Ferrua (2016).

5.3.9 Modelling the ß-carotene Release Kinetics

Immediately after each digestion time, the digesta sample retained in the simulated latex stomach chamber was removed. These samples were snap-frozen using liquid N_2 and stored at −80 °C. Subsequent β carotene extraction and analysis was carried out as described in the Chapter 4 and section 4.3.6.

The Weibull distribution function is widely used to describe nutrient release kinetics during *in vitro* analysis (Kong & Singh, 2011). The experimental β-carotene release data were fitted with the Weibull distribution function as follows.

$$\text{β-carotene release (\%)} = 1 - e^{-kt(\beta)} \qquad \text{(Eq. 5.4)}$$

Where k defines the time scale of the process (min^{-1}) associated with the rate constant of β-carotene release and β is a shape parameter that characterises the shape of the release curves. The half-time ($t_{1/2}$), the time to reach 50% loss of total β-carotene is calculated as the following equation;

$$t_{(\frac{1}{2})} = \left(\frac{-\ln 0.5}{k}\right)^{\frac{1}{\beta}} \qquad \text{(Eq. 5.5)}$$

5.3.10 Statistical Analysis

An ANOVA was conducted using a 2-factor factorial design to determine differences in hardness (N), mixing weight parameter (α) and β-carotene release during static *in vitro* gastric digestion. The factors were cooking treatment (steamed and fried sweet potatoes), and digestion time (0-240 min). The Tukey test was used to analyse the differences between means and statistical significance was assessed at a level of $p<0.05$. The student t-test was used to assess differences in the Weibull model parameters and softening and β-carotene release half-time. Minitab 17 software was used for statistical analysis.

5.4 Results and Discussion

5.4.1 Choice of Experimental Parameters

The size of the sweet potatoes cubes was selected to be 5 mm in length, width and thickness which is similar to the upper limit of the actual size range of vegetable particulates after oral mastication (Jalabert-Malbos *et al.,* 2007). In order to achieve the objectives of this study, namely, to quantify textural changes and particle size breakdown processes during digestion, the upper fragment size limit after oral mastication was chosen to ensure that the sweet potato samples did not completely break down during the 4 hours of gastric digestion. In addition, the use a simple geometry (cubes) was selected to limit possible variation of textural measurements.

In this study, four hours of digestion time was selected because most solid foods are cleared from the human stomach approximately within 3 to 4 hours (Minekus *et al.,* 2014). Moreover, the HGS test used in this study was not intended to reproduce the actual physicochemical reactions that develop during digestion, but to provide an initial framework to characterise the influence of gastric juice on the break down mechanics of the sweet potato samples. Thus, preliminary studies were conducted and these identified that soaked steamed/fried sweet potatoes cube samples that were exposed to the mechanical forces generated by the HGS for 10 min provided a representative particle size distribution which would enable us to identify key mechanisms underlying the breakdown behaviour. Moreover, soaked steamed/fried sweet potato cube samples exposed to the mechanical forces generated by the HGS for more than 10 min resulted in a fine debris of all the end-products whereas less than 10 min left many particles undamaged.

5.4.2 Softening Kinetics of Sweet Potatoes during Gastric Phase is Influenced by the Initial Cooked Sweet Potatoes Characteristics

The hardness (peak force of the first compression cycle in N) of the steamed and fried sweet potato matrix during simulated gastric digestion is shown in Table 5.1. Changes in the hardness of the sweet potato cubes during digestion were significantly influenced by the cooking method (SSP or FSP) and length of digestion time ($p<0.05$). Textural changes occurring during thermal processing and digestion in starch-based plant foods (i.e. potatoes and rice) are mainly associated with the gelatinisation behaviour of starch and degradation of cell wall and middle lamella structural components (Mennah-Govela & Bornhorst, 2016ab; Kong *et al,* 2011).

Hardness measured at time 0 min in FSP was not significantly different from the corresponding SSP ($p>0.05$). The similarity in hardness we measured may appear to contradict the different microstructural changes of sweet potatoes after these two cooking methods as observed through LM (Chapter 4, section 4.4.2). SSP parenchyma cells were observed to be completely filled with gelatinised starch matrix after steaming. In contrast, the interior microstructure of fried samples showed that the cells were more separated and cell arrangement was extensively disrupted, which may be expected to lower the initial hardness of fried sweet potatoes compared to SSP. However, although, the fried sweet potato interior microstructure is porous, the high initial hardness of the fried sweet potato is likely due to the crust formation during frying (Chapter 4, section 4.4.2).

As seen in Table 5.1, the hardness of steamed and fried sweet potatoes significantly decreased during digestion time ($p<0.05$). After 240 min of digestion, FSP exhibited the greatest decrease (58%) compared to its initial hardness value, whereas only a 37% decrease in hardness was observed in the case of SSP. During the first hour of gastric digestion, the hardness of the FSP decreased significantly from 4.83±0.36 N to 3.75±0.16 N (22% of change). The rapid decrease of hardness in FSP during digestion may be associated with to the rapid softening of the crust (As described in the Chapter 3). Furthermore, the disrupted structure and high porosity developed during frying process leads to rapid loss of the firmness and integrity of cell walls of FSP after absorption of gastric juice as observed in light micrographs (see the Chapter 4). Similar rapid decreases in hardness were not observed in the SSP.

The Weibull distribution function is widely used to describe the softening kinetics of solid foods during static *in vitro* gastric digestion (Bornhorst *et al.,* 2015; Drechsler & Bornhorst, 2018). The softening curves (Figure 5.2) determined by monitoring changes in steamed and fried sweet potatoes hardness during digestion fit well to the Weibull model (Eq. (5.1)), as evidenced by the high R^2 values (0.97-0.99, Table 5.2) and low SSE (<0.002, Table 5.2). The reported softening rate constants of the Weibull function (k) demonstrated that the FSP showed higher rate of softening ($k=0.004\ min^{-1}$) compare to SSP ($k=0.002\ min^{-1}$). The β values for both the steamed and fried sweet potatoes are $\beta<1$, indicating a higher rate of hardness reduction at the initial stage of the gastric digestion process followed by an exponential decrease in the hardness of sweet potatoes with digestion time.

Table 5.1: Changes in the hardness (N) of the steamed and fried sweet potatoes during *in vitro* gastric digestion

Digestion time (min)	Hardness of SSP (N)*	Hardness of FSP (N)*
0	4.61 ± 0.24^{ab}	4.83 ± 0.36^{a}
10	4.50 ± 0.34^{ab}	4.26 ± 0.15^{abc}
20	4.48 ± 0.13^{ab}	3.97 ± 0.14^{bc}
40	4.28 ± 0.08^{abc}	3.91 ± 0.38^{bcd}
60	4.09 ± 0.25^{bc}	3.75 ± 0.16^{d}
120	3.75 ± 0.33^{cd}	2.97 ± 0.07^{ef}
180	3.24 ± 0.11^{de}	2.40 ± 0.26^{fg}
240	2.91 ± 0.31^{ef}	2.04 ± 0.03^{g}

*Values are represented as averages (n=24 cubes) ± SD of the mean. Different letters within each column and raw represent statistically different means ($p<0.05$). SSP: Steamed sweet potatoes. FSP: Fried sweet potatoes

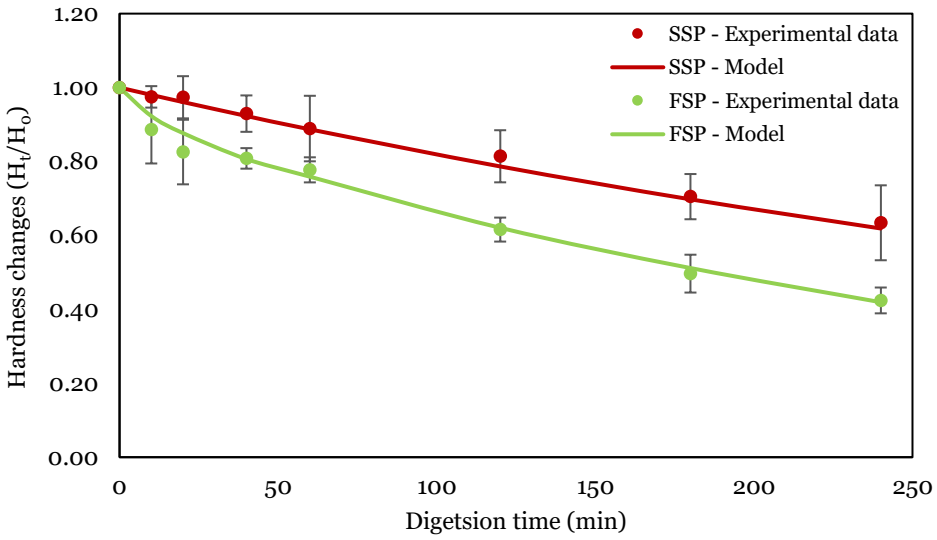

Figure 5.2: Softening curves of the steamed and fried sweet potatoes matrix during *in vitro* gastric digestion based on the hardness (N) measurements. Values are given as averages (n = 3) with error bars as SD (some are too small to be visible). The solid lines represent the predicted values from the average Weibull model parameters shown in Table 5.2. SSP: Steamed sweet potatoes. FSP: Fried sweet potatoes

The half-time ($t_{1/2}$), defined as the time to reach 50% reduction in initial hardness incorporates both the k and β parameters from the Weibull model, and will more

appropriately describe the overall curve properties than either one of the fitted parameters on its own (Bornhorst *et al.,* 2015). Results revealed that while no significant differences ($p>0.05$) were observed between the initial hardness of the steamed and fried samples (4.61±0.24N and 4.83±0.36 N, respectively), the softening half-time varied from 381±97 (SSP) to 218±32 min (FSP). Thus, foods with similar initial hardness may not have comparable softening rates, as previously observed by Bornhorst *et al.,* (2015). The differences in the softening half-time observed between the sweet potatoes tested may be attributed to their initial microstructure as well as the rate of acid diffusion. In FSP, the porous microstructure leads to more rapid acid diffusion and subsequent collapsing as well as faster softening during *in vitro* gastric digestion compared to the compact and denser structure of SSP, which is in agreement with previous findings (Chapter 3 and 4). The relevance of these findings on the breakdown response of the sweet potatoes samples is discussed in the following sections.

Table 5.2: Parameter values of Weibull function (Eq. 5.1) fitted to the softening curves of the steamed and fried sweet potatoes during *in vitro* gastric digestion.

	k	ß	R^2	SSE	$t_{1/2}$ (min)
SSP	0.002 ± 0.00^{b}	0.99 ± 0.02^{a}	0.99	0.000	381 ± 97^{a}
FSP	0.004 ± 0.00^{a}	0.91 ± 0.07^{a}	0.97	0.002	218 ± 32^{b}

R^2 is the goodness of fit; SSE is error sum of squares

k is the rate of change in hardness (min^{-1})

ß is the distribution shape factor (dimensionless)

$t_{1/2}$ is the softening half-time (min)

SSP: Steamed sweet potatoes and FSP: Fried sweet potatoes

Values represent the average model parameters or softening half-time from 3 digestion trials ± SD

Means within each column followed by different superscript letters are significantly different ($p<0.05$)

5.4.3 Mechanisms of Particle Breakdown Depend on the Initial Structure of Steamed and Fried Sweet Potatoes

In the *in vitro* gastric phase, gastric juice was diffused into the sweet potatoes structure and thereby leads to biochemical digestion. The influence of gastric juice diffusion on the mechanical breakdown mechanics of the steamed and fried sweet

potatoes matrixes were determined by exposing the soaked sweet potatoes samples (digested or not) to the mechanical forces generated by the HGS.

The distributions of particle surface area in the disintegrated steamed and fried sweet potatoes samples are depicted in Figure 5.3 and 5.4. In the gastric digestion process, it is important to describe the amount of nutrient/s that is entrapped within the digested particles. Thus, analysing the breakdown behaviour of food during gastric digestion in terms of the surface area of particles is a better indicator of the amount of nutrients associated with the food matrix than distributions of the number of particles (Drechsler & Ferrua, 2016).

Fragmentation, chipping and erosion are the major mechanisms responsible for solid food disintegration in a simulated gastric environment (Drechsler & Ferrua, 2016; Kong & Singh, 2009). According to the Figure 5.3 and 5.4, the progressive size reduction of the steamed and fried sweet potatoes samples due to the exposure of gastric juice followed different type of break down mechanisms. Without exposure to gastric juice (0 min, control sample) and after 10 min exposure to gastric juice, the SSP exhibited mainly undamaged (5%) particles and fine debris particles (4-5%), without any progressive reduction in size due to fracture or chipping mechanisms (Figure 5.3). This result highlighted that at the beginning SSP might demonstrate resistance to breakdown, due to exposure of the mechanical forces generated by the HGS. However, the breakdown of the SSP appeared to be driven by fragmentation, chipping as well as surface erosion mechanisms when they were exposed to simulated gastric fluid from 20 min to 240 min, due to the increased softening and biochemical digestion of the SSP matrix. A similar breakdown behaviour of steamed potatoes has been reported previously by Drechsler and Ferrua, (2016).

According to the Figure 5.4, without exposure to gastric juice (0 min, control sample), the FSP exhibited mainly undamaged 5%) particles compared to the fine debris particles (<2%). This distribution revealed a significant amount of nutrients still present in the form of large particles in the disintegrated control samples. However, even if there are mainly large particles, some small soluble nutrients (i.e. gelatinised starch) and β-carotene could be released into the gastric medium from the damaged cells within the fried matrix. Unlike SSP, the breakdown of the FSP appeared to be driven by fragmentation, chipping as well as surface erosion mechanisms when they were exposed to simulated gastric fluid for varying times up to 240 min probably due to the rapid softening increased acid diffusion into the fried matrix and associated biochemical digestion of the FSP matrix.

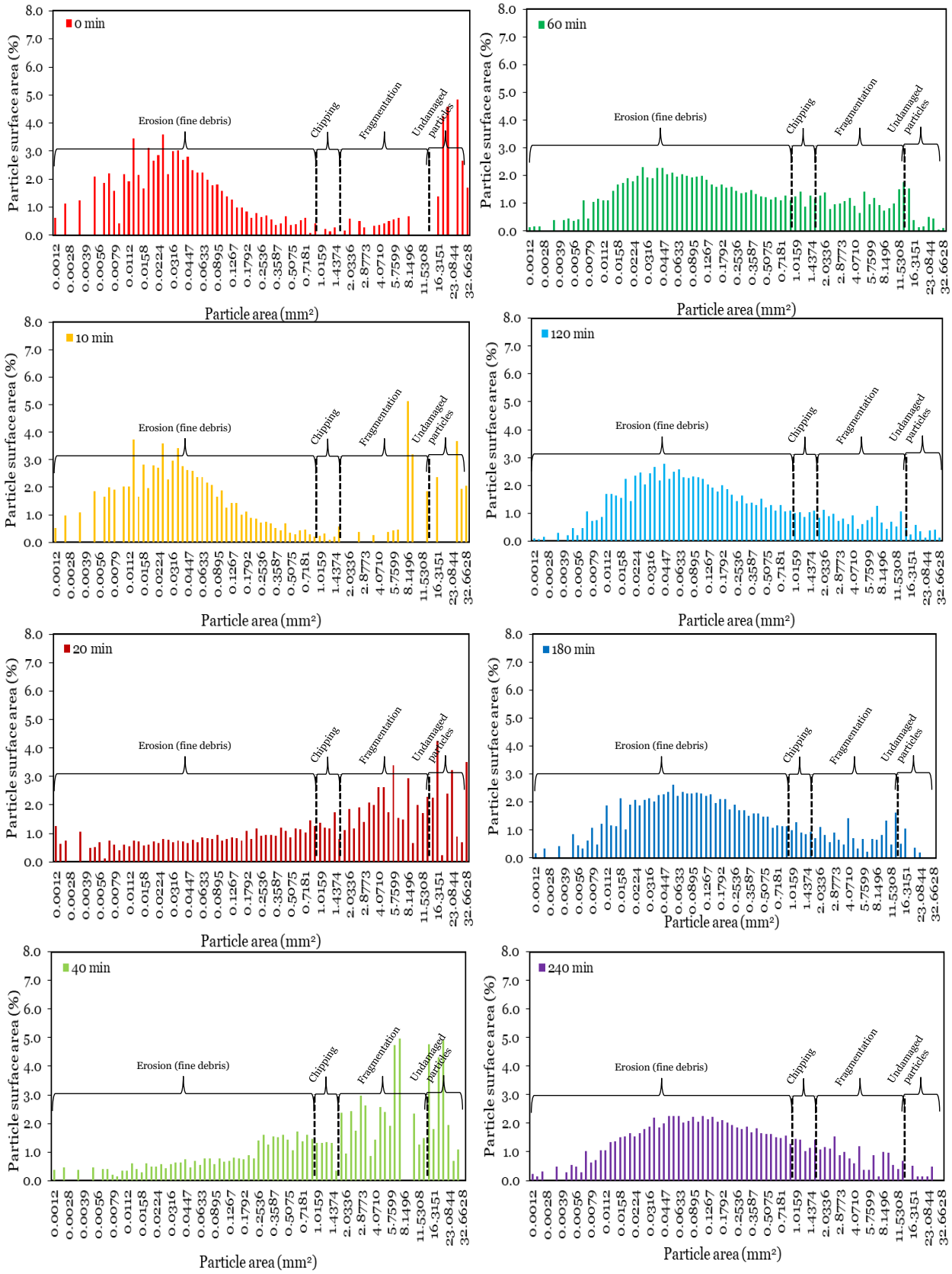

Figure 5.3: Examples illustrating the characterisation of broken SSP particles surface area (0-240 min digestion time) to determine the underlying mechanisms of SSP breakdown during the gastric phase.

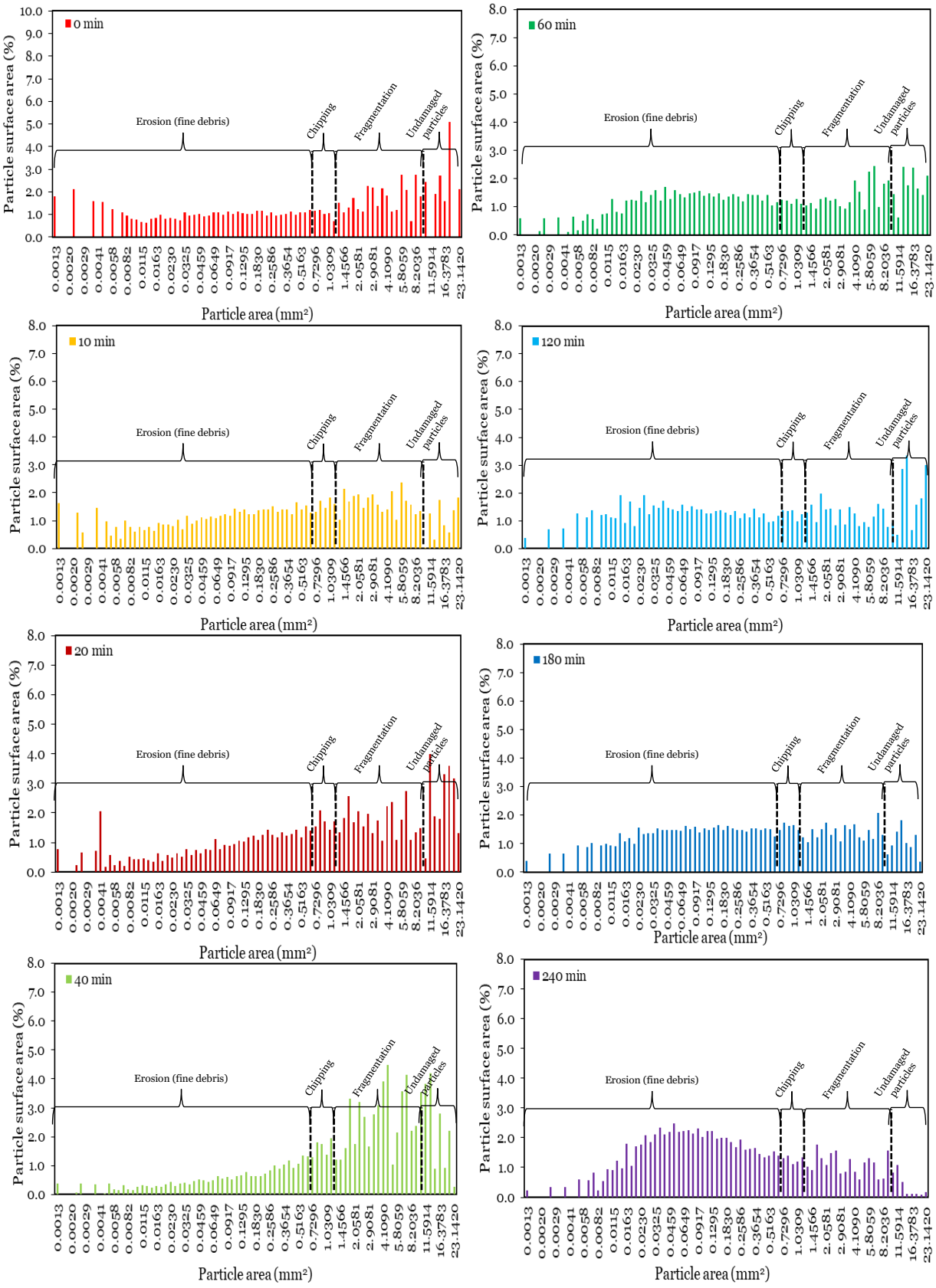

Figure 5.4: Examples illustrating the characterisation of broken FSP particles surface area (0-240 min digestion time) to determine the underlying mechanisms of FSP breakdown during the gastric phase.

In addition to that, both SSP and FSP showed the weight percentage of large particles and chips decreased progressively, while the percentage of fine particles increased gradually, during the gastric phase. The maximum magnitude of the destructive force from the human stomach and the HGS is around 1.9 N and 2.5 N, respectively. Thus, it is difficult for the stomach to fragment hard food particles (Hardness>2.5 N) into smaller pieces (Kamba *et al.,* 2000; Kong & Singh, 2010). Consequently, cooked sweet potatoes with high initial hardness (4.61±0.24N and 4.83±0.36 N) are broken down into different fragments in the HGS. On the other hand, cooked sweet potatoes were easier to break apart after exposure to gastric juice, which may lead to the formation of chips from the different fragments in the HGS. As the length of time the cooked sweet potato was exposed to gastric juice increased, the distribution of fine debris and chips shifted towards smaller sizes, presumably due to the increased softening of the sweet potato matrix.

5.4.4 Role of Biochemical and Mechanical Effects on the Breakdown Process of Steamed and Fried Sweet Potatoes

The cumulative particle surface area distribution of steamed and fried sweet potatoes over 240 min gastric digestion time is shown in Figure 5.5. The breakdown behaviour of the SSP and FSP exposed to gastric juice was characterised by fitting the cumulative distributions of particle surface areas to a mixed Weibull function. The model parameters including the coefficient of determinations (R^2) are given in Table 5.3. As can be noted by the large R^2 values (R^2>0.99), the mixed Weibull function model is a good fit for the data. The particle surface area distribution exhibited a bimodal distribution behaviour, with one component associated with fine debris (first mode of the mixed Weibull distribution) and another with particles similar in size to the original cubes (second mode of the mixed Weibull distribution). In agreement with expectations, when the exposure of gastric juice progress had a positive effect on the extent of damage incurred by the cooked sweet potatoes particles (Figure 5.5). The scale parameter (λ) is a constant representing the broadness (i.e. When λ is increased, the height of the Weibull distribution decreases and the broadness increases) whereas the shape parameter (k) is a constant representing the shape (i.e. sigmoidal shape when k >1, or parabolic shape when k < 1) of the Weibull distribution (Krifa, 2009). It is interesting to note that, in one hand, the scale parameter of the first mode of the mixed Weibull distribution (λ_1) value increased over the 240 min digestion period in both SSP and FSP, which indicate a broader distribution spread of the fine particles with increased digestion time (Table 5.3). On the other hand, the scale parameter of the second mode of the mixed Weibull distribution (λ_2) value decreased over the 240 min digestion period in both SSP and FSP,

which indicate a narrower distribution spread of the large particles with increased digestion time (Table 5.3).

The extent of damage to the sweet potatoes due to exposure of gastric juice and mechanical forces generated by the HGS was characterised based on the mixed Weibull parameter (α), that describe the weight of fine particles (first mode of the mixed Weibull distribution) within the breakdown sample. The temporal evolution of the weight of fine particles (α) of steamed and fried sweet potatoes is shown in Figure 5.6.

The weight of fine particles (α) was significantly influenced by the cooking treatment and the digestion time ($p<0.05$, Figure 5.6). As expected, both steamed and fried sweet potatoes had significant increases in the weight of fine particles during the 240 min gastric digestion period ($p<0.05$). Results showed that the weight of fine particles (α) between cooking methods at most of the times during digestion were similar, with the exception of a few time points. The weight of fine particles value of the SSP exposed to the gastric fluid was not significantly different compared to the FSP during the first 60 min of digestion time. However, between 60 and 240 min of digestion time, the α value of the FSP exposed to the gastric fluid was significantly higher than that of the SSP ($P<0.05$), indicating that the FSP had a higher disintegration rate than SSP. As reported in Chapter 3, frying not only led to dehydration of the samples, it also caused a disruption of cell arrangement, creation of a porous network and crust formation. These factors could directly contribute to the higher diffusivity of gastric juice within the fried samples compared to the steamed samples and lead to a decrease in the firmness and the integrity of cell walls of FSP after absorption of gastric juice. This disintegration pattern is in good agreement with the softening kinetics of sweet potatoes during simulated *in vitro* gastric phase. Thus, the softening half-time may be a good indicator of the relative rate of breakdown of food products.

Table 5.3: Mixed Weibull distribution parameters. Values are given as averages (n = 3) with SD.

Digestion time (min)	λ1		k1		λ2		k2		R^2	
	SSP	FSP	SSP	FSP	SSP	FSP	SSP	FSP	SSP	FSP
0	0.04±0.02	0.06±0.09	1.15±0.10	0.71±0.08	14.52±1.97	15.16±2.5	0.72±0.39	0.42±0.13	>0.998	>0.997
10	0.01±0.00	0.05±0.05	1.23±0.06	0.93±0.04	11.51±1.53	11.04±0.02	0.75±0.15	0.50±0.15	>0.991	>0.998
20	0.01±0.00	0.10±0.09	0.69±0.12	0.58±0.06	1.58±0.90	12.54±0.21	0.71±0.08	0.30±2.34	>0.997	>0.999
40	0.26±0.30	0.18±0.28	0.51±0.04	0.68±0.89	2.62±0.06	9.44±0.57	0.84±0.09	0.33±0.04	>0.991	>0.998
60	0.03±0.01	0.47±0.04	1.07±0.11	0.69±0.85	0.69±0.23	2.70±0.07	0.58±0.01	0.64±0.07	>0.996	>0.996
120	0.03±0.00	0.43±0.31	0.91±0.03	0.56±0.07	0.30±0.11	3.04±0.30	0.64±0.03	0.94±0.49	>0.996	>0.997
180	0.68±0.18	0.46±0.06	0.87±0.28	0.68±0.10	0.11±0.10	0.14±0.23	0.79±0.15	0.87±0.11	>0.997	>0.997
240	0.69±0.02	0.41±0.26	0.67±0.04	0.57±0.01	0.07±0.00	0.03±0.00	0.97±0.03	0.89±0.03	>0.997	>0.997

SSP: Steamed sweet potatoes and FSP: Fried sweet potatoes

λ1 and λ2 are the scale parameters established by left (first mode) and right (second mode) Weibull distribution, respectively

k1 and k2 are the shape parameters established by left (first mode) and right (second mode) Weibull distribution, respectively

R^2 is the coefficient of determinations

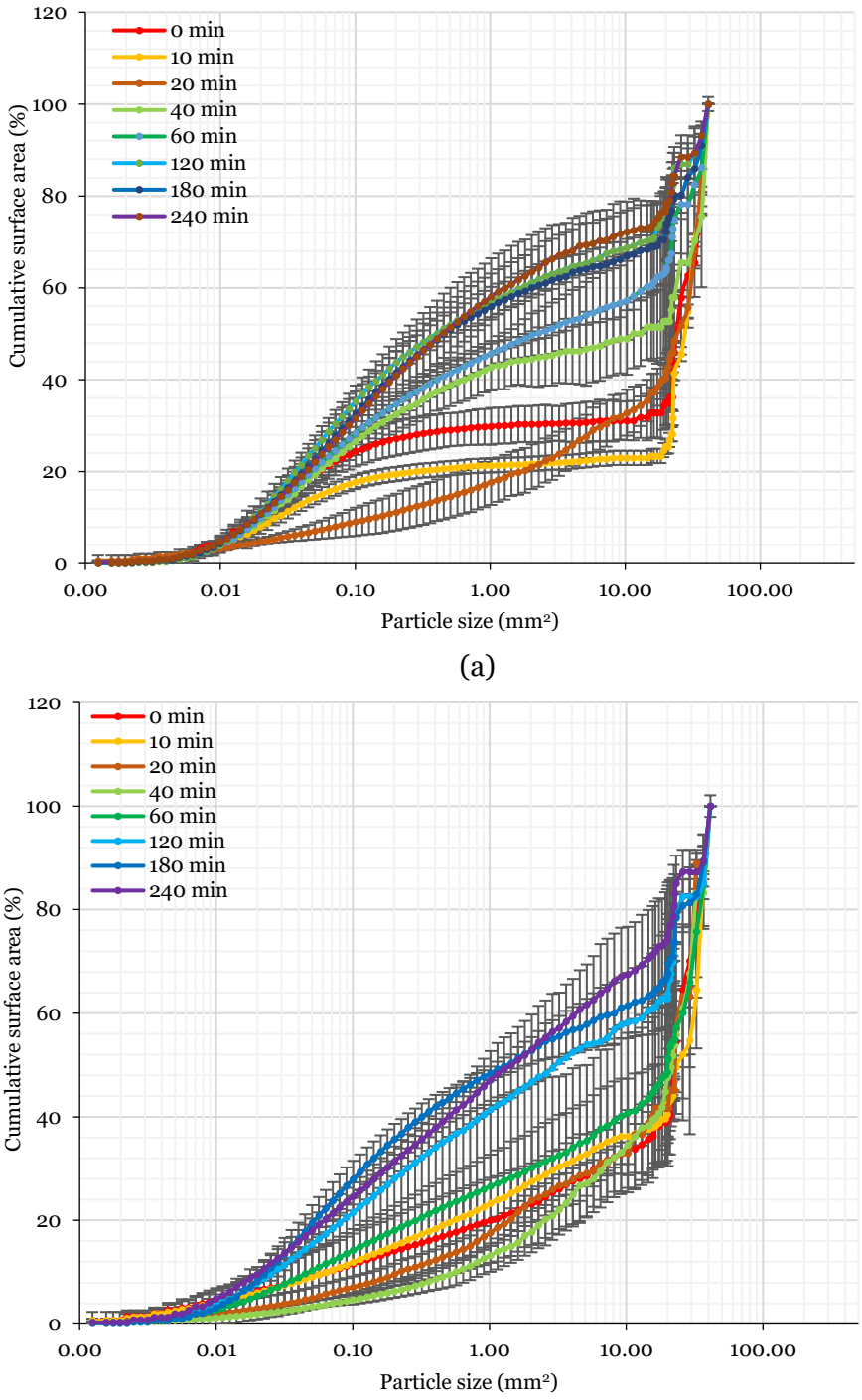

Figure 5.5: Graphical illustration of the influence of gastric juice soaking time on the cumulative size distribution of particle surface areas of (a) SSP and (b) FSP. Values are given as averages (n=3) with error bars as SD.

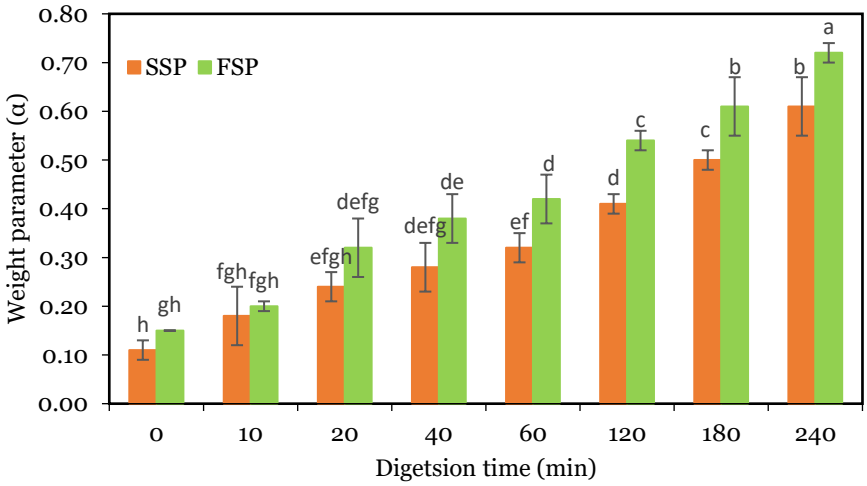

Figure 5.6: Temporal evolution of weight parameter (α) of the Mixed Weibull function (proportion of small particles within breakdown sweet potatoes samples). Values are given as averages (n = 3) with error bars as SD. The different letters within each bar correspond to significance level ($p<0.05$) as determined using multiple comparison of means (Tukey test). SSP: Steamed sweet potatoes and FSP: Fried sweet potatoes.

5.4.5 Role of Biochemical and Mechanical Effects on the ß-Carotene Release from Steamed and Fried Sweet Potatoes

Figure 5.7 shows the β-carotene release profiles of the steamed and fried sweet potatoes, when they were exposed to gastric juice absorption over 240 min during static *in vitro* gastric phase and subsequent mechanical disintegration in the HGS. As expected, digestion time significantly ($p<0.05$) increased the total amount of β-carotene released from both steamed and fried sweet potatoes. Moreover, β-carotene release was also statistically ($p<0.05$) influenced by the cooking method.

Based on the coefficient values ($R^2>0.95$), the Weibull function fitted well to the β-carotene release data for both steamed and fried sweet potatoes (Table 5.4). The Weibull parameters are shown in Table 5.4 demonstrate that there is not a significant difference between rate constant (k) and shape parameter (β) from the different cooking methods. However, there is a trend of faster rate of β-carotene release ($k = 0.002\ min^{-1}$) in FSP and slower rate of β-carotene release ($k = 0.001\ min^{-1}$) in steamed sweet potatoes. The β parameter was used as a structure factor to determine the pattern of β-carotene release during digestion. Both steamed and fried sweet potatoes showed the value of $\beta < 1$ which suggested that β-carotene release proceeded in two phases: 1) a higher initial rate of β-carotene release followed by; 2) an exponential decrease in the release of β-carotene with increased digestion time.

The half-time ($t_{1/2}$), the time to reach 50% decrease in the release of total β-carotene, incorporates both the k and β parameters from the Weibull model, and more appropriately describes the overall curve properties than either one of the fitted parameters on their own (Bornhorst *et al.,* 2015). The 50% of total β-carotene released from the fried sweet potatoes due to exposure of gastric juice and mechanical forces generated by the HGS within ~466 min whereas the steamed sweet potatoes had a β-carotene release half-time of ~694 min. This suggests that the cooking induced differences in sweet potato microstructure may result in variations in the rate of β-carotene release half-time. We have already described that gaps between cells and more intercellular and intracellular spaces can be observed after digestion of FSP and as a result, gastric juice penetrates this food matrix faster than SSP. Thus, fried matrix underwent collapsing as well as quickest softening during *in vitro* gastric digestion compared to the compact and denser structure of steamed sweet potatoes, which may lead to the faster disintegration and subsequent β-carotene release in the HGS. This is in line with the results of Tumuhimbise *et al.* (2009), who showed that the FSP had the highest percentage of bioaccessible all-trans-β-carotene compared to steamed once. These authors also highlighted that the presence of fat in the FSP may improve the bioaccessibility of fat-soluble β-carotene. Similarly, using a dynamic *in vitro* digestion model, Van Loo-Bouwman *et al.* (2014), highlighted that the bioaccessibility of β-carotene was two times higher in the oil-based diet compared to the vegetable based-mixed diet. These trends in the β-carotene release may correspond to the structural changes and softening kinetics observed through texture analysis (section 5.4.2).

In Chapter 3 it was shown that, in the absence of mechanical forces of human stomach, β-carotene release from the sweet potato food matrix during static *in vitro* gastric digestion, was not affected by the different structures in steamed and fried samples. In contrast, findings of this chapter suggest that, in the presence of the mechanical forces of the human stomach, β-carotene release from the sweet potato food matrix during gastric digestion is influenced by the different structure of steamed and fried samples. Thus, mechanical forces generated by the human stomach, had a greater effect on the breakdown of cell walls and the release of ß-carotene entrapped within cells in both steamed and fried sweet potatoes.

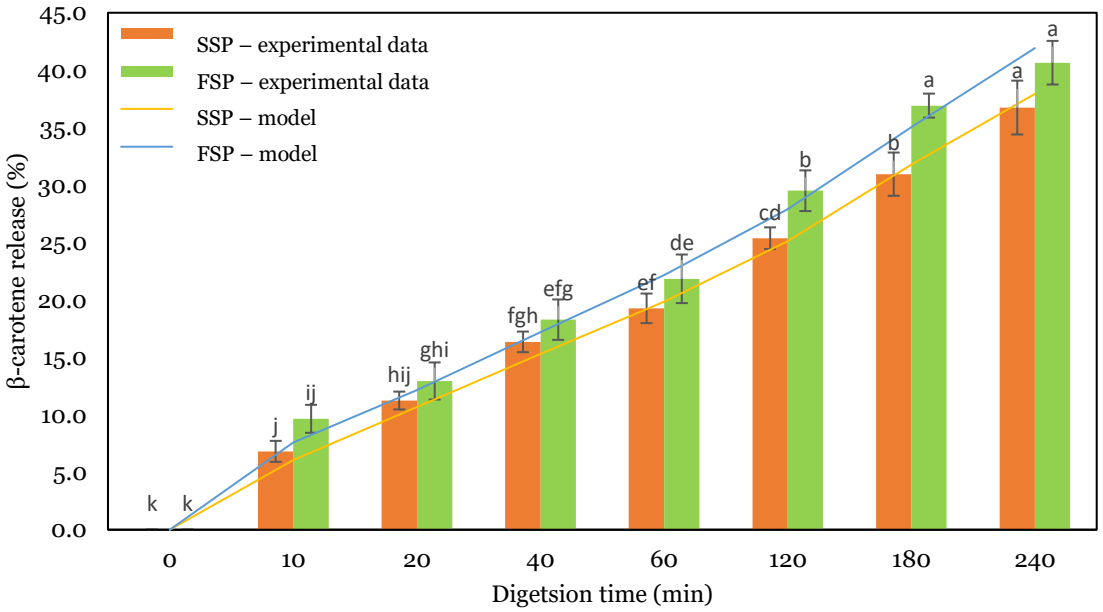

Figure 5.7: Graphical illustration of the influence of gastric juice soaking time on the ß-carotene (%) release profiles of the steamed and fried sweet potato matrix. Values are given as averages (n = 3) with error bars as SD. The prediction of the model of the Weibull function (Eq. 5.4) are represented by solid lines.

Table 5.4: Parameter values of Weibull function (Eq. 5.4 and Eq. 5.5) fitted to the ß-carotene (%) release profiles of the steamed and fried sweet potatoes.

	k	ß	R^2	SSE	$t_{1/2}$ (min)
SSP	0.001 ± 0.00^a	0.91 ± 0.01^a	0.96	0.002	694 ± 39^a
FSP	0.002 ± 0.00^a	0.89 ± 0.01^a	0.95	0.003	466 ± 85^b

R^2 is the goodness of fit; SSE is error sum of squares

k is the rate of ß-carotene release (min^{-1})

ß is the distribution shape factor (dimensionless)

$t_{1/2}$ is the ß-carotene release half-time (min)

SSP: Steamed sweet potatoes and FSP: Fried sweet potatoes

Values represent the average model parameters or ß-carotene release half-time from 3 digestion trials ± SD

Means within each column followed by different superscript letters are significantly different ($p<0.05$)

5.5 Conclusions

Steamed and fried sweet potatoes microstructure was expected to play an important role in the food matrix softening, disintegration as well as the release of ß-carotene during *in vitro* gastric digestion. In this study, the dynamic HGS model was employed to investigate the gastric juice diffusion on softening and disintegration kinetics of steamed and fried sweet potatoes. The rate of softening during *in vitro* gastric digestion was related to the disintegration kinetics and ß-carotene release of steamed and fried sweet potatoes. The mixed Weibull function can successfully be used to describe the cumulative distributions of particle surface areas of steamed and fried sweet potatoes during gastric digestion. Particle surface area distributions revealed that the kinetics of breakdown differed when the sweet potato was exposed to different cooking methods. FSP samples that were exposed to simulated gastric juice had a faster disintegration in the HGS, which contributed to both the erosion and chipping as well as to some extent fragmentation. The SSP samples exposed to simulated gastric juice had a much slower disintegration compared to FSP. Similarly, the rate of softening during *in vitro* gastric digestion was associated to the disintegration kinetics of steamed and fried sweet potatoes. Finally, findings of this chapter also highlighted that, in the presence of mechanical forces of human stomach, β-carotene release from sweet potato food matrix during gastric digestion was influenced by the different microstructure of steamed and fried samples. The effect of food microstructure on the disintegration kinetics of solid foods in the stomach described here will be important for developing innovative foods with desired functional properties.

Chapter Six

6. Characterisation of Egg White Gels Microstructure and its Relationship with Pepsin, Acid and Moisture Diffusivity during Static *In Vitro* Gastric Digestion*

6.1 Abstract

Fundamental knowledge of the diffusion of pepsin, acid and moisture into food structures during gastric digestion is crucial to better control the disintegration and release of nutrients. This chapter aimed to investigate how protein-based food microstructure, in the form of two different egg white gels (EWGs) with similar protein concentration (10%), impacts the pepsin, acid and moisture diffusion. The two different EWG models were prepared by heating fresh egg white, previously adjusted to two different pH values (pH 5 and pH 9). Their microstructures were evaluated using a high-resolution confocal microscopic technique followed by image analysis. To better understand the ability of pepsin to diffuse within each EWG's structure, the effective diffusivity (D_{eff}) of fluorescein isothiocyanate (FITC)-pepsin and FITC-dextran were measured in the native EWGs, using the fluorescence recovery after photobleaching (FRAP) technique. The neutral FITC-dextran (40 kDa) was used as a control to highlight the potential effects of electrostatic interactions between the egg white proteins and FITC-pepsin. The acid and moisture diffusion into the EWG structures were investigated using the hyperspectral imaging (HSI) technique. The microstructure of pH 5 EWG was characterised by a more porous and interconnected void network (mean particle size of 0.76±0.07 μm, with a mean interparticle distance of 1.79±0.57 μm) than that compact and homogeneous structure of pH 9 EWG (mean particle size of 0.32±0.02 μm, with a mean interparticle distance of 0.76±0.07 μm). As a result, the diffusivity of FITC-pepsin was significantly higher ($p<0.05$) for the pH 5 EWG than the pH 9 EWG (D_{eff} = 5.25±0.53 x10^{-11} m^2/s vs D_{eff} = 4.42±0.61x10^{-11} m^2/s). Similarly, it can be observed that pH 5 EWG had considerably ($p<0.05$) higher D_{eff} of water (5.6±1.4 x10^{-9} m^2/s) than pH 9 EWG (2.1±0.1 x10^{-9} m^2/s). However, both pH 5 EWG (2.4±0.1x10^{-9} m^2/s) and pH 9 EWG (2.3±0.6x10^{-9} m^2/s) had a similar ($p>0.05$) D_{eff} of acid during *in vitro* gastric digestion. Comparison of FITC-dextran and FITC-pepsin diffusivities confirmed the existence of electrostatic interactions between the egg white proteins and FITC-pepsin in the pH 5 EWG, but not in pH 9 EWG. In conclusion, the diffusion of gastric juice constituents

within the EWGs appeared to be not only modulated by the initial gel microstructure, but also by environmental conditions such as pH.

*Chapter six published as peer-reviewed papers as follows:

Somaratne, G., Nau, F., Ferrua, M. J., Singh, J., Ye, A., Dupont, D., Singh, R. P. and Floury, J. (2019). Characterization of egg white gel microstructure and its relationship with pepsin diffusivity. *Food Hydrocolloids*, Accepted.

Somaratne, G., Reis, M. M., Ferrua, M. J., Ye, A., Nau, F., Floury, J., Dupont, D., Singh, R. P. and Singh, J. (2019). Mapping the spatiotemporal distribution of acid and moisture in food structures during gastric juice diffusion using Hyperspectral Imaging. *Journal of Agricultural and Food Chemistry*, Accepted.

6.2 Introduction

Proteins, when present as the main constituent in a food matrix, are important for their nutritional properties and various functionalities such as gelling, emulsifying and foaming abilities (Foegeding & Davis, 2011). Digestion of food protein initiates in the stomach by the action of pepsin (Akimov & Bezuglov, 2012; Inglingstad *et al.,* 2010). The mobility of pepsin into food matrices and their subsequent breakdown in the gastric environment are strongly correlated with the food matrix structure (Guo *et al.,* 2015; Luo *et al.,* 2017; Nyemb *et al.,* 2016a; Thevenot *et al.,* 2017). Since food structure can have a critical role in determining the rate of peptide release in the stomach and absorption of amino acids/peptides in the small intestine, it is of ultimate importance to nutrition and health (Lorieau *et al.,* 2018; Luo *et al.,* 2017; Nyemb *et al.,* 2016a, b).

Egg white proteins mainly including ovalbumin, ovotransferrin, ovomucoid and lysozyme, are widely available and show a well-balanced profile of amino acids with high bioavailability (Abeyrathne, Lee, & Ahn, 2013; Matsuoka *et al.,* 2017). Besides their nutritional characteristics, the denaturation and aggregation behaviour of these proteins is of particular relevance toward the manufacture of hydro- or emulsion gel structures which can act as nutrients or drug delivery systems (Drakos & Kiosseoglou, 2006; Opazo-Navarrete *et al.,* 2018; Tomczyńska-Mleko *et al.,* 2016). Without altering the protein composition of egg white, changes in pH and ionic strength, followed by heat treatment can produce gels with varying macro- and micro-structural designs (Nyemb *et al.,* 2016a). Thus, EWGs provide interesting protein-based model food for investigating the food matrix effect on the diffusion kinetics of pepsin into food matrices.

A number of studies have provided evidence that the structure of egg white protein gelled with different pH conditions play a predominant role in their rate of *in vitro* and *in vivo* protein digestion as well as in the nature of peptides released (Nyemb *et al.,* 2016a, b; Nyemb *et al.,* 2015). Furthermore, these findings reported the microstructure of EWGs using TEM and SEM and demonstrated its impact on the digestion behaviour of these protein gels (Nyemb *et al.,* 2016a). However, there are no

systematic studies in the literature aimed at the quantitative description of the microstructure of the EWGs and their impact on the gastrointestinal digestion. This is partly due to a lack of appropriate techniques for undisturbed visualisation and quantification of dense microstructures of EWGs at an appropriate high resolution. The other unexplored aspect of the previous findings is the extent and rate to which digestive enzymes, particularly gastric pepsin can penetrate into the gel microstructure and contribute to hydrolyse the protein in EWGs.

Recent advances in CLSM and in fluorescent tracers make it possible to quantitatively characterise the microstructure and diffusion rate of the digestive enzyme within food matrix. The Airyscan technology was recently introduced by ZEISS using a new detector concept for CLSM. It mainly replaces the physical pinhole aperture with a 32-channel area detector to acquire the pinhole-plane image at each and every scan position (Huff, 2015). Thereby, this approach allows to enhance both the spatial resolution and signal-to-noise-ratio information of the micrographs, without increasing the excitation power and image acquisition time by averaging of multiple images, as it is often the case in conventional confocal microscopy (Huff, 2015; Korobchevskaya *et al.,* 2017). To our knowledge, this super-resolution imaging technique has never been applied for EWG microstructure observation. Yet it could allow visualisation and quantification of the morphological features of the microstructures of EWGs by simply using fluorescent dyes for labelling the egg white proteins. This technique could therefore represent an interesting alternative to other imaging techniques requiring laborious preparation of samples such as electron microscopy.

FRAP is a widely established CLSM based method for the estimation of effective diffusion coefficients of fluorescently labelled molecules. It has recently been used to study the mobility of the digestive enzymes within the food matrix (Guo *et al.,* 2017; Thevenot *et al.,* 2017). Techniques related to confocal microscopy including FRAP and FCS have been used to characterise the diffusion of pepsin in different dairy-based gel microstructures (Luo *et al.,* 2017; Thevenot *et al.,* 2017). Luo *et al.* (2017), has shown that the architecture of the dairy-based gel matrix could affect the overall proteolysis reaction rate and the gels breakdown properties. However, the diffusion of pepsin into the protein-based gel matrix depends on the type of protein and thus, it is required to investigate the pepsin diffusivity within the individual sources of protein.

Apart from pepsin, the gastric digestion of protein also related to the acidic environment of the gastric juice (Van Wey *et al.,* 2014). The hydrochloric acid was capable of activating pepsin whereas moisture in gastric juice capable of hydrating the food matrix which contributes to mechanical disintegration during gastric digestion (Minekus *et al.,* 2014; Ozvural & Bornhorst, 2018). However, there is still a limited

understanding of the diffusivity of hydrochloric acid and water into the protein-based gel matrixes.

With all the above background information, the objectives of this chapter were to gain an understanding of the microstructural characteristics of egg white protein gels (pH 5 and pH 9 EWGs) using a high-resolution confocal microscopy, and to identify how the diffusion properties of fluorescently labeled FITC-pepsin and FITC-dextran (40 kDa) is affected by the EWG matrices using the FRAP technique. Moreover, this chapter was also explored the feasibility of HSI, in the range 550–1700 nm, for predicting total acid and moisture distributions in EWG matrices during *in vitro* gastric juice diffusion process. Finally, the microstructural parameters of EWGs were qualitatively related to the diffusivity of FITC-pepsin, water and acid. Furthermore, the diffusivity of FITC-dextran (40 kDa) was used to identify any electrostatic interactions (if presence) between the egg white proteins and FITC-pepsin.

6.3 Materials and Methods

6.3.1 Materials

Fresh eggs were purchased from a local supermarket (Rennes, France). The total protein (N×6.25) in the egg white was determined using the Kjeldahl method (AOAC method, 2005). Fast Green, pepsin from porcine gastric mucosa, FITC, and FITC–dextran of the average molecular weight of 40 kDa were purchased from Sigma-Aldrich (St. Louis, MO, USA). Pepsin was labelled with FITC as described in section 6.3.6. The FITC-pepsin was used to evaluate the diffusion rate of pepsin within the different EWG structures. The FITC–dextran was dissolved in sterile water to a concentration of 50 mg/mL and used to investigate the diffusion rate of a chemically inert molecule within the EWG matrices. All the reagents used were analytical grade. Milli-Q water (Millipore Corp., Bedford, MA, USA) was used for all experiments.

6.3.2 Preparation of Egg White Solution

The eggs were manually broken, and the egg whites were carefully separated from the yolks. The whole egg white solution (250 mL) was homogenized using an IKA T-18 Ultra Turrax Digital Homogenizer (10,000 rpm for 1 min). Two sub-samples of egg white solution were taken, and the pH of each sub-sample was adjusted to pH 5.0 or pH 9.0, respectively, using 2 M HCl or 2 M NaOH. Egg white solutions were then diluted with Milli-Q water to 10% protein concentration.

6.3.3 Egg White Gel Preparation for Microstructure Study

For the gel microstructure study, about 600 μL of the pH 5 or of the pH 9 egg white solution were poured into 1 mL Eppendorf tubes. They were mixed with 6 μL aliquot of 1% (wt/v) of Fast Green. The mixture was vortexed, and then each solution (100 μL) was slowly injected into the chamber of an IBIDI μ-Slide I Luer system (IBIDI GmbH, Martinsried, Germany). The IBIDI system was then covered using aluminum foils to prevent photo-bleaching of fluorescent molecules. The IBIDI systems were horizontally heated at 80 °C for 5 min in a temperature-controlled water bath. After heating, the samples were cooled to room temperature and stored at 19 °C in an air-conditioned room until measurements.

6.3.4 EWG Preparation for the FRAP Analysis

For the FRAP analysis, about 150 μL of each egg white solution was poured into the individual wells of an open IBIDI μ-Slide (chambered coverslip) with 8 wells system (IBIDI GmbH, Martinsried, Germany), and covered with a coverslip. As described earlier, the IBIDI systems were horizontally heated at 80 °C for 5 min in a temperature-controlled water bath. After heating, the samples were cooled to room temperature and stored at 19 °C in an air-conditioned room until measurements.

6.3.5 EWG Preparation for the Hyperspectral Imaging

For the HSI analysis, pH adjusted egg white solutions were put in sealed plastic cylindrical containers (inner diameter 20 mm) and were heated in a water bath at 80 °C for 60 min. After heating, the gels were cooled and kept at 4 °C for 20 min. Then gels were removed from the plastic casings and cut into 30 mm length using a surgical scalpel blade.

Preliminary studies were conducted to identify the time and temperature combinations of each EWG preparation methods (Sections 6.3.3, 6.3.4 and 6.3.5) that generate the similar microstructural properties of prepared pH 5 and pH 9 EWGs. The details of the development of protein-based product models and their initial parameters such as weight of the sample, microstructure, diameter and length were given in Appendix 2.

6.3.6 Pepsin Labeling

For the FRAP analysis, FITC-pepsin was kindly provided from the UMR1253 laboratory, INRA, Agrocampus Ouest, Rennes, France. According to the UMR1253 laboratory records, pepsin was labelled with FITC according to the manufacturer's

instructions as described in a previous study (Thevenot *et al.,* 2017). Moreover, UMR1253 laboratory records reported that the pepsin inactivation by the labelling reaction was checked by measuring the FITC-pepsin activity using haemoglobin as the substrate according to the method described in Minekus *et al.* (2014) (Appendix 3). The FITC-pepsin was dissolved in sterile water to a concentration of 50 mg/mL before FRAP analysis.

6.3.7 Confocal Imaging

The EWGs labeled with Fast Green were imaged with the inverted LSM 880 confocal laser scanning microscope (Carl Zeiss AG, Oberkochen, Germany) using the Airyscan detection unit. To maximize the resolution enhancement, a Plan Apochromat 63x with a high numerical aperture (NA = 1.40) oil objective was used. A He/Ne laser with a wavelength of 633 nm was used to excite the Fast-Green dye, with appropriate emission in each system. Laser power, detector gain, and pixel dwell times were adjusted for each dataset keeping them at their lowest values in order to avoid saturation and bleaching effects.

Airyscan images were acquired with 7% of the maximum with a main beam splitter MBS488/561/633, no additional emission filter, a gain setting of 700 to 780, a pixel dwell time of 1.54 µs and no averaging. The zoom was automatically set at 1.8 as requested by the system. For further image analysis, at least ten micrographs of 1336x1336 pixels (1 µm = 18.17 pixels) were taken on different regions in a constant z-position (at a depth of 8 µm from the surface) of three independent samples of each of the two EWGs.

Zen Black 2.1 (Version 13.0.0.0) software was used to process the acquired datasets using the 2D mode at default settings of the Airyscan processing function. The software processes each of the 32 Airy detector channels separately by performing filtering, deconvolution and pixel reassignment in order to obtain images with enhanced spatial resolution and improved signal-to-noise-ratio. This processing includes a Wiener filter deconvolution with options of either 2D or a 3D reconstruction algorithm as described in Huff (2015).

6.3.8 Image Analysis

The microstructure of the EWGs were characterised from the Airyscan confocal micrographs using FIJI software and according to the image analysis technique previously described by Silva *et al.* (2015a), with slight modifications. The egg white protein network was enhanced using a white top-hat filter by removing the artifacts, and

smoothening was done to remove acquisition noise. The enhanced image was converted to a binary image using the Otsu thresholding algorithm with egg white protein phase contributing black pixels and aqueous phase contributing white pixels. The segmentation procedure was validated by visual comparison of the resulted binary image with its original image. Figure 6.1 shows the schematic representation of the confocal micrographs segmentation procedure.

Quantification of microstructural parameters was performed using MorphoLibJ, Granulometry and Geodesics plugins as previously reported in Legland, Arganda-Carreras, & Andrey, (2016); Legland *et al.,* (2012); Silva *et al.* (2015a) and Thevenot *et al.* (2017). Five different microstructural parameters were determined. They are particle area fraction (ratio between the protein matrix area with respect to the total area of the image), boundary length per unit area (ratio between the length of the perimeter around all the protein particle aggregate edges or boundaries with respect to the total image area), size of particle aggregates, inter-particle aggregate distances and the tortuosity parameter, which is defined as the ratio of the actual flow path length through the pores to the shortest distance between the beginning and the end of the flow path (the Euclidean distance) (Silva *et al.,* 2015a; Thevenot *et al.,* 2017).

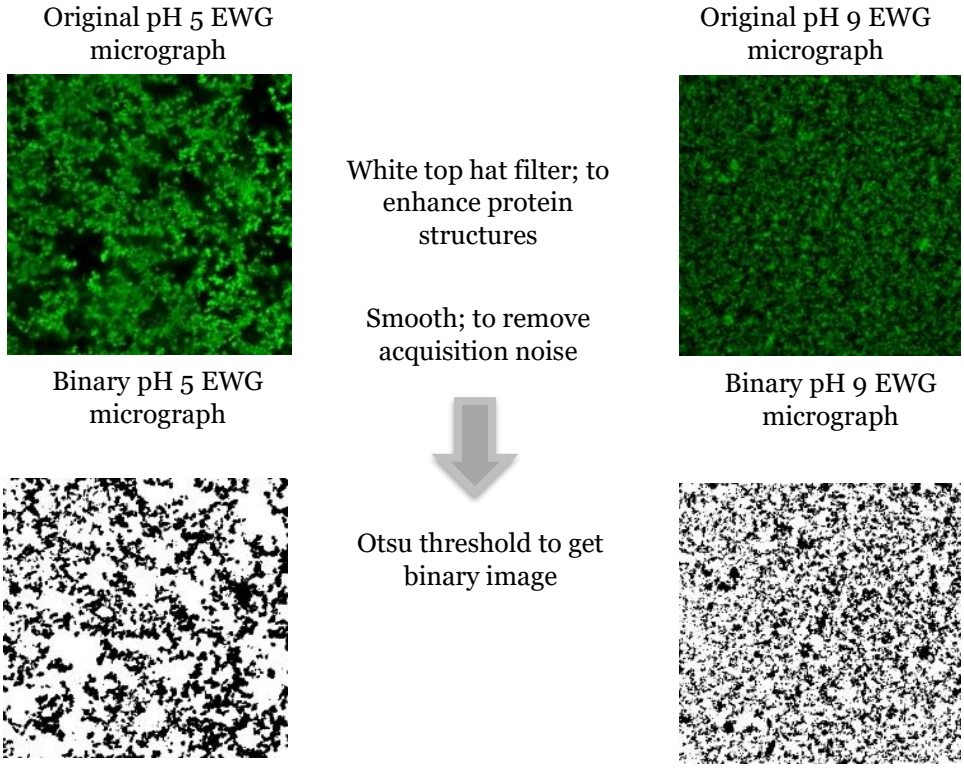

Figure 6.1: Schematic representation of the confocal micrographs segmentation procedure

6.3.9 Fluorescence Recovery After Photobleaching Analysis

Effective diffusion coefficients of fluorescently labelled pepsin, as well as labelled dextran within EWGs were determined using an adaptation of the FRAP protocol described by Floury *et al.,* (2012) and Thevenot *et al.* (2017). EWGs were prepared in the individual wells of an open IBIDI µ-Slide system as described earlier (section 6.3.4) and then a 20 µL aliquot of 50 mg/mL FITC-pepsin and FITC-dextran (40 kDa) was added to the surface of the gel sample. To ensure fluorescent molecules to migrate from the surface of the gel toward the bottom of the sample, the samples were kept at room temperature (20 °C) for approximately 30 min before measuring. For each gel type, three different gels were prepared separately to ensure the reproducibility of the gel-processing stage.

The FRAP analysis was performed on the CLSM (Zeiss LSM880, Oberkochen, Germany). All diffusion measurements were performed at 20 °C in an air-conditioned room. The FITC-pepsin and the FITC–dextran were excited using the argon laser system at a wavelength of 488 nm and detected on a 495–580 nm spectral bandwidth. The 488 nm argon laser was set to between 0.5 and 5% for imaging and 100% for bleaching step. The pinhole was set to one airy unit. Samples were observed at a constant depth of 15 µm from the sample surface using a 40×objective lens (oil immersion) with a numerical aperture of 1.30. The bleached region was a circular region within each image with a radius of 5 µm. A rectangle region was selected as the background. The bleached region was scanned with 20 pre-bleach images and then bleached with 150 iterations followed by fluorescence recovery. A total of 480 images were captured during post-bleaching at 0.1 ms intervals until full recovery was reached. Ten FRAP acquisitions were carried out on the different locations of each EWG.

Control FRAP experiments were achieved in the same conditions in water with the FITC-dextran (40 kDa) and FITC-pepsin with a concentration of 0.5 mg/mL, according to the method as described in Silva, Lortal, & Floury (2015b). Briefly, the fluorescent water (100 µL) was poured between a glass slide and a cover slip sealed with an adhesive frame (Geneframe, ABgene House, UK).

6.3.10 Fluorescence Recovery After Photobleaching Data Analysis

Data were analysed by using the analytical method described in Thevenot *et al.* (2017), with the assumptions of pure isotropic diffusion in a homogeneous medium and a two-dimensional diffusion process using the classical diffusion equation given by Fick's second law. Analyses of the recorded images were performed using FIJI software and the

D_{eff} were obtained by data fitting via nonlinear least squares with RStudio software as follows.

The normalization of FRAP recovery

The mean intensity $F_{ROI(t)}$ within a ROI of radius W_B= 2.5 µm and the background region was obtained as a function of time using the Zen black software. The centre coordinates (x and y) of the ROI was noted. The FRAP recovery curves were normalized to correct the loss of fluorescence caused by photobleaching that might have occurred during the imaging of the recovery phase (Silva *et al.,* 2013). The normalized fluorescence recovery inside the ROI was calculated using the following equation:

$$F_M^{2D}(t) = \frac{I(t)-(BG(t)-BGi)}{Ii} \qquad \text{(Eq. 6.1)}$$

Where I(t) and BG(t) are the fluorescence in the ROI and in a background region obtained from the ROI at recovery time t, respectively. BGi and Ii are the average fluorescence during the pre-bleach phase in the background region and in ROI, respectively.

After the photobleaching of the ROI, the bleached fluorophore molecules will be replaced by intact fluorophores by diffusion. This fluorophore concentration distribution at a time t after photobleaching is assumed to be isotropic two-dimensional diffusion in a homogenous medium which can be calculated by solving Fick's second law:

$$\frac{\partial}{\partial t} C(\vec{r},\ t) = D\nabla^2 C(\vec{r},\ t) \qquad \text{(Eq. 6.2)}$$

Where $C(\vec{r},\ t)$ is the concentration of the unbleached fluorophores at position $\vec{r}$ and time t.

The analytical solution of Fick's second law for a radial direction normalized fluorescence recovery inside a region of interest of radius W_B is given by:

$$F_M^{2D}(t) = \frac{Fo}{2}\left(\left(\frac{W_M^2}{W_B^2}\right)\left[\sum_{n=1}^{+\infty}\frac{(K_M)^n}{n!n}\left(1 - exp\left(\frac{-2n}{1+2n\frac{t}{\tau_D}}\cdot\frac{W_B^2}{W_M^2}\right)\right)\right] + 2\right) \qquad \text{(Eq. 6.3)}$$

Where F_M^{2D} is the mean normalized fluorescence intensity inside the ROI, W_B is the radius of ROI (m), W_M is the profile width in the radial direction (m) and K_M is the bleach efficiency for the mobile molecule (the origin of the coordinates is the centre of the bleach region).

Unknown parameters of W_M and K_M were estimated by fitting the following Eq. (6.4) to the experimental first post-bleach image intensity profile using an ImageJ macro developed by Waharte *et al.* (2010):

$$F_M(r,0) = exp\left(-K_M \exp\left(-2\,\frac{r^2}{W_M^2}\right)\right) \qquad \text{(Eq. 6.4)}$$

FRAP recovery curves were then fitted with Eq. (6.3) (n = 100) using the function *nls* in RStudio (version 3.4.3), yielding to the characteristic recovery time τD (s). The D_{eff} was obtained from the best-fit value of τD using the following relation:

$$D_{eff} = \frac{W_M^2}{4\tau_D} \qquad \text{(Eq. 6.5)}$$

The reduced diffusion coefficient (D_r) was calculated as the ratio of the D_{eff} for the FITC–pepsin or FITC–dextran in the gel matrix divided by the D_{eff} of the same probe in water.

6.3.11 Determination of Acid and Moisture Diffusivity using hyperspectral imaging

HSI technique developed in chapter 3 (section 3.3 Materials and Methods) was used to characterise the diffusion of acid and water within EWG structures during gastric digestion. EWG structures were prepared for the diffusion study and exposed to *in vitro* gastric digestion before scanning by HSI (as described in section 3.3.5). Then, cylindrical EWG samples were removed at different gastric digestion times (0 to 240 min) and two slices (5 mm thickness) were obtained from their central parts (as described in section 3.3.5). The spatial distribution of moisture and acid within the digested samples were determined by scanning each of the slices with the HSI system (as described in section 3.3.6). After that, each corresponding EWG slice was used to determine (using gravimetric analytical methods) the total amount of moisture (section 3.3.7) or acid (section 3.3.8) present in it for calibration purposes. Calibration models were subsequently built using PLS (as described in the section 3.3.9 and 3.3.10). The spatiotemporal distributions of moisture and acid were mapped across the digested EWG matrix (as described in section 3.3.11). Finally, the kinetics and mechanism of acid and moisture diffusion into the pH 5 and pH 9 EWGs was described mathematically using Fick's second law and the power-law model (as described in section 3.3.12).

6.3.12 Statistical Analysis

The Student's t-test was applied in order to compare the microstructural parameters of the two EWGs. One-way ANOVA and Tukey's paired comparison test were applied to the FITC-pepsin and FITC-dextran diffusion coefficient data of the two different EWGs and water to determine which mean values were significantly different from one another at the 95% confidence level.

An ANOVA was conducted using a 2-factor factorial design to determine differences in acid and moisture uptake during simulated gastric digestion. The factors were EWG types (pH 5 and pH 9 EWG), and digestion time (0–240 min). A Tukey multiple comparison test was implemented to investigate the differences among means when the main effects were significant. The Student's t-test was used to assess differences in Fick's second law and the power-law model parameters. Minitab 17 software was used for statistical analysis.

6.4 Results and Discussion

6.4.1 Observation of Native Egg White Gels Microstructure

The EWG microstructure can be defined as the arrangement of egg white protein aggregate particles. Figure 6.2 shows the two different EWGs (pH 5 and pH 9) micrographs obtained from confocal imaging. Thanks to Fast Green labelling, proteins appear coloured in green on the confocal micrographs, while associated pores in aqueous phase appear in black.

As shown in micrographs, the microstructural organization strongly differs between pH 5 EWG (Figure 6.2(a)) and pH 9 EWG (Figure 6.2(b)). When the pH is adjusted to pH 5 before heat gelation, egg white produced a more porous, loosely packed and heterogeneous protein network. Conversely, when the pH of the egg white solution is adjusted to pH 9, it produced a dense and more homogeneous protein network. This result was in precise agreement with earlier reported SEM and TEM observations for pH 5 granular and pH 9 smooth EWGs microstructure (Nyemb *et al.,* 2016a). These authors also observed large spherical aggregates in pH 5 EWG and both small spherical and linear aggregates in pH 9 EWG.

6.4.2 Microstructural Parameters of Native Egg White Gels

From the series of micrographs of each gel microstructure, particle area fraction, boundary length per unit area and tortuosity were calculated (Table 6.1). Particle area fractions were not statistically different ($p>0.05$) between the pH 5 and pH 9 EWGs. This result is not surprising because the protein concentration was the same in both gels (10%). However, the boundary length per unit area was significantly ($p<0.05$) larger for the pH 9 EWG (1.93±0.11 μm/μm^2) than for the pH 5 EWG (0.92±0.20 μm/μm^2), consistently with the significantly smaller particle size at pH 9 when compared to pH 5. Indeed, the mean particle size was 0.76±0.07 μm for pH 5 EWG and 0.32±0.02 μm for pH 9 EWG (Table 6.1). On the contrary, the tortuosity parameter was significantly ($p<0.05$) larger for the pH 5 EWG (1.14±0.14) than for the pH 9 EWG (1.07±0.01).

Similarly, inter-particle aggregate distance was significantly longer for the pH 5 EWG (1.79±0.57 μm) than for the pH 9 EWG (0.76±0.07). This indicates smaller voids between particles in the pH 9 EWG when compared to the pH 5 EWG.

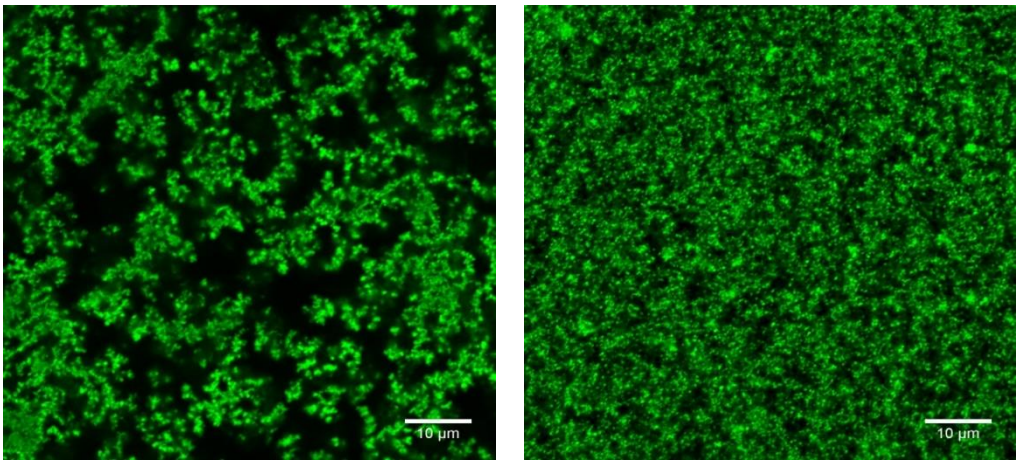

(a) (b)

Figure 6.2: pH 5 EWG (a) and pH 9 EWG (b) micrographs obtained from the confocal imaging.

Table 6.1: Quantitative parameters characterising the microstructure of pH 5 and pH 9 EWGs obtained from image analysis on binary confocal micrographs.

Parameter	pH 5 EWG	pH 9 EWG
Particle area fraction	0.31±0.08[a]	0.29±0.02[a]
Boundary length per unit area (μm/μm²)	0.92±0.20[b]	1.93±0.11[a]
Tortuosity	1.14±0.14[a]	1.07±0.01[b]
Particle aggregate size (μm)	0.76±0.07[a]	0.32±0.02[b]
Inter-particle aggregate distance (μm)	1.79±0.57[a]	0.76±0.07[b]

The results are expressed as the mean ± SD (n=30)
Means within each line followed by different superscript letters are significantly different ($p<0.05$)

Thus, consistently with the qualitative analysis of the micrographs presented above, the quantitative parameters measured on the images confirm that the pH 5 EWG presented both mean particle size and an inter-particle aggregate distance significantly greater ($p<0.05$) than that for the pH 9 EWG. Moreover, Figure 6.3 highlights broader distributions of both particle size and inter-particle aggregate distance for the pH 5 EWG, meaning that this latter EWG is more heterogeneous than the pH 9 EWG. The dense and homogeneous structure of the pH 9 EWG, made of small protein aggregates with

abundant small pores, explains the lower tortuosity value of this gel than that of the pH 5 EWG, made of non-homogeneously distributed large protein aggregates and many interconnected large pores.

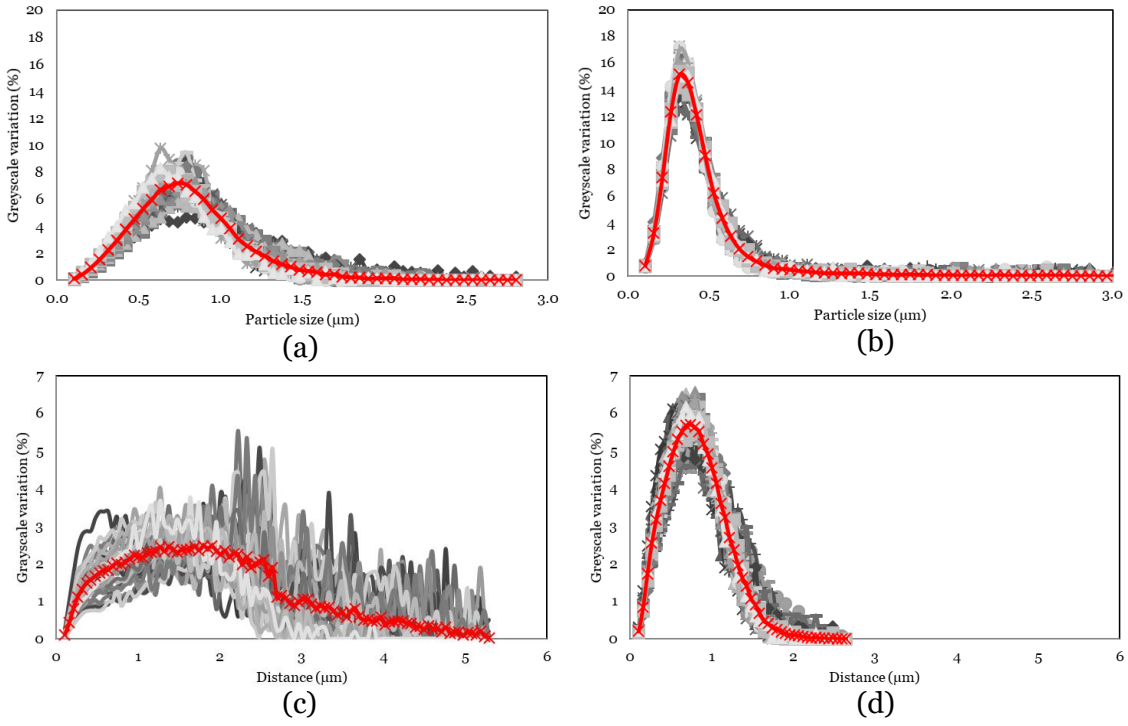

Figure 6.3: Distribution of particle aggregate sizes (µm) in confocal micrographs of (a) pH 5 EWG and (b) pH 9 EWG. Distribution of inter-particle aggregate distances in confocal micrographs of (c) pH 5 EWG and (b) pH 9 EWG. The average curve (red solid line) of each graph was obtained from 30 individual curves (grey solid lines).

These results are very much in line with the mechanism of globular protein heat gelation, and especially with the impact of pH conditions on the equilibrium between the denaturation and aggregation steps that occur during such gelation (Doi, 1993). At pH 5, close to the isoelectric point of most egg white proteins, electrostatic repulsions between proteins are minimal, thus favoring aggregation which leads to spherical aggregates and finally coarse particulate EWG (Nyemb *et al.,* 2016a). In contrast, at pH 9, electrostatic repulsions between proteins are much higher, favoring denaturation more than aggregation, and leading to linear aggregates which produce a more homogeneous protein network (Clark, Kavanagh, & Ross-Murphy, 2001; Nyemb *et al.,* 2016a).

6.4.3 Effective Diffusion Coefficients of FITC-pepsin and FITC–dextran in EWG

Typical fluorescence recovery curves with the FITC-labeled solutes in the EWG matrices and in water are presented in Figure 6.4. Diffusion profiles along with selected FRAP images before, during, and after photo-bleaching revealed distinct profiles for each gel matrices and water (Figure 6.4). Nearly complete fluorescence recovery for all the FITC-pepsin and FITC-dextran curves was observed, suggesting isotropic diffusion of fluorescent molecules within gel matrices and water.

The D_{eff} obtained from the modelling of the experimental data are summarised in Table 6.2. The measure of the activity of the fluorescently labelled pepsin using FITC showed that the enzyme was fully inactivated (see Appendix 3). This may be due to the alkaline pH (around pH 8) experienced by the pepsin during the labelling process. It is reported that pepsin can inactivate as a result of a completely irreversible alkaline denaturation in a narrow pH range (between pH 6 and pH 7) (Kamatari, Dobson, & Konno, 2003; Lin *et al.,* 1993). Thus, FITC-pepsin diffusion does not affect the microstructure of the EWGs, and the reported values of FITC-pepsin diffusion in this study represent the D_{eff} value within the native gels.

In agreement with the fluorescence recovery curves (Figure 6.4), the calculated D_{eff} of FITC-pepsin is higher than that of FITC-dextran, regardless of the treatment. The larger D_{eff} of FITC-pepsin compared to that of FITC-dextran may be the result of its smaller size, due to a lower molecular mass, a globular molecular shape and a smaller hydrodynamic radius (Braga, Desterro, & Carmo- Fonseca, 2004; Thevenot *et al.,* 2017). The FITC-pepsin has a hydrodynamic radius of 3.6 nm and the average molecular weight is 32.4 kDa (Thevenot *et al.,* 2017). On the other hand, FITC-dextran is a linear glucose-based polysaccharide and has a hydrodynamic radius of 4.5 nm and the average molecular weight is 40 kDa (Braga *et al.,* 2004).

The FITC-pepsin and FITC-dextran diffusion coefficients in water are 10.45±1.07 $x10^{-11}$ m^2/s and 4.57±0.61 $x10^{-11}$ m^2/s, respectively, which is in agreement with previous studies (Braga *et al.,* 2004; Tyn & Gusek, 1990). As expected, compared with the diffusion coefficients measured in water, those measured within the EWG matrices were significantly ($p<0.05$) lower, more particularly within the pH 9 EWG. The sterical hindrance effect imposed by the microstructure of the EWGs may be the main factor that influences the extent of fluorescent probes mobility.

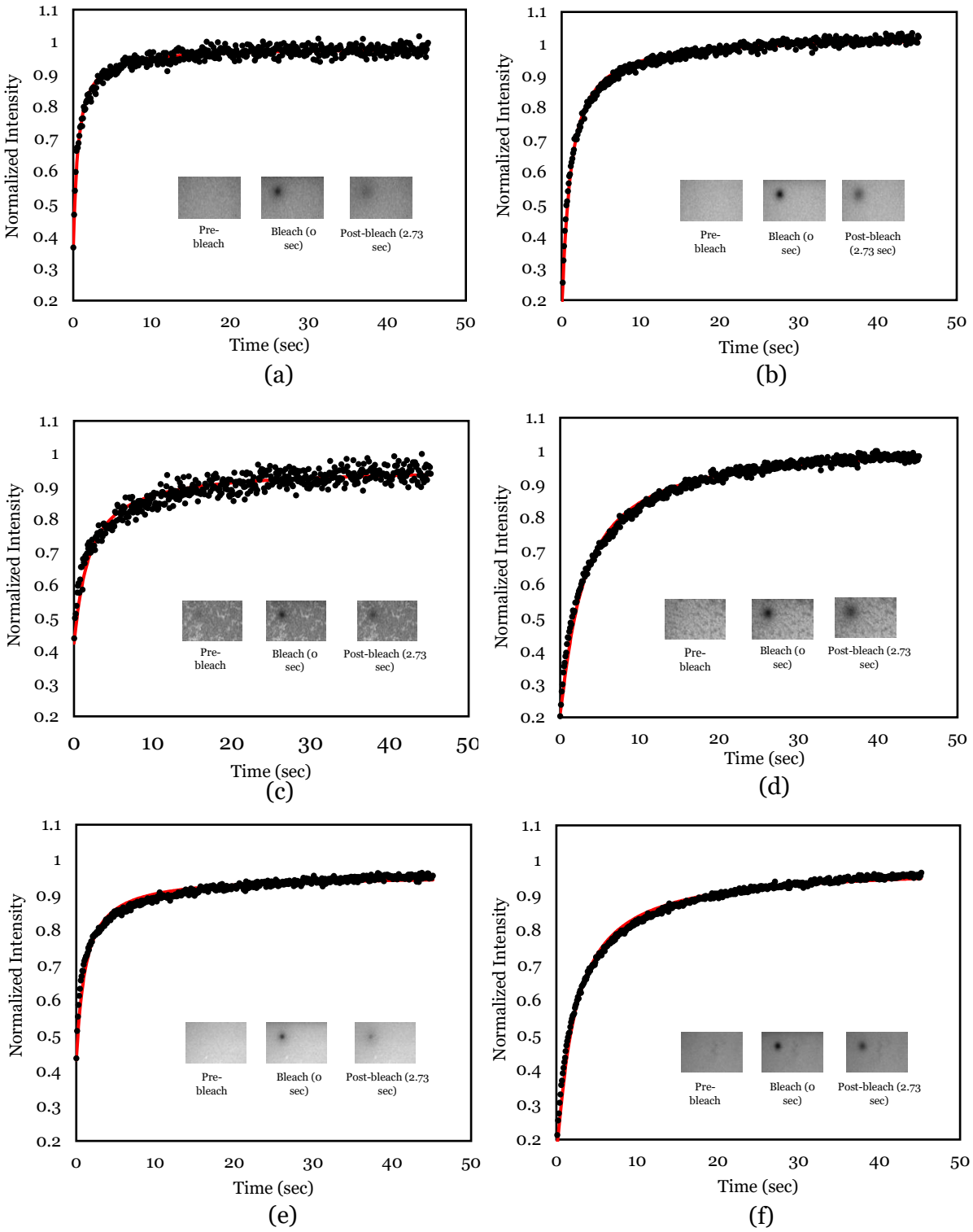

Figure 6.4: Representative FRAP profiles and images before bleaching and after 0 and 2.73 s (30th post-bleaching image) for diffusion of (a) FITC-pepsin in water, (b) FITC-dextran in water, (c) FITC-pepsin in pH 5 EWG, (d) FITC-dextran in pH 5 EWG, (e) FITC-pepsin in pH 9 EWG and (f) FITC-dextran in pH 9 EWG. Data points (black colour) denote the normalized experimental data and solid lines (red colour) denote the data curve fit.

Table 6.2: D_{eff} values relating to the mobility of FITC-pepsin and FITC-dextran in water and EWGs.

	D_{eff} (x10^{-11} m^2/s)	
	FITC-pepsin	FITC-dextran
Water	10.45±1.07^a	4.57±0.21^c
pH 5 EWG	5.25±0.53^b	2.59±0.41^d
pH 9 EWG	4.42±0.61^c	1.90±0.31^e

Effective diffusion coefficient: D_{eff}

Values are expressed as the mean ± SD (n=30)

Different letters represent statistically significant differences ($p<0.05$)

Previous studies highlighted that microstructural characteristics such as particle area fraction, pore size, pore connectivity and tortuosity are key variables required to understand the flow and transport behaviour of digestive enzymes within the food matrix (Grundy *et al.,* 2016; Thevenot *et al.,* 2017). In fact, the results of this study show that EWGs with the same particle area fraction, but differing in tortuosity, inter-particle aggregate distance and particle aggregate size, do not present the same efficiency for FITC-pepsin and FITC-dextran diffusion. It could be therefore hypothesized that the larger inter-connected pores and heterogeneous nature of the pH 5 EWGs contribute to higher tortuosity and inter-particle aggregate distance, and thereby increased FITC-dextran and FITC-pepsin diffusivity. In contrast, the more homogeneous and denser pH 9 EWG, with smaller unconnected pores, leads to smaller tortuosity and inter-particle aggregate distance, and thereby reduced the D_{eff} of FITC-dextran and FITC-pepsin.

6.4.4 Reduced Diffusion Coefficients of FITC-pepsin and FITC–dextran in Egg White Gels

The diffusion of fluorescent probes across protein-based food systems is a multiplex phenomenon that is based on several variables, such as microstructure of the systems, shape and size of the fluorescent molecule with respect to the pore shape and size of food architecture, as well as molecular interactions (Silva *et al.,* 2015b; Silva *et al.,* 2013). Interactions between neutral FITC–dextran and the components of the protein gels were found to be negligible (Floury *et al.,* 2012; Silva *et al.,* 2013). However, highly pH-dependent interactions can be observed between pepsin and substrate protein molecules (Campos & Sancho, 2003; Nyemb *et al.,* 2016a; Yasnoff & Bull, 1953). Thus, in this study, FRAP-based diffusion of FITC-dextran within EWGs was used as a proxy to assess any interaction effects of FITC-pepsin and egg white protein molecules.

Table 6.3 shows the D_r (i.e. the ratio of effective diffusion coefficient in the gel matrix to the diffusion coefficient in water) of FITC–dextran and FITC-pepsin in the two different EWGs. The D_r is considered as an indicator of the effects of the presence of any interactions between protein particles and FITC-pepsin (if they take place) on the diffusion behaviour of the enzyme (Floury *et al.,* 2012).

Table 6.3: Reduced diffusion coefficient (Dr) values relating to the mobility of FITC-pepsin and FITC-dextran.

	Dr	
	FITC-pepsin	FITC-dextran
pH 5 EWG	0.50±0.05[a]	0.57±0.09[b]
pH 9 EWG	0.42±0.06[c]	0.42±0.07[c]

Values are expressed as the mean ± SD (n=30)
Different letters represent statistically significant differences ($p<0.05$)

Table 6.4: Net charge of the pepsin and major egg white proteins at pH 5 and pH 9. The given net charge values and the estimated pI (isoelectric point) of the proteins were calculated by using the online Protein Calculator v3.4 (http://protcalc.sourceforge.net/).

	% of egg white proteins	net charge at pH 5 (mV)	net charge at pH 9 (mV)	Estimated pI (isoelectric point)
Pepsin	-	-18.0	-38.8	4.23
Lysozyme	3.5	10.8	0.2	9.04
Ovotransferrin	12.5	27.9	-33.0	7.00
Ovalbumin	54	4.2	-20.2	5.29
Ovomucoid	11	-0.3	-26.3	4.97

Interestingly, the Dr was similar for FITC-pepsin and FITC-dextran within the pH 9 EWG (Dr=0.42), indicating no interaction between egg white proteins and FITC-pepsin during the diffusion process in this EWG. By contrast, the Dr was significantly smaller for FITC-pepsin (Dr=0.50±0.05) than for FITC-dextran (Dr=0.57±0.09) within the pH 5 EWG, suggesting interactions between FITC-pepsin and this EWG matrix. Such difference between both EWGs is consistent with the modification in the net charge of the diffusing pepsin and of the main egg white proteins as a function of the pH of the system (Table 6.4). Most of egg white proteins are positively charged at pH 5, whereas

the net charge of pepsin is negative, thereby enhancing egg white proteins-pepsin electrostatic interactions. In contrast, at pH 9 both egg white proteins and pepsin net charges are negative. Thus, the interactions between the FITC-pepsin and the egg protein matrix could be negligible in the pH 9 EWG, due to electrostatic repulsions.

6.4.5 Moisture and Acid Content of Egg White Gels

Moisture content evolution during simulated gastric digestion for both EWGs is shown in Table 6.5. Moisture content was significantly influenced by digestion time ($p<0.05$, Table 6.5). Although, moisture at times 180 and 240 min in both pH 5 and pH 9 EWG was significantly different from the other digestion times ($p<0.05$) but did not change significantly between 0 and 180 min of digestion. The moisture content between pH 5 and pH 9 EWGs at all most all the times during digestion were similar.

The acid content for each EWGs during the 240 min digestion period in gastric juice is shown in Table 6.5. The acid content of the EWGs was significantly influenced by the type of EWGs, digestion time, and their interaction ($p<0.05$). pH 5 EWG exhibited comparatively high acid content whereas pH 9 EWG had no initial acid compared to the pH 5 EWG (0.0 mg HCl/g of the sample compared to <1.1 mg HCl/g of the sample). pH 5 EWG had significant increases in acid content during the 240 min gastric digestion period ($p<0.05$). However, despite the gradual increase in acid content over the 240 min digestion period, no significant ($p>0.05$) changes in acid content during digestion were observed for pH 9 EWG.

6.4.6 Moisture Content Prediction

Table 6.6 shows the main statistics used to evaluate the performance of the developed calibration and prediction models for predicting the moisture content of the examined pH 5 and pH 9 EWG samples. Calibration models generated using hyperspectral data with R^2 values of greater than 0.70 can be considered as good enough for prediction purposes (Caporaso *et al.,* 2018; Williams & Sobering, 1996). Thus, it was observed that the PLS calibration models based on full spectra had a very good ($R_{cal}^2>0.70$) (Caporaso *et al.,* 2018; Williams & Sobering, 1996) moisture prediction accuracy for both pH 5 and pH 9 EWG food matrices, with $R_{cal}^2>0.88$ and RMSEC<0.13 (Table 6.6). The application of HSI has been reported previously for moisture determination in biological products (i.e. mango, banana and strawberry), demonstrating a similar prediction performance of $R^2\geq0.90$ of PLS regression calibration built on the wavelengths of 400 nm and 1000 nm (ElMasry *et al.,* 2007; Pu & Sun, 2015; Rajkumar *et al.,* 2012).

Table 6.5: Moisture contents (% wet basis) and acid contents (mg HCl/g of sample) of EWGs during 240 min of *in vitro* gastric digestion.

Moisture content (% wet basis)	Digestion time (min)							
	0	10	20	40	60	120	180	240
pH 5 EWG	87.66 ± 0.13^{Ab}	87.79 ± 0.10^{Ab}	88.44 ± 0.01^{Aa}	88.70 ± 0.06^{Aa}	88.75 ± 0.07^{Aa}	88.73 ± 0.10^{Aa}	88.75 ± 0.04^{Aa}	88.78 ± 0.04^{Aa}
pH 9 EWG	87.89 ± 0.40^{Ab}	88.34 ± 0.09^{Aa}	88.28 ± 0.21^{Aab}	88.67 ± 0.09^{Aa}	88.33 ± 0.15^{Aa}	88.52 ± 0.13^{Aa}	88.17 ± 0.44^{Aa}	88.60 ± 0.17^{Aa}
Acid contents (mg HCl/g of sample)								
pH 5 EWG	1.11 ± 0.02^{Ac}	1.13 ± 0.01^{Ac}	1.19 ± 0.05^{Abc}	1.26 ± 0.04^{Ab}	1.27 ± 0.04^{Ab}	1.31 ± 0.03^{Aab}	1.33 ± 0.02^{Aa}	1.32 ± 0.02^{Aa}
pH 9 EWG	0.00 ± 0.00^{Ba}	0.01 ± 0.02^{Ba}	0.08 ± 0.01^{Ba}	0.14 ± 0.01^{Ba}	0.17 ± 0.01^{Ba}	0.14 ± 0.05^{Ba}	0.13 ± 0.02^{Ba}	0.16 ± 0.02^{Ba}

A-B Means within each column followed by different superscript letters are significantly different ($p<0.05$).

a-c Means within each line followed by different superscript letters are significantly different ($p<0.05$).

Values represent averages ($n = 3$) ± SD.

The predicted versus measured plots for the best PLS calibration models for moisture content are shown in Figure 6.5. It can be observed that the measured and predicted moisture values of pH 5 EWG (Figure 6.5(a)) are separated into two different regions. This could be due to the initial moisture content of the sample (87-88%) immediately (after 10 min, as seen in Table 6.5) reach the equilibrium moisture content (88.5-89.0%) after immersion in the gastric fluid.

In this study, all PLS models appeared to be acceptable since not more than four factors (LVs) were used in the development of calibration models (Table 6.6). When the calibrated model was used to predict the samples, the prediction results were also desirable, with a R_{pred}^2>0.80 between the measured and the predicted values for both EWGs and the RMSEP<0.19 for pH 5 and pH 9 EWGs (Table 6.6).

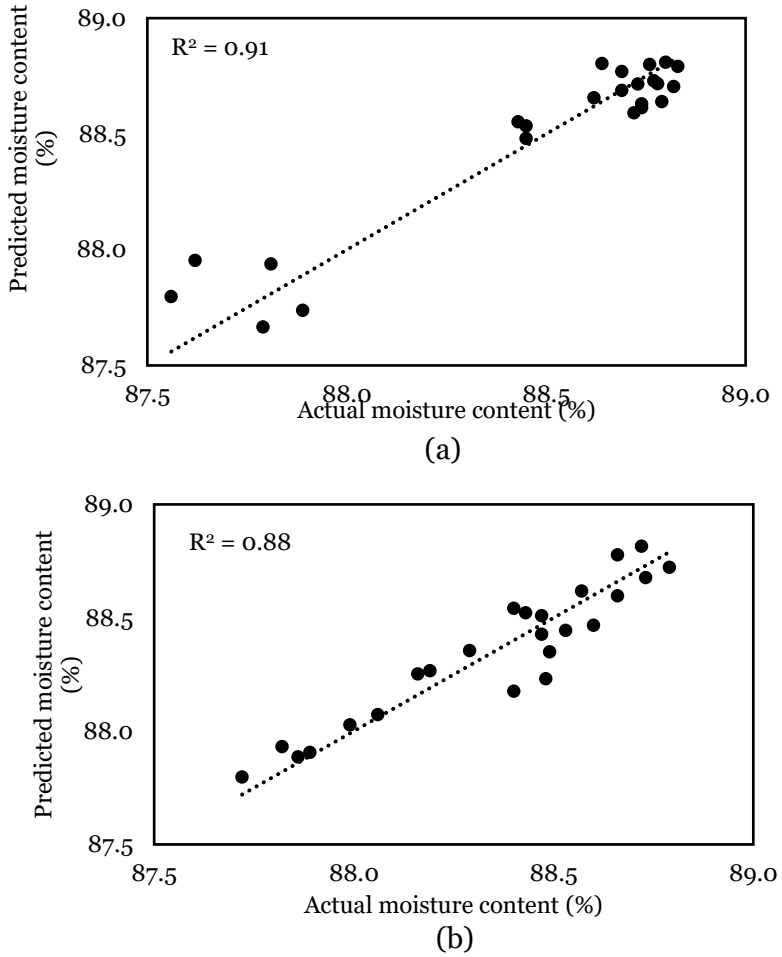

Figure 6.5: Predicted versus measured values of moisture in (a) pH 5 EWG and (b) pH 9 EWG for the best PLS models (calibration data set), expressing the moisture content as wet basis. The solid line shows the calibration line of the PLS regression model. Performance of the PLS regression model for moisture indicated as the determination coefficients (R^2).

Table 6.6: Performance of the PLS regression model for moisture content, for HSI quantification on pH 5 and pH 9 EWGs

		Calibration		Prediction	
	LVs	R_{cal}^2	RMSEC	R_{pred}^2	RMSEP
pH 5 EWG	3	0.91	0.13	0.83	0.19
pH 9 EWG	4	0.88	0.11	0.80	0.16

LVs: latent variables. Sample size (n): 24. Spectral range: 550–1700 nm. R_{cal}^2 = coefficient of determination of calibration, R_{pred}^2 = coefficient of determination of prediction, RMSEC = root mean square error of calibration. RMSEP = root mean square error of prediction.

6.4.7 Acid Content Prediction

The main statistics used to evaluate the performance of the developed calibration and prediction models for predicting acid content of the examined pH 5 and pH 9 EWG samples are given in Table 6.7. The predicted versus measured plots for the best PLS regression models for acid content are shown in Figure 6.6. The performance of the PLS model was good ($Rcal^2 > 0.7$) (Caporaso *et al.,* 2018; Williams & Sobering, 1996) for acid prediction in pH 5 EWG (R_{cal}^2 = 0.87) and pH 9 EWG (R_{cal}^2 = 0.82). It was also demonstrated that all calibrated models had good performance with the low RMSEC<0.15. The R_{cal}^2>0.82 of the PLS calibration models obtained in this study was comparable to those reported previously by the application of HSI on vinegar culture to investigate their acid content, with R^2 of the PLS model equal to 0.86 (Zhu *et al.,* 2016). The PLS regression model appeared to be robust since less than four factors (LVs) were used in the calibration model development (Table 6.7). When the acid calibrated model was applied to the prediction set, the results were applicable with R_{pred}^2>0.80 between the measured and the predicted values and the RMSEP<0.25 for pH 5 and pH 9 EWGs (Table 6.7).

Table 6.7: Performance of the PLS regression model for acid content, for HSI quantification on pH 5 and pH 9 EWGs

		Calibration		Prediction	
	LVs	R_{cal}^2	RMSEC	R_{pred}^2	RMSEP
pH 5 EWG	3	0.87	0.03	0.82	0.25
pH 9 EWG	4	0.82	0.02	0.80	0.02

LVs: latent variables. Sample size (n): 24. Spectral range: 550–1700 nm. R_{cal}^2 = coefficient of determination of calibration, R_{pred}^2 = coefficient of determination of prediction, RMSEC = root mean square error of calibration. RMSEP = root mean square error of prediction.

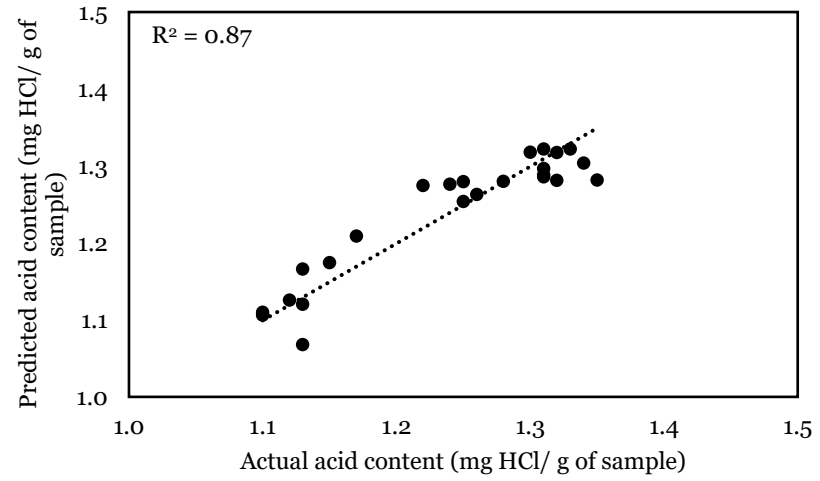

(a)

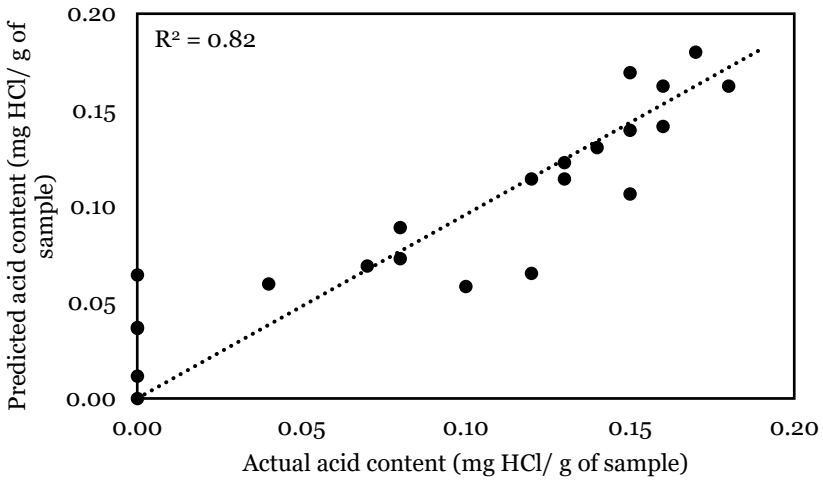

(b)

Figure 6.6: Predicted versus measured values of acid in (a) pH 5 EWG and (b) pH 9 EWG for the best PLS models (calibration data set), expressing the acid content as mg HCl/g of sample. The solid line shows the calibration line of the PLS regression model. Performance of the PLS regression model for acid indicated as determination coefficients (R^2).

6.4.8 Spatiotemporal Distribution of Moisture in Egg White Gel Structures during Gastric Digestion

The developed PLS regression models for the prediction of moisture in pH 5 and pH 9 EWG matrixes were applied to HSI hypercubes to visualise the spatial moisture distribution of digested samples with different digestion times. Figure 6.7 shows the final visualised image of the moisture distribution of pH 5 and pH 9 EWG product models at eight different gastric digestion times. Although there was variation in the distribution

in moisture content across the pH 5 and pH 9 EWG food matrices, there was a general trend of increase in overall moisture content represented by the shift from blue to red (Figure 6.7). This is an indication of EWG food matrices absorbing moisture during their gastric digestion.

More specifically, in pH 5 EWG, initially at around 87% moisture, gastric juice advanced rapidly: a homogeneous and stable moisture content (89%) was reached in after only 20 min of digestion. This is consistent with the porous nature of this EWG, as previously characterised by section 6.4.1 and 6.4.2. In contrast, the diffusion of moisture into the pH 9 EWG matrix is slower, the equilibrium is reached after approximately one-hour digestion. This is consistent with the more compact-dense microstructure of pH 9 EWG (section 6.4.1 and 6.4.2) which might hinder the penetration of gastric moisture.

6.4.9 Spatiotemporal Distribution of Acid in Egg White Gel Structures during Gastric Digestion

The spatiotemporal distribution of acid in EWG structures during gastric digestion is displayed in Figure 6.8. Figure 6.8 (a) clearly shows that acid diffusion into the pH 5 EWG matrix is anisotropic in the radial plane. This may be due to the irregular and interconnected pore paths distribution within the gel matrix (section 6.4.1 and 6.4.2). In pH 9 EWG, the acid diffusion process can be described as an anisotropical increase over a limited range from 0 to 0.4 mg HCl/g of the sample within 4 hours of gastric digestion. This could be due to the diffusion of gastric acid may be limited by the compact dense nature of pH 9 EWG (as described in section 6.4.1 and 6.4.2) and negligible initial acid content of pH 9 EWG matrix.

6.4.10 Impact of Egg White Gel Structures on Diffusion Kinetics of Water during Gastric Digestion

Figure 6.9 illustrates the concentration ratio of moisture uptake into the pH 5 and pH 9 EWG structures as a function of digestion time. The *in vitro* moisture gain concentration profiles of different EWG structures could be expressed by the Fick's second law and the D_{eff} of gastric moisture was estimated for each EWG structure and is shown in Table 6.8.

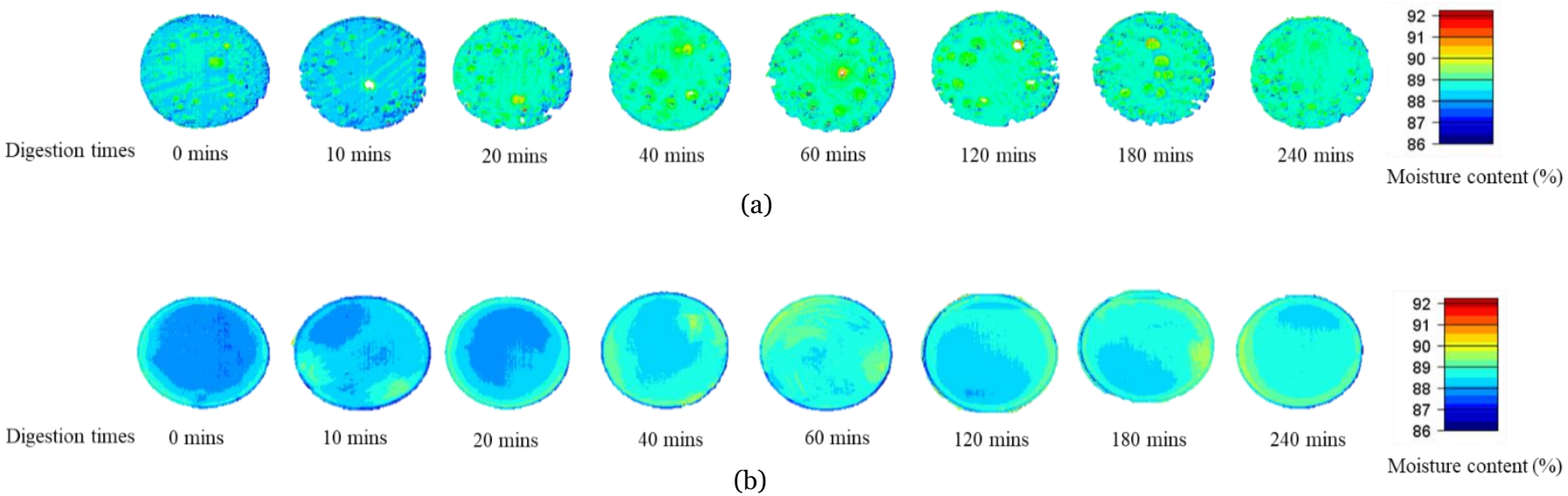

Figure 6.7: Spatiotemporal moisture content distribution maps of (a) pH 5 EWG and (b) pH 9 EWG generated by using the optimal PLS models.

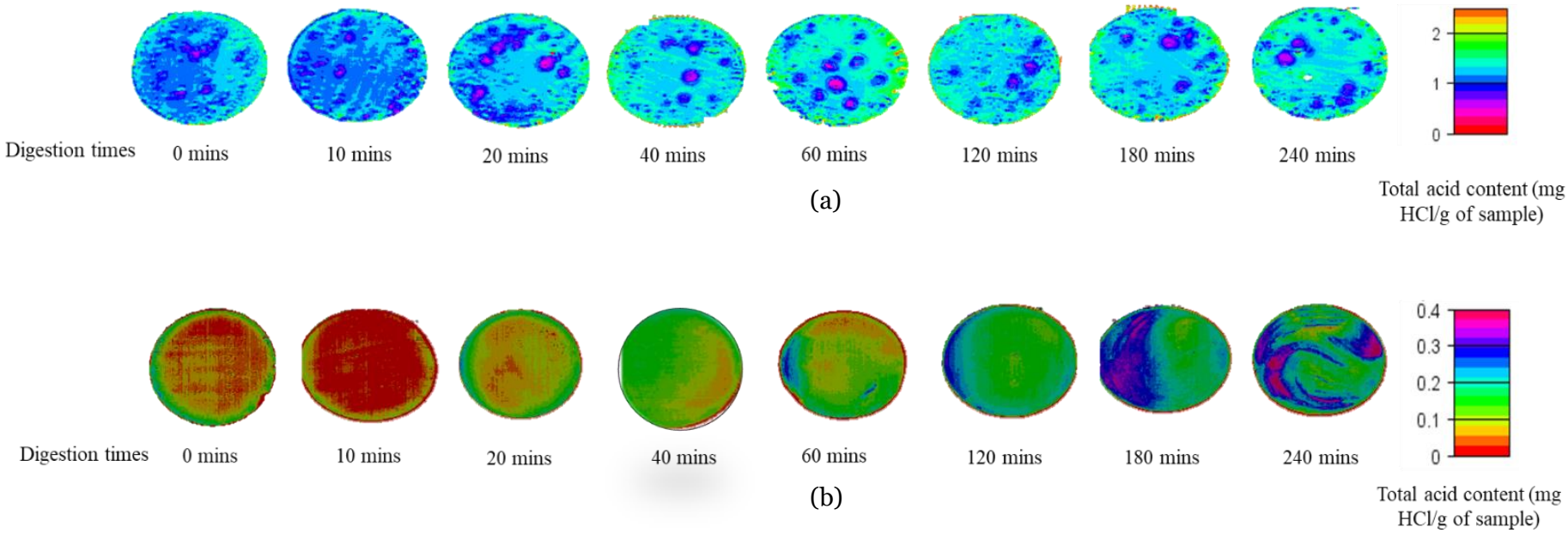

Figure 6.8: Spatiotemporal acid content distribution maps of (a) pH 5 EWG and (b) pH 9 EWG generated by using the optimal PLS models. (Note that the colour scale of an individual EWG structure represents a different range of acid (mg HCl/g of sample) content)

The EWG structure significantly affected the diffusion kinetics of moisture during gastric digestion ($p<0.05$). It can be observed that pH 5 EWG had considerably ($p<0.05$) higher D_{eff} of water ($5.6\pm1.4 \times 10^{-9}$ m²/s) than pH 9 EWG ($2.1\pm0.1 \times 10^{-9}$ m²/s). At pH 5, which is close to the isoelectric point of most egg white protein, the formation of spherical aggregates of egg white protein are predominate which leads to the formation of the porous and spatially heterogeneous structure of the pH 5 EWG (Nyemb *et al.,* 2016a). This loosely packed, more porous and spatially heterogeneous structure of the pH 5 EWG (as described in section 6.4.1 and 6.4.2) allows the water to diffuse at a faster rate. In contrast, pH 9 EWG has a less porous and a more rigid structure due to the formation of small linear and spherical aggregates of egg white protein at pH 9, (Nyemb *et al.,* 2016a) which likely hinders the water mobility within the structure. This fact could be further strengthened using the results reported in the section 6.4.3 in which the loosened microstructure in the pH 5 EWG may lead to faster pepsin diffusion and subsequent gel disintegration compared to the smooth-gel structure of pH 9 EWG.

To confirm the diffusion mechanism, the data were fitted with the power-law model. The model parameters and goodness of fit ($R^2>0.97$) are shown in Table 6.8. The moisture uptake in the pH 5 EWG followed the Fickian diffusion ($n=0.22$) whereas, in the pH 9 EWG, the water transport could not be described using a Fickian diffusion ($n=0.49$). Similarly, Fick's law model provided a good fit for diffusion of moisture into pH 5 EWG ($R^2=0.98$), with the exception of pH 9 EWG ($R^2=0.94$), because diffusion of moisture into pH 9 EWG regulated by both erosion-controlled and Fickian diffusion mechanism.

The porous microstructure of the pH 5 EWG may enable diffusion of water as a result of the moisture concentration gradient (Fickian diffusion). As illustrated in section 6.4.1 and 6.4.2, interconnecting empty pores of the pH 5 EWG matrix served as pathways for diffusion of water that enters the EWG matrix. In contrast to the pH 5 EWG matrix, a complex interplay between the concentration gradient of moisture and the polymer erosion due to acid and pepsin hydrolysis of the protein-gel matrix (non-Fickian diffusion) governed the water diffusion within the pH 9 EWG. In here, the water diffusion may be hindered by the compact microstructure of pH 9 EWG (Section 6.4.1 and 6.4.2). Thus, the degradation of the pH 9 EWG by pepsin action would give more free space between the polymer chains, which makes it easier for water molecules to mobile in the gel matrix. However, in the presence of pepsin, no substantial dimensional changes were observed within 4 hours of gastric digestion for both EWGs. In these experimental conditions, even though the EWG cylinders had not completely disintegrated during simulated digestion, microstructural changes may occur within the gel matrix during gastric digestion which merits in future investigation.

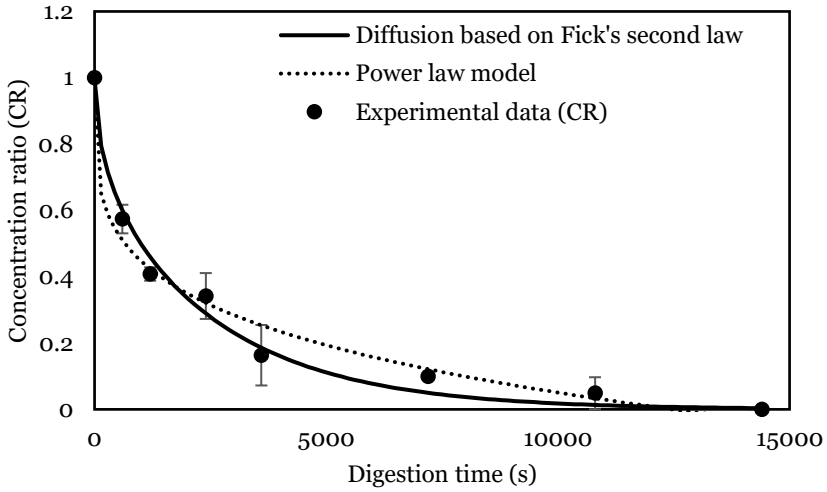

(a)

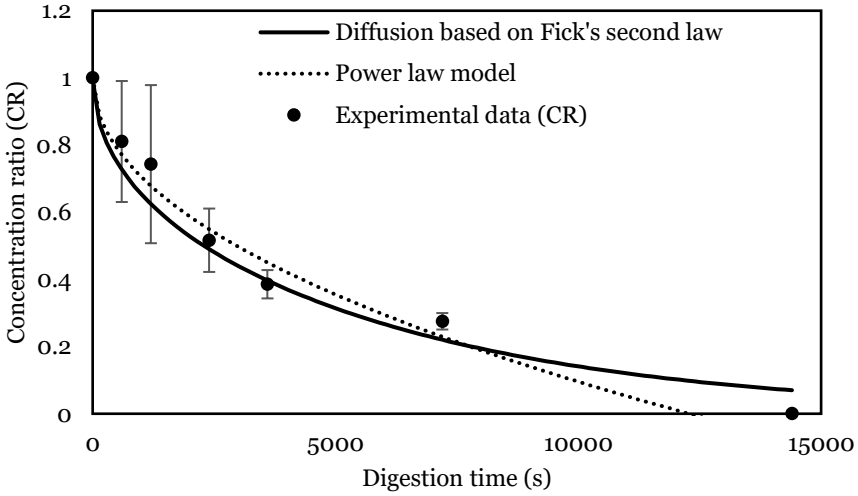

(b)

Figure 6.9: Plots of moisture concentration ratio as a function of digestion time (s) for the (a) pH 5 EWG and (b) pH 9 EWG. Circles represent average experimental values (n = 3) and error bars represent the SD of the mean. The prediction of the model of the Fick's second law (Eq. 3.1) and the power-law model (Eq. 3.2) are represented by solid and dashed lines, respectively.

Table 6.8: The rate of moisture diffusion (k), diffusion exponent (n), diffusion mechanism and effective diffusivity (D_{eff} ± SD of n=3) for water in pH 5 and pH 9 EWGs.

	The power-law model					The Fick's second law model		
	R^2	SSE	k	n	Diffusion mechanism	R^2	SSE	D_{eff} (m^2/s) ± SD
pH 5 EWG	0.98	0.08	0.106 ± 0.014^{a}	0.22 ± 0.05^{b}	Fickian diffusion	0.98	0.02	$5.6\pm1.4x10^{-9\ a}$
pH 9 EWG	0.97	0.03	0.011 ± 0.004^{b}	0.49 ± 0.04^{a}	Erosion controlled + Fickian diffusion	0.94	0.05	$2.1\pm0.1x10^{-9\ b}$

R^2: Coefficient of determination, SSE: Error sum of squares

a-b Means within each column followed by different superscript letters are significantly different ($p<0.05$)

k is the rate constant and n is the release exponent for the power-law model

D_{eff} is the effective diffusivity (m^2/s)

6.4.11 Impact of Egg White Gel Structures on Diffusion Kinetics of Acid during Gastric Digestion

The acid concentration ratio data as a function of the digestion time (t) were fitted into the Fick's second law and the power-law models as listed in Eq. 3.1 and Eq. 3.2, respectively (Figure 6.10). The results of the model parameters and the R^2 are listed and compared in Table 6.9.

The acid diffusion based on the Fick's second law model provided a good fit for pH 5 and pH 9 EWG data set (R^2>0.97). Both pH 5 EWG (2.4±0.1x10^{-9} m^2/s) and pH 9 EWG (2.3±0.6x10^{-9} m^2/s) had a similar ($p>0.05$) D_{eff} of acid. Limited information was found related to the D_{eff} of acid and water within EWG matrices during simulated gastric digestion. The factors influencing acid diffusion of both EWGs might include macro-structural properties (i.e. textural properties), microstructural properties (i.e. porosity, tortuosity), electrostatic interactions between egg gel matrices and H^+ ions, as well as buffering capacity. Elucidation on these specific properties of EWGs that control diffusion is an area that merits future investigation.

The power-law model had an acceptable R^2 (>0.98) for both EWG product models. Both pH 5 and pH 9 EWGs followed a Fickian acid diffusion mechanism during *in vitro* gastric digestion. This finding also highlights the fact that the D_{eff} of acid does not follow the same trend as the moisture D_{eff} during simulated gastric digestion of EWGs and should be estimated separately. Moreover, limited information was found related to the mechanism of acid diffusion into EWG structures during simulated gastric digestion which merits in future investigations.

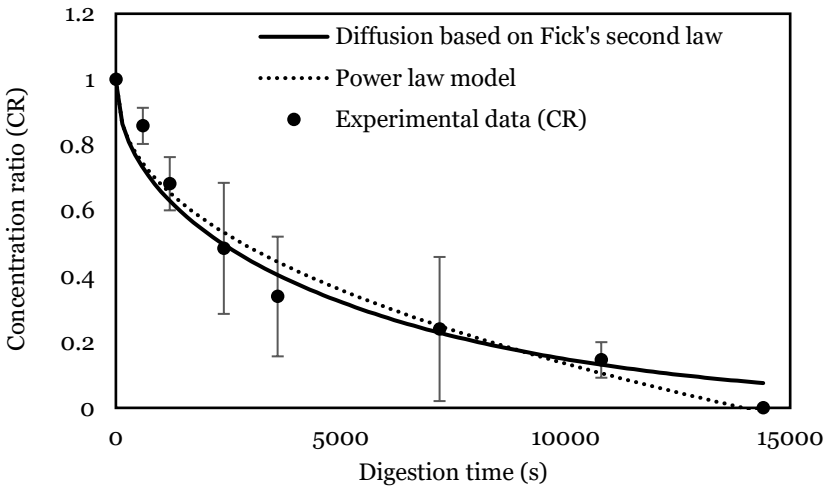

(a)

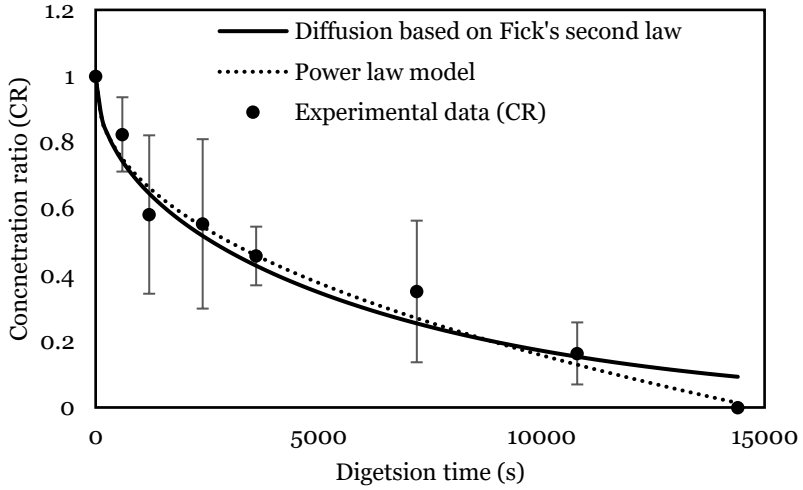

(b)

Figure 6.10: Plots of acid concentration ratio as a function of digestion time (s) for the (a) pH 5 EWG and (b) pH 9 EWG. Circles represent average experimental values (n = 3) and error bars represent the SD of the mean. The prediction of the model of the Fick's second law (Eq. 3.1) and the power-law model (Eq. 3.2) are represented by solid and dashed lines, respectively.

Table 6.9: The rate of acid diffusion (k), diffusion exponent (n), diffusion mechanism and effective diffusivity (D_{eff} ± SD of n=3) for acid in pH 5 and pH 9 EWGs.

	The power-law model					The Fick's 2nd law model		
	R^2	SSE	k	n	Diffusion mechanism	R^2	SSE	D_{eff} (m^2/s) ± SD
pH 5 EWG	0.97	0.02	0.016±0.0002[a]	0.43±0.03[a]	Fickian diffusion	0.97	0.02	$2.4\pm0.1x10^{-9}$ [a]
pH 9 EWG	0.99	0.01	0.016±0.0002[a]	0.44±0.05[a]	Fickian diffusion	0.98	0.02	$2.3\pm0.6x10^{-9}$ [a]

R^2: Coefficient of determination, SSE: Error sum of squares

a-b Means within each column followed by different superscript letters are significantly different ($p<0.05$)

k is the rate constant and n is the release exponent for the power-law model

D_{eff} is the effective diffusivity (m^2/s)

6.5 Conclusions

This study is the first reported quantitative characterisation of the microstructural differences observed on EWGs of the same composition but exposed to different pHs during the heat gelation process. Results indicate that, when gelled at pH 5, a more open and the heterogeneous microstructure is formed, in comparison to the dense and more homogeneous structure of the pH 9 gel. This study also showed that pepsin diffusion within the gel structures is largely controlled by the egg white protein gel microstructure and to some extent by the pH conditions that determine electrostatic interactions between pepsin and egg white proteins. Thus, the loose protein network of the pH 5 EWG exhibited a significantly higher rate of FITC-pepsin diffusion than the more dense pH 9 EWG, despite likely electrostatic interactions between pepsin and the protein network at pH 5, as suggested by the lower Dr than FITC-dextran in the pH 5 EWG.

These results suggested that pepsin diffusion in protein-based hydrogels can be modulated by the microstructure of the matrix. Such knowledge could assist the food industry in developing novel protein-based formulations to control the digestion kinetics for desired health outcomes. However, this chapter studied the diffusion behaviour of inactivated pepsin, due to the labelling with the fluorescent dye. During gastric digestion, the pepsin is active and therefore its diffusion through the gel matrix might be accompanied by the disintegration of the EWG microstructure, and thereby might strongly influence the further pepsin mobility. There is not much information about the effect of pepsin activity on further pepsin diffusion within the food protein-based gel microstructures. As well as, research on the link between microscopic investigations of the disintegration of EWGs microstructure due to diffusion of pepsin also remains scarce and merits future investigation.

The results of this chapter also offer convincing evidence that HSI provides more qualitative and quantitative information on the nature of the moisture and acid penetration into pH 5 and pH 9 EWG structures during the gastric juice diffusion process. Overall, moisture transport processes in EWGs were influenced by microstructural characteristics. It can be observed that pH 5 EWG had considerably ($p<0.05$) higher D_{eff} of water ($5.6\pm1.4 \times 10^{-9}$ m^2/s) than pH 9 EWG ($2.1\pm0.1 \times 10^{-9}$ m^2/s). However, the microstructural difference may not influence the rate of acid diffusion into the EWG structure during static *in vitro* gastric digestion. To better elucidate the gastric fluid diffusion observed in the gastric environment, the proposed HSI can be improved in the future to investigate the pH changes, pepsin diffusion and associated structural changes in digested EWG matrix while diffusion of gastric fluid.

Chapter Seven

7. Characterisation of Microstructural Disintegration and Nutrient Release in pH 5 and pH 9 Egg White Gels during Static *In Vitro* Gastric Digestion*

7.1 Abstract

Digestion behaviour of food protein-based hydrogels is greatly influenced by the gel characteristics and, in particular, the microstructure. Using egg white gels (EWGs) as a model food, this chapter aimed to explore the real-time disintegration by pepsin of different microstructures and the subsequent nutrient release kinetics. Using thermal treatment at 80 °C, EWGs with two different microstructures, but similar protein concentration (10%), were produced by varying the pH conditions (pH 5 and pH 9). The *in situ* spatiotemporal disintegration of the microstructure during static *in vitro* gastric digestion was followed using high-resolution confocal microscopy. Tetramethylrhodamine isothiocyanate (TRITC)-dextran (4.4 kDa) was incorporated into the gels as a marker fluorescent molecule of peptide-like size, to trace its release following pepsin action on the gel. The looser microstructure of pH 5 EWG caused the gel to disintegrate more quickly, and to a greater extent, leading to a higher rate of TRITC-dextran release. In contrast, the compact-dense microstructure of the pH 9 EWG showed slower kinetics of disintegration and TRITC-dextran release, likely due to reduced accessibility of pepsin to its substrates. Pepsin activity is highly pH-dependent, therefore the high local pH and high buffering capacity of pH 9 EWG may also play a pivotal role in the slower disintegration observed for this gel. In both EWGs, spatial degradation was mainly observed at the gel surface while the interior area fractions remained unchanged. Thus, surface erosion is possibly the underlying mechanism of EWG disintegration by pepsin in these experimental conditions.

*Chapter six submitted as a peer-reviewed paper: Somaratne, G., Nau, F., Ferrua, M. J., Singh, J., Ye, A., Dupont, D., Singh, R. P. and Floury, J. (2019). *In situ* disintegration of egg white gels by pepsin and kinetics of nutrient release followed by time-lapse confocal microscopy. *Food Hydrocolloids*, Accepted. Volume 98, January 2020, 105258.

7.2 Introduction

There has been growing interest in gaining insights into the design of novel food systems whose digestibility is controllable based on life stages and health conditions (Gonçalves *et al.,* 2018). In this respect, food protein-based hydrogels have received great attention, as versatile platforms for the encapsulation and controlled delivery of major nutrients and bioactive compounds (Chen, Remondetto, & Subirade, 2006; Jonker, Löwik, & Van-Hest, 2012; Zúñiga & Troncoso, 2012). They can be defined as cross-linked, three-dimensional and hydrophilic structures that are swollen in an aqueous environment (Jonker *et al.,* 2012; Nam, Watanabe, & Ishihara, 2004).

Food protein-based hydrogels have often been formulated to control the release of active ingredients at desired sites in the gastrointestinal tract. In order to achieve this, the microstructure and/or the physicochemical properties of the gel network can be manipulated through various processing techniques, such as control of ionic strength, change in pH, temperature or high pressure (Guo *et al.,* 2014; Nyemb *et al.,* 2016a; Zúñiga & Troncoso, 2012). Indeed, it is now well established that the hydrogel structure can influence the kinetics of protein hydrolysis during gastro-intestinal digestion (Guo *et al.,* 2014; Le Feunteun *et al.,* 2014; Nau *et al.,* 2019; Nyemb *et al.,* 2016a; Opazo-Navarrete *et al.,* 2018).

Protein digestibility inside the gastric compartment plays a significant role in contributing to the overall nutritional value of proteins (Guerra *et al.,* 2012; Wen *et al.,* 2015). It is mainly controlled by the action of gastric pepsin which facilitates the proteolysis of proteins into smaller peptides (Luo, Boom, & Janssen, 2015; Zúñiga & Troncoso, 2012). The evaluation of pepsin action through hydrogel networks is an important consideration in the design of functional protein-based hydrogel systems (Chen *et al.,* 2006; Luo *et al.,* 2015). However, current understanding of the mechanisms by which the microstructure of gels can affect the gastric pepsin action remain largely unknown; in part because of the limited methods available to evaluate pepsin diffusion through hydrogels and subsequent matrix disintegration, (Luo *et al.,* 2015; Luo *et al.,* 2017; Thevenot *et al.,* 2017). Using confocal based microscopy techniques, Thevenot *et al.* (2017) and Luo *et al.* (2017), reported that pepsin diffusion in dairy gels depends on native gel composition and microstructure. The major drawback of these techniques is that the pepsin is fully inactivated due to the fluorescent tag labelling process (Thevenot *et al.,* 2017). As a result, it was impossible to quantitatively describe the coupled diffusion and enzymatic action of pepsin using these techniques.

Egg white is comprised of a set of globular proteins mainly including ovalbumin (54%), ovotransferrin (12%), ovomucoid (11%), ovomucin (3.5%), and lysozyme (3.5%)

(Abeyrathne *et al.,* 2013; Tomczyńska-Mleko *et al.,* 2016; Nyemb *et al.,* 2014). Gelation of egg white proteins have received much attention among food scientists because it is a useful way to modulate the functional attributes that make egg white proteins suitable for the encapsulation of bioactive agents, such as nutraceuticals and pharmaceuticals (Tomczyńska-Mleko, 2015; Tomczyńska-Mleko *et al.,* 2016). A great deal of *in vivo* and *in vitro* research has been directed towards the understanding of the basic mechanisms affecting egg white protein digestibility (Nyemb *et al.,* 2016a, b; Nyemb *et al.,* 2014; Nyemb *et al.,* 2015). Moreover, in Chapter 6 of this thesis provided a thorough initial microstructure characterisation of two different egg white gels (EWGs) and their effect on the diffusion of fluorescently labelled pepsin. However, to the best of our knowledge, no comprehensive study has been carried out to study the effect of EWG microstructure on pepsin action and subsequent gel disintegration.

The aim of this Chapter (Chapter 7) was to investigate the real-time disintegration behaviours of two EWGs (as protein-based model foods) of identical protein content (10 wt% proteins), but with different structures and pH, using an *in situ* gastric digestion methodology based on high-resolution time-lapse confocal microscopy. Concurrently, we also investigated the release kinetics of a TRITC-dextran (4.4 kDa) during EWGs disintegration by pepsin. TRITC-dextran was chosen as a marker as it is similar in size to the peptides released by pepsin during proteolysis and is therefore a good model of nutrients released during protein disintegration.

7.3 Materials and Methods

7.3.1 Materials

Fresh eggs were purchased from the local supermarket (Rennes, France). The protein content was 10.5 wt% measured by the Kjeldahl method (Nx6.25) in triplicate. A 5 wt% solution of TRITC-dextran (Sigma–Aldrich, St Louis, USA), with an average molecular weight 4.4 kDa, was used. A solution of 1 wt% of Fast Green (Sigma–Aldrich, St Louis, USA) was used to stain the egg white proteins. Simulated gastric fluid (SGF) was prepared according to Minekus *et al.* (2014) (Section 3.3.4). Pepsin from porcine gastric mucosa (3200–4500 U/mg protein, Sigma, UK) was used. Porcine pepsin (80,000 U/mL) stock solutions (1 mL) were prepared fresh before each confocal microscopy observation and stored on ice until it was used. All the reagents used were analytical grade.

Before the microscopic observations, the activity of pepsin stock solution was re-adjusted to 8,000 U/mL using SGF (pH 2). Preliminary experiments were conducted using the pepsin concentration of 2,000 U/mL at pH 2 as recommended in the

INFOGEST protocol. However, we did not observe any significant pepsin-mediated degradation of either EWGs during two hours using these experimental conditions. Therefore, in order to observe changes during the two-hour digestion period, we selected 8,000 U/mL pepsin concentration for the study, which increased the kinetics of degradation.

7.3.2 Preparation of Heat-induced Egg White Gels

pH 5 and pH 9 egg white solutions (10 wt% proteins) were prepared as described in Chapter 6 (section 6.3.2). *In-situ* gastric digestion of EWGs was performed inside a 100 µL channel slide (µ-Slide I0.4 Luer systems, IBIDI GmbH, Martinsried, Germany) to impose one-dimensional pepsin diffusion and gel disintegration. To prepare the gel, approximately 600 µL of pH adjusted egg white solution was poured into 1 mL Eppendorf tubes. Then 6 µL of Fast Green (1 wt%) and 30 µL of TRITC-dextran (5 wt%) was added to each tube. The mixture was vortexed, and then 100 µL of the solution was slowly injected into the chamber of a µ-Slide system, and carefully spread to cover the two-third of the channel length (50 mm). The system was covered using aluminium foil to prevent photo-bleaching of fluorescent molecules and it was horizontally heated at 80°C for 5 min in a temperature-controlled water bath. After heating, the samples were cooled to room temperature and kept at 20°C in an air-conditioned room before microscopic analysis.

7.3.3 Spectral Properties of TRITC-dextran in Egg White Gels at Different pH

The effect of pH change in the EWGs due to penetration of the SGF on the fluorescence emission properties of TRITC-dextran was investigated. Indeed, in order to be able to quantify the evolution of the fluorescent intensity of the dye during the disintegration of the EWGs under digestion by pepsin, its spectral properties must be independent of the environmental pH.

The pH of the SGF was adjusted to pH 2, 3, 4, 5, 6, 7 or 8 using 0.1 M/1 M HCl or NaOH. One mL of each pH adjusted SGF solutions were then mixed with 10 µL of TRITC-dextran solution (50 mg/mL). Small pieces of pH 5 EWG samples were deposited onto the individual wells of the µ-Slide (8 well) IBIDI plates (IBIDI GmbH, Martinsried, Germany) and left in contact with the TRITC-dextran fluorescent SGF solutions (100 µL) at different pH (pH 2, 3, 4) for 30 minutes at room temperature. Similarly, small pieces of pH 9 EWG were left in contact with the TRITC-dextran fluorescent SGF solutions (100 µL) at different pH (pH 2, 3, 4, 5, 6, 7, 8) for 30 minutes. In addition, 100 µl of TRITC-dextran solutions (50 mg/mL) were directly added into the small pieces of pH 5 and pH 9 EWG samples to obtain the emission spectrum at pH 5 and pH 9, respectively.

Emission spectra measurements of TRITC-dextran were performed using the confocal microscope (LSM 880, Carl Zeiss AG, Oberkochen, Germany) with the 20× dry objective lens (NA = 0.5). Excitation of TRITC-dextran was achieved using the DPSS laser (561 nm) and the emitted light was collected between 560 nm – 675 nm. The spectral analyses were performed using the unmixing function of the Zen black software. Emission spectrum intensities were normalized by dividing all intensities with the maximum peak intensity.

7.3.4 Time-lapse Confocal Microscopic Observations during *In Vitro* Gastric Digestion

Two different sets of experiments were conducted separately, using an inverted confocal microscope (LSM 880, Carl Zeiss AG, Oberkochen, Germany):

(i) The disintegration of EWGs microstructure during static *in vitro* gastric digestion was observed inside the channel slide system using the high-resolution mode of the confocal microscope equipped with the Airyscan detection unit and a Plan Apochromat 63x with high numerical aperture (NA = 1.40) oil objective. The Fast Green was excited using a HeNe laser system at a wavelength of 633 nm.

(ii) The release of TRITC-dextran, as a result of EWGs disintegration by pepsin, was monitored using the conventional confocal mode with a x20 dry objective lens (NA = 0.5) and the DPSS laser system with an excitation wavelength of 561 nm.

To optimise pepsin activity over the digestion period the temperature was maintained at 37 °C using a microscope cage incubator. Samples were placed on the microscope stage and the gel sample surface inside the IBIDI system was found by moving the stage in the x and y planes such that the gel sample surface was centred in the imaging window (Figure 7.1).

In order to observe the disintegration of the protein network due to pepsin action, first, a tile scan was set up to cover the region of gel surface towards the center with an area of 68 μm x 1019 μm (1 x 15 tiles, 10% overlap in between each tile) fields of view by automatically moving the motorized stage. Then the initial gel microstructure was recorded as a tile Airyscan image with optimum resolution (1360x1360 pixel) prior to digestion. For this, Airyscan images were acquired with 7% of the maximum laser power with a main beam splitter MBS488/561/633, no additional emission filter, a gain setting of 700 to 780, a pixel dwell time of 1.54 μs and without averaging. The acquisition was performed at 8 μm from the sample surface with a zoom 1.8. Then, the Zen Black 2.1

(Version 13.0.0.0) software was used to process the acquired datasets using the 2D mode at default settings of the Airyscan processing function.

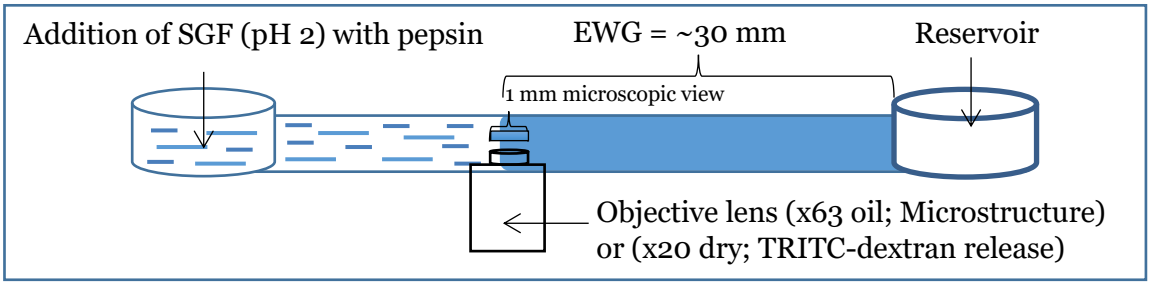

Figure 7.1: Diagram of the IBIDI gel system experimental device for monitoring the *in situ* disintegration of the model EWGs

For quantification of TRITC-dextran release from the gels under digestion, the tile scan was set up to cover an area of 213 µm x 1934 µm (1 x 10 tiles, 10% overlap in between each tile) fields of view and the tile scan image with resolution (512x512 pixel). Images were acquired using a PMT detector with a 570 – 630 nm emission wavelength, a pixel dwell time of 4.10 µs and one averaging. The TRITC-dextran fluorescence intensity can be affected by photobleaching effects of laser exposure. Thus, preliminary trials were also carried out to confirm that the selected laser power (0.7%) and the gain setting of 750 was not the cause of any fluorescence intensity loss during the 2 hours of digestion time.

After optimising the confocal microscopy configuration, the IBIDI system was carefully removed without altering the stage position of the microscope. Then, 150 µL SGF (pH 2) containing pepsin was injected into the other side of the IBIDI channel using a thin pipette (Microlance 3, 19GA2), so that air inclusion was minimized and to facilitate the direct contact between the digestive fluid and the gel surface. The two reservoirs were covered with caps to avoid any evaporation during further digestion by pepsin at 37 °C. As soon as possible, the sample was placed in the pre-warmed stage and the time-lapse imaging was started every 15 min for the 120 min period of digestion for microstructural observation of the protein gels, and every 5 min over 120 min for the TRITC-dextran release. Each set of experiments was performed in triplicate for both types of EWGs.

Control experiments were performed in the same manner on both EWGs, either without any fluid or with the SGF only (without adding pepsin). This aimed to check for any photo-bleaching effect over the imaging period, or for any microstructural changes due to the acidification, or for passive diffusion of TRITC-dextran with water in SGF, respectively.

7.3.5 Quantification of Protein Particle Area Fraction

The time-lapse sequences of 16 bits-grayscale images were analysed using the Fiji software package (Schindelin *et al.,* 2012). The applied image analysis technique was previously described by Silva *et al.* (2015). Binary images were generated by choosing the Otsu thresholding algorithm after applying, first the white top-hat and then the smooth filters, to remove artifacts. In a 2 bits image, black pixels represent the egg white protein phase whereas white pixels represent aqueous phase. The segmentation procedure was validated by visual comparison of the resulting binary image with its original image. The protein particle area fraction (ratio between the protein matrix area with respect to the total area of the image) was quantified on each image using the "Analyse Particles" function in FIJI.

The result of protein particle area fraction quantification was displayed on a heat map in which columns represent digestion time points and rows represent the distance from the gel surface (μm). The colour scale was used to map the corresponding particle area fraction data in individual cells. The colour gradient was set for no protein particle area fraction (0%) in the heat map to red, and the highest particle area fraction (50%) to green.

7.3.6 Modeling the Kinetics of TRITC-Dextran Release over Digestion Time

The kinetics of TRITC-dextran release from the protein gels into the SGF solution was determined by quantification of the decrease in the average fluorescence intensity in a region of the gel over the digestion period. The average fluorescence intensity (I_t) was quantified in a region of the gel surface towards the center with an area of 213 μm x 1000 μm at each digestion time, using Zen Black 2.1 (Version 13.0.0.0) software. The fraction of TRITC-dextran released at a digestion time (t) was calculated as:

$$F_{(t)} = \frac{(I_0 - I_t)}{I_0} \qquad \text{(Eq.7.1)}$$

Where $F_{(t)}$ is the release TRITC-dextran fraction at digestion time t, I_o is the initial TRITC-dextran intensity and I_t is the TRITC-dextran intensity after digestion time (t).

The Weibull model: The Weibull distribution function, widely used to describe drug dissolution and nutrient release kinetics during *in vitro* analysis (Carbinatto *et al.,* 2014; Kong & Singh, 2011), was used to model the TRITC-dextran release during static *in vitro* gastric digestion. The experimental data were fitted with the Weibull distribution function using the Curve Fitting Toolbox of Matlab (R2016a, Mathworks, Natick, MA, USA):

$$F_{(t)} = 1 - e^{-kt(\beta)} \qquad \text{(Eq. 7.2)}$$

Where k defines the time scale of the process (min^{-1}) associated with the rate constant of TRITC-dextran release and β is a shape parameter that characterizes the shape of the release curves (Langenbucher, 1972). Coefficient of determination (R^2) and error sum of squares (SSE) were used to determine the quality of the goodness of fit. The half-time ($t_{1/2}$), i.e. the time to reach 50% loss of total TRITC-dextran, was calculated as:

$$t_{(\frac{1}{2})} = \left(\frac{-\ln 0.5}{k}\right)^{\frac{1}{\beta}} \qquad \text{(Eq. 7.3)}$$

The power law (Krosmeyer-Peppas) model: In order to gain some insight into the TRITC-dextran release rate and mechanism from the pH 5 and pH 9 EWG during static *in vitro* gastric digestion, a very simple and semi-empirical equation to describe drug release from polymeric systems, the power-law model (Krosmeyer-Peppas model), was applied (Carbinatto *et al.,* 2014; Sankalia, Sankalia, & Mashru, 2008; Sriamornsak, Thirawong, & Korkerd, 2007).

$$F_{(t)} = kt^n \qquad \text{(Eq. 7.4)}$$

In this equation, k is the rate constant and n is the release exponent, indicative of the mechanism of the TRITC-dextran release. The parameters k and n were obtained from the initial portion of the curve (% released < 70%), according to the literature (Sankalia *et al.,* 2008). When the exponent n assumes a value of $n<0.5$, the TRITC-dextran release mechanism can be hypothesized as purely Fickian diffusion. When $0.5<n<1.0$, the TRITC-dextran release mechanisms are hypothesized to be both Fickian diffusion and erosion controlled. When the value of n is greater than 1.0, a pure erosion-controlled mechanism is generally governed the TRITC-dextran release mechanism (Sriamornsak *et al.,* 2007).

7.3.7 Statistical Analysis

A one-way ANOVA was used to assess differences in the Weibull model and the power-law model parameters and the half-time ($t_{1/2}$). A Tukey multiple comparison test was implemented to investigate the differences between means when the main effects were significant. Minitab 17 software was used for statistical analysis.

7.4 Results and Discussion

Time-lapse confocal microscopy in the (xy)-plane was employed to observe in real-time effect of the diffusion of SGF containing pepsin on the microstructural changes of EWGs over the 2 hours of static *in vitro* digestion. First, two control experiments were conducted to identify any artefactual microstructural modifications. The first control conducted with no SGF or pepsin showed that the mean Fast Green fluorescence intensity remained stable over 2 hours, meaning that no significant photo bleaching of the fluorescent dye was occurring with time due to confocal imaging (Figure 7.2). The second control, conducted using the SGF solution without pepsin, did not cause any detectable changes in the typical microstructures of EWGs (Figure 7.3). Overall, this demonstrates that any observed spatiotemporal modifications of the EWGs will be due to the action of pepsin.

7.4.1 Egg White Gel Microstructure Impacts the Disintegration by Pepsin

Figures 7.4 (a) and 7.5 (a) show typical sets of 15 tile-scan images obtained along the x-axis from the surface of the gel (tile 1) during the 2 hours digestion, with pH 5 and pH 9 EWGs, respectively. The first image was captured at t=0 minutes, immediately prior to the addition of SGF-pepsin, to demonstrate the initial microstructure organisation of the EWG. Images were then captured at 4 min after addition of SGF-pepsin and then every 15 minutes thereafter over the 2 hours of the digestion. Due to Fast Green labelling, protein aggregate particles appeared coloured in green on the confocal micrographs, while associated pores in the aqueous phase are black. As reported in Chapter 6, the microstructural organisation of the EWGs strongly differs depending on the adjusted pH before heat gelation. At pH 5, the egg white proteins formed a highly anisotropic, granular network, and protein aggregates were unevenly distributed through the aqueous phase (Figure 7.4 (a)). At pH 9, the proteins formed a highly isotropic, smooth network and protein aggregates were evenly distributed through the aqueous phase (Figure 7.5 (a)). Figure 7.4 (b) and Figure 7.5 (b) show the corresponding relative protein particle area fractions (%) of both EWGs calculated on each individual (x,t) tile-scan images, in order to quantify the extent of protein network disintegration over the digestion period. The initial (t = 0 min) protein particle area fraction of both gels varied from 50 to 30%.

Changes to the spatial pattern of the protein network of both EWGs were apparent as early as 4 minutes after the addition of the SGF-pepsin solution, although the extent of the change differed between the two gels (Figure 7.4 (a) and Figure 7.5 (a)). Visually, Figure 7.4 (a) and Figure 7.4 (b) show that protein particles progressively disappeared from the surface of the pH 5 EWG after 4 min digestion, but the extent of

disintegration remained quite limited during the first 34 min of digestion. Then, the disintegration process seemed to accelerate after 49 min digestion. After 2 hours of digestion by pepsin, the front gel surface had shrunk to almost 700 μm from its initial position. In contrast, the disintegration process was much slower and of a much more limited extent for the pH 9 EWG (Figure 7.5 (a) and Figure 7.5 (b)), with a decrease in the interface's position between the enzymatic solution and the gel of less than 100 μm in 2 hours of digestion. These results clearly demonstrate that pepsinolysis was affected by the characteristics of the EWGs, in agreement with Nyemb *et al.* (2016a, b).

Based on the dimensions of pepsin (5.5 nm x 3.6 nm x 7.4 nm) (Luo *et al.,* 2015) and the average inter-particle aggregate distances of pH 5 EWG (1.79±0.57 μm) and pH 9 EWG (0.76±0.07 μm) (Chapter 6, Section 6.4.2), pepsin is able to penetrate into both protein gel matrices. However, the loose microstructure of the pH 5 EWG leads to faster pepsin diffusion than the dense structure of pH 9 EWG (Chapter 6, Section 6.4.3). This could explain why the extent of gel disintegration observed in the present study was much higher in the pH 5 EWG than in the pH 9 EWG.

7.4.2 pH Cannot Be Avoided as A Key Parameter for Egg White Gel Disintegration by Pepsin

The activity of pepsin has been shown to be very pH dependent, with an optimum of pH 1.7 to 2.0 (Luo *et al.,* 2018). Therefore, any change in this pH within the digestion environment is likely to significantly affect the enzymic activity (Campos & Sancho, 2003; Schlamowitz & Peterson, 1959). It is probably the main limiting factor in the present static experimental set-up, in which there is neither renewal nor mixing of the SGF throughout the digestion experiment. Yet, the local pH at the interface between SGF and EWG during the digestion is of paramount importance on pepsin activity and subsequent gel disintegration. Due to the higher buffering effect of the EWG at pH 9 than at pH 5, the local pH at the interface between SGF and EWG is probably much higher with pH 9 EWG than with pH 5 EWG over the digestion period.

Therefore, in addition to the lower pepsin diffusivity, the difference in local pH within the gel may also contribute to the much more limited proteolysis we observed within the pH 9 EWG compared to the pH 5 EWG. Further investigation is needed to characterise the changes of local pH within the digestion system that control the degradation of protein in the food matrix. In addition, the apparent size of pepsin has been reported to increase at pH greater than 6.5 (Campos & Sancho, 2003; Nyemb *et al.,* 2016a) and this may have hindered its diffusion into the pH 9 EWG.

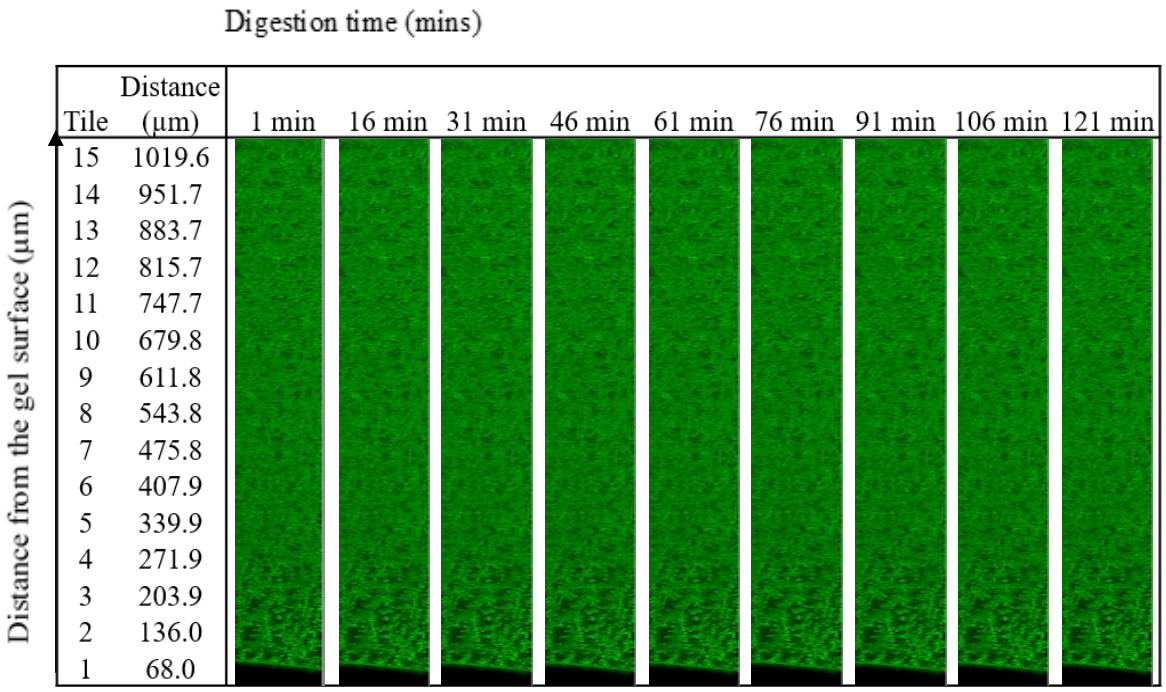

(a)

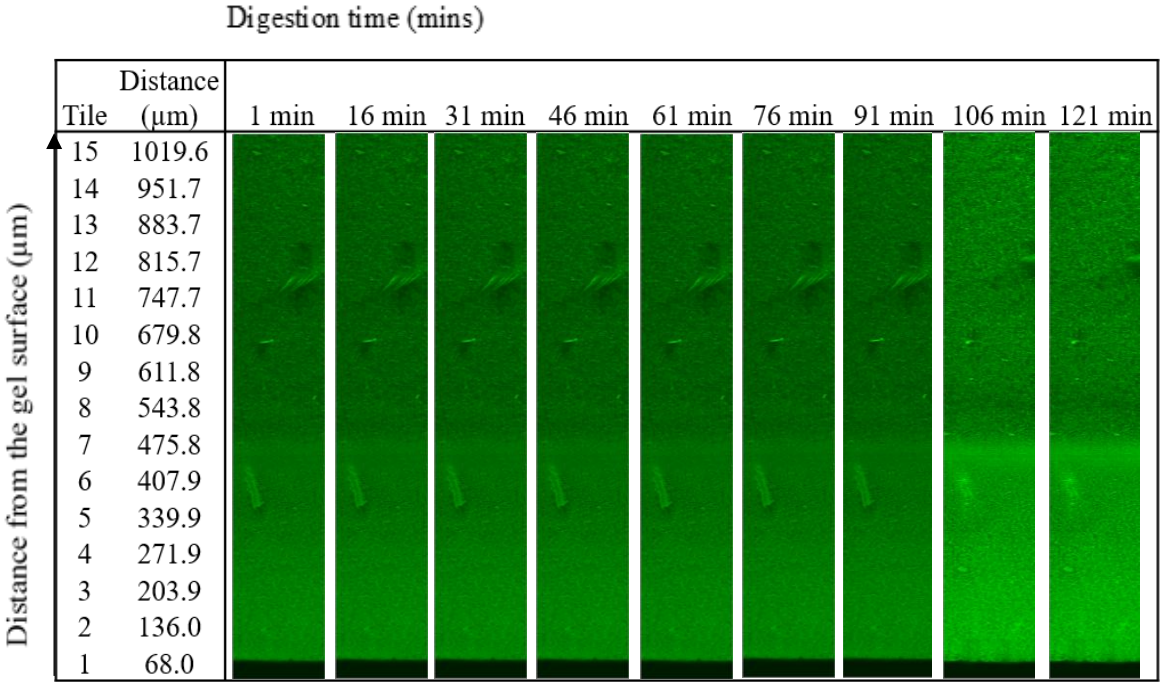

(b)

Figure 7.2: Typical time-lapse fluorescence imaging of changes of (a) pH 5 EWG and (b) pH 9 EWG microstructure with no SGF or pepsin (control experiment). No change of microstructure and no photo bleaching of the fluorescent dye was occurring with time due to confocal imaging in both (a) pH 5 EWG and (b) pH 9 EWG

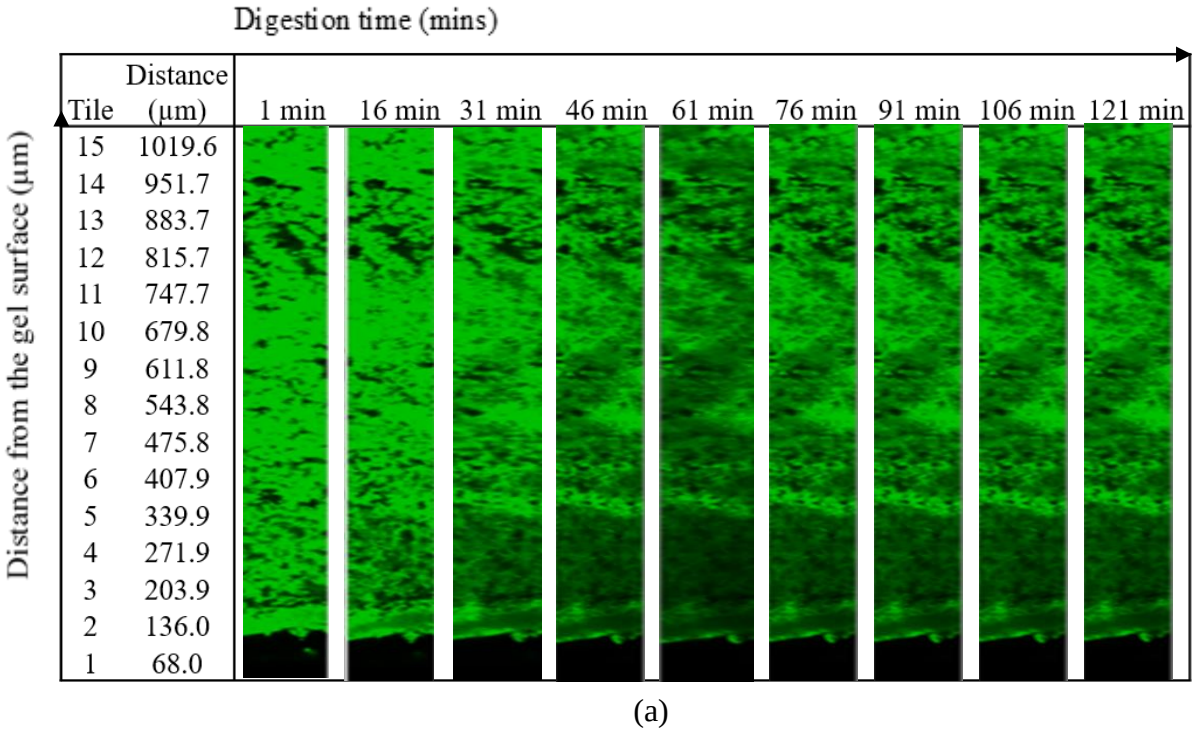

(a)

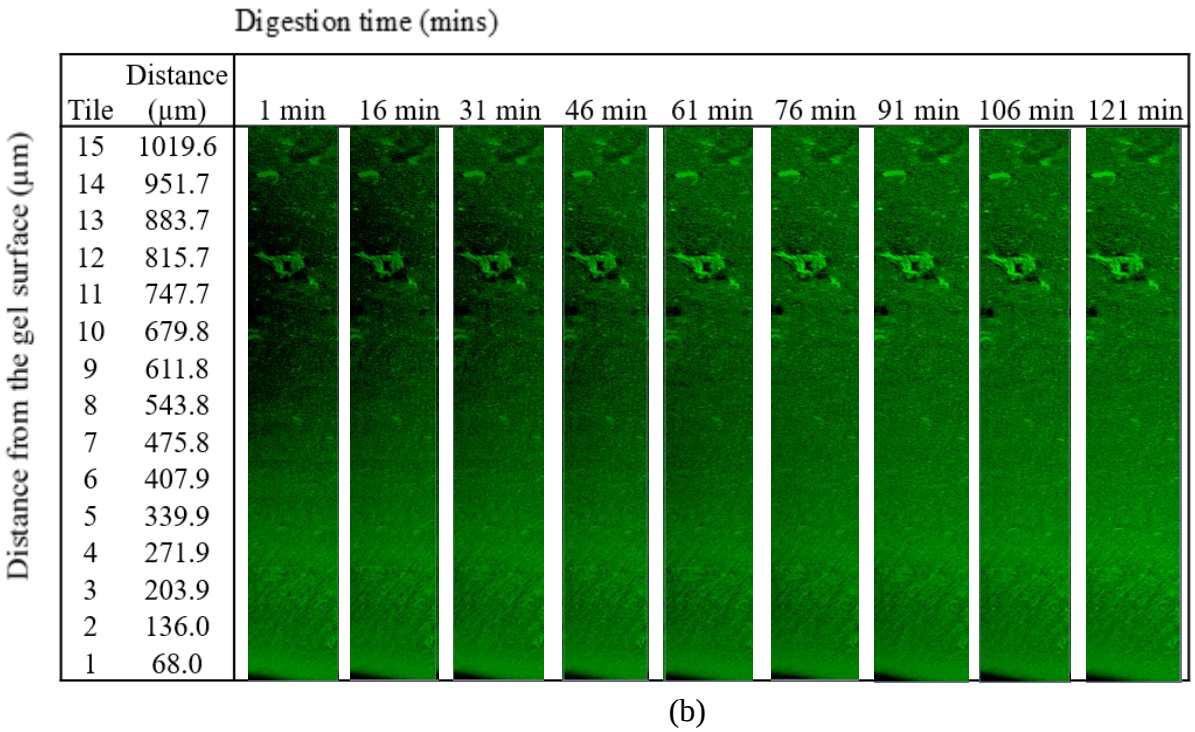

(b)

Figure 7.3: Typical time-lapse fluorescence imaging of changes of (a) pH 5 EWG and (b) pH 9 EWG microstructure during diffusion of SGF at pH 2 (Control experiment). No change of network microstructure and fluorescence intensity was observed in both (a) pH 5 EWG and (b) pH 9 EWG microstructure during diffusion of SGF at pH 2.

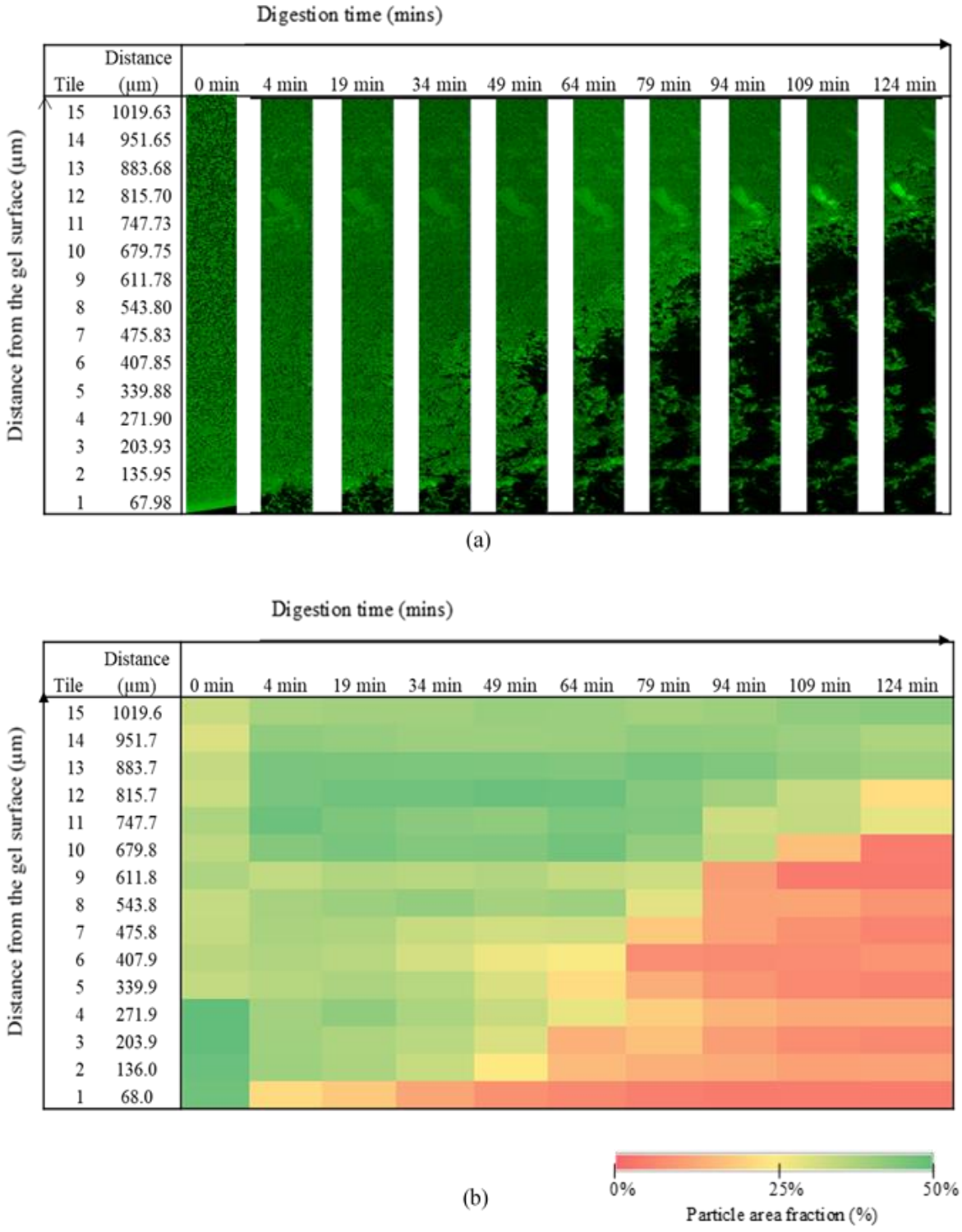

Figure 7.4: (a) Typical time-lapse fluorescence imaging of changes of pH 5 EWG microstructure during diffusion of SGF at pH 2 containing 8,000 U/mL of pepsin. (b) Visualisation of changes of corresponding area fraction of pH 5 EWG microstructure during gastric digestion through a heat-map diagram (red = no particle on the confocal image)

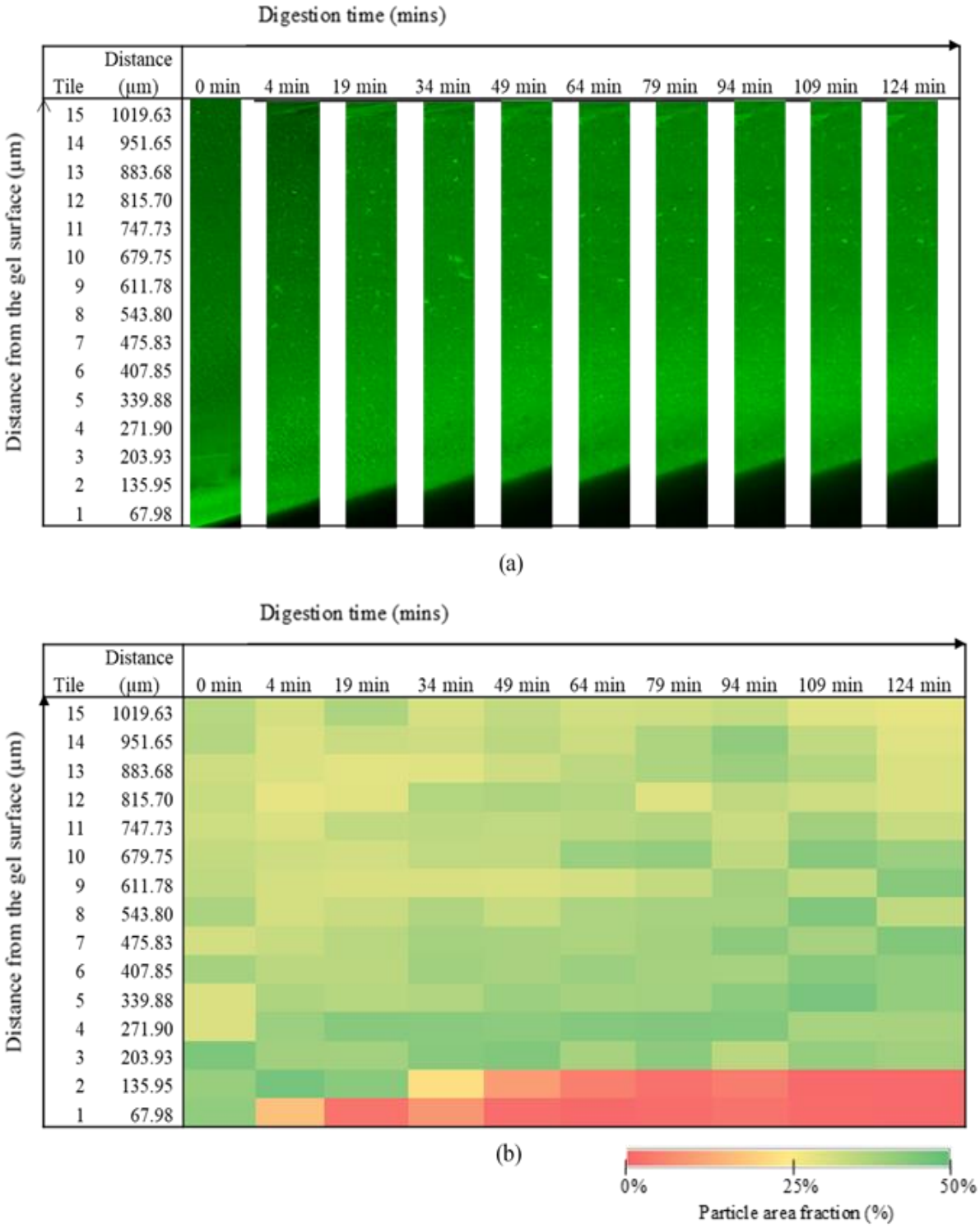

Figure 7.5: (a) Typical time-lapse fluorescence imaging of changes of pH 9 EWG microstructure during diffusion of SGF at pH 2 containing 8,000 U/mL of pepsin. (b) Visualisation of changes of corresponding area fraction of pH 9 EWG microstructure during gastric digestion through a heat-map diagram (red = no particle on the confocal image)

7.4.3 In These Experimental Conditions, Egg White Gel Disintegration by Pepsin was Mainly Driven by a Surface Erosion Phenomenon

Changes in the gel structure during digestion by pepsin was observed to occur within a very thin region near the surface of the gel in contact with the SGF-pepsin solution, of less than 500 μm length, over the 2 hours of digestion (Figure 7.4 (a) and Figure 7.5 (a)). Moreover, image analysis of the particle area fractions on each set of tile-scan images obtained from high-resolution confocal microscopy clearly showed that the microstructure of the protein gel networks remained unchanged inside the bulk of both EWGs during the digestion experiment (Figure 7.4 (b) and Figure 7.5 (b)). The disintegration process of both types of the gel was therefore very slow, with an action of pepsin mostly located at the interface in contact with the enzyme solution. These results suggest that the rate of enzymatic degradation is much faster than the diffusion of pepsin into the EWGs. In other words, we assume that in these experimental conditions, namely using a static digestion set-up with a small and finite volume of SGF-pepsin solution, most of the enzyme molecules reacted with the nearest substrate molecules of egg proteins within their surrounding environment, and then diffused further into the gel. This mode of action leads to a localized degradation in the immediate vicinity of the gel surface compared to a minimal gel degradation further in the bulk. Such surface erosion phenomenon has been previously reported by Floury *et al.* (2018), for the digestion of dairy protein (i.e. acid and rennet gels) gels by the simulated gastric juice, observed by time-lapse synchrotron deep-UV fluorescence microscopy.

7.4.4 TRITC-dextran (4.4 kDa) can be considered as a peptide release marker in Egg White Gel matrices during gastric digestion

In pharmaceutical technology, TRITC-dextran has been used as a model of drug delivery due to the stability of TRITC over a wide pH range (i.e. pH 2–11) and resistance to photo-bleaching (Geisow, 1984; Varshosaz, 2012). In the present study, TRITC-dextran of 4.4 kDa has been used as a fluorescent model of peptide-like size. The pH dependence of the TRITC-dextran emission spectrum is summarized in Figure 7.6 (a) for pH 9 EWG in the pH range of 2.0–9.0 and in Figure 7.6 (b) for pH 5 EWG in the pH range 2.0–5.0. It yields identical emission spectral distributions for both pH 5 and pH 9 EWGs over 2.0–9.0 pH range. These results suggest that TRITC-dextran is a pH-insensitive dye. Similar results have been reported previously (Geisow, 1984). Consequently, TRITC-dextran (4.4 kDa) can be considered as an appropriate marker of peptide release from EWG matrices during simulated gastric digestion.

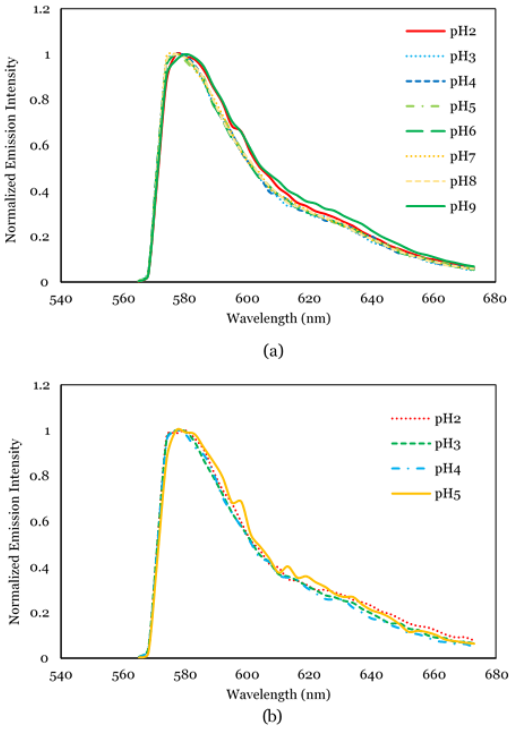

Figure 7.6: TRITC-dextran emission spectra of (a) pH 9 EWG, and (b) pH 5 EWG at different pH conditions

7.4.5 Egg White Gel Characteristics Determine the Extent of TRITC-Dextran Release by Pepsin Action

The TRITC-dextran release profiles of both EWGs as a function of time in the presence and absence of pepsin are illustrated in Figure 7.7. Control experiments using SGF without pepsin were performed to evaluate the kinetics of release of TRITC-dextran due to the diffusion driven by only the concentration gradient between the SGF solution and the gels. In the absence of pepsin, we found that the kinetics and the percentage of TRITC-dextran release was greater from the pH 5 EWG than from the pH 9 EWG. This is consistent with the microstructure of the gels, which is loose for the pH 5 EWG *versus* dense for the pH 9 EWG (Chapter 6, sections 6.4.1 and 6.4.2). When pepsin was added to the SGF solution, both the kinetics and the percentage of TRITC-dextran release significantly increased compared to the control (SGF without pepsin) for both kinds of gels, consistent with the EWG disintegration due to the action of pepsin. In addition, in the presence of pepsin, the release of TRITC-dextran was higher from the pH 5 EWG, consistent with the disintegration by pepsin, which was higher in the pH 5 EWG compared to the pH 9 EWG.

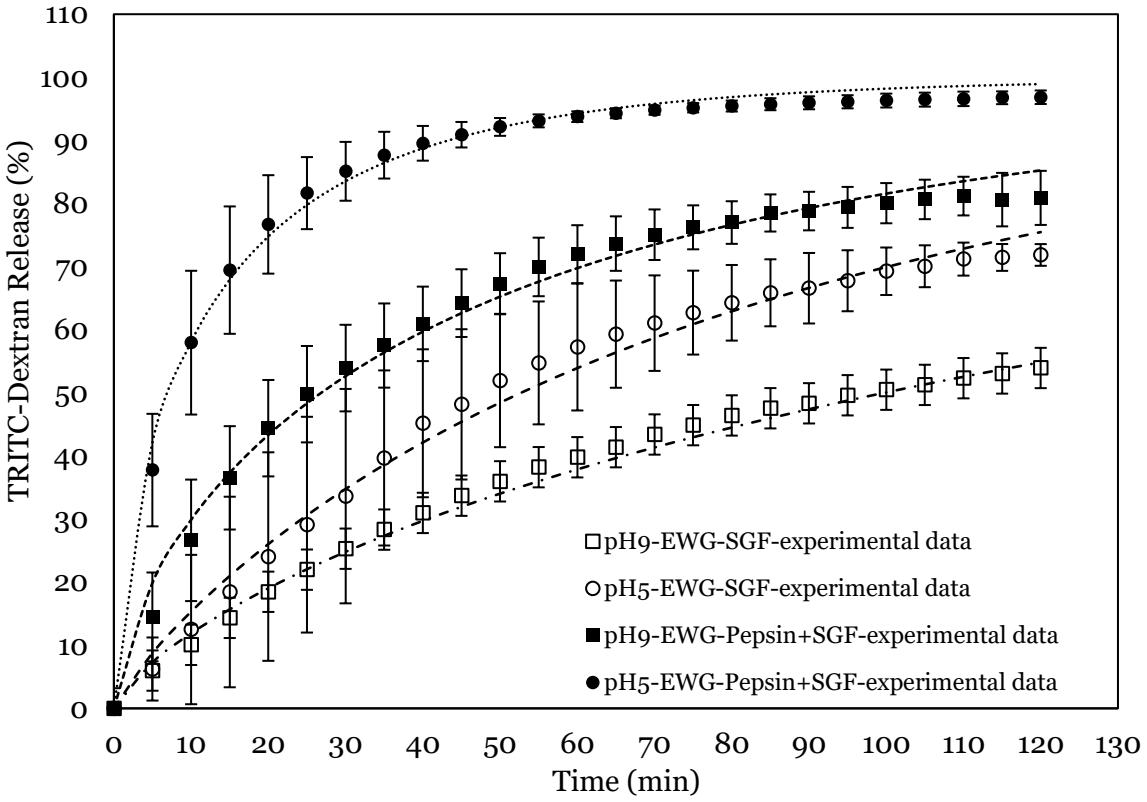

Figure 7.7: Percentage of TRITC-dextran release from pH 9 EWG (squares) and pH 5 EWG (circles) over time using either SGF-pepsin solution (filled symbols) or SGF solution without pepsin (open symbols). Values represent averages (n=3 replicates) with error bars representing the SD. Dashed lines show the model representations of the Weibull function applied to the entire TRITC-dextran release profiles.

In order to quantify the differences of kinetics highlighted in Figure 7.7, modelling of the curves was performed. The Weibull distribution function and the power-law model are widely used to describe drug dissolution and nutrient release kinetics during *in vitro* analysis (Carbinatto *et al.,* 2014; Kong & Singh, 2011; Kosmidis, Argyrakis, & Macheras, 2003). The Weibull function and and the power-law model fitted well to the TRITC-dextran release data as stated by the coefficients of determination (R^2>0.97), in the presence and absence of pepsin for both EWGs (Table 7.1).

Table 7.1: Fitting parameters for the TRITC-dextran release data fitted with the Weibull model and the power-law model

Experimental condition	k (min^{-1})	β	$t_{1/2}$ (min)	R^2	SSE
pH 5 EWG, SGF-pepsin	0.19 ± 0.010^a	0.64 ± 0.01^c	7 ± 1^d	0.99	0.01
pH 9 EWG, SGF-pepsin	0.08 ± 0.003^b	0.66 ± 0.01^c	27 ± 2^c	0.99	0.01
pH 5 EWG, SGF only	0.02 ± 0.002^c	0.86 ± 0.02^a	53 ± 2^b	0.99	0.01
pH 9 EWG, SGF only	0.02 ± 0.001^c	0.74 ± 0.01^b	99 ± 6^a	0.99	0.00
	Power law model fitting parameters				
Experimental condition	k (min^{-1})	n	R^2	SSE	Release mechanism
pH 5 EWG, SGF-pepsin	0.17 ± 0.008^a	0.53 ± 0.01^c	0.99	0.000	Anomalous
pH 9 EWG, SGF-pepsin	0.08 ± 0.003^b	0.54 ± 0.01^c	0.98	0.006	Anomalous
pH 5 EWG, SGF only	0.04 ± 0.002^c	0.62 ± 0.01^a	0.97	0.025	Anomalous
pH 9 EWG, SGF only	0.04 ± 0.002^c	0.58 ± 0.01^b	0.98	0.008	Anomalous

Anomalous transport indicates the erosion controlled and fickian diffusion mechanisms

k (min^{-1}) is the rate constant, β is a shape parameter and $t_{1/2}$ (min) is the time to reach 50% loss of total TRITC-dextran for the Weibull function

k (min^{-1}) is the rate constant and n is the release exponent for the power-law model

R^2 is the coefficient of determination; SSE is error sum of squares

Values represent averages (n = 3) ± SD

Means within each column followed by different superscript letters are significantly different ($p<0.05$)

The Weibull parameters (k and β), power-law model parameters (k and n) and $t_{1/2}$ were significantly ($p<0.05$) influenced by the experimental conditions. The reported release rate constants of the Weibull function and the power-law model (k) confirmed that, in the presence of pepsin, the pH 5 EWG showed significant ($p<0.05$) higher rate of TRITC-dextran release compared to the pH 9 EWG. The k values of both gels in the absence of pepsin (SGF only) were lower than those in the presence of SGF-pepsin. These results confirm that the presence of pepsin accelerates the EWG disintegration and subsequent TRITC-dextran release.

The β parameter of the Weibull function was used as a shape parameter to determine the pattern of TRITC-dextran release during digestion (Carbinatto *et al.,* 2014). Both EWGs showed the value of $\beta<1$, in the presence as well as the absence of pepsin. This suggests that TRITC-dextran release proceeded in two phases: first, a high

initial rate of TRITC-dextran release, followed by, a subsequent exponential decrease in the TRITC-dextran release with time. Furthermore, the β parameter of the TRITC-dextran release profiles in the presence of SGF-pepsin was lower than the TRITC-dextran release profiles in the absence of pepsin (SGF only). This indicates that TRITC-dextran release profiles in the presence of SGF-pepsin had a higher initial slope than the TRITC-dextran release profiles in the absence of pepsin. This could be due to rapid erosion of the gel matrix by pepsin accompanied by the faster release of TRITC-dextran during the initial release phase.

The EWGs disintegration behaviour as described in Figure 7.4 and Figure 7.5 do not exactly follow the suggested two-phase TRITC-dextran release behaviour. For example, as explained before, Figure 7.4 (a) and Figure 7.4 (b) show that the extent of the disintegration of the pH 5 EWG remained quite limited during the first 34 min of digestion. Indeed, this different behaviour of both the gel disintegration and the TRITC-dextran release could suggest that more than one mechanism may be involved in the release of TRITC-dextran from the EWG matrix in the presence of the proteolytic enzyme, pepsin.

To prove that, the release exponent (n) value of the power-law model was used to identify the mechanism that drives the nutrient release process during gastric digestion (Carbinatto *et al.,* 2014). The release exponent (n) values of studied samples presented between 0.53 and 0.62 (Table 7.1) indicate that the TRITC-dextran release occurred according an anomalous mechanism (non-Fickian transport). More specifically, in the presence of pepsin, the combination of EWG matrix erosion due to pepsin activity and passive diffusion of the TRITC-dextran could be the two possible mechanisms responsible for TRITC-dextran release. In the absence of pepsin, the kinetics of TRITC-dextran release may mainly be governed by the combination of egg protein matrix relaxation as a result of hydration and the passive diffusion of the TRITC-dextran due to the concentration gradient. According to Nam *et al.* (2004), hydrated hydrogels triggers the release of the loaded active compound within the hydrogels through the widened space within the gel network.

Moreover, any single parameter (k or β) of the Weibull function does not adequately characterise the release kinetics of TRITC-dextran from the EWGs. Thus, in the end, release half-time ($t_{1/2}$) is arguably the most informative parameter. Being the time required to reach 50% loss of total TRITC-dextran, $t_{1/2}$ incorporates both the k and β parameters from the Weibull model. Consequently, it describes more adequately the overall curve properties compared with either one of the fitted parameters on its own (Bornhorst *et al.,* 2015). In SGF without pepsin, TRITC-dextran release half-times were 53 min and 99 min from pH 5 EWG and pH 9 EWG, respectively. These results show that

the presence of acidic SGF alone is ineffective at releasing TRITC-dextran from both EWGs, but especially from the dense pH 9 EWG. However, when pepsin was added to the SGF solution, half-time ($t_{1/2}$) dramatically ($p<0.05$) declined to around 7 min and 27 min for the pH 5 and pH 9 EWGs, respectively. This clearly demonstrates that the EWG disintegration due to the action of pepsin leads to a massive release of TRITC-dextran initially embedded inside the gels. The significantly ($p<0.05$) lower half-time ($t_{1/2}$) value determined for the pH 5 EWG, compared to the pH 9 EWG, may result from the differences in EWG architecture. This is in accordance with the results of Nyemb *et al.* (2016a), who showed that pH 5 EWG, consisting of a less-dense structure, underwent greater protein hydrolysis during gastrointestinal digestion than a pH 9 EWG, with a dense-compact structure.

7.5 Conclusions

This study aimed at understanding microstructure-related effects of two model EWG protein matrices on their disintegration by pepsin using an *in-situ* methodology based on confocal imaging. In conclusion, the overall gel disintegration, and concomitant peptide-like molecule release rates were greatly influenced by the microstructure characteristics of the egg white protein gels. However, the effect of varied local pH at the interface between SGF solution and EWG also needs to be taken into consideration, since pH may also influence the overall disintegration kinetics. This issue merits future investigations. This study also demonstrated that the Weibull function can successfully be used to describe the rate and mechanism that drives the nutrient release process from EWGs during gastric digestion in the model investigated here.

The proposed novel methodology utilising time-lapse confocal microscopy might enable the study in real-time, and with a high resolution, of the spatiotemporal degradation behaviour of food protein hydrogels during the *in vitro* digestion process. This could help in the optimization of the design of biomaterial delivery food vehicles in the future. However, improvement of the proposed methodology is still required to monitor the simultaneous spatiotemporal mapping of pH changes within the digestion system during simulated gastric digestion. In addition, dual labelling of the hydrogel protein and enzyme could allow a better understanding of the mechanism of enzyme action during digestion of food matrices.

Chapter Eight

8. Role of Gastric Juice Diffusion on Softening and Mechanical Disintegration of pH 5 And pH 9 Egg White Gels during *In Vitro* Gastric Digestion*

8.1 Abstract

Fundamental knowledge of the influence of gastric juice diffusion into food structures on rate of softening and mechanical disintegration of the food matrix during gastric digestion is crucial to better control the disintegration and release of nutrients. The aim of this work was to investigate the gastric juice diffusion on softening and disintegration kinetics of pH 5 and pH 9 egg white gel (EWG) structures during *in vitro* gastric digestion. EWG samples (5 cm^3 cubes) underwent *in vitro* digestion by incubation in the simulated gastric fluid at different time intervals for up to 240 min. The hardness of the digested EWG cubes were measured using a Texture Analyser; softening kinetics were fit to the Weibull model. Results revealed that pH 9 EWG (Initial hardness: 4.83±0.13 N) had the longest softening halftime (458±86 min), indicating the slowest softening, whereas pH 5 EWG (Initial hardness: 2.39±0.07 N) had shortest softening halftime (197±12 min), indicating the quickest softening. The digested samples were immediately exposed to mechanical forces generated by the human gastric simulator (HGS) for 10 min to investigate the influence of gastric juice on the breakdown behaviour of the pH 5 and pH 9 EWG cubes. When described in terms of the particle surface area, results suggested that EWG breakdown within the HGS followed a bimodal distribution. The breakdown behaviour of the disintegrated samples was characterised by fitting the cumulative distributions of particle surface areas to a mixed Weibull function (R^2>0.99). The weight of fine particles (α) showed that regardless of gastric juice diffusion, the pH 5 EWG (α = 0.22±0.03) disintegrated into more fine particles than those resulting from pH 9 EWG disintegration (α = 0.07±0.02). As expected, the diffusion of gastric juice enhanced erosion of the EWG particles into fine particles (<1 mm^2) after 240 min of gastric digestion. Result generated from the particle surface area distribution is in good agreement with the softening kinetics of EWGs during the simulated *in vitro* gastric phase.

*Chapter eight submitted as a peer-reviews paper: Somaratne, G., Ferrua, M. J., Ye, A., Nau, F., Dupont, D., Singh, R. P. and Singh, J. (2019). Egg white gel structures determines gastric juice diffusion with consequences on softening and mechanical disintegration during *in vitro* gastric digestion. *Food Research International*, Submitted.

8.2 Introduction

As the primary stage in the digestion of food by the human body, mastication breaks down nearly all solid or semi-solid foods into small particles in the oral cavity (Bornhorst & Singh, 2012; Chen, 2009, 2015). One of the foremost roles of mastication is the formation of a cohesive food bolus for safe swallowing and as a result of mastication, flavour and aroma release from disintegrated food structure (Bornhorst & Singh, 2012). The bolus of food resulting from chewing is disintegrated into small particles under both repeated shearing and grinding of gastric contents by the antral contraction waves together with the biochemical degradation of acids and enzymes in the human stomach (Kong & Singh, 2008a; Kong & Singh, 2009a, b). For all forms of food, gastric digestion is greatly influenced by the initial characteristics of the food material properties, especially food composition and food structure (Ferrua *et al.,* 2011; Kong & Singh, 2008b; Singh *et al.,* 2015). Thus, by altering the material properties of the ingested food, the structural variations will positively modify the nutrient release process through altering the gastric juice diffusion, biochemical disintegration as well as mechanical disintegration when exposed to the peristaltic activity of the stomach (Bornhorst & Singh, 2014; Singh *et al.,* 2015). This might be taken into consideration for optimal design of novel foods towards the targeted and controlled delivery of nutrients.

For solid and semi solid foods, the disintegration kinetics in the stomach is a very important factor controlling the gastric emptying and subsequent nutrient release kinetics (Guo *et al.,* 2014, 2015; Kong & Singh, 2008b, 2009). However, there is still a limited understanding of the mechanisms such as acid and enzyme diffusion into the food matrix, biochemical digestion, softening, erosion and fragmentation of food matrix driving the disintegration kinetics and structural breakdown of food during gastric digestion and few models exist to describe these processes (Bornhorst & Singh, 2014; Drechsler & Ferrua, 2016). Due to the importance of monitoring food particle breakdown in the gastric environment, few analysis techniques including image analysis, sieving and laser diffraction were proposed to quantify changes in particle size distribution of foods during *in vitro* and *in vivo* gastric digestion (Bornhorst *et al.,* 2013; Drechsler & Ferrua, 2016; Guo *et al.,* 2015; Nau *et al,* 2019). Moreover, previous studies have attempted to describe the disintegration of food during digestion with the use of texture analysis methods and these studies also proposed that softening half time is a good indicator to monitor food breakdown during digestion (Bornhorst *et al.,* 2015; Drechsler & Bornhorst, 2018).

Protein is one of the most important macronutrients in food and the digestion of protein is initiated by the acid and pepsin in the stomach (Luo *et al.,* 2015). Eggs have

been widely consumed around the world as an important source of protein in the human diet (Miranda *et al.,* 2015). Due to their functional properties, egg white proteins are extensively used in the formation of food gels with different structures that have considerable potential to serve as a functional food with controlled delivery properties (Nyemb *et al.,* 2016a). The behaviour of different EWG structures in simulated gastric environments has recently received much attention. In particular, Nyemb *et al.* (2016a, b), reported that the overall proteolysis of egg white protein is higher when granular spongy EWGs are submitted to *in vitro* gastric digestion, as compared to smooth rigid EWG. Similarly, micro- and macro-structural changes on EWG matrices have been presumed responsible for different *in vivo* rates of protein digestion and gastric emptying (Nau *et al.,* 2019). Using FRAP analysis and HSI technique, the previous chapter of this thesis (Chapter 6) has shown that the EWG microstructure strongly influences the extent of gastric pepsin and acid diffusion into pH 5 and pH 9 EWGs. However, despite these observations, there remains a poor understanding of the influence of the diffusion of gastric juice on the mechanical disintegration and softening kinetics of EWGs during *in vitro* gastric digestion.

With the aim of making up the insufficiency of the current studies, this chapter proposes to identify the role of gastric juice diffusion and simultaneous biochemical digestion on the rate of softening and mechanical disintegration of pH 5 and pH 9 EWG structures during *in vitro* gastric digestion. The human gastric simulator (HGS) was employed to investigate the disintegration kinetics of pH 5 and pH 9 EWGs under simulated gastric conditions. The texture analysis was used to determine the softening kinetics, with a focus on the effect of the gastric juice diffusion into different EWGs on their breakdown behaviour in the gastric environment.

8.3 Materials and Methods

8.3.1 Materials

Fresh eggs were purchased from a local supermarket in Palmerston North, New Zealand. Eggs were stored at room temperature (25 °C) and used within no more than five days. To reduce the influence of possible variations among the initial samples, the same batch of eggs was used for the entire study. The protein concentration of egg white (10.5±0.28%) was determined by the Kjeldahl method (N×6.25).

All chemicals and enzymes were used in this study is similar as described in the previous 4.3.1 materials section. The SSF and SGF were prepared using the electrolyte stock solutions according to the harmonised INFOGEST protocol, described in section 3.3.4.

8.3.2 Preparation of Egg White Gels

pH adjusted egg white solution was prepared as described previously in section 6.3.2. Then EWGs were prepared as described previously in section 6.3.5. After the preparation of EWGs, they were removed from the plastic casings and cut into 5 mm^3 cubes using a metal wire mesh cutter.

8.3.3 Static *In Vitro* Digestion

EWGs were exposed to *in vitro* oral and gastric phase of digestion at different time intervals up to 4 hours as described in section 5.3.3. Then pH 5 and pH 9 EWGs cubes were separated from the gastric juice using a sieve and then following textural and breakdown measurements of EWG cubes were measured, immediately.

8.3.4 Hardness Determination using Texture Profile Analysis

The texture profile analysis of digested pH 5 and pH 9 EWG cubes was performed using a Texture Analyser TA-XTPlus (Texture Technologies, Stable Microsystems, Surrey, UK) with a 5 kg load cell as described in section 5.3.4.

8.2.5 Weibull Model Parameters and Softening Half-Time Determination

The hardness change kinetics of pH 5 and pH 9 EWGs was described mathematically using the Weibull model as described in section 5.3.5.

8.3.6 Mechanical Disintegration of Egg White Gels Using a Human Gastric Simulator

The influence of gastric juice diffusion into the pH 5 and pH 9 EWG cubes on their breakdown behaviour were analysed by exposing the soaked samples to a dynamic HGS for 10 min as described in section 5.3.6.

8.3.7 Determination of Particle Size Distribution using Image Analysis

The breakdown mechanics of the pH 5 and pH 9 EWGs was assessed on combined digesta, which include the cumulative emptied digesta and the digesta retained in the simulated latex stomach chamber as described in section 5.3.7. Instead of Iodine dye solution used in section 5.3.7, EWG particles were dyed with a 0.5% Bromophenol blue to increase their contrast against the background.

8.3.8 Modelling of Particle Breakdown during Gastric Digestion

To quantify the extent of breakdown, the cumulative distribution of particles in terms of their surface areas was fit to a mixed Weibull distribution function as described in section 5.3.8.

8.3.9 Statistical Analysis

An ANOVA was conducted using a 2-factor factorial design to determine differences in hardness and mixing weight parameter (α) during static *in vitro* gastric digestion. The factors were the type of EWG (pH 5 and pH 9 EWGs) and digestion time (0-240 min). The Tukey test was used to analyse the differences between means and statistical significance was assessed at a level of $p<0.05$. The student t-test was used to assess differences in the Weibull model parameters and softening half-time. Minitab 17 software was used for statistical analysis.

8.4 Results and Discussion

8.4.1 Softening Kinetics of Egg White Gels during Gastric Phase is Influenced by the Initial Egg White Gel Characteristics

The hardness (peak force at the first compression cycle, in N) of the pH 5 and pH 9 EWGs over the 240 min gastric digestion is shown in Table 8.1. Changes in the hardness of the EWG cubes were significantly ($p<0.05$) influenced by the type of EWG and digestion time. For both pH 5 and pH 9 EWGs, the hardness significantly decreased with increasing digestion time. The softening thus occurring during digestion in EWGs could be due to the proteolysis behaviour of egg white protein due to gastric pepsin. In addition to that water uptake from the EWG matrix during gastric digestion process (Chapter 6) may also be associated with the hardness reduction of EWGs during gastric digestion.

pH 9 EWG had a significantly highest initial hardness compared to the pH 5 EWG (4.83±0.13 N compared to 2.39±0.07 N), likely due to the more compact and microstructurally homogeneous gel formed by egg white proteins at pH 9 (Chapter 6). In contrast, the microstructure of the pH 5 EWG was characterised by a spatially heterogeneous loose protein matrix made of larger aggregate particles (Chapter 6, sections 6.4.1 and 6.4.2), which lead to the lowest initial hardness. Throughout the gastric digestion, pH 9 EWG maintained a higher hardness compared to pH 5 EWG. Results further indicate that initial EWG texture and microstructure impact hardness reduction during gastric digestion. In particular, after 240 min of digestion, pH 5 EWG exhibited the greatest change (66% decrease) from its initial hardness value, whereas only 40% decrease was observed in the case of pH 9 EWG.

Table 8.1: Changes in the hardness (N) of the pH 5 and pH 9 EWGs during *in vitro* gastric digestion

Digestion time (min)	Hardness of pH 5 EWG (N)*	Hardness of pH 9 EWG (N)*
0	2.39 ± 0.07^{f}	4.83 ± 0.13^{a}
10	2.10 ± 0.02^{fg}	4.41 ± 0.30^{ab}
20	1.96 ± 0.07^{fgh}	4.31 ± 0.16^{b}
40	1.83 ± 0.03^{gh}	4.17 ± 0.17^{b}
60	1.63 ± 0.18^{hi}	4.01 ± 0.14^{bc}
120	1.38 ± 0.12^{ij}	3.62 ± 0.18^{cd}
180	1.07 ± 0.05^{jk}	3.43 ± 0.18^{d}
240	0.81 ± 0.08^{k}	2.88 ± 0.16^{e}

*Values are represented as averages (n=24 cubes) ± SD of the mean. Different letters within each column and raw represent statistically different means ($p<0.05$).

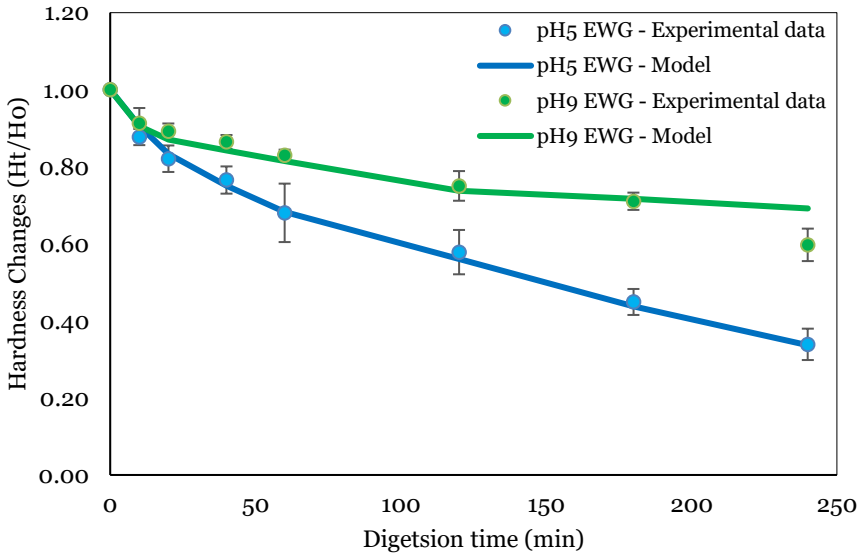

Figure 8.1: Softening curves of the pH 5 and pH 9 EWGs during *in vitro* gastric digestion based on the hardness (N) measurements. Values are means (n = 3) with error bars as SD (some are too small to be visible). The solid lines represent the predicted values from the average Weibull model parameters shown in Table 8.2.

The Weibull distribution function has been widely used to describe the softening kinetics of solid foods during static *in vitro* gastric digestion (Bornhorst *et al.,* 2015; Drechsler & Bornhorst, 2018). In the present study also, the experimental data of softening during gastric digestion (Figure 8.1) fit well to the Weibull model (Eq. (5.1)), as evidenced by the high coefficient of determination values (R^2 = 0.95-0.98, Table 8.2) and

low error sum of squares (SSE <0.01, Table 8.2). The reported softening rate constants of the Weibull function (k) demonstrated that the pH 5 EWG showed a higher rate of softening (k=0.004 min^{-1}) compared to pH 9 EWG (k=0.002 min^{-1}). The β values for both pH 5 and pH 9 EWGs are lower than 1, indicating a higher rate of softening at the initial stage of the gastric digestion process followed by an exponential decrease in the hardness of EWG with digestion time.

The half-time ($t_{1/2}$), i.e. the time to reach 50% reduction of initial hardness, incorporates both the k and β parameters from the Weibull model, and thus more appropriately describes the overall curve properties than either one of the fitted parameters on its own (Bornhorst *et al.,* 2015). Results show that pH 9 EWG, which had the highest initial hardness (4.83±0.13 N), also had the highest softening half-time (458±86 min), indicating a slowest softening than pH 5 EWG which had the lowest initial hardness (2.39±0.07 N) and the lowest softening half-time (197±12 min). These differences observed between both EWGs probably reflect the differences in their initial texture and microstructure that may result in different rates of pepsin, moisture and/or acid diffusion. Indeed, it was previously established that the loosened microstructure of the pH 5 EWG leads to faster pepsinolysis, moisture and acid diffusion during *in vitro* gastric digestion compared to the denser structure of pH 9 EWG (Chapters 6 and 7). The relevance of these findings on the breakdown response of the EWG samples are discussed in the following sections.

Table 8.2: Parameter values of Weibull function (Eq. 5.1) fitted to the softening curves of the pH 5 and pH 9 EWGs during *in vitro* gastric digestion.

	k	ß	R^2	SSE	$t_{1/2}$ (min)
pH 5 EWG	0.004±0.00^a	0.90±0.02^a	0.98	0.01	197±12^b
pH 9 EWG	0.002±0.00^b	0.92±0.03^a	0.95	0.00	458±86^a

R^2 is the goodness of fit; SSE is error sum of squares

k is the rate of change in hardness (min^{-1})

ß is the distribution shape factor (dimensionless)

$t_{1/2}$ is the softening half-time (min)

Values represent the average model parameters or softening half-time from 3 digestion trials ± SD

Means within each column followed by different superscript letters are significantly different ($p<0.05$)

8.4.2 Mechanisms of Particle Breakdown Depend on the Initial Structure of the Egg White Gels

During the *in vitro* gastric phase, gastric juice diffused into the EWG structure, thus simultaneously favouring the softening of gel particles and pepsinolysis of egg white protein inside the gel cubes/particles (Nyemb *et al.,* 2016a), and both phenomena might have some impact on the mechanical disintegration of the EWGs due to the stomach movements. Therefore, the influence of gastric juice diffusion on the breakdown mechanics of the pH 5 and pH 9 EWGs was investigated by exposing the soaked EWG samples (digested or not) to the mechanical forces generated by the HGS.

As described earlier in section 5.4, from a nutritional point of view, the amount of nutrients that are entrapped within the digested particles or, on the contrary, those released from the food particles is an important indicator. Thus, analysing the breakdown behaviour of food during gastric digestion in terms of the particle surface area is a better indicator of the amount of nutrients associated with food matrix than distributions of the number of particles (Drechsler & Ferrua, 2016). The distributions of particle size (surface area) in the disintegrated pH 5 and pH 9 EWG samples are depicted in Figure 8.2 and 8.3.

Fragmentation, chipping and erosion are the major mechanisms responsible for solid food disintegration in a simulated gastric environment (Drechsler & Ferrua, 2016; Kong & Singh, 2009a). Based on the classification framework proposed by Drechsler and Ferrua (2016), (Figure 5.1), an attempt was made to evaluate the contribution of surface erosion and particle fragmentation on the breakdown of EWG particles due to the exposure of gastric juice and the mechanical forces generated by the HGS.

According to the Figure 8.2 and 8.3, without exposure to gastric juice (0 min, control sample), the pH 5 and pH 9 EWGs exhibited mainly undamaged (5-10%) particles compared to the fine debris particles (<0.5-1%). These distributions revealed the significant amount of nutrients still present inside large particles (A_0>15 mm²) in the disintegrated control samples. However, even if there are mainly large particles, some small hydro soluble nutrients (i.e. peptides) could be released into the gastric medium.

On the contrary, as the digestion proceeds, the particle size progressively decreased for both EWGs as demonstrated by the increasing percentages of the small particles such as chips (1 mm²<A_0<1.75 mm²) and fine debris (A_0<1 mm²). Interestingly, this progressive size reduction due to previous exposure to gastric juice followed different types of breakdown mechanisms for the pH 5 and pH 9 EWG samples.

The breakdown of the pH 5 EWG appears to be driven by fragmentation, chipping as well as surface erosion mechanisms when the gel is exposed to gastric juice up to 20 min, since mainly fragmented, chips and fine debris particles are observed within the

samples (Figure 8.2). It can be assumed that the diffusion of gastric juice into the pH 5 EWG causes the fast reduction of the internal cohesive forces that hold the pH 5 EWG matrix together, consistently with the fast softening previously reported (Table 8.2). Consequently, when the stress applied by the HGS was greater than the internal cohesive forces inside the pH 5 EWG matrix, it may lead to extensive fragmentation of particles as soon as the digestion began. When the exposure to gastric juice progressed, the percentage of fragmented particles decreased markedly, and the percentage of chipped particles increased steadily; this is especially visible within the pH 5 EWG samples exposed to 120 min of gastric digestion. As further exposure to gastric juice increases, the distribution of chips shifted towards smaller sizes, likely due to the increased softening of the pH 5 EWG. Finally, the pH 5 EWG exposed to SGF-pepsin more than 120 min exhibited considerable breakdown as the number of fine debris particles (<1 mm^2) increased and the distribution curve shifted towards the left (Figure 8.2). Somewhat similar breakdown behaviour has been previously reported by Guo *et al.* (2015), for a soft whey protein emulsion gel. This soft gel had a faster disintegration than hard gels in the HGS, which resulted from both abrasion and to some extent fragmentation.

The pH 9 EWG showed the weight percentage of large particles (>15 mm^2) decreased progressively over gastric digestion (Figure 8.3). The main mechanisms that can explain the particle size distributions of pH 9 EWG expose to gastric digestion over 240 min are the eroding of the matrix into fine debris, with a progressive reduction in size due to fracture or chipping mechanisms. Unlike pH 5 EWG, smaller particles (<0.008 mm^2) of pH 9 EWGs are increasing the most rapidly. On the contrary, for the size classes between 0.012 mm^2 -1.5 mm^2 do not appear to change sizably. Thus, surface erosion of the pH 9 EWG may be one of the predominant mechanisms of pH 9 EWG disintegration during *in vitro* gastric phase. A similar trend was observed by Guo *et al.* (2015), when they examined the simulated gastric digestion of whey protein emulsion gels using the HGS; those gel samples that had a hard texture had a much slower disintegration largely governed by abrasion compared to soft gels.

Therefore, the disintegration mechanism, in the HGS, of the EWGs previously exposed to the gastric juice can be explained based on their initial hardness and microstructure. The maximum magnitude of the destructive force from the HGS is around 2.5 N (Kong & Singh, 2010). Then, the low initial hardness of pH 5 EWG (around 2.4 N) suggests this gel can be broken down quickly into smaller fragments in the HGS, whereas the much higher initial hardness of pH 9 EWG (around 4.8 N) might explain the relevance of the erosion mechanism in the disintegration of this gel and the particular low impact of fragmentation mechanism. On the other hand, EWGs became softer and

then likely easier to break apart after diffusion of gastric juice. Then, as reported in the previous chapters 6 and 7, pepsin diffusivity was higher inside the flexible, highly anisotropic, porous and the granular network of the pH 5 EWG than inside the rigid, highly isotropic, less porous and smooth network of the pH 9 EWG. The result was greater changes of the microstructure of pH 5 EWG, and a greater effect on the weakening and disintegration of this gel. Another factor possibly contributing to the greater resistance of the pH 9 EWG to breakdown under the stomach conditions could be the higher initial pH of the gel (as also reported in Chapter 7). Indeed, this could locally induce high pH despite the addition of gastric fluid, thus limiting the proteolytic action of pepsin on the pH 9 gel proteins in agreement with the observations of Nau *et al.* (2019). These authors further underlined that smooth-rigid EWG (similar to pH 9 EWG) is more elastic, cohesive and viscoelastic than the granular-spongy EWGs (similar to pH 5 EWG). Thus, the smooth-rigid EWG is more resistant to breakdown and likely to break up forming harder particles.

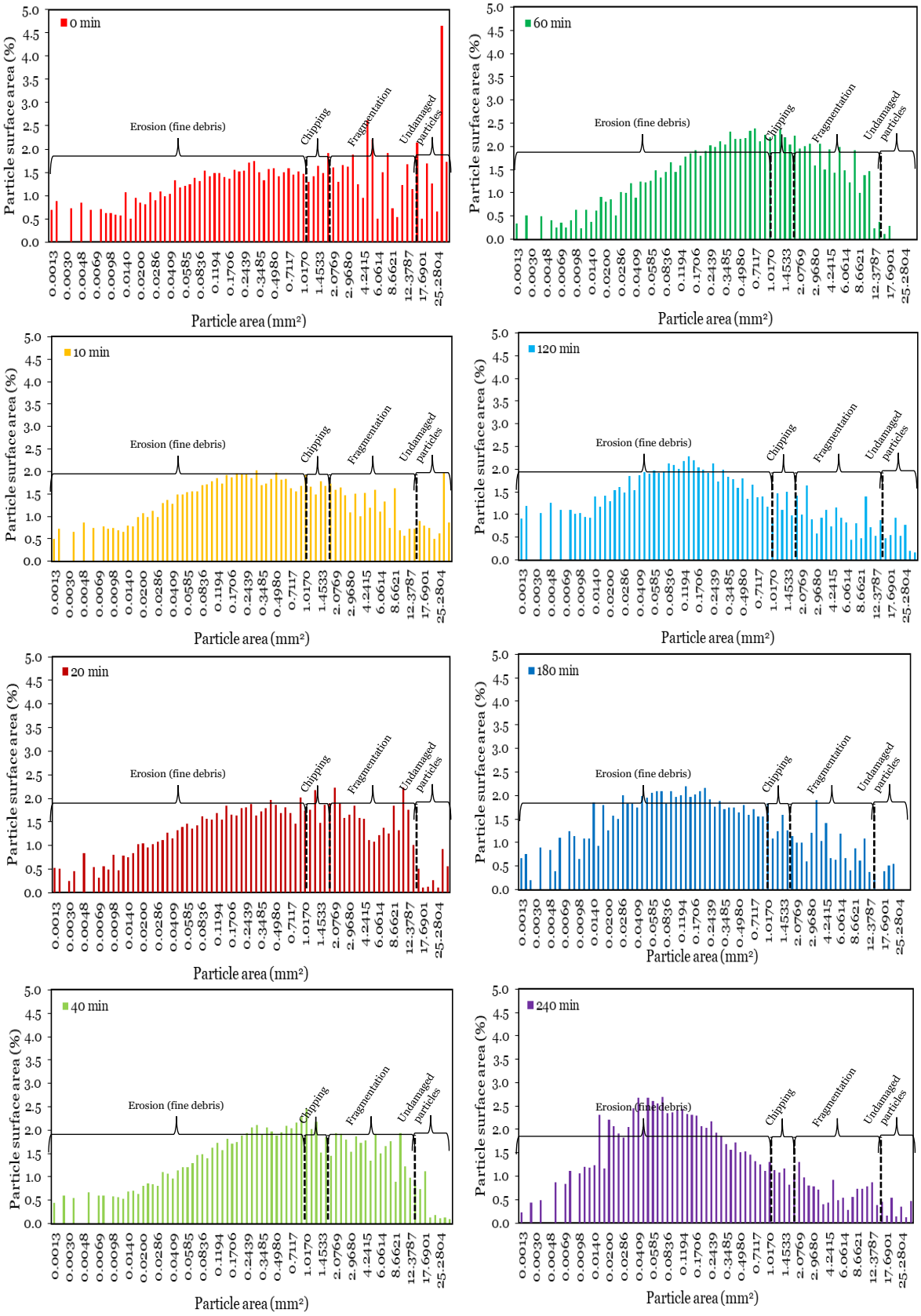

Figure 8.2: Examples illustrating the characterisation of broken pH 5 EWG particles surface area (0-240 min digestion time) to determine the underlying mechanisms of EWG breakdown during the gastric phase.

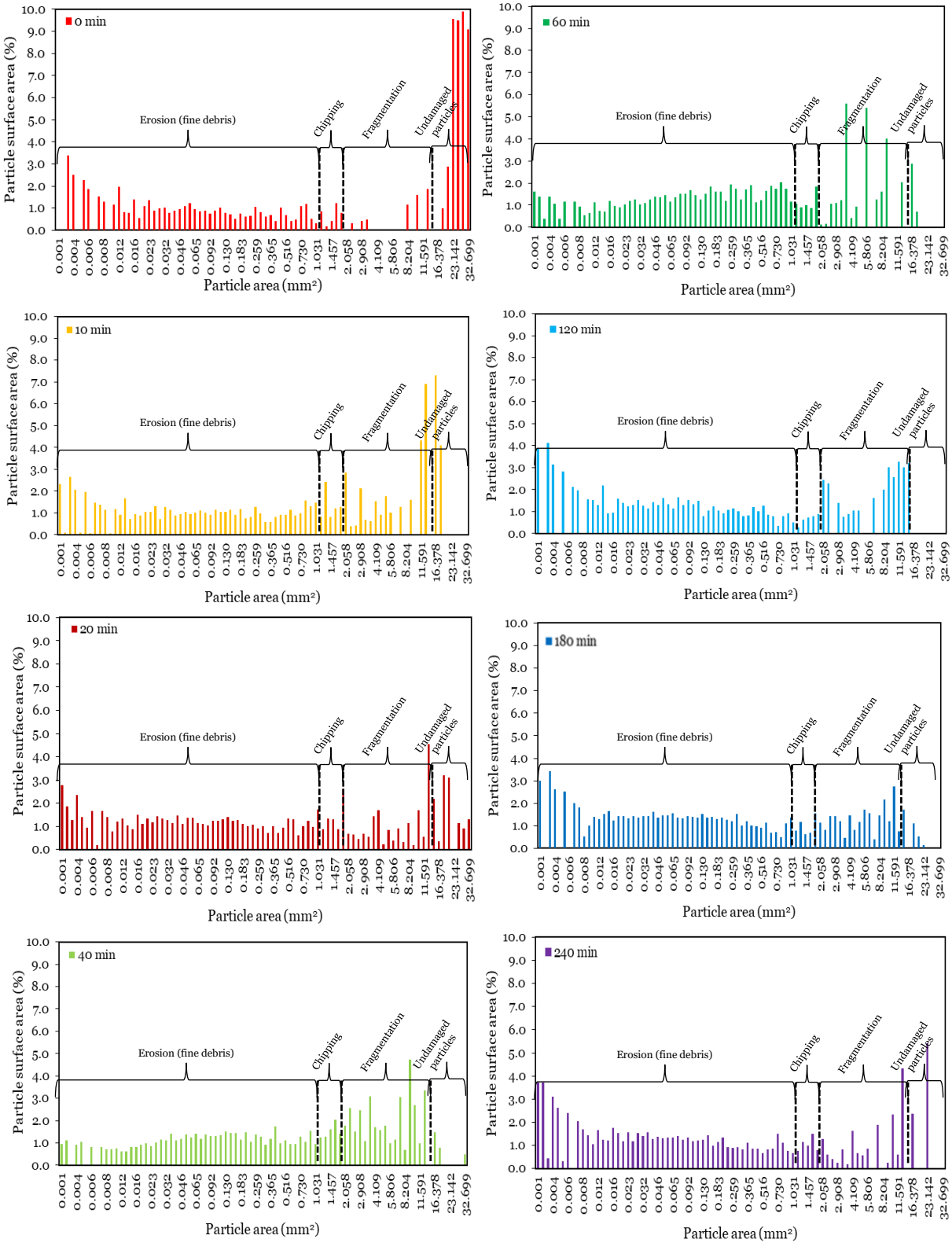

Figure 8.3: Examples illustrating the characterisation of broken pH 9 EWG particles surface area (0-240 min digestion time) to determine the underlying mechanisms of EWG breakdown during the gastric phase.

8.4.3 Role of Biochemical and Mechanical Effects on the Breakdown Process of pH 5 and pH 9 Egg White Gels

The cumulative particle surface area distributions of pH 5 and pH 9 EWG after 10 min HGS and for 0 to 240 min prior gastric digestion is shown in Figure 8.4. At the beginning of gastric digestion, curves exhibited a bimodal distribution behaviour, with one component associated with fine debris (<1 mm^2) and another with particles similar in size to the original cubes (~25 mm^2). As expected, longer the exposure to gastric juice, curves shifted towards the left and smaller the EWG particles (Figure 8.4).

All the cumulative distributions of particle surface areas well fitted to mixed Weibull models, as indicated by correlation coefficients (R^2) all higher than 0.99 (Table 8.3). The particle surface area distribution exhibited a bimodal distribution behaviour, with one component associated with fine debris (first mode of the mixed Weibull distribution) and another with particles similar in size to the original cubes (second mode of the mixed Weibull distribution). The scale parameter (λ) is a constant representing the broadness (i.e. When λ is increased, the height of the Weibull distribution decreases and the broadness increases) whereas the shape parameter (k) is a constant representing the shape (i.e. sigmoidal shape when $k>1$, or parabolic shape when $k<1$) of the Weibull distribution (Krifa, 2009). It is interesting to note that, in one hand, the scale parameter of the first mode of the mixed Weibull distribution (λ_1) value increased over the 240 min digestion period in both pH 5 and pH 9 EWGs, which indicate a broader distribution spread of the fine particles with increased digestion time (Table 8.3). On the other hand, the scale parameter of the second mode of the mixed Weibull distribution (λ_2) value decreased over the 240 min digestion period in both pH 5 and pH 9 EWGs, which indicate a narrower distribution spread of the large particles with increased digestion time (Table 8.3).

The extent of damage to the EWGs due to exposure to gastric juice and mechanical forces generated by the HGS was assessed based on the mixed Weibull parameter (α) that describes the weight of fine particles within the breakdown sample. The temporal evolution of α parameter for pH 5 and pH 9 EWGs is shown in Figure 8.5. The weight of fine particles (α) was significantly influenced by the EWG type, digestion time, and their interaction ($p<0.05$, Figure 8.5). As expected, the weight of fine particles significantly increased ($p<0.05$) during the 240 min gastric digestion period for both pH 5 and pH 9 EWGs. Results showed that in the absence of gastric juice diffusion, the pH 5 EWG ($\alpha = 0.22\pm0.03$) disintegrated into more fine particles than the pH 9 EWG ($\alpha = 0.07\pm0.02$). Moreover, the weight of fine particles values of the pH 5 EWG remained significantly higher than that of the pH 9 EWG ($p<0.05$) throughout the 240 min gastric digestion, indicating the pH 5 EWG underwent a higher disintegration rate than pH 9

EWG. These disintegration patterns are in good agreement with the softening kinetics of EWGs during the simulated *in vitro* gastric phase reported above (section 8.4.1). Thus, the softening half-time may be a good indicator of the relative rate of breakdown of protein-based hydrogels.

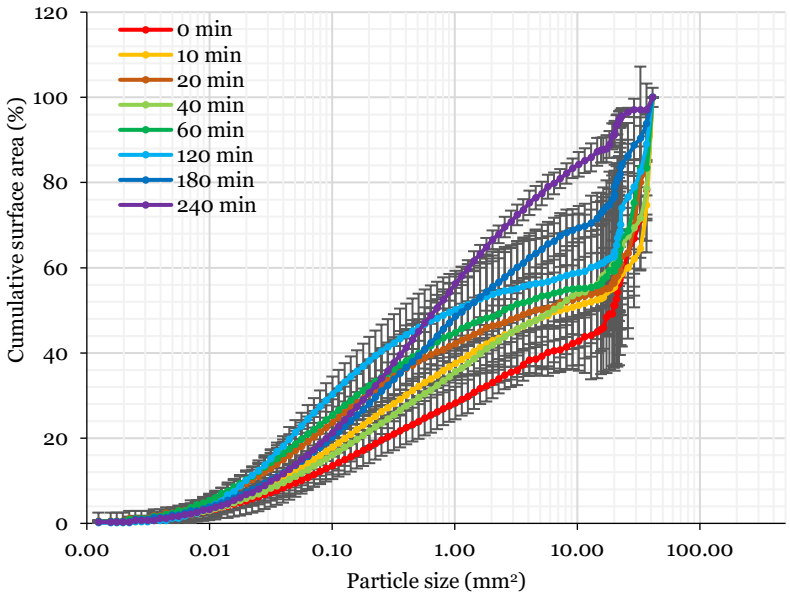

(a)

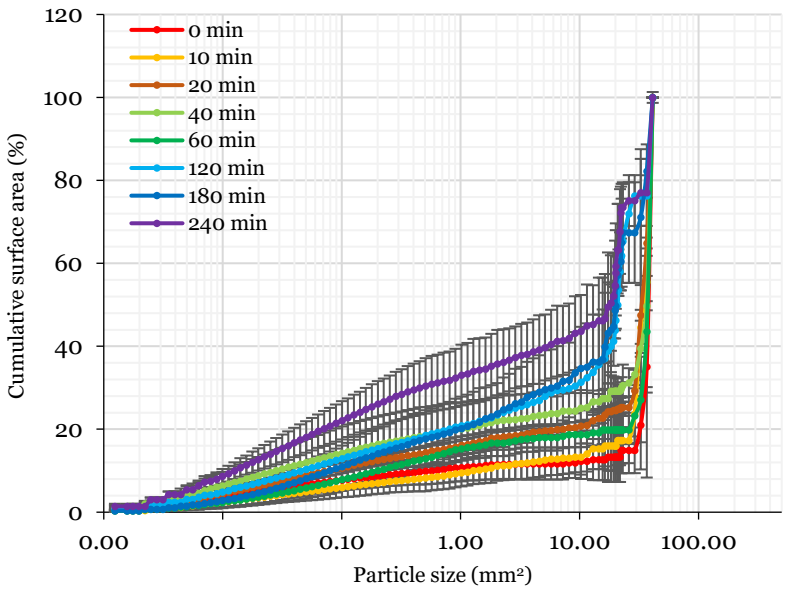

(b)

Figure 8.4: Cumulative particle surface area distributions for (a) pH 5 and (b) pH 9 EWGs after 10 min HGS, depending on the time of prior gastric juice soaking. Values are given as averages (n = 3) with error bars as SD.

Table 8.3: Mixed Weibull Distribution Parameters. Values are given as averages (n = 3) with SD.

Digestion time (min)	λ1		k1		λ2		k2		R^2	
	pH 5 EWG	pH 9 EWG	pH 5 EWG	pH 9 EWG	pH 5 EWG	pH 9 EWG	pH 5 EWG	pH 9 EWG	pH 5 EWG	pH 9 EWG
0	0.01±0.01	0.01±0.00	0.70±0.06	0.79±0.07	3.01±1.54	27.3±2.5	0.58±0.00	0.50±0.04	>0.998	>0.993
10	0.21±0.00	0.01±0.13	0.79±0.01	0.70±0.19	1.34±1.07	17.2±3.0	0.63±0.02	0.56±0.24	>0.999	>0.997
20	0.69±0.19	0.02±0.03	0.79±0.07	0.75±0.05	0.61±0.27	12.6±4.2	0.67±0.06	0.69±0.20	>0.999	>0.998
40	0.61±0.01	0.01±0.00	0.79±0.01	0.75±0.06	0.38±0.18	9.4±1.4	0.67±0.03	0.49±0.05	>0.997	>0.992
60	0.64±0.05	0.03±0.00	0.80±0.04	0.67±0.04	0.09±0.08	5.7±1.2	0.75±0.07	0.47±0.12	>0.998	>0.997
120	0.79±0.83	0.05±0.00	0.64±0.09	0.68±0.08	0.03±0.00	2.6±0.5	0.96±0.06	0.67±0.24	>0.998	>0.994
180	1.46±0.23	0.09±0.04	0.66±0.02	0.68±0.16	0.03±0.00	2.9±1.12	0.87±0.06	0.98±1.49	>0.997	>0.993
240	2.98±0.45	0.11±0.00	0.62±0.09	0.73±0.05	0.01±0.00	2.6±0.3	0.80±0.07	0.53±0.03	>0.996	>0.998

λ1 and λ2 are the scale parameters established by left (first mode) and right (second mode) Weibull distribution, respectively

k1 and k2 are the shape parameters established by left (first mode) and right (second mode) Weibull distribution, respectively

R^2 is the coefficient of determinations

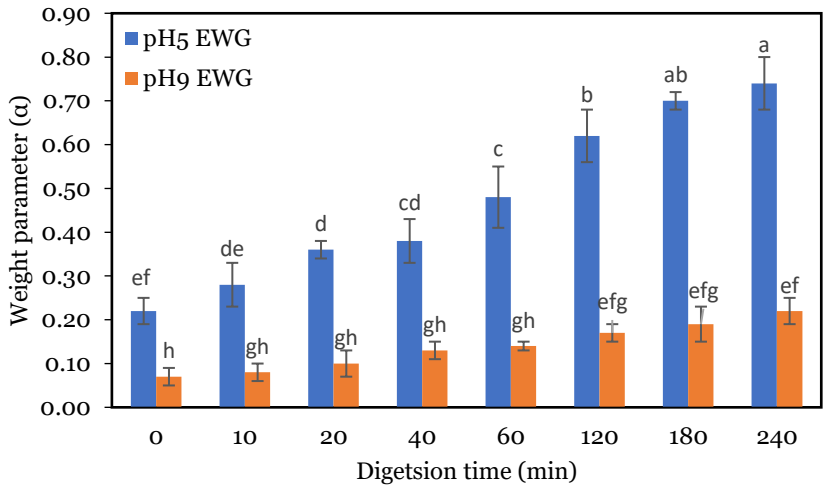

Figure 8.5: Temporal evolution of weight parameter (α) of the Mixed Weibull function (proportion of small particles within samples) for pH 5 and pH 9 EWG submitted to 10 min HGS after 0 to 240 min prior gastric digestion. Values are given as averages (n = 3) with error bars as SD. Different letters indicate significant difference ($p<0.05$) as determined using multiple comparison of means (Tukey test).

8.5 Conclusions

In this study, the dynamic HGS model was employed to investigate the effect of gastric juice diffusion on softening and disintegration kinetics of two differently structured egg white protein gels (pH 5 and pH 9 EWGs). The rate of softening during *in vitro* gastric digestion was qualitatively related to the disintegration kinetics of pH 5 and pH 9 EWGs. The mixed Weibull function can successfully be used to describe the cumulative distributions of particle surface areas of EWGs during gastric digestion. Particle surface area distributions revealed that pH 5 and pH 9 EWGs follow distinct breakdown patterns when they are exposed to HGS after prior gastric digestion up to 240 min. To summarize, the pH 5 EWG had a faster disintegration which results from both erosion and chipping mechanisms, as well as to some extent fragmentation. In contrast, the pH 9 EWG had a much slower disintegration largely governed by erosion. It was assumed these modes of disintegration depend on the internal cohesive forces of the EWG matrices which are closely related to the EWG texture and microstructure. In conclusion, the overall gel softening and disintegration as a result of gastric juice diffusion and mechanical strains was greatly influenced by the characteristics of the EWGs. These findings support the role of EWG structure and biochemical effects on the disintegration patterns of gels during *in vitro* and *in vivo* gastric digestion. The derived findings of this study regarding the disintegration kinetics of foods in the stomach should be important for designing novel foods with desired functional properties.

Chapter Nine

9. Overall Discussion, Conclusions and Future Recommendations

9.1 Overall Discussion and Conclusions

This PhD programme investigated the physicochemical processes of gastric digestion in order to understand how food composition and structure influences the relative roles that the biochemical and mechanical processes have on the disintegration of the solid food matrix. The use of static *in vitro* digestion followed by dynamic HGS enabled us to mimic the main mechanisms (i.e. gastric acid and enzyme diffusion, biochemical digestion and physical disintegration) of solid food breakdown in the stomach and the subsequent nutrient release that occurs during the gastric phase (Figure 9.1).

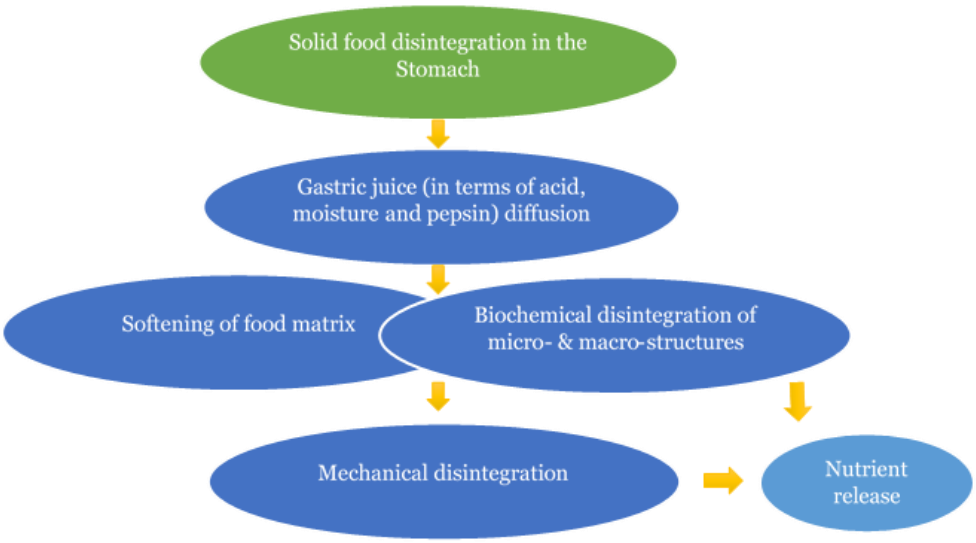

Figure 9.1: Schematic overview of unravelling the physicochemical process of gastric digestion

The overview of existing literature provided in chapter 2 highlighted the knowledge gap regarding the role of food material properties on major solid food breakdown mechanisms in the stomach and subsequent nutrient release. This chapter starts with a discussion of stomach physiology and the composition of gastric secretion, then focuses on the important mechanisms such as gastric juice diffusion, biochemical digestion and physical disintegration and the influence that the chemical and physical properties of the solid food matrix has on these processes. *In vivo* and *in vitro* approaches used for studying gastric digestion of foods are also highlighted in this section. The chapter concludes with an outlook on future research in this area to increase

our fundamental understanding of the food digestion process in the stomach as related to the food material properties (i.e. composition, texture and microstructure).

As a starting point for the investigations of this overall research, sweet potatoes and EWGs were selected as representative starch and protein-based product models respectively, to simulate the different stages of *in vitro* gastric digestion. In order to introduce different structures to the food matrix, each food product model was processed in different ways.

Orange-fleshed sweet potato has been identified as a good source of starch and β-carotene. Sweet potato is normally cooked in a variety of ways, including boiled, fried or steamed, prior to consumption (Tumuhimbise *et al.,* 2009; Van Jaarsveld *et al.,* 2006). The cooking methods, steaming and frying were chosen here as thermal treatments that may be used by a typical consumer and result in quite different changes to the sweet potato structure. To gain a better understanding of sweet potato microstructural changes after cooking, LM, CLSM and SEM were used to observe the surface and cross-sectional slices of sweet potato tissues, before and after cooking for each thermal treatment. In addition, the moisture content and hardness of the SSP and FSP matrix were determined. Results revealed that the different cooking methods not only influenced the microstructure but also the moisture content of the sweet potato matrix. More specifically, SSP contained a high moisture content and were characterised by a densely packed cellular network. In contrast, frying not only dehydrated the sweet potato matrix, but also caused a disruption in the cellular arrangement, created a porous cellular network and resulted in the formation of a crust. However, the texture analysis method used revealed that both steamed and fried sweet potato samples had a similar hardness when assessed immediately after cooking irrespective of their different microstructure. Although, FSP samples had a porous interior structure compared to SSP samples, the high initial hardness of FSP is probably due to the crust formation during frying.

Egg white was chosen as the protein-based model food because it is a rich source of various functional proteins, which can form a wide range of hydro gel structures while keeping a constant chemical composition (Nyemb *et al.,* 2016a, b). In this study, two different EWG models, with similar protein concentration (10%), were prepared by heating fresh egg white that had previously been adjusted to either pH 5 or pH 9. The microstructures of the two different EWGs were quantitatively evaluated using a high-resolution confocal microscopic technique followed by image analysis. Texture analysis was performed by measuring hardness where it was related to the peak force of the first compression cycle. Results showed that egg white protein formed compact and microstructurally homogeneous hydrogels at pH 9. In contrast, gels made at pH 5 formed

a loose and microstructurally heterogeneous protein matrix. At pH 5, which is close to the isoelectric point of most egg white protein, we observed that the egg white protein predominately formed spherical aggregates, leading to the formation of a porous and spatially heterogeneous structure of the pH 5 EWG. In contrast, pH 9 EWG had a less porous and a more rigid structure due to the formation of linear aggregates of egg white protein at pH 9 (Nyemb *et al.,* 2016a, b).

The diffusion of gastric juice within the food matrix was one of the key parameters that helped to describe the overall food breakdown within the stomach and was crucial for our understanding of nutrient release during digestion. Gastric juice is made up predominantly of gastric acid, moisture and enzymes (i.e. pepsin and lipase). During gastric digestion, this gastric juice gradually penetrates from the external surface towards the centre of the food bolus promoting the biochemical degradation and subsequent softening of the food micro- and macro- structure, thus improving its overall disintegration rate. In this study, a novel HSI based methodology was developed to characterise the diffusion of acid and moisture within food structures during gastric digestion. HSI results provided more qualitative and quantitative information on the nature of the moisture and acid penetration into solid food structures during the gastric juice diffusion process.

The gastric juice mapping results revealed that the mechanism and the rate of gastric acid and moisture diffusion was determined by the properties of the food matrix. Interestingly, the rate of acid diffusion did not follow the same trend as the rate of moisture diffusion during simulated gastric digestion of cooked sweet potato or EWGs. More specifically, in FSP the diffusivity of acid (D_{eff} = 3.2±0.2x10^{-9} m^2/s) was higher than in SSP (D_{eff} = 1.6±0.4x10^{-9} m^2/s). This higher acid diffusivity was related to the interconnected porous microstructure inside the FSP compared to the compact and dense cellular microstructure of SSP. However, in contrast to acid diffusivity, the diffusivity of water in SSP (D_{eff} = 2.2±0.8 x10^{-9} m^2/s) was higher than that in FSP (D_{eff} = 1.9±0.5 x10^{-9} m^2/s) during gastric digestion. Although the reason for different trends of moisture and acid diffusivity across steamed and fried sweet potatoes are not clear, Mennah-Govela and Bornhorst (2016b) hypothesized that these differences are due to the water holding capacity differences between steamed and fried matrices.

As reported in this research (Chapter 4), the diffusion of acid and moisture into the sweet potato matrices influenced the cellular breakdown of cooked sweet potatoes microstructure and was associated with the gradual release of β-carotene from the matrices with the increase in digestion time. The degradation of the cell wall may be related to the acidic environment of the gastric juice (pH 3) and the hydrochloric acid was capable of hydrolyse the pectin in the cell wall (Kong & Singh, 2011). Previous studies

have shown that fruit cell walls are more susceptible to degradation in a highly acidic environment compared to an environment with a pH>4.0, due to acid hydrolysis of pectin in the cell wall (Knee, 1982; McFeeters & Fleming, 1991). However, it is important to note that gastric acid alone had no major effect on the complete breakdown of steamed/fried sweet potato cell walls even after 4 hours of gastric digestion. Thus, cell walls in the plant-food matrix may act as a physical 'barrier' towards the interactions of gastric juice and the release of nutrients into the aqueous phase of the gastric digesta. In the absence of mechanical forces generated by the stomach, biochemical digestion did not have a greater effect on the breakdown of cell walls and the release of ß-carotene in steamed or fried sweet potato. The microscopic observations also highlighted that, in the fried samples, gastric acid rapidly diffused into the porous food matrix, but did not enter the cells, possibly due to the accumulated canola oil around the cell walls inhibiting the degradation of the cell walls by the gastric acid. Thus, gastric juice content including acid, moisture and pepsin, may not have a major influence on digestion and release of nutrients from plant based starchy foods. This observation is in agreement with both steamed and fried samples having the similar rate of ß-carotene release during gastric digestion.

The EWGs had different trends of water and acid diffusion rates during gastric digestion parallel when compared with those observed for the cooked sweet potato. We observed that the loosened microstructure in the pH 5 EWG had a significantly ($p<0.05$) higher D_{eff} of water (D_{eff} = 5.6±1.4 x10^{-9} m^2/s) compared to the smooth, less porous gel structure of pH 9 EWG (D_{eff} = 2.1±0.1 x10^{-9} m^2/s). The rate of acid diffusion (D_{eff}) did not differ significantly between the pH 5 EWG (D_{eff} = 2.4±0.1x10^{-9} m^2/s) and pH 9 EWG (D_{eff} = 2.3±0.6x10^{-9} m^2/s). Limited information was found related to the D_{eff} of acid within EWG matrices during simulated gastric digestion. However, it could be hypothesized that water holding capacity, interactions between egg white protein and acid, as well as buffering capacity of EWG may influencing the rate of acid diffusion in both EWGs.

As a key enzyme in the gastric fluid, pepsin plays a significant role in breaking down the protein within the food matrix. Thus, the D_{eff} of pepsin into the EWG matrix is an important parameter to help describe the breakdown behaviour and overall disintegration rate of the EWG during gastric digestion. As a part of this study, the impact of the two different EWG structures on pepsin diffusion was investigated. To characterise the ability of pepsin to diffuse within each EWG's structure, the D_{eff} of FITC-pepsin and FITC-dextran were measured in the native EWGs, using the FRAP technique. The neutral FITC-dextran (40 kDa) was used as a control to highlight the potential effects of electrostatic interactions between the egg white proteins and FITC-pepsin. The diffusion of FITC-dextran and FITC-pepsin were explained by microstructural parameters of

EWGs. The diffusivity of FITC-pepsin was significantly higher ($p<0.05$) in the more porous and heterogeneous pH 5 EWG network compared to the more compact and homogeneous structure of pH 9 EWG (D_{eff} = 5.25±0.53 x10^{-11} m^2/s vs D_{eff} = 4.42±0.61 x10^{-11} m^2/s). Comparison of FITC-dextran and FITC-pepsin diffusivities confirmed the existence of electrostatic interactions between the egg white proteins and FITC-pepsin in the pH 5 EWG, but not in pH 9 EWG. Moreover, the diffusion of pepsin within the EWG appeared to be not only modulated by the initial gel microstructure, but also by environmental conditions such as pH of the EWG.

In this research, a novel methodology based on time-lapse confocal microscopy was developed to monitor the spatiotemporal microstructural changes of EWGs due to the diffusion of gastric juice (Chapter 7). TRITC-dextran (4.4 kDa), chosen as a model fluorescent molecule of nutrients (i.e. peptide-like size), was incorporated into the EWGs. Microscopic observations showed that the loosest network of pH 5 EWG disintegrated more quickly and to a greater extent, leading to a higher rate of TRITC-dextran release than the most tightened network of pH 9 EWG. Moreover, experiments with SGF without pepsin showed that the acid and moisture in gastric juice do not affect the release of TRITC-dextran from the egg white protein structure, especially in the pH 9 EWG. Pepsin activity is highly dependent on local pH therefore, the high buffering capacity of EWGs may also affect the disintegration rate that was slower in the pH 9 EWG. In both gels, spatial degradation was mainly observed at the gel surface, while the interior gel microstructure remained unchanged. Thus, surface erosion is possibly the underlying mechanism of EWG disintegration by pepsin in these experimental conditions.

All these microstructural changes that occur in foods during biochemical digestion within the gastric environment may lead to substantial softening of the food matrix. Characterisation of the softening kinetics of solid foods during gastric digestion is crucial in formulating food that delivers desirable nutrient bioavailability. Thus, this thesis (chapter 5 and 8) investigated the relationship that exists between the initial structural properties of sweet potatoes and EWGs and their subsequent softening kinetics during gastric digestion. The pH 9 EWG, with highest initial hardness (4.83 N) had the longest softening half-time (458 min), indicating the slowest softening, whereas the pH 5 EWG (Initial hardness: 2.39 N) had shortest softening half-time (197 min), indicating the quickest softening. It is interesting to note that steamed and fried sweet potatoes had similar initial hardness (4.61 N compared with 4.83 N), but the softening half-time varied from SSP = 381 min to FSP = 218 min. The microstructural observations suggested that the rate of softening during *in vitro* gastric digestion was also related to the initial microstructure of the food. Products with a porous and heterogeneous

microstructure were easily softened during gastric digestion, such as the FSP and pH 5 EWG. In contrast, those foods that had a more compact and homogeneous microstructure, such as SSP and pH 9 EWG, were less easily broken down and had slower rates of softening.

The influence of gastric juice on the breakdown mechanics of the food matrix was determined by exposing the food samples that had been soaked in simulated gastric juice to the mechanical forces generated by the HGS. An attempt was made to evaluate the contribution that surface erosion and particle fragmentation had on the subsequent breakdown of the food particles during exposure to the mechanical forces generated by the HGS. The mixed weibull model provided a reasonable description for the disintegration performance of the tested foods. The weight of fine particles (α) showed that regardless of gastric juice diffusion, the pH 5 EWG ($\alpha = 0.22 \pm 0.03$) disintegrated into finer particles followed by FSP ($\alpha = 0.15 \pm 0.01$), SSP ($\alpha = 0.11 \pm 0.02$) and pH 9 EWG ($\alpha = 0.07 \pm 0.02$). As expected, the diffusion of gastric juice enhanced the abrasion of the solid food particles into fine particles during gastric digestion. In particular, pH 5 EWG and FSP exhibited considerably more breakdown as the weight of fine particles significantly increased over time ($p<0.05$). Finally, findings of this study also highlighted that, FSP matrix underwent quickest softening and collapsing during *in vitro* gastric digestion compared to the compact and denser structure of SSP. This may lead to the faster cell wall breakdown and subsequent β-carotene release from FSP cellular matrix than SSP in the presence of the mechanical forces of the human stomach.

In conclusion, food matrix structure and composition play a pivotal role in the different stages of gastric digestion, including gastric juice in terms of moisture, acid and pepsin diffusion, biochemical and mechanical disintegration (Figures 9.2 and 9.3). However, other factors in the gastric environment, such as local pH changes within the interface of food and gastric fluid, may also play a significant role in the overall gastric digestion process. This study has provided a more complete understanding of the mechanisms of solid food breakdown and demonstrated a relationship between food material properties and solid food disintegration during gastric digestion. Such knowledge will be useful for food scientists and nutritionists to consider when developing new generation of foods with improved health and wellness and to validate health claims for functional foods. This research also offers a platform for further research into the development of mathematical and theoretical modelling of solid food disintegration in the stomach.

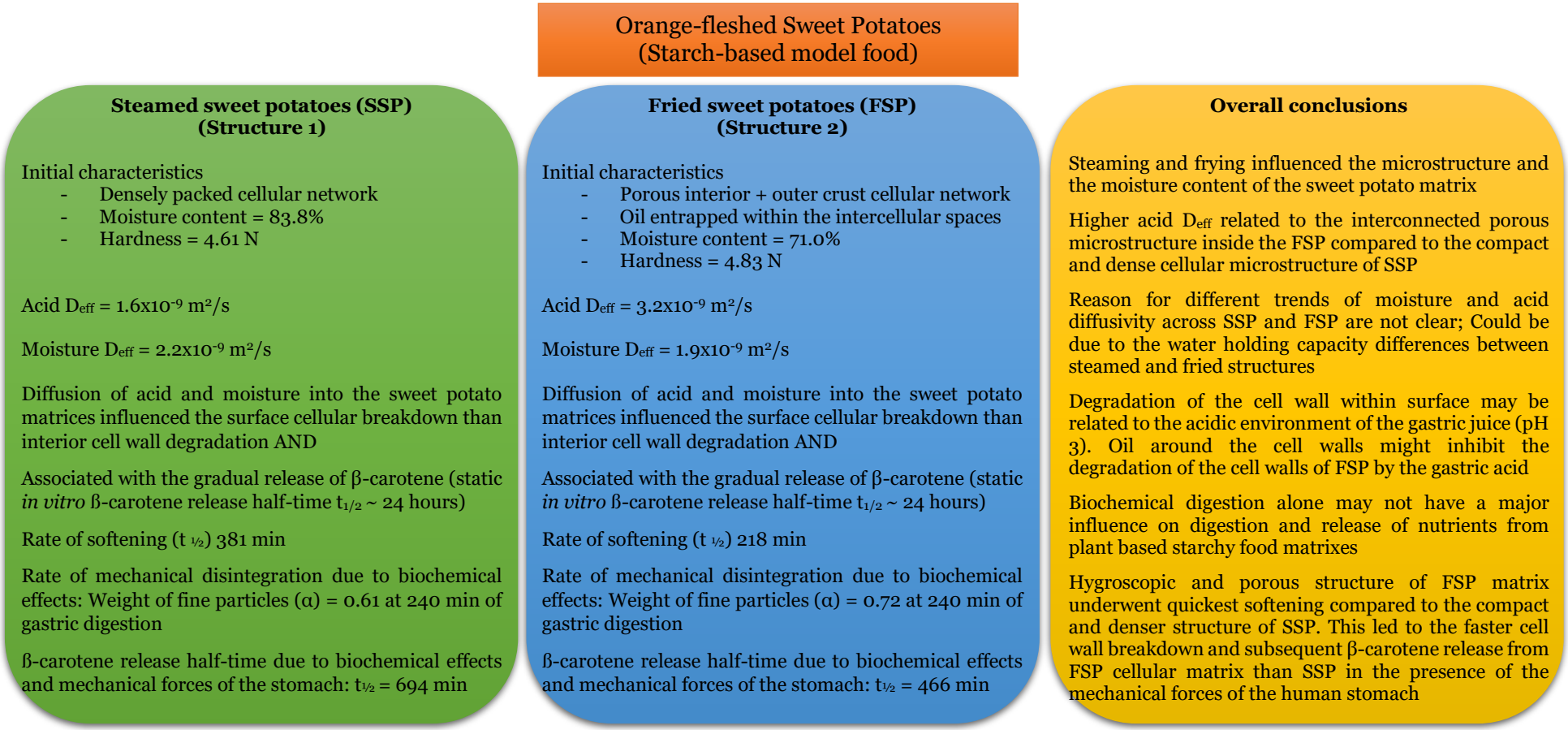

Figure 9.2: Summary of role of starch-based model food structures on the mechanisms of solid food disintegration during *in vitro* gastric digestion

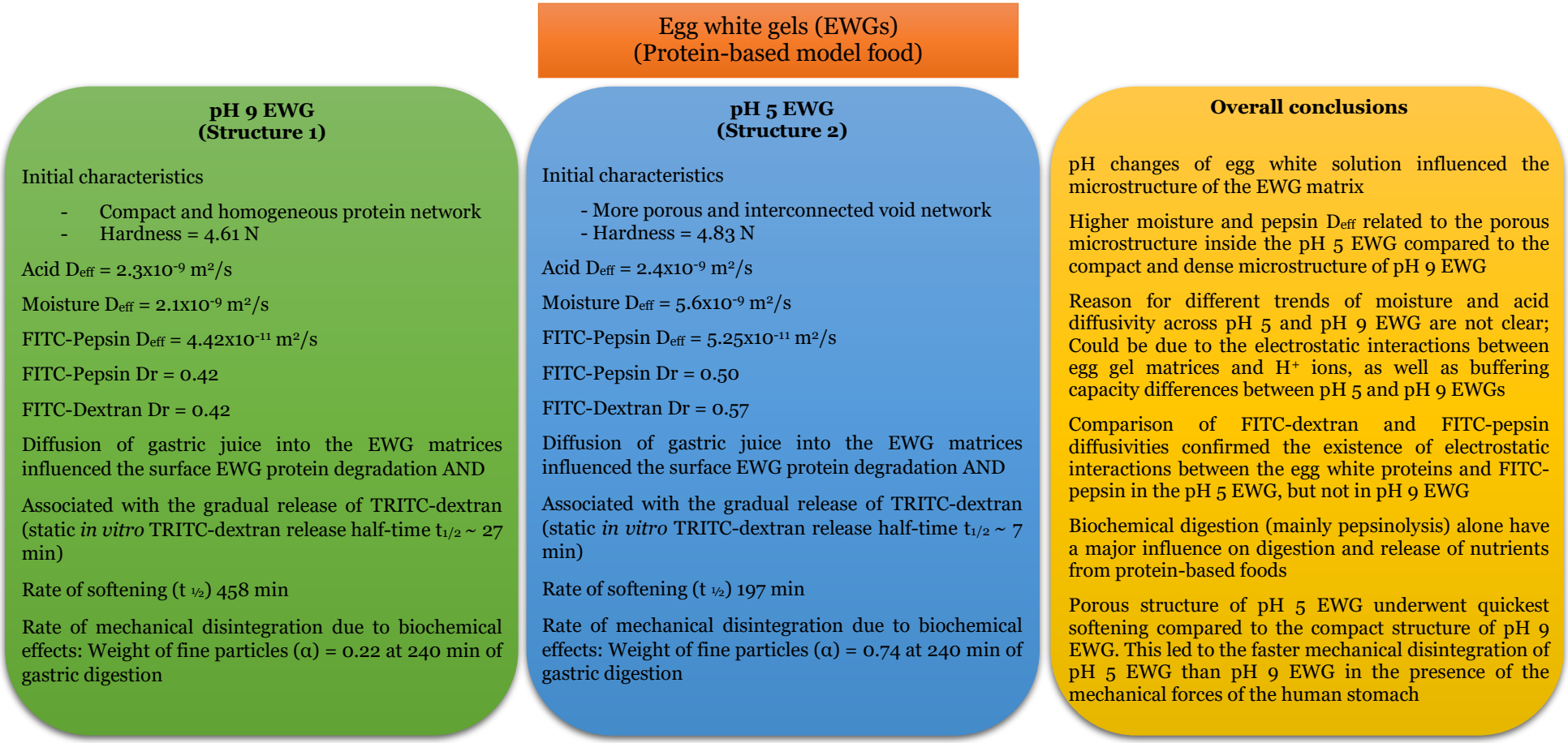

Figure 9.3: Summary of role of protein-based model food structures on the mechanisms of solid food disintegration during *in vitro* gastric digestion

9.2 Future Recommendations

The following important areas need to be considered in future studies to further strengthen the knowledge of how different food material properties influence the biochemical and mechanical degradation and subsequent nutrient release of foods during digestion; underpinning knowledge critical for the development of innovative foods with enhanced functionalities.

- *Quantification of the microstructural parameters of cooked sweet potatoes and their changes as a result of digestion*

In this thesis, CLSM based systematic methodology was developed to visualise and quantify the morphological features (i.e. porosity, tortuosity and area fractions) of the microstructures of pH 5 and pH 9 EWGs and their changes as a result of digestion. Several microscopic techniques, including CLSM, SEM, LM and TEM were used to qualitatively observe SSP and FSP microstructures and their changes as a result of digestion. However, this research was unable to develop a systematic study to provide a quantitative description of the microstructure of the cooked sweet potatoes and their impact on the gastric digestion. This was due to the inaccessibility and/or lack of appropriate techniques for undisturbed visualisation and quantification of dense and complex microstructures of sweet potatoes at an appropriate high resolution. However, these microstructural properties are very important in modelling mass transfer during gastric digestion process (Mennah-Govela & Bornhorst, 2016b).

The application of X-ray micro-computed tomography on fried potato has shown that this technique has the potential to provide more reliable microstructural information with higher resolution (Alam & Takhar, 2016). Several investigations have been successfully carried out, in particularly to identify the effect of frying conditions on porosity, pore size distribution, pore shape, and pore interconnectivity of deep-fat fried foods (Adedeji & Ngadi, 2011; Alam & Takhar, 2016). Thus, an investigation of the feasibility of using X-ray micro-computed tomography technique to quantitatively characterise the cooked sweet potato microstructural characteristics (i.e. porosity, pore volume, pore size distribution) and their changes due to diffusion of gastric juice merits future investigation.

- *Mapping the spatiotemporal distribution of pH in food structures during gastric juice diffusion using HSI*

Findings of this thesis have highlighted that the diffusion of pepsin within the EWG appeared to be modulated not only by the initial gel microstructure, but also by environmental conditions such as pH, likely because of the impact on electrostatic interactions between pepsin and the egg white proteins. Moreover, pepsin activity is

highly dependent on local pH and the high buffering capacity of foods may therefore also affect the disintegration rate during gastric digestion. Thus, to better elucidate the spatiotemporal pH changes within the food structure due to the diffusion of the gastric fluid observed in gastric environment, the proposed HSI technique (Chapter 3 and 6) could be improved in the future.

- *Investigation of factors that influence the different spatiotemporal distribution pattern of acid and moisture within food matrices during gastric digestion*

From the gastric acid and moisture mapping results, the spatiotemporal distribution pattern of gastric acid does not follow a similar trend during simulated gastric digestion of cooked sweet potatoes when compared to that of EWGs. Although the reason for the different acid and moisture distribution patterns is not clear, it is hypothesized that these differences are due to molecular interactions and water holding capacity in the different food matrices. Thus, elucidation of the specific microstructural and physical properties of the foods that control diffusion of gastric acid and moisture into differing food matrices is an area that merits future investigation.

- *Modelling the temporal changes of the effective acid, moisture and pepsin diffusivity in solid food matrix during in vitro gastric digestion*

The reported findings of this thesis highlighted that initial food structure has a pronounced effect on the overall rate of acid, moisture and pepsin diffusion due to the variation of initial microstructural properties of cooked sweet potatoes and EWGs. During the diffusion of gastric juice, pepsin hydrolyses the protein matrix of EWGs (Chapter 7) whereas hydrochloric acid reduces the intracellular adhesion of the plant cell wall and may induce structural breakdown and pore path increments in the sweet potatoes matrix (Chapter 4). These phenomena are consequently reducing the ability of food structure to hinder the gastric juice diffusion. Thus, the D_{eff} of acid, moisture and pepsin into foods may increase with digestion time due to structural changes induced by biochemical digestion within the gastric environment (Widjaja, 2010). However, temporal changes of the D_{eff} of acid, moisture and pepsin in food in the literature are very rare.

In this study, the spatiotemporal distribution of the acid and moisture concentration within the food structure during the gastric digestion was investigated using HSI technique. For future studies, it is important to incorporate a mathematical modelling approach to quantify the temporal changes of the D_{eff} of acid and moisture within the food structures. The temporal changes of the diffusivity of pepsin within

protein-based model foods due to pepsinolysis occurring in the stomach is another area for future studies.

- *Investigation of the mechanism of pepsin action during gastric digestion of EWG matrices*

Chapter 7 of this thesis proposed a novel methodology based on time-lapse confocal microscopy that enabled the study in real-time, and with a high resolution, of the spatiotemporal degradation behaviour of food protein hydrogels during the *in vitro* digestion process. However, improvement of the proposed methodology is still required to monitor the mechanism of pepsin diffusion and its action within the digestion system during simulated gastric digestion. For example, dual labelling of the hydrogel protein and enzyme could enable a better understanding of the mechanism of enzyme action during digestion of food matrices.

- *Investigation of nutrient release from EWGs due to the gastric juice diffusion and subsequent mechanical disintegration*

In this thesis, β-carotene in sweet potatoes was used as a target nutrient and its release due to diffusion of gastric juice and subsequent mechanical disintegration was studied. Likewise, TRITC-dextran (4.4 kDa) was incorporated into the EWG matrix and it was used as a model fluorescent molecule of a nutrient (i.e. peptide-like size) to study its release during the biochemical process of *in vitro* gastric digestion. However, this research was unable to develop a systematic study to provide a quantitative description of the release of TRITC-dextran (4.4 kDa) from EWGs due to diffusion of gastric juice and subsequent mechanical disintegration by the HGS; an investigation in this area merits future investigation. Moreover, the investigation of the impact of EWG structure on the extent of digestion and nature of peptides released is essential since the efficiency of EWG digestion is directly linked to the protein bioaccessibility and bioavailability. Thus, further studies are needed to improve the proposed methodologies in this research to investigate the differences in the profile of peptides released from the EWG matrixes due to diffusion of gastric juice and subsequent mechanical disintegration during gastric digestion.

- *Application of the developed in vitro methodologies to evaluate the gastric digestion behaviour of a wider variety of food products*

This thesis successfully applied methodologies to monitor the spatiotemporal acid and moisture distribution within the food matrix and to monitor the pepsin diffusivity and real-time spatiotemporal degradation profile of food protein hydrogels during the *in*

vitro digestion process. After *in vitro* gastric digestion, soaked food particles were exposed to the dynamic HGS model, to identify the role of gastric juice and stomach forces have on the breakdown behaviour of different solid food matrices during gastric digestion. These results demonstrated the effect that food composition and structure have on the overall breakdown mechanism and nutrient release during digestion. However, natural food structures are highly complex and heterogeneous, and thus it is necessary to further expand the methods applied here to a wider variety of food products, including fruits, vegetables, cereals, meats, cheeses, and other manufactured food products.

- *Investigation of in vivo gastric digestion behaviour of food matrices and the establishment of valid in vitro and in vivo correlation*

The *in vitro* studies described here, demonstrated that egg white proteins formed a compact and microstructurally homogeneous gel at pH 9, which was associated with a lower rate of pepsin diffusion and subsequent slower rate of softening as well as mechanical disintegration when compared to the relatively spatially heterogeneous loose protein matrix of the pH 5 EWG, which correlate well with the previous *in vivo* study (Nau *et al.,* 2019). In this study, different *in vitro* gastric digestion models (i.e. static *in vitro* digestion model and HGS) were also used to identify the role of gastric juice absorption and biochemical degradation on the physical breakdown mechanism of steamed and fried sweet potatoes. Results of the present study indicate that, in the presence of mechanical forces generated by the HGS, biochemical digestion had a greater effect on the breakdown of cell walls and the release of ß-carotene in FSP compared to SSP. However, it should be noted that we have used *in vitro* digestion models only. While these models have provided an insight into key physicochemical processes of gastric digestion, they do not take into account all the processes that contribute to β-carotene release during the entire digestion and absorption at the intestinal level. Therefore, it is important to carry out *in vivo* studies to assess the potential health and physiological consequences of β-carotene.

Finally, the establishment of valid correlations between the conclusions of this thesis and the *in vivo* behaviour of foods during digestion will be essential to, not only prove the value of the outcome of this thesis, but also to help initiate a framework with which to classify food products based on their initial material properties and their predominant disintegration behaviour during *in vitro* gastric digestion. Such knowledge will be invaluable for food scientists and nutritionists developing the rational design and fabrication of a new generation of foods with improved health and wellness and to validate the health claims of functional foods.

References

Abeyrathne, E., Lee, H., & Ahn, D. (2013). Egg white proteins and their potential use in food processing or as nutraceutical and pharmaceutical agents—A review. *Poultry Science, 92*(12), 3292-3299.

Adedeji, A. A., & Ngadi, M. O. (2011). Microstructural characterization of deep-fat fried breaded chicken nuggets using x-ray micro-computed tomography. *Journal of Food Process Engineering*, *34*(6), 2205-2219.

Akimov, M., & Bezuglov, V. (2012). Methods of protein digestive stability assay-state of the art. In *New Advances in the Basic and Clinical Gastroenterology*: InTech.

Alam, T., & Takhar, P. S. (2016). Microstructural Characterization of Fried Potato Disks Using X-Ray Micro Computed Tomography. *Journal of Food Science, 81*(3), E651-E664.

Allen, A., & Flemström, G. (2005). Gastroduodenal mucus bicarbonate barrier. protection against acid and pepsin. *American Journal of Physiology-Cell Physiology*. *288*(1), C1-C19.

Allen, A., & Garner, A. (1980). Mucus and bicarbonate secretion in the stomach and their possible role in mucosal protection. *Gut, 21*(3), 249.

Association of Official Analytical Chemists (AOAC) (2005). Official methods of analysis of AOAC International. Rockville, MD, USA.

Barbé, F., Menard, O., Le Gouar, Y., Buffiere, C., Famelart, M. H., Laroche, B., Feunteun, S. L., Remond, D., & Dupont, D. (2014). Acid and rennet gels exhibit strong differences in the kinetics of milk protein digestion and amino acid bioavailability. *Food Chemistry, 143*, 1-8.

Barbé, F., Ménard, O., Le Gouar, Y., Buffière, C., Famelart, M.-H., Laroche, B., Le Feunteun, S., Dupont, D., & Rémond, D. (2013). The heat treatment and the gelation are strong determinants of the kinetics of milk proteins digestion and of the peripheral availability of amino acids. *Food Chemistry, 136*(3), 1203-1212.

Bengtsson, A., Brackmann, C., Enejder, A., Alminger, M. L., & Svanberg, U. (2010). Effects of thermal processing on the *in vitro* bioaccessibility and microstructure of β-carotene in orange-fleshed sweet potato. *Journal of Agricultural and Food Chemistry, 58*(20), 11090-11096.

Biswas, A., Sahoo, J., & Chatli, M. (2011). A simple UV-Vis spectrophotometric method for determination of β-carotene content in raw carrot, sweet potato and supplemented chicken meat nuggets. *LWT-Food Science and Technology, 44*(8), 1809-1813.

Bohn, T., Carriere, F., Day, L., Deglaire, A., Egger, L., Freitas, D., Golding, M., Le Feunteun, S., Macierzanka, A., Menard, O., Miralles, B., Moscovici, A., Portmann,

R., Recio, I., Remond, D., Sante-Lhoutelier, V., Wooster, T. J., Lesmes, U., Mackie, A. R., & Dupont, D. (2018). Correlation between *in vitro* and *in vivo* data on food digestion. What can we predict with static *in vitro* digestion models? *Critical Reviews in Food Science and Nutrition, 58*(13), 2239-2261.

Bordoloi, A., Kaur, L., & Singh, J. (2012a). Parenchyma cell microstructure and textural characteristics of raw and cooked potatoes. *Food Chemistry, 133*(4), 1092-1100.

Bordoloi, A., Singh, J., & Kaur, L. (2012b). *In vitro* digestibility of starch in cooked potatoes as affected by guar gum. Microstructural and rheological characteristics. *Food Chemistry, 133*(4), 1206-1213.

Bornhorst, G. M., & Singh, R. P. (2014). Gastric digestion *in vivo* and *in vitro*: how the structural aspects of food influence the digestion process. *Annual Review of Food Science and Technology, 5*, 111-132.

Bornhorst, G. M., & Singh, R. P. (2012). Bolus formation and disintegration during digestion of food starchs. *Comprehensive Reviews in Food Science and Food Safety, 11*(2), 101-118.

Bornhorst, G. M., Ferrua, M. J., & Singh, R. P. (2015). A proposed food breakdown classification system to predict food behavior during gastric digestion. *Journal of Food Science, 80*(5), R924-R934.

Bornhorst, G. M., Gouseti, O., Wickham, M. S., & Bakalis, S. (2016). Engineering digestion: Multiscale processes of food digestion. *Journal of Food Science, 81*(3). R534-R543.

Bornhorst, G. M., Kostlan, K., & Singh, R. P. (2013). Particle size distribution of brown and white rice during gastric digestion measured by image analysis. *Journal of Food Science, 78*(9), E1383-E1391.

Bornhorst, G. M., Roman, M. J., Dreschler, K. C., & Singh, R. P. (2014). Physical property changes in raw and roasted almonds during gastric digestion *in vivo* and *in vitro*. *Food Biophysics, 9*(1), 39-48.

Bornhorst, G. M. (2017). Gastric Mixing During Food Digestion: Mechanisms and Applications. *Annual Review of Food Science and Technology, 8*, 523-542.

Bornhorst, G. M., Singh, R., & Heldman, D. (2011). Rate kinetics of bread bolus disintegration during *in vitro* digestion. Paper presented at the *International Congress of Engineering and Food*.

Braga, J., Desterro, J. M. P., & Carmo-Fonseca, M. (2004). Intracellular macromolecular mobility measured by fluorescence recovery after photobleaching with confocal laser scanning microscopes. *Molecular Biology of the Cell*, *15*(10), 4749–4760.

Campos, L. A., & Sancho, J. (2003). The active site of pepsin is formed in the intermediate conformation dominant at mildly acidic pH. *FEBS Letters, 538*(1-3), 89-95.

Caporaso, N., Whitworth, M. B., Grebby, S., & Fisk, I. D. (2018). Non-destructive analysis of sucrose, caffeine and trigonelline on single green coffee beans by hyperspectral imaging. *Food Research International, 106,* 193-203.

Capuano, E. (2017). The behavior of dietary fiber in the gastrointestinal tract determines its physiological effect. *Critical Reviews in Food Science and Nutrition, 57*(16), 3543-3564.

Carbinatto, F. M., de Castro, A. D., Evangelista, R. C., & Cury, B. S. (2014). Insights into the swelling process and drug release mechanisms from cross-linked pectin/high amylose starch matrices. *Asian Journal of Pharmaceutical Sciences, 9*(1), 27-34.

Castell, D. O., Murray, J., Tutuian, R., Orlando, R., & Arnold, R. (2004). The pathophysiology of gastro-oesophageal reflux disease – Oesophageal manifestations. *Alimentary Pharmacology & Therapeutics, 20*, 14-25.

Chen, J. (2009). Food oral processing—A review. *Food Hydrocolloids, 23*(1), 1-25.

Chen, J. (2015). Food oral processing: Mechanisms and implications of food oral destruction. *Trends in Food Science & Technology, 45*(2), 222-228.

Chen, J., Gaikwad, V., Holmes, M., Murray, B., Povey, M., Wang, Y., & Zhang, Y. (2011). Development of a simple model device for *in vitro* gastric digestion investigation. *Food Function, 2*(3-4), 174-182.

Chen, L., Remondetto, G. E., & Subirade, M. (2006). Food protein-based materials as nutraceutical delivery systems. *Trends in Food Science & Technology, 17*(5), 272-283.

Clark, A., Kavanagh, G., & Ross-Murphy, S. (2001). Globular protein gelation—Theory and experiment. *Food Hydrocolloids, 15*(4-6), 383-400.

Costa, P., & Lobo, J. M. S. (2001). Modeling and comparison of dissolution profiles. *European Journal of Pharmaceutical Sciences, 13*(2), 123-133.

Crank, J. (1979). *The mathematics of diffusion*. Oxford university press.

Dekkers, B. L., Kolodziejczyk, E., Acquistapace, S., Engmann, J., & Wooster, T. J. (2016). Impact of gastric pH profiles on the proteolytic digestion of mixed betalg-Xanthan biopolymer gels. *Food Function, 7*(1), 58-68.

Deshpande, A., Rhodes, C., Shah, N., & Malick, A. (1996). Controlled-release drug delivery systems for prolonged gastric residence: An overview. *Drug Development and Industrial Pharmacy, 22*(6), 531-539.

De-Wijk, R. A., Janssen, A. M., & Prinz, J. F. (2011). Oral movements and the perception of semi-solid foods. *Physiology & Behavior, 104*(3), 423-428.

Diaz, J. V., Anthon, G. E., & Barrett, D. M. (2007). Nonenzymatic degradation of citrus pectin and pectate during prolonged heating. effects of pH, temperature, and degree of methyl esterification. *Journal of Agricultural and Food Chemistry, 55*(13), 5131-5136.

Doi, E. (1993). Gels and gelling of globular proteins. *Trends in Food Science & Technology, 4*(1), 1-5.

Drakos, A., & Kiosseoglou, V. (2006). Stability of acidic egg white protein emulsions containing xanthan gum. *Journal of Agricultural and Food Chemistry, 54*(26), 10164-10169.

Drechsler, K. C., & Bornhorst, G. M. (2018). Modeling the softening of starch-based foods during simulated gastric digestion. *Journal of Food Engineering, 222*, 38-48.

Drechsler, K. C., & Ferrua, M. J. (2016). Modelling the breakdown mechanics of solid foods during gastric digestion. *Food Research International, 88*, 181-190.

Dupont, D., Alric, M., Blanquet-Diot, S., Bornhorst, G., Cueva, C., Deglaire, A., Denis, S., Ferrua, M., Havenaar, R., Lelieveld, J., Mackie, A. R., Marzorati, M., Menard, O., Minekus, M., Miralles, B., Recio, I., & Van den Abbeele, P. (2018). Can dynamic *in vitro* digestion systems mimic the physiological reality? *Critical Reviews in Food Science*, 1-17.

ElMasry, G., Kamruzzaman, M., Sun, D.W., & Allen, P. (2012). Principles and applications of hyperspectral imaging in quality evaluation of agro-food products: A review. *Critical Reviews in Food Science and Nutrition, 52*(11), 999-1023.

ElMasry, G., Wang, N., ElSayed, A., & Ngadi, M. (2007). Hyperspectral imaging for nondestructive determination of some quality attributes for strawberry. *Journal of Food Engineering, 81*(1), 98-107.

Farinu, A., & Baik, O. D. (2007). Heat transfer coefficients during deep fat frying of sweetpotato: Effects of product size and oil temperature. *Food Research International, 40*(8), 989-994.

Ferrua, M. J., & Singh, R. P. (2015). Human Gastric Simulator (Riddet Model): *The Impact of Food Bioactives on Health* (pp. 61-71). Springer, Cham.

Ferrua, M. J., & Singh, R. P. (2010). Modeling the fluid dynamics in a human stomach to gain insight of food digestion. *Journal of Food Science, 75*(7), R151-R162.

Ferrua, M. J., Kong, F., & Singh, R. P. (2011). Computational modeling of gastric digestion and the role of food material properties. *Trends in Food Science & Technology, 22*(9), 480-491.

Flores, F. P., & Kong, F. (2017). *In vitro* release kinetics of microencapsulated materials and the effect of the food matrix. *Annual Review of Food Science and Technology, 8*, 237-259.

Floury, J., Bianchi, T., Thévenot, J., Dupont, D., Jamme, F., Lutton, E., Panouillé, M., Boué, F., & Le Feunteun, S. (2018). Exploring the breakdown of dairy protein gels during *in vitro* gastric digestion using time-lapse synchrotron deep-UV fluorescence microscopy. *Food Chemistry, 239*, 898-910.

Floury, J., Madec, M. N., Waharte, F., Jeanson, S., & Lortal, S. (2012). First assessment of diffusion coefficients in model cheese by fluorescence recovery after photobleaching (FRAP). *Food Chemistry*, *133*(2), 551–556.

Foegeding, E. A., & Davis, J. P. (2011). Food protein functionality: A comprehensive approach. *Food Hydrocolloids, 25*(8), 1853-1864.

Foegeding, E., Daubert, C., Drake, M., Essick, G., Trulsson, M., Vinyard, C., & Van de Velde, F. (2011). A comprehensive approach to understanding textural properties of semi-and soft-solid foods. *Journal of Texture Studies, 42*(2), 103-129.

Fried, M., Abramson, S., & Meyer, J. (1987). Passage of salivary amylase through the stomach in humans. *Digestive Diseases and Sciences, 32*(10), 1097-1103.

Gardner, J., Ciociola, A., Robinson, M., & McIsaac, R. (2002). Determination of the time of onset of action of ranitidine and famotidine on intra-gastric acidity. *Alimentary Pharmacology & Therapeutics, 16*(7), 1317-1326.

Garna, H., Mabon, N., Nott, K., Wathelet, B., & Paquot, M. (2006). Kinetic of the hydrolysis of pectin galacturonic acid chains and quantification by ionic chromatography. *Food Chemistry, 96*(3), 477-484.

Geisow, M. J. (1984). Fluorescein conjugates as indicators of subcellular pH. A critical evaluation. *Experimental Cell Research, 150*(1), 29-35.

Ghosal, K., Chandra, A., Rajabalaya, R., Chakraborty, S., & Nanda, A. (2012). Mathematical modeling of drug release profiles for modified hydrophobic HPMC based gels. *An International Journal of Pharmaceutical Sciences, 67*(2), 147-155.

Gonçalves, R. F., Martins, J. T., Duarte, C. M., Vicente, A. A., & Pinheiro, A. C. (2018). Advances in nutraceutical delivery systems: From formulation design for bioavailability enhancement to efficacy and safety evaluation. *Trends in Food Science & Technology*, *78*, 270-291.

Grassby, T., Picout, D. R., Mandalari, G., Faulks, R. M., Kendall, C. W., Rich, G. T., Wickham, M. S., Lapsley, K, & Ellis, P. R. (2014). Modelling of nutrient bioaccessibility in almond seeds based on the fracture properties of their cell walls. *Food Function, 5*(12), 3096-3106.

Grassi, M., & Grassi, G. (2005). Mathematical modelling and controlled drug delivery. matrix systems. *Current Drug Delivery, 2*(1), 97-116.

Gray-Stuart, E. M. (2016). Modelling food breakdown and bolus formation during mastication. A thesis presented in partial fulfilment of the requirements for the degree of Doctor of Philosophy in Bioprocess Engineering at Massey University, Palmerston North, New Zealand. Massey University.

Grover, V. P., Tognarelli, J. M., Crossey, M. M., Cox, I. J., Taylor-Robinson, S. D., & McPhail, M. J. (2015). Magnetic resonance imaging: Principles and techniques-lessons for clinicians. *Journal of Clinical and Experimental Hepatology, 5*(3), 246-255.

Grundy, M. M., Carrière, F., Mackie, A. R., Gray, D. A., Butterworth, P. J., & Ellis, P. R. (2016). The role of plant cell wall encapsulation and porosity in regulating lipolysis during the digestion of almond seeds. *Food & Function, 7*(1), 69-78.

Grundy, M. M., Wilde, P. J., Butterworth, P. J., Gray, R., & Ellis, P. R. (2015). Impact of cell wall encapsulation of almonds on *in vitro* duodenal lipolysis. *Food Chemistry, 185*, 405-412.

Guerra, A., Etienne-Mesmin, L., Livrelli, V., Denis, S., Blanquet-Diot, S., & Alric, M. (2012). Relevance and challenges in modeling human gastric and small intestinal digestion. *Trends in Biotechnology, 30*(11), 591-600.

Guo, Q., Bellissimo, N., & Rousseau, D. (2017). Role of gel structure in controlling *in vitro* intestinal lipid digestion in whey protein emulsion gels. *Food Hydrocolloids, 69*, 264-272.

Guo, Q., Ye, A., Lad, M., Dalgleish, D., & Singh, H. (2014). Effect of gel structure on the gastric digestion of whey protein emulsion gels. *Soft Matter, 10*(8), 1214-1223.

Guo, Q., Ye, A., Lad, M., Ferrua, M., Dalgleish, D., & Singh, H. (2015). Disintegration kinetics of food gels during gastric digestion and its role on gastric emptying: An *in vitro* analysis. *Food & Function, 6*(3), 756-764.

Hedren, E., Diaz, V., & Svanberg, U. (2002). Estimation of carotenoid accessibility from carrots determined by an *in vitro* digestion method. *European Journal of Clinical Nutrition, 56*(5), 425.

Hellstrom, P. M., Gryback, P., & Jacobsson, H. (2006). The physiology of gastric emptying. *Best Practice & Research Clinical Anaesthesiology, 20*(3), 397-407.

Higuchi, T. (1963). Mechanism of sustained-action medication; Theoretical analysis of rate of release of solid drugs dispersed in solid matrices. *Journal of Pharmaceutical Sciences, 52*(12), 1145-1149.

Hoebler, M. F. D., Karinthi, A., Belleville, C., & Barry, J. L. C. (2000). Particle size of solid food after human mastication and *in vitro* simulation of oral breakdown. *International Journal of Food Sciences and Nutrition, 51*(5), 353-366.

Howard, L., Wong, A., Perry, A., & Klein, B. (1999). β-Carotene and ascorbic acid retention in fresh and processed vegetables. *Journal of Food Science, 64*(5), 929-936.

Huff, J. (2015). The Airyscan detector from ZEISS: Confocal imaging with improved signal-to-noise ratio and super-resolution. *Nature Methods, 12*(12).

Hunt, R. H., Camilleri, M., Crowe, S. E., El-Omar, E. M., Fox, J. G., Kuipers, E. J., Malfertheiner, P., McColl, K. E., Pritchard, D. M., Rugge, M., Sonnenberg, A., Sugano, K., & Tack, J. (2015). The stomach in health and disease. *Gut, 64*(10), 1650-1668.

Hyslop, E. (1980). Stomach contents analysis—A review of methods and their application. *Journal of Fish Biology, 17*(4), 411-429.

Inglingstad, R. A., Devold, T. G., Eriksen, E. K., Holm, H., Jacobsen, M., Liland, K. H., Rukke, E. O., & Vegarud, G. E. (2010). Comparison of the digestion of caseins and whey proteins in equine, bovine, caprine and human milks by human gastrointestinal enzymes. *Dairy Science & Technology, 90*(5), 549-563.

Islam, S. N., Nusrat, T., Begum, P., & Ahsan, M. (2016). Carotenoids and β-carotene in orange-fleshed sweet potato: A possible solution to vitamin A deficiency. *Food Chemistry, 199*, 628-631.

Jalabert-Malbos, M. L., Mishellany-Dutour, A., Woda, A., & Peyron, M. A. (2007). Particle size distribution in the food bolus after mastication of natural foods. *Food Quality and Preference, 18*(5), 803-812.

Jenkins, D., Thorne, M. J., Wolever, T., Jenkins, A. L., Rao, A. V., & Thompson, L. U. (1987). The effect of starch-protein interaction in wheat on the glycemic response and rate of *in vitro* digestion. *The American Journal of Clinical Nutrition, 45*(5), 946-951.

Jeong, S. H., Berhane, N. H., Haghighi, K., & Park, K. (2007). Drug release properties of polymer coated ion-exchange resin complexes: Experimental and theoretical evaluation. *Journal of Pharmaceutical Sciences, 96*(3), 618-632.

Jonker, A. M., Löwik, D. W. P. M., & Van Hest, J. C. M. (2012). Peptide-and protein-based hydrogels. *Chemistry of Materials, 24*(5), 759-773.

Kamatari, Y. O., Dobson, C. M., & Konno, T. (2003). Structural dissection of alkaline-denatured pepsin. *Protein Science, 12*(4), 717-724.

Kamba, M., Seta, Y., Kusai, A., Ikeda, M., & Nishimura, K. (2000). A unique dosage form to evaluate the mechanical destructive force in the gastrointestinal tract. *International Journal of Pharmaceutics*, *208*(1-2), 61-70.

Kamruzzaman, M., Makino, Y., & Oshita, S. (2016a). Hyperspectral imaging for real-time monitoring of water holding capacity in red meat. *LWT-Food Science and Technology, 66*, 685-691.

Kamruzzaman, M., Makino, Y., & Oshita, S. (2016b). Parsimonious model development for real-time monitoring of moisture in red meat using hyperspectral imaging. *Food Chemistry, 196,* 1084-1091.

Kelly, K. A. (1980). Gastric emptying of liquids and solids: Roles of proximal and distal stomach. *The American Journal of Physiology-Gastrointestinal and Liver Physiology, 239*(2), G71-G76.

Knee, M. (1982). Fruit softening III. Requirement for Oxygen and pH effects. *Journal of Experimental Botany*, *33*(6), 1263-1269.

Kondjoyan, A., Daudin, J. D., & Santé-Lhoutellier, V. (2015). Modelling of pepsin digestibility of myofibrillar proteins and of variations due to heating. *Food Chemistry, 172*, 265-271.

Kong, F., & Singh, R. P. (2008a). Disintegration of solid foods in human stomach. *Journal of Food Science, 73*(5), R67-R80.

Kong, F., & Singh, R. P. (2008b). A model stomach system to investigate disintegration kinetics of solid foods during gastric digestion. *Journal of Food Science, 73*(5), E202-E210.

Kong, F., & Singh, R. P. (2009a). Digestion of raw and roasted almonds in simulated gastric environment. *Food Biophysics, 4*(4), 365-377.

Kong, F., & Singh, R. P. (2009b). Modes of disintegration of solid foods in simulated gastric environment. *Food Biophysics, 4*(3), 180-190.

Kong, F., & Singh, R. P. (2010). A human gastric simulator (HGS) to study food digestion in human stomach. *Journal of Food Science, 75*(9), E627-E635.

Kong, F., & Singh, R. P. (2011). Solid loss of carrots during simulated gastric digestion. *Food Biophysics, 6*(1), 84-93.

Kong, F., Oztop, M. H., Singh, R. P., & McCarthy, M. J. (2013). Effect of boiling, roasting and frying on disintegration of peanuts in simulated gastric environment. *LWT - Food Science and Technology, 50*(1), 32-38.

Kong, F., Oztop, M. H., Singh, R. P., & McCarthy, M. J. (2011). Physical changes in white and brown rice during simulated gastric digestion. *Journal of Food Science, 76*(6), E450-E457.

Korobchevskaya, K., Lagerholm, B. C., Colin-York, H., & Fritzsche, M. (2017). Exploring the potential of airyscan microscopy for live cell imaging. In *Photonics* (Vol. 4, pp. 41). Multidisciplinary Digital Publishing Institute.

Kosmidis, K., Argyrakis, P., & Macheras, P. (2003). A reappraisal of drug release laws using Monte Carlo simulations: The prevalence of the Weibull function. *Pharmaceutical Research, 20*(7), 988-995.

Koufman, J. A., & Johnston, N. (2012). Potential benefits of pH 8.8 alkaline drinking water as an adjunct in the treatment of reflux disease. *Annals of Otology, Rhinology, and Laryngology, 121*(7), 431-434.

Kozlov, L., Meshcheriakova, E., Zavada, L., Efremov, E., & Rashkovetskiĭ, L. (1979). Dependence of pepsin conformational states on pH and temperature. *Biokhimiia (Moscow, Russia), 44*(2), 339-349.

Kozu, H., Kobayashi, I., Nakajima, M., Uemura, K., Sato, S., & Ichikawa, S. (2010). Analysis of flow phenomena in gastric contents induced by human gastric peristalsis using CFD. *Food Biophysics, 5*(4), 330-336.

Kozu, H., Nakata, Y., Nakajima, M., Neves, M. A., Uemura, K., Sato, S., Kobayashi, I., & Ichikawa, S. (2014). Development of a human gastric digestion simulator equipped with peristalsis function for the direct observation and analysis of the food digestion process. *Journal of Food Science and Technology, 20*(2), 225-233.

Krifa, M. A. (2009). Mixed Weibull model for size reduction of particulate and fibrous materials, *Powder Technology*, *194*, 233-238.

Krall, S. M., & McFeeters, R. F. (1998). Pectin hydrolysis. effect of temperature, degree of methylation, pH, and calcium on hydrolysis rates. *Journal of Agricultural and Food Chemistry, 46*(4), 1311-1315.

Langenbucher, F. (1972). Letters to the Editor. Linearization of dissolution rate curves by the Weibull distribution. *Journal of Pharmacy and Pharmacology, 24*(12), 979-981.

Le Feunteun, S., Barbé, F., Rémond, D., Ménard, O., Le Gouar, Y., Dupont, D., & Laroche, B. (2014). Impact of the dairy matrix structure on milk protein digestion kinetics: Mechanistic modelling based on mini-pig *in vivo* data. *Food and Bioprocess Technology, 7*(4), 1099-1113.

Legland, D., Arganda-Carreras, I., & Andrey, P. (2016). MorphoLibJ: Integrated library and plugins for mathematical morphology with ImageJ. *Bioinformatics, 32*(22), 3532-3534.

Legland, D., Devaux, M. F., Bouchet, B., Guillon, F., & Lahaye, M. (2012). Cartography of cell morphology in tomato pericarp at the fruit scale. *Journal of Microscopy, 247*(1), 78-93.

Lemmens, L., Van Buggenhout, S., Van Loey, A. M., & Hendrickx, M. E. (2010). Particle size reduction leading to cell wall rupture is more important for the β-carotene bioaccessibility of raw compared to thermally processed carrots. *Journal of Agricultural and Food Chemistry, 58*(24), 12769-12776.

Lentle, R. G., & Janssen, P. W. (2011). *The physical processes of digestion*. Springer Science & Business Media.

Lin, X., Loy, J. A., Sussman, F., & Tang, J. (1993). Conformational instability of the N- and C-terminal lobes of porcine pepsin in neutral and alkaline solutions. *Protein Science, 2*(9), 1383-1390.

Lorieau, L., Halabi, A., Ligneul, A., Hazart, E., Dupont, D., & Floury, J. (2018). Impact of the dairy product structure and protein nature on the proteolysis and amino acid bioaccessiblity during *in vitro* digestion. *Food Hydrocolloids, 82*, 399-411.

Low, D. Y., D'Arcy, B., & Gidley, M. J. (2015). Mastication effects on carotenoid bioaccessibility from mango fruit tissue. *Food Research International, 67*, 238-246.

Lu, P. J., Hsu, P. I., Chen, C. H., Hsiao, M., Chang, W. C., Tseng, H. H., Lin, K. H., Chuah, S.K., & Chen, H. C. (2010). Gastric juice acidity in upper gastrointestinal diseases. *World Journal of Gastroenterology, 16*(43), 5496-5501.

Luo, Q., Boom, R. M., & Janssen, A. E. (2015). Digestion of protein and protein gels in simulated gastric environment. *LWT-Food Science and Technology, 63*(1), 161-168.

Luo, Q., Borst, J. W., Westphal, A. H., Boom, R. M., & Janssen, A. E. (2017). Pepsin diffusivity in whey protein gels and its effect on gastric digestion. *Food Hydrocolloids, 66*, 318-325.

Luo, Q., Chen, D., Boom, R. M., & Janssen, A. E. M. (2018). Revisiting the enzymatic kinetics of pepsin using isothermal titration calorimetry. *Food Chemistry, 268*. 94-100.

Malagelada, J. R., Go, V. L., & Summerskill, W. H. (1979). Different gastric, pancreatic, and biliary responses to solid-liquid or homogenized meals. *Digestive Diseases and Sciences, 24*(2), 101-110.

Marciani, L., Gowland, P. A., Fillery-Travis, A., Manoj, P., Wright, J., Smith, A., Young, P., Moore, R. & Spiller, R. C. (2001). Assessment of antral grinding of a model solid meal with echo-planar imaging. *The American Journal of Physiology-Gastrointestinal and Liver Physiology, 280*(5), G844-G849.

Marimuthu, P., & Schätzlein, A. G. (2013). Biological barriers. transdermal, oral, mucosal, blood brain barrier, and the blood eye barrier. In *Fundamentals of Pharmaceutical Nanoscience* (pp. 301-336). Springer.

Matsuoka, R., Takahashi, Y., Kimura, M., Masuda, Y., & Kunou, M. (2017). Heating has no effect on the net protein utilisation from egg whites in rats. *The Scientific World Journal, 2017*.

McClements, D. J., Decker, E. A., Park, Y., & Weiss, J. (2008). Designing food structure to control stability, digestion, release and absorption of lipophilic food components. *Food Biophysics, 3*(2), 219-228.

McFeeters, R. F., & Fleming, H. P. (1991). pH effect on calcium inhibition of softening of cucumber mesocarp tissue. *Journal of Food Science*, *56*(3), 730-732.

Mennah-Govela, Y. A., & Bornhorst, G. M. (2016a). Acid and moisture uptake in steamed and boiled sweet potatoes and associated structural changes during *in vitro* gastric digestion. *Food Research International, 88*, 247-255.

Mennah-Govela, Y. A., & Bornhorst, G. M. (2016b). Mass transport processes in orange-fleshed sweet potatoes leading to structural changes during *in vitro* gastric digestion. *Journal of Food Engineering, 191*, 48-57.

Mennah-Govela, Y. A., Bornhorst, G. M., & Singh, R. P. (2015). Acid diffusion into rice boluses is influenced by rice type, variety, and presence of alpha-amylase. *Journal of Food Science, 80*(2). E316-E325.

Minekus, M. (2015). The TNO Gastro-Intestinal Model (TIM). In K. Verhoeckx, P. Cotter, I. López-Expósito, C. Kleiveland, T. Lea, A. Mackie, T. Requena, D. Swiatecka and H. Wichers (Eds.), *The Impact of Food Bioactives on Health. in vitro and ex vivo models*, (pp. 37-46). Cham. Springer International Publishing.

Minekus, M., Alminger, M., Alvito, P., Ballance, S., Bohn, T., Bourlieu, C., Carriere, F., Boutrou, R., Corredig, M., Dupont, D., Dufour, C., Egger, L., Golding, M., Karakaya, S.; Kirkhus, B., Le Feunteun, S., Lesmes, U., Macierzanka, A., Mackie, A., Marze, S., McClements, D. J., Menard, O., Recio, I., Santos, C. N., Singh, R. P., Vegarud, G. E., Wickham, M. S., Weitschies, W., & Brodkorb, A. (2014). A standardised static *in vitro* digestion method suitable for food–An international consensus. *Food & Function, 5*(6), 1113-1124.

Miranda, J., Anton, X., Redondo-Valbuena, C., Roca-Saavedra, P., Rodriguez, J., Lamas, A., Franco, C. M., & Cepeda, A. (2015). Egg and egg-derived foods: Effects on human health and use as functional foods. *Nutrients, 7*(1), 706-729.

Mishra, S., Hardacre, A., & Monro, J. (2012). Food structure and starch digestibility. In *Starchs-Comprehensive studies on glycobiology and glycotechnology*). IntechOpen.

Montgomery, R. K., Mulberg, A. E., & Grand, R. J. (1999). Development of the human gastrointestinal tract: Twenty years of progress. *Gastroenterology, 116*(3), 702-731.

Moore, J. G., Christian, P. E., Brown, J. A., Brophy, C., Datz, F., Taylor, A., & Alazraki, N. (1984). Influence of meal weight and caloric content on gastric emptying of meals in man. *Digestive Diseases and Sciences, 29*(6), 513-519.

Nam, K., Watanabe, J., & Ishihara, K. (2004). Modeling of swelling and drug release behavior of spontaneously forming hydrogels composed of phospholipid polymers. *International Journal of Pharmaceutics, 275*(1-2), 259-269.

Nau, F., Nyemb, K., Lechevalier, V., Floury, J., Serrière, C., Stroebinger, N., Boucher, T., Guérin-Dubiard, C., Ferrua, M. J., & Dupont, D. (2019). Spatial-temporal changes in pH, structure and rheology of the gastric chyme in pigs as influenced by egg white gel properties. *Food Chemistry*, *280*, 210-220.

Nyemb, K., Guerin-Dubiard, C., Dupont, D., Jardin, J., Rutherfurd, S. M., & Nau, F. (2014). The extent of ovalbumin *in vitro* digestion and the nature of generated peptides are modulated by the morphology of protein aggregates. *Food Chemistry, 157*, 429-438.

Nyemb, K., Guérin-Dubiard, C., Pézennec, S., Jardin, J., Briard-Bion, V., Cauty, C., Rutherfurd, S. M., Dupont, D., & Nau, F. (2016a). The structural properties of egg white gels impact the extent of *in vitro* protein digestion and the nature of peptides generated. *Food Hydrocolloids, 54*, 315-327.

Nyemb, K., Rutherfurd, M. S., Guérin, C., Dupont, D., & Nau, F. (2015). How the matrix characteristics of egg white gel influence the *in vivo* gastric digestion process. Spatio-temporal mapping. In *6th International Symposium on "Delivery of Functionality in Complex Food Systems. Physically inspired approaches from the nanoscale to the microscale"*, July 2015, Paris, France.

Nyemb, K., Causeur, D., Jardin, J., Briard-Bion, V., Guérin-Dubiard, C., Rutherfurd, S. M., Dupont, D., & Nau, F. (2016b). Investigating the impact of egg white gel structure on peptide kinetics profile during *in vitro* digestion. *Food Research International, 88*, 302-309.

Opazo-Navarrete, M., Altenburg, M. D., Boom, R. M., & Janssen, A. E. M. (2018). The effect of gel microstructure on simulated gastric digestion of protein gels. *Food Biophysics, 13*(2), 124-138.

Ozvural, E. B., & Bornhorst, G. M. (2018). Chemical and structural characteristics of frankfurters during *in vitro* gastric digestion as influenced by cooking method and severity. *Journal of Food Engineering, 229*, 102-108.

Pal, A., Brasseur, J. G., & Abrahamsson, B. (2007). A stomach road or "Magenstrasse" for gastric emptying. *Journal of Biomechanics, 40*(6), 1202-1210.

Parada, J., & Aguilera, J. (2007). Food microstructure affects the bioavailability of several nutrients. *Journal of Food Science, 72*(2), R21-R32.

Parada, J., & Santos, J. L. (2016). Interactions between starch, lipids, and proteins in foods. Microstructure control for glycemic response modulation. *Critical Reviews in Food Science and Nutrition, 56*(14), 2362-2369.

Pavelka, M. & Roth, J. (2010). Parietal Cells of Stomach. Secretion of Acid. In. *Functional Ultrastructure*. Springer, Vienna

Pedersen, A., Bardow, A., Jensen, S. B., & Nauntofte, B. (2002). Saliva and gastrointestinal functions of taste, mastication, swallowing and digestion. *Oral Diseases*, *8*(3), 117-129.

Pedreschi, F., Cocio, C., Moyano, P., & Troncoso, E. (2008). Oil distribution in potato slices during frying. *Journal of Food Engineering, 87*(2), 200-212.

Peng, H., Xiong, H., Li, J., Xie, M., Liu, Y., Bai, C., & Chen, L. (2010). Vanillin cross-linked chitosan microspheres for controlled release of resveratrol. *Food Chemistry, 121*(1), 23-28.

Peppas, N. A., & Sahlin, J. J. (1989). A simple equation for the description of solute release III. Coupling of diffusion and relaxation. *International Journal of Pharmaceutics, 57*(2), 169-172.

Pu, Y. Y., & Sun, D. W. (2015). Vis–NIR hyperspectral imaging in visualizing moisture distribution of mango slices during microwave-vacuum drying. *Food Chemistry, 188*, 271-278.

Punčochová, K., Ewing, A. V., Gajdošová, M., Sarvašová, N., Kazarian, S. G., Beránek, J., & Štěpánek, F. (2015). Identifying the mechanisms of drug release from amorphous solid dispersions using MRI and ATR-FTIR spectroscopic imaging. *International Journal of Pharmaceutics*, *483*(1-2), 256-267.

Rajkumar, P., Wang, N., EImasry, G., Raghavan, G., & Gariepy, Y. (2012). Studies on banana fruit quality and maturity stages using hyperspectral imaging. *Journal of Food Engineering, 108*(1), 194-200.

Richardson, J. C., Bowtell, R. W., Mäder, K., & Melia, C. D. (2005). Pharmaceutical applications of magnetic resonance imaging (MRI). *Advanced Drug Delivery Reviews, 57*(8), 1191-1209.

Ritger, P. L., & Peppas, N. A. (1987). A simple equation for description of solute release II. Fickian and anomalous release from swellable devices. *Journal of Controlled Release, 5*(1), 37-42.

Russo, M. A., Strounina, E., Waret, M., Nicholson, T., Truss, R., & Halley, P. J. (2007). A study of water diffusion into a high-amylose starch blend: The effect of moisture content and temperature. *Biomacromolecules, 8*(1), 296-301.

Sams, L., Paume, J., Giallo, J., & Carriere, F. (2016). Relevant pH and lipase for *in vitro* models of gastric digestion. *Food Function, 7*(1), 30-45.

Sankalia, J. M., Sankalia, M. G., & Mashru, R. C. (2008). Drug release and swelling kinetics of directly compressed glipizide sustained-release matrices: Establishment of level A IVIVC. *Journal of Controlled Release, 129*(1), 49-58.

Schindelin, J., Arganda-Carreras, I., Frise, E., Kaynig, V., Longair, M., Pietzsch, T., Preibisch, S., Rueden, C., Saalfeld, S., Schmid, B., Tinevez, J. Y., White, D. J., Hartenstein, V., Eliceiri, K., Tomancak, P. & Cardona, A. (2012). Fiji. an open-source platform for biological-image analysis. *Nat Methods, 9*(7), 676-682.

Schlamowitz, M. & Peterson, L. U. (1959). Studies on the optimum pH for the action of pepsin on "native" and denatured bovine serum albumin and bovine hemoglobin. *Journal of Biological Chemistry, 234*(12), 3137-3145.

Schulze, K. (2006). Imaging and modelling of digestion in the stomach and the duodenum. *Neurogastroenterol Motil, 18*(3), 172-183.

Schweiggert, R. M., Kopec, R. E., Villalobos-Gutierrez, M. G., Högel, J., Quesada, S., Esquivel, P., Schwartz S. J., & Carle, R. (2014). Carotenoids are more bioavailable from papaya than from tomato and carrot in humans: A randomised cross-over study. *British Journal of Nutrition, 111*(3), 490-498.

Sicard, J., Mirade, P. S., Portanguen, S., Clerjon, S., & Kondjoyan, A. (2018). Simulation of the gastric digestion of proteins of meat bolus using a reaction-diffusion model. *Food Function*, *9*, 6455–6469.

Siepmann, J., & Peppas, N. (2012). Modeling of drug release from delivery systems based on hydroxypropyl methylcellulose (HPMC). *Advanced Drug Delivery Reviews, 64*, 163-174.

Siepmann, J., Kranz, H., Bodmeier, R., & Peppas, N. (1999). HPMC-matrices for controlled drug delivery: A new model combining diffusion, swelling, and dissolution mechanisms and predicting the release kinetics. *Pharmaceutical Research, 16*(11), 1748-1756.

Silva, J. V. C., Peixoto, P. D. S., Lortal, S. & Floury, J. (2013). Transport phenomena in a model cheese. The influence of the charge and shape of solutes on diffusion. *Journal of Dairy Science*, *96*(10), 6186–6198.

Silva, J. V., Legland, D., Cauty, C., Kolotuev, I. & Floury, J. (2015a). Characterization of the microstructure of dairy systems using automated image analysis. *Food Hydrocolloids, 44*, 360-371.

Silva, J. V., Lortal, S. & Floury, J. (2015b). Diffusion behavior of dextrans in dairy systems of different microstructures. *Food Research International, 71*, 1-8.

Singh, H., & Gallier, S. (2014). Processing of food structures in the gastrointestinal tract and physiological responses. In *Food Structures, Digestion and Health* (pp. 51-81). Elsevier.

Singh, H., Ye, A., & Ferrua, M. J. (2015). Aspects of food structures in the digestive tract. *Current Opinion in Food Science, 3,* 85-93.

Sriamornsak, P., Thirawong, N., & Korkerd, K. (2007). Swelling, erosion and release behavior of alginate-based matrix tablets. *European Journal of Pharmaceutics and Biopharmaceutics, 66*(3), 435-450.

Sumnu, S. G., & Sahin, S. (2008). *Advances in deep-fat frying of foods*. CRC Press.

Thérien-Aubin, H., Baille, W. E., Zhu, X. X., & Marchessault, R. H. (2005). Imaging of high-amylose starch tablets. 3. Initial diffusion and temperature effects. *Biomacromolecules, 6*(6), 3367-3372.

Thevenot, J., Cauty, C., Legland, D., Dupont, D., & Floury, J. (2017). Pepsin diffusion in dairy gels depends on casein concentration and microstructure. *Food Chemistry, 223,* 54-61.

Thuenemann, E. C., Mandalari, G., Rich, G. T., & Faulks, R. M. (2015). Dynamic Gastric Model (DGM); In K. Verhoeckx, P. Cotter, I. López-Expósito, C. Kleiveland, T. Lea, A. Mackie, T. Requena, D. Swiatecka and H. Wichers (Eds.), *The Impact of Food Bioactives on Health: In vitro and ex vivo models*, (pp. 47-59). Cham. Springer International Publishing.

Tian, J., Chen, S., Wu, C., Chen, J., Du, X., Chen, J., Liu, D., & Ye, X. (2016). Effects of preparation methods on potato microstructure and digestibility: An *in vitro* study. *Food Chemistry, 211*, 564-569.

Tomczyńska-Mleko, M. (2015). Development of a new product. egg white albumen gels with differentiated magnesium release. *Journal of Elementology, 20*(2), 463–475.

Tomczyńska-Mleko, M., Handa, A., Wesołowska-Trojanowska, M., Terpiłowski, K., Kwiatkowski, C., & Mleko, S. (2016). New controlled release material. aerated egg white gels induced by calcium ions. *European Food Research and Technology, 242*(8), 1235-1243.

Tortora, G. J., & Derrickson, B. H. (2008). The digetsive system, In *Principles of Anatomy and Physiology*, 902-903. John Wiley and Sons.

Treuting, P. M., Dintzis, S. M., & Montine, K. S. (2017). In *Comparative Anatomy and Histology. a mouse, rat, and human atlas*. Academic Press.

Tumuhimbise, G. A., Namutebi, A., & Muyonga, J. H. (2009). Microstructure and *in vitro* beta carotene bioaccessibility of heat processed orange fleshed sweet potato. *Plant foods for human nutrition, 64*(4), 312-318.

Tydeman, E. A., Parker, M. L., Faulks, R. M., Cross, K. L., Fillery-Travis, A., Gidley, M. J., Fillery-Travis, A., & Waldron, K. W. (2010). Effect of carrot (*Daucus carota*) microstructure on carotene bioaccessibility in the upper gastrointestinal tract. 2.

In vivo digestions. *Journal of Agricultural and Food Chemistry, 58*(17), 9855-9860.

Tyn, M. T., & Gusek, T. W., (1990). Prediction of diffusion coefficients of proteins. *Biotechnology and Bioengineering, 35*(4), 327-338.

Ulleberg, E. K., Comi, I., Holm, H., Herud, E. B., Jacobsen, M. & Vegarud, G. E. (2011). Human gastrointestinal juices intended for use in *in vitro* digestion models. *Food Digestion, 2*(1-3), 52-61.

Urbain, J. L. C., Siegel, J. A., Charkes, N. D., Maurer, A. H., Malmud, L. S. & Fisher, R. S. (1989). The two-component stomach. effects of meal particle size on fundal and antral emptying. *European Journal of Nuclear Medicine and Molecular Imaging, 15*(5), 254-259.

Van Loo-Bouwman, C. A., Naber, T. H. J., Minekus, M., Van-Breemen, R. B., Hulshof, P. J. M., & Schaafsma, G. (2014). Food matrix effects on bioaccessibility of β-carotene can be measured in an *in vitro* gastrointestinal model. *Journal of Agricultural and Food Chemistry, 62*(4), 950-955.

Van Wey, A., Cookson, A., Roy, N., McNabb, W., Soboleva, T., Wieliczko, R., & Shorten, P. (2014). A mathematical model of the effect of pH and food matrix composition on fluid transport into foods. An application in gastric digestion and cheese brining. *Food Research International, 57*, 34-43.

Van Jaarsveld, P. J., Harmse, E., Nestel, P., & Rodriguez-Amaya, D. B. (2006). Retention of β-carotene in boiled, mashed orange-fleshed sweet potato. *Journal of Food Composition and Analysis*, *19*(4), 321-329.

Varshosaz, J. (2012). Dextran conjugates in drug delivery. *Expert Opinion on Drug Delivery, 9*(5), 509-523.

Von-Burkersroda, F., Schedl, L., & Göpferich, A. (2002). Why degradable polymers undergo surface erosion or bulk erosion. *Biomaterials, 23*(21), 4221-4231.

Waharte, F., Steenkeste, K., Briandet, R., & Fontaine-Aupart, M. P. (2010). Diffusion Measurements inside Biofilms by Image-Based Fluorescence Recovery after Photobleaching (FRAP) Analysis with a Commercial Confocal Laser Scanning Microscope. Applied and Environmental Microbiology, *76*(17), 5860.

Weiner, K., Graham, L., Reedy, T., Elashoff, J., & Meyer, J. (1981). Simultaneous gastric emptying of two solid foods. *Gastroenterology, 81*(2), 257-266.

Wen, S., Zhou, G., Song, S., Xu, X., Voglmeir, J., Liu, L., Zhao, F., Li, M., Li, L., & Yu, X. (2015). Discrimination of *in vitro* and *in vivo* digestion products of meat proteins from pork, beef, chicken, and fish. *Proteomics, 15*(21), 3688-3698.

Widjaja, J. M. (2010). Kinetics of gastric juice diffusion to solid food during digestion. Master of Science Thesis, University of California, Davis.

Williams, P. C., & Sobering, D. (1996). How do we do it? A brief summary of the methods we use in developing near infrared calibrations. *Near infrared spectroscopy. The Future Waves*, 185-188.

Wu, D., Shi, H., Wang, S., He, Y., Bao, Y., & Liu, K. (2012). Rapid prediction of moisture content of dehydrated prawns using online hyperspectral imaging system. *Analytica Chimica Acta, 726*, 57-66.

Wu, P., Deng, R., Wu, X., Wang, Y., Dong, Z., Dhital, S., & Chen, X. D. (2017). *In vitro* gastric digestion of cooked white and brown rice using a dynamic rat stomach model. *Food Chemistry, 237*, 1065-1072.

Yao, C. K., Gibson, P. R. & Shepherd, S. J. (2013). Design of clinical trials evaluating dietary interventions in patients with functional gastrointestinal disorders. *The American Journal of Gastroenterology, 108*(5), 748-758.

Yasnoff, D. S., & Bull, H. B. (1953). Interaction of egg albumin and pepsin. *Journal of Biological Chemistry, 200*(2), 619-628.

Yin, X, Li H, Guo Z, Wu L, Chen F, de Matas M, Shao Q, Xiao T, York P, He Y, & Zhang J. (2013). Quantification of swelling and erosion in the controlled release of a poorly water-soluble drug using synchrotron X-ray computed microtomography. *AAPS Journal*, *15*(4), 1025-1034.

Zhu, Y., Zou, X., Shen, T., Shi, J., Zhao, J., Holmes, M., & Li, G. (2016). Determination of total acid content and moisture content during solid-state fermentation processes using hyperspectral imaging. *Journal of Food Engineering, 174*, 75-84.

Zúñiga, R. N., & Troncoso, E. (2012). Improving nutrition through the design of food matrices. In *Scientific, Health and Social Aspects of the Food Industry*. IntechOpen, 295-320.

Appendix 1

Starch-based Product Model Development

Identification of the Suitable Sweet Potato (Kumara) Variety for the Further Analysis

Introduction: Sweet potatoes (*Ipomoea batatas* [L.] Lam) are an extremely important starchy dietary staples of the tropical and subtropical areas in many parts of the world and therefore have nutritional advantage for the rural and urban people of these regions. The sweet potato could be considered as an excellent source of natural health-promoting constituents, such as β-carotene and anthocyanins (Okwadi, 2015; Zulu *et al.,* 2012). The kumara or sweet potato in New Zealand is one of the Maori food plants that have been adopted as a common component of the present New Zealand daily diet (Yen, 1963). The following varieties of sweet potatoes (Table 1) were used to identify the suitable variety for the development of starch rich product model for the study. β-carotene was used as target nutrient to study its release during gastric digestion. There basic chemical composition was analysed.

Table 1: Main Types of Kumara grown in New Zealand

Variety	Main/less cultivar	Morphology and sensory characteristics
Owairaka Red (most common)	Main cultivars in commercial production	Red-purple skin/Cream flesh sometimes marbled with red
Beauregard	Main cultivars in commercial production	Orange skin and flesh the sweetest of the 3 main varieties
Toka Toka Gold	Main cultivars in commercial production	Yellow-cream skin/ Deep cream flesh sometimes marbled with orange a sweeter taste than red kumara

Source: http://www.kumara.co.nz/types-of-kumara.html

Owairaka Red Toka Toka Gold Beauregard

Figure 1: Main Types of kumara grown in New Zealand

Raw Material: Kumara sweet potatoes were purchased from a local grocery store (Pack and Save, Palmerston North, New Zealand). Same size (approximately 10 cm in diameter

and 10-15 cm in length) and weight (200–250 g) tubers were chosen for each and every experimental determination.

Chemical Analysis: Composition analysis (AOAC, 2005) of the above selected varieties was carried out. Moisture content (%) of the fresh sweet potatoes were determined by drying weighed kumara slices in an aluminium dish, in a vacuum oven, at 105 °C to constant weight. Then sweet potatoes dry matter was obtained by freeze-drying small sweet potato pieces (1×1 cm) and lyophilised and ground to pass through the sieve number 72 (British Sieve Standards). Fat content of sweet potatoes was determined using the Mojonnier method. Total nitrogen was measured by Kjeldahl method. Crude protein was calculated by multiplying the total nitrogen content by a factor of 6.25. A total starch assay kit (K-TSTA, Megazyme International Ireland Ltd., Ireland) was used to determine the total starch content of the freeze-dried sweet potato samples.

β-carotene analysis (Biswas, Sahoo, & Chatli, 2011)

Standard preparation: Standard of β-carotene Type I (95% purity, UV) was obtained from Sigma Aldrich. The standard stock solution at 1 mg/mL concentration was prepared by dissolving standard in acetone. The working standard solutions of 16, 8, 4, 2, 1 and 0.50 mg/mL were prepared. All solutions were protected against light with aluminium foil.

β-carotene extraction and analysis: For β-carotene extraction, 0.5 g of freeze-dried sweet potato sample was accurately weighed in a glass test tube. Then 5 mL of chilled acetone was added to it, and the tube was held for 15 min with occasional shaking, vortex at high speed for 10 min, and finally centrifuged at 1370 g for 10 min. Supernatant was collected into a separate test tube, and the remaining β-carotene compound was re-extracted (until it gives a white residue) with 5 mL of an acetone followed by centrifugation once again as above. Both of the supernatants were pooled together and then passed through the Whatman filter paper No. 42 into 25 mL volumetric flask. The carotenoid extract was then made up to 25 mL using acetone. The absorbance of the extract was determined at 449 nm wavelength in a UV-Vis spectrophotometer.

Results and Discussion: All the selected sweet potato varieties differed in their chemical composition content (Table 2). The results of β-carotene analytical data (Table 2) indicated that Beauregard orange-fleshed sweet potatoes had the highest levels of β-carotene than their corresponding values of nearly 10 and 14 μg/g of red and gold fleshed sweet potato samples, respectively. β-carotene content of Beauregard orange variety is approximately 34 times greater than other selected varieties. β-carotene content of up to

276.98 µg/g fresh weights and 315.71 µg/g of dry weight basis has been found in orange-fleshed sweet potatoes varieties (Tumuhimbise, Namutebi, & Muyonga, 2009).

Table 2: Chemical Composition of the Three Different Sweet Potatoes Varieties

Values are in means ± SD on dry matter basis.

Variety	Fat (% dry weight basis)	Protein (% dry weight basis)	Ash (% dry weight basis)	Starch (% dry weight basis)	Total β-carotene (µg of ß-carotene/dry matter g)
Owairaka Red	0.98±0.02	2.62±0.01	3.37±0.09	78.10±0.4	10.01 ±0.58
Beauregard Orange	1.35±0.05	4.45±0.04	2.57±0.10	65.83±0.3	345.18± 0.62
Toka Toka Gold	0.86±0.06	6.13±0.04	2.54±0.10	66.37±0.1	14.29± 0.85

Conclusions: Beauregard orange kumara was selected as a starch rich product model for future studies. β-carotene was selected as the target nutrient of study in this selected product model.

Sweet Potatoes Product Sample Preparation

Orange-fleshed sweet potatoes (Beauregard orange variety of Kumara) were purchased from a local grocery store (Pack and Save, Palmerston North, New Zealand). Same size (approximately 10 cm in diameter and 10-15 cm in length) and weight (200–250 g) tubers were chosen for each and every experimental determination. Orange-fleshed sweet potatoes were peeled with a hand-peeler.

For the gastric juice diffusion study (Chapter 3), cylindrical sweet potatoes (30 mm length x 20 mm diameter) were cut from sweet potato core (parallel to the length) using a cutting bore (20 mm diameter).

For the microstrucral analysis (Chapter 4) and mechanical breakdown study (Chapter 6), sweet potatoes were cut into strips using a DiTo-Sama® vegetable slicer dicer, followed by cutting the strips into cubes (5 mm^3) using a knife. Cubes were selected from the interior of the sweet potato; any strips containing curve surfaces were discarded.

Preliminary Studies for the Development of Steamed Sweet Potatoes Product Model

Introduction: The objective of this preliminary study was to develop a moderately soft and cooked (gelatinised starch) steamed sweet potatoes product model for the analysis of gastric digestion studies. Preliminary studies were conducted by changing different steaming time in order to identify optimum steaming conditions. Moreover, preliminary studies were conducted by changing different steaming time in order to get the similar initial moisture and microstructure of steamed sweet potato cylinders and cubes used in the study.

Sweet potato sample preparation prior to cooking: The steam sweet potatoes were prepared according to the method described by Drechsler and Ferrua, (2016) with slight modification.

Prior to steaming, water was placed at the bottom of the steam cooker and heated up to boiling during 15 min. The temperature of the generated steam reached up to 100±3 ◦C. Then, orange-fleshed sweet potato cubes (50 g) were steamed over 1500 mL of boiling water using a steamer pot (25 cm diameter) with a 1.5 mm stainless steel sieve mesh for 5 min, and then removed.

Ten cylindrical sample of sweet potatoes were steamed for 10 min according to the same method in order to get the similar initial moisture and microstructure of steamed sweet potato cubes (Table 3). Microstructural analysis was done by light microscopy. The dimension of foods was measured using an electronic digital caliper (Ampro T74615 stainless-steel digital caliper). The oven-drying method was used for determination of moisture content (% dry basis).

Preliminary studies were conducted by changing different steaming time in order to identify optimum steaming conditions (data not shown). After preliminary studies, 5 min steam cooking sweet potatoes cubes and 10 min steam cooking sweet potatoes cylinders was used as a product model for future studies, because all starch granules were gelatinised compare to raw sample (Figure 2).

Table 3: Average initial weight, dimensions and moisture of steamed sweet potatoes cubes and cylinders. Values are given as an average ± SD (n = 5)

	Initial weight (g)	Length (mm)	Diameter (mm)	Moisture (%)
SSP cylinders	6.38±0.3	30.0±1.0	20.2±0.2	83.25±1.24
SSP cubes	0.92±0.2	4.8±0.4	-	82.89±0.96

SSP: Steamed sweet potatoes

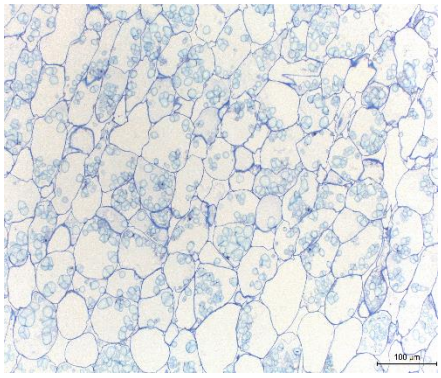

(a)

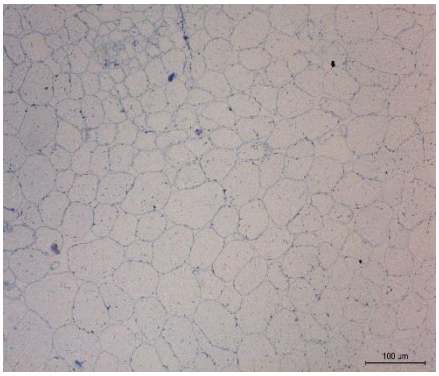

(b)

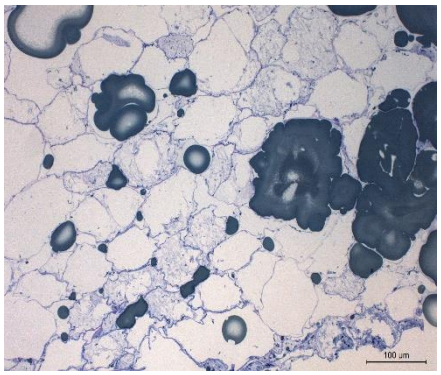

(d)

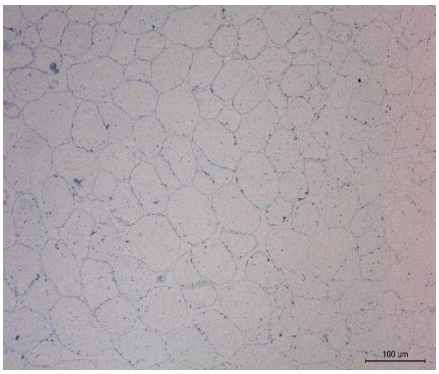

(c)

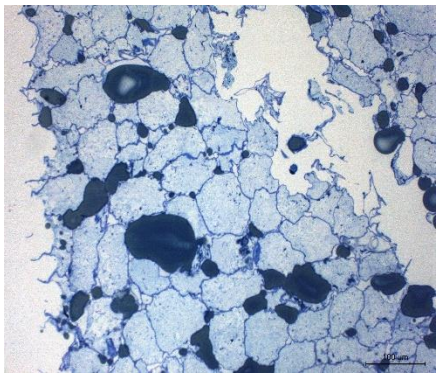

(e)

Figure 2: Light microscopy images of (d) raw, steamed sweet potatoes (b) cubes and (c) cylinders, fried sweet potatoes (d) cubes and (e) cylinders.

Preliminary Studies for the Development of Fried Sweet Potatoes Product Model

The frying method adopted in this study is a method that is typically used in the production of deep-fried potato chips (Odenigbo *et al.,* 2012; Tumuhimbise, Namutebi, & Muyonga, 2009). Initially, the canola oil was filled in a Breville Deep Fryer and pre-heated to 180±2 °C before frying.

The orange-fleshed sweet potato cubes (50 g) were placed in a wire mesh basket, which was immersed in the oil for 1.5 min, after the set temperature was reached. A thermocouple was kept inside frying container during cooking to measure the temperature profile over time to ensure similar cooking conditions for each batch. After frying, the batch of sample was taken out of the oil and allowed to drain for 5 min before blotting off the surface oil using an absorbent paper.

Ten cylindrical sample of sweet potatoes were fried for 5 min according to the same method in order to get the similar initial moisture, fat and microstructure of fried sweet potato cubes (Table 4). Microstructural analysis was done by light microscopy. The dimension of foods was measured using an electronic digital caliper (Ampro T74615 stainless-steel digital caliper). The oven-drying method was used for determination of moisture content (% dry basis). Fat content of sweet potatoes was determined using the Mojonnier method.

Preliminary studies were conducted by changing different frying time in order to identify optimum frying conditions (data not shown). After preliminary studies, 1.5 min fried sweet potatoes cubes and 5 min fried sweet potatoes cylinders was used as a product model for future studies, because all starch granules were gelatinised compare to raw sample (Figure 2).

Table 4: Average initial weight, dimensions, moisture and fat of fried sweet potatoes cubes and cylinders. Values are given as an average ± SD (n = 5)

	Initial weight (g)	Length (mm)	Diameter (mm)	Moisture (%)	Fat (%)
FSP cylinders	4.92±0.2	27.7±0.4	18.2±0.1	72.10±1.28	6.95±1.07
FSP cubes	0.65±0.8	4.3±0.7	-	71.79±1.96	7.45±0.97

FSP: Fried sweet potatoes

References

Biswas, A., Sahoo, J., & Chatli, M. (2011). A simple UV-Vis spectrophotometric method for determination of β-carotene content in raw carrot, sweet potato and supplemented chicken meat nuggets. *LWT-Food Science and Technology*, *44*(8), 1809-1813.

Drechsler, K. C., & Ferrua, M. J. (2016). Modelling the breakdown mechanics of solid foods during gastric digestion. *Food Research International*, *88*, 181-190.

Association of Official Analytical Chemists (AOAC) (2005). Official methods of analysis of AOAC International. Rockville, MD, USA.

Odenigbo, A., Rahimi, J., Ngadi, M., Wees, D., Mustafa, A., & Seguin, P. (2012). Quality changes in different cultivars of sweet potato during deep-fat frying. *Journal of Food Processing & Technology*, *3*(5), 1000156.

Okwadi, J. (2015). Introducing a pro-vitamin a rich staple crop: Analysis of decision making along the orange-fleshed sweet potato value chain in Uganda. University of Greenwich.

Tumuhimbise, G. A., Namutebi, A., & Muyonga, J. H. (2009). Microstructure and *in vitro* beta carotene bioaccessibility of heat processed orange-fleshed sweet potato. *Plant Foods for Human Nutrition*, *64*(4), 312-318.

Yen, D. E. (1963). The New Zealand Kumara or Sweet Potato. Economic Botany, *17*(1), 31-45.

Zulu, L., Adebola, P., Shegro, A., Laurie, S., & Pillay, M. (2012). Progeny Evaluation of Some Sweet Potato [*Ipomoea batatas* (L.) Lam.] Breeding Lines in South Africa. Paper presented at the II All Africa Horticulture Congress 1007.

Appendix 2

Protein-based Product Model Development

EWGs are used in this study as a model protein-based food. It is highly used in food industry as food gels mainly due to their functional and nutritional properties Nyemb *et al.,* (2016). In the present study, the egg white hydrogels were created using various pH conditions before heating in order to form two differently structured gels as follows;

Fresh eggs were purchased from a local supermarket (Pack and Save, Palmerston North, New Zealand). The total protein (N×6.25) in the egg white was determined using the Kjeldahl method.

Table 1: Protein analysis in egg white

Initial Weight (g)	HCL volume (mL)	N%	Protein %
1.6256	20.2	1.74	10.87
1.6456	20.0	1.70	10.63
1.4924	17.6	1.65	10.32
		Average	10.61
		SD	0.28

Preparation of Egg White Solution: EWGs were prepared as described previously in Nyemb *et al.,* (2016). The eggs were manually broken, and the egg whites were carefully separated from the yolks. The whole egg white solution (250 mL) was homogenized using an IKA T-18 Ultra Turrax Digital Homogenizer (10,000 rpm for 1 min). Two sub-samples of egg white solution were taken, and the pH of each sub-sample was adjusted to pH 5.0 or pH 9.0, respectively, using 2 M HCl or 2 M NaOH. Egg white solutions were then diluted with Milli-Q water to 10% protein concentration as follows;

For pH 9 EWG preparation;

Protein (%)	= 10.61%
Volume of egg white solution after adjustment of pH	= 90+0.58 = <u>90.58 mL</u>
Amount of water required to adjust the protein to 10%	= ((10*100)/10.61)-90.58 = <u>3.67 mL</u>
Final volume	= 90+0.58+3.67 mL = <u>94.25 mL</u>
Protein (%) in final volume	= (10.61/100)*94.25 = <u>10%</u>

For pH 5 EWG preparation;

Protein (%)	= 10.61%
Volume of egg white solution after adjustment of pH	= 90+3.43 = 93.43 mL
Amount of water required to adjust the protein to 10%	= ((10*100)/10.61)-93.43 = 0.82 mL
Final volume	= 90+3.43+0.82 mL = 94.25 mL
Protein (%) in final volume	= (10.61/100)*94.25 = 10%

EWG preparation: pH adjusted egg white solutions were put in sealed plastic cylindrical containers (inner diameter 20 mm) and were heated in a water bath for 60 min at 80 °C. After heating, the gels were cooled and kept at 4 °C for 20 min. Then gels were removed from the plastic casings and cut into 30 mm length using a surgical scalpel blade.

As shown in Table 2, the dimension of foods was measured using an electronic digital caliper (Ampro T74615 stainless-steel digital caliper).

Table 2: Average initial weight of the sample, diameter and length for each food structures after cooking that were used in the static *in vitro* digestion model. Values are given as an average ± SD (n = 5)

	Initial weight of the sample (g)	Length (mm)	Diameter (mm)
pH 5 EWG	9.10±0.3	29.6±0.6	20.3±0.2
pH 9 EWG	11.09±0.4	29.9±0.9	20.1±0.7

As shown in Figure 1, microstructural analysis was done by SEM according to the method described by Nyemb *et al.,* (2016). SEM images confirmed that the microstructre observed within pH 5 and pH 9 EWG is agreement with previous findings (Nyemb *et al.,* 2016).

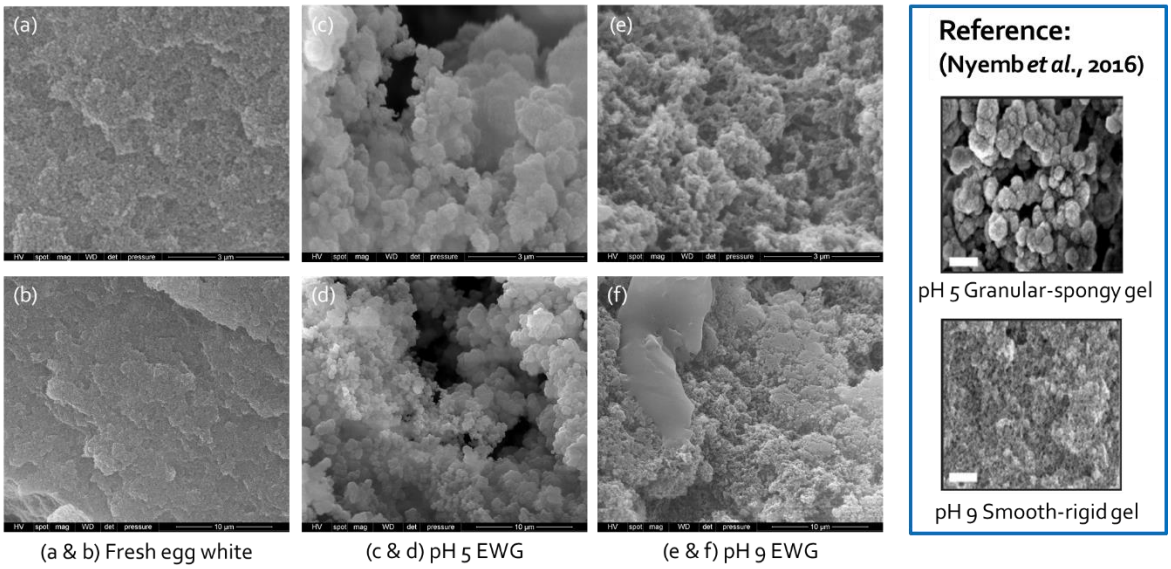

Figure 1: SEM images of pH 5 and pH 9 EWGs

References

Nyemb, K., Causeur, D., Jardin, J., Briard-Bion, V., Guérin-Dubiard, C., Rutherfurd, S. M., Dupont, D., & Nau, F. (2016). Investigating the impact of egg white gel structure on peptide kinetics profile during *in vitro* digestion. *Food Research International*, *88*, 302-309.

Appendix 3

Determination of Pepsin Activity

Pepsin activity (Spectrophotometric Stop Reaction) was measured as described in the INFOGEST harmonized digestion protocol (Minekus *et al.,* 2014).

Principle:

Haemoglobin + H2O $\xrightarrow{\text{pepsin}}$ TCA soluble tyrosine containing peptides

Substrate: haemoglobin 2% (w/v) (bovine blood haemoglobin, Sigma-Aldrich)

A stock solution of pepsin (porcine pepsin, ref P6887 Sigma-Aldrich) 1 mg/mL stock solution was dissolved in NaCl 150 mM at pH 6.5 and several dilutions (5–35 µg/mL) were prepared with HCl 10 mM just before the activity test. For the test, 500 µL of substrate solution was incubated at 37 °C for 4 min, 100 µL of enzyme solution was added and after precisely 10 min the reaction was stopped with trichloroacetic acid (TCA, 5%). The samples were centrifuged at 6000 g for 30min and the absorbance (280 nm) was measured. During the assay, a linear curve was obtained. The absorbance is a function of the pepsin concentration. For each sample, a blank was run in parallel according to the same procedure was followed but the pepsin was added after the addition of TCA, which stops the reaction. The blank absorbance was noted A_{280} Blank.

Calculation:

$$\frac{Units}{mg} = \frac{[\,A280\,Test - \,A280\,Blank] \times 1000}{(\Delta t \times X)}$$

Δt: duration of the reaction, i.e. 10 minutes

X: concentration of pepsin powder in the final reaction mixture (quartz cuvette) [mg/mL]

Table 1: Pepsin Activity of different pepsin used in this study

Thesis Chapter	Type of Pepsin	Pepsin Activity
Chapter 6	FITC-pepsin	0.0±0.00 U/mg
Chapter 3 & 6	Pepsin (>250 U/mg)	271±10 U/mg
Chapter 4, 5 & 8	Pepsin (>250 U/mg)	281±15 U/mg
Chapter 7	Pepsin (>3200–4500 U/mg)	2971±54 U/mg

Reference:

Minekus, M., *et al.,* A standardized static *in vitro* digestion method suitable for food - An international consensus. *Food Function*, *5*(6), 1113-24.

Appendix 4

Diameter changes of the Cylindrical Sweet Potatoes and EWGs during *In Vitro* Gastric Digestion; To Prove Negligible Shrinkage

Diameter changes after digestion. The diameter of food cylinders (three different sides) was measured before and after digestion (Chapter 3, section 3.3.5) for each food system using an electronic digital caliper (Ampro T74615 stainless-steel digital caliper). An ANOVA was conducted using a 2-factor factorial design to determine differences in diameter during simulated gastric digestion. The factors were food types (SSP, FSP, pH 5 EWG and pH 9 EWG), and digestion time (0–240 min). The diameter was not significantly ($p<0.05$) influenced by the food type, digestion time, and their interaction (Table 1).

Table 1: Diameter (mm) of sweet potatoes and EWGs during 240 min of *in vitro* gastric digestion. Values represent averages (n = 3) ± SD. Means within each column and raw followed by different superscript letters are significantly different ($p<0.05$)

Treatment	Digestion time (min)							
	0	10	20	40	60	120	180	240
SSP	20.6 ± 0.2^{a}	20.5 ± 0.3^{a}	20.4 ± 0.1^{a}	20.3 ± 0.4^{a}	20.4 ± 0.4^{a}	20.2 ± 0.1^{a}	20.2 ± 0.1^{a}	20.2 ± 0.2^{a}
FSP	18.3 ± 0.1^{b}	18.3 ± 0.1^{b}	18.3 ± 0.2^{b}	18.3 ± 0.2^{b}	18.1 ± 0.1^{b}	18.1 ± 0.1^{b}	18.1 ± 0.1^{b}	18.2 ± 0.1^{b}
pH 5 EWG	20.6 ± 0.1^{a}	20.5 ± 0.2^{a}	20.4 ± 0.3^{a}	20.5 ± 0.3^{a}	20.5 ± 0.1^{a}	20.2 ± 0.1^{a}	20.3 ± 0.3^{a}	20.2 ± 0.1^{a}
pH 9 EWG	20.7 ± 0.5^{a}	20.7 ± 0.5^{a}	20.5 ± 0.1^{a}	20.4 ± 0.1^{a}	20.5 ± 0.2^{a}	20.4 ± 0.1^{a}	20.4 ± 0.3^{a}	20.3 ± 0.2^{a}

SSP: Steamed sweet potatoes, FSP: Fried sweet potatoes, EWG: Egg white gel

DRC 16 Forms

DRC 16

MASSEY UNIVERSITY
GRADUATE RESEARCH SCHOOL

STATEMENT OF CONTRIBUTION
DOCTORATE WITH PUBLICATIONS/MANUSCRIPTS

We, the candidate and the candidate's Primary Supervisor, certify that all co-authors have consented to their work being included in the thesis and they have accepted the candidate's contribution as indicated below in the *Statement of Originality*.

Name of candidate:	Geeshani Maduwanthi Somaratne
Name/title of Primary Supervisor:	Dr. Jaspreet Singh
Name of Research Output and full reference:	
Somaratne, G., Ferrua, M. J., Ye, A., Nau, F., Floury, J., Dupont, D. and Singh, J. (2019). Food material properties as determining factors in nutrient release during human gastric digestion: A Review. Critical Reviews in Food Science and Nutrition, Submitted.	
In which Chapter is the Manuscript /Published work:	Chapter 2
Please indicate:	
• The percentage of the manuscript/Published Work that was contributed by the candidate:	85%
and	
• Describe the contribution that the candidate has made to the Manuscript/Published Work:	
The candidate was involved in planning, designing and wrote the first draft of the review manuscript.	
For manuscripts intended for publication please indicate target journal:	
Critical Reviews in Food Science and Nutrition	
Candidate's Signature:	Somaratne.
Date:	09/09/2019
Primary Supervisor's Signature:	
Date:	9/09/2019

(This form should appear at the end of each thesis chapter/section/appendix submitted as a manuscript/publication or collected as an appendix at the end of the thesis)

GRS Version 4- January 2019

MASSEY UNIVERSITY
GRADUATE RESEARCH SCHOOL

STATEMENT OF CONTRIBUTION
DOCTORATE WITH PUBLICATIONS/MANUSCRIPTS

We, the candidate and the candidate's Primary Supervisor, certify that all co-authors have consented to their work being included in the thesis and they have accepted the candidate's contribution as indicated below in the *Statement of Originality*.

Name of candidate:	Geeshani Maduwanthi Somaratne
Name/title of Primary Supervisor:	Dr. Jaspreet Singh
Name of Research Output and full reference:	
Somaratne, G., Reis, M. M., Ferrua, M. J., Ye, A., Nau, F., Floury, J., Dupont, D., Singh, R. P. and Singh, J. (2019). Mapping the spatiotemporal distribution of acid and moisture in food structures during gastric juice diffusion using Hyperspectral Imaging. Journal of Agricultural and Food Chemistry, Accepted.	
In which Chapter is the Manuscript /Published work:	Chapter 3 and Part of Chapter 6
Please indicate:	
• The percentage of the manuscript/Published Work that was contributed by the candidate:	85%
and	
• Describe the contribution that the candidate has made to the Manuscript/Published Work:	
The candidate was involved in planning, designing and carrying out the experiments. The candidate compiled and summarised the results for discussion with supervisors, and wrote the first draft of the manuscript. The candidate also drafted answers to the queries from reviewers during the peer-review process.	
For manuscripts intended for publication please indicate target journal:	
Journal of Agricultural and Food Chemistry	
Candidate's Signature:	Somaratne.
Date:	09/09/2019
Primary Supervisor's Signature:	
Date:	9/9/2019

(This form should appear at the end of each thesis chapter/section/appendix submitted as a manuscript/publication or collected as an appendix at the end of the thesis)

GRS Version 4- January 2019

MASSEY UNIVERSITY
GRADUATE RESEARCH SCHOOL

STATEMENT OF CONTRIBUTION
DOCTORATE WITH PUBLICATIONS/MANUSCRIPTS

We, the candidate and the candidate's Primary Supervisor, certify that all co-authors have consented to their work being included in the thesis and they have accepted the candidate's contribution as indicated below in the *Statement of Originality*.

Name of candidate:	Geeshani Maduwanthi Somaratne
Name/title of Primary Supervisor:	Dr. Jaspreet Singh
Name of Research Output and full reference: Somaratne, G., Ferrua, M. J., Ye, A., Nau, Dupont, D., Singh, R. P. and Singh, J. (2019). Role of biochemical and mechanical disintegration on β-carotene release from steamed and fried sweet potatoes during *in vitro* gastric digestion. *Food Research*	
In which Chapter is the Manuscript /Published work:	Chapter 4 & 5
Please indicate:	
• The percentage of the manuscript/Published Work that was contributed by the candidate:	85%
and	
• Describe the contribution that the candidate has made to the Manuscript/Published Work:	
The candidate was involved in planning, designing and carrying out the experiments. The candidate compiled and summarised the results for discussion with supervisors. The candidate is writing the first draft of the manuscript for publication purpose.	
For manuscripts intended for publication please indicate target journal:	
Food Research International	
Candidate's Signature:	Somaratne
Date:	09/09/2019.
Primary Supervisor's Signature:	
Date:	9/9/2019.

(This form should appear at the end of each thesis chapter/section/appendix submitted as a manuscript/publication or collected as an appendix at the end of the thesis)

GRS Version 4- January 2019

MASSEY UNIVERSITY
GRADUATE RESEARCH SCHOOL

STATEMENT OF CONTRIBUTION
DOCTORATE WITH PUBLICATIONS/MANUSCRIPTS

We, the candidate and the candidate's Primary Supervisor, certify that all co-authors have consented to their work being included in the thesis and they have accepted the candidate's contribution as indicated below in the *Statement of Originality*.

Name of candidate:	Geeshani Maduwanthi Somaratne
Name/title of Primary Supervisor:	Dr. Jaspreet Singh
Name of Research Output and full reference:	
Somaratne, G., Nau, F., Ferrua, M. J., Singh, J., Ye, A., Dupont, D., Singh, R. P. and Floury, J. (2019). Characterization of egg white gel microstructure and its relationship with pepsin diffusivity. Food Hydrocolloids, Accepted.	
In which Chapter is the Manuscript /Published work:	Part of Chapter 6
Please indicate:	
• The percentage of the manuscript/Published Work that was contributed by the candidate:	85%
and	
• Describe the contribution that the candidate has made to the Manuscript/Published Work:	
The candidate was involved in planning, designing and carrying out the experiments. The candidate compiled and summarised the results for discussion with supervisors, and wrote the first draft of the manuscript. The candidate also drafted answers to the queries from reviewers during the peer-review process.	
For manuscripts intended for publication please indicate target journal:	
Food Hydrocolloids	
Candidate's Signature:	Somaratne
Date:	09/09/2019.
Primary Supervisor's Signature:	
Date:	9/9/19

(This form should appear at the end of each thesis chapter/section/appendix submitted as a manuscript/publication or collected as an appendix at the end of the thesis)

GRS Version 4- January 2019

MASSEY UNIVERSITY
GRADUATE RESEARCH SCHOOL

STATEMENT OF CONTRIBUTION
DOCTORATE WITH PUBLICATIONS/MANUSCRIPTS

We, the candidate and the candidate's Primary Supervisor, certify that all co-authors have consented to their work being included in the thesis and they have accepted the candidate's contribution as indicated below in the *Statement of Originality*.

Name of candidate:	Geeshani Maduwanthi Somaratne
Name/title of Primary Supervisor:	Dr. Jaspreet Singh
Name of Research Output and full reference:	
Somaratne, G., Nau, F., Ferrua, M. J., Singh, J., Ye, A., Dupont, D., Singh, R. P. and Floury, J. (2019). In situ disintegration of egg white gels by pepsin and kinetics of nutrient release followed by time-lapse confocal microscopy. Food Hydrocolloids, Accepted.	
In which Chapter is the Manuscript /Published work:	Chapter 7
Please indicate:	
• The percentage of the manuscript/Published Work that was contributed by the candidate:	85%
and	
• Describe the contribution that the candidate has made to the Manuscript/Published Work:	
The candidate was involved in planning, designing and carrying out the experiments. The candidate compiled and summarised the results for discussion with supervisors, and wrote the first draft of the manuscript. The candidate also drafted answers to the queries from reviewers during the peer-review process.	
For manuscripts intended for publication please indicate target journal:	
Food Hydrocolloids	
Candidate's Signature:	Somaratne
Date:	09/09/2019
Primary Supervisor's Signature:	
Date:	9/9/2019

(This form should appear at the end of each thesis chapter/section/appendix submitted as a manuscript/publication or collected as an appendix at the end of the thesis)

GRS Version 4- January 2019

MASSEY UNIVERSITY
GRADUATE RESEARCH SCHOOL

STATEMENT OF CONTRIBUTION
DOCTORATE WITH PUBLICATIONS/MANUSCRIPTS

We, the candidate and the candidate's Primary Supervisor, certify that all co-authors have consented to their work being included in the thesis and they have accepted the candidate's contribution as indicated below in the *Statement of Originality*.

Name of candidate:	Geeshani Maduwanthi Somaratne
Name/title of Primary Supervisor:	Dr. Jaspreet Singh
Name of Research Output and full reference:	
Somaratne, G., Nau, F., Ferrua, M. J., Ye, A., Floury, J., Dupont, D., Singh, R. P. and Singh, J. (2019). Egg white gel structure determines gastric juice diffusion with consequences on softening and mechanical disintegration during in vitro gastric digestion. Targeted journal Food Hydrocolloids, In preparation.	
In which Chapter is the Manuscript /Published work:	Chapter 8
Please indicate:	
• The percentage of the manuscript/Published Work that was contributed by the candidate:	85%
and	
• Describe the contribution that the candidate has made to the Manuscript/Published Work:	
The candidate was involved in planning, designing and carrying out the experiments. The candidate compiled and summarised the results for discussion with supervisors. The candidate is writing the first draft of the manuscript for publication purpose.	
For manuscripts intended for publication please indicate target journal:	
Food Hydrocolloids	
Candidate's Signature:	Gsomaratne
Date:	09/09/2019.
Primary Supervisor's Signature:	
Date:	9/9/2019.

(This form should appear at the end of each thesis chapter/section/appendix submitted as a manuscript/ publication or collected as an appendix at the end of the thesis)

GRS Version 4- January 2019

Copyright Permission